University of Alberta
Department of Civil &
Environmental Engineering

NUMERICAL SIMULATIONS OF THE BEHAVIOUR OF PARTIALLY ENCASED COMPOSITE COLUMNS

by

Mahbuba Begum

Robert G. Driver

and

Alaa E. Elwi

July 2007

Numerical Simulations of the Behaviour of Partially Encased Composite Columns

by

Mahbuba Begum

Robert G. Driver
and

Alaa E. Elwi

Structural Engineering Report 269

Department of Civil and Environmental Engineering
University of Alberta
Edmonton, Alberta, Canada

July 2007

ACKNOWLEDGEMENTS

ABSTRACT

This study presents a wide range of numerical investigations on partially encased composite (PEC) columns based on finite element analysis. The PEC columns studied herein are fabricated from thin-walled built-up H-shaped steel sections with links provided between the opposing flanges to improve the resistance to local buckling. The regions between the flanges and web are filled with concrete. Prediction of the behaviour of this relatively new composite system by finite element modelling presents a challenging problem due to local buckling of the thin steel flange plates and crushing of the concrete near the ultimate load. These challenges were overcome in the current finite element model through the implementation of a dynamic explicit formulation along with a damage plasticity model for concrete and a contact pair algorithm at the steel–concrete interface.

The model was applied successfully to simulate the behaviour of 34 PEC columns from five experimental programs. The model was able to trace a stable and complete load–strain history accurately for PEC columns with small and large cross-sections, with different link spacings, constructed with normal strength, high strength and steel fibre reinforced high strength concrete, and tested under concentric and eccentric axial loads. The model reliably reproduced the peak load, axial deformation at the peak load, the post-peak behaviour and the failure mode observed in the tests.

Studies were performed to quantify the effects of local imperfections and residual stresses on the capacity of these columns using the developed model. The results revealed that the ultimate capacity of the column was not affected significantly by the

presence of local imperfections and residual stresses in the steel section. Finally, a comprehensive parametric study was carried out by varying the overall column slenderness ratio, load eccentricity, link spacing, slenderness ratio of the steel flange plate and concrete strength to explore the behaviour of these columns under the combined effect of axial compression and bending about the strong axis.

TABLE OF CONTENTS

LIST OF TABLES

LIST OF FIGURES

LIST OF SYMBOLS

A_c	Cross-sectional area of concrete
A_r	Cross-sectional area of additional reinforcing steel bars
A_s	Cross-sectional area of steel shape
A_{se}	Effective cross-sectional area of steel shape
b/t	Width-to-thickness ratio of flange plate
b	Unsupported flange width
b_c	Width of concrete stress block
b_e	Full effective flange width
b_f	Full flange width (equals $2b$)
c	Distance between extreme compression fibre and neutral axis
c_1, c_2 and c_3	Empirical factors used in the double-exponential stress-strain model for concrete (Barr and Lee 2003)
C_c	Total force in concrete stress block
C_r	Cross-sectional strength of PEC column
d	Depth of the column cross-section
d_c	Compression damage parameter for concrete
d_t	Tensile damage parameter for concrete
d_f	Diameter of the steel fibre
e	Initial load eccentricity used in the parametric study
e_{top}	Initial load eccentricity at top surface of the column
e_{bottom}	Initial load eccentricity at the bottom surface of the column
e_x	Initial load eccentricity for bending about strong axis
e_y	Initial load eccentricity for bending about the weak axis
e/d	Initial load eccentricity ratio used in the parametric study
E_c	Modulus of elasticity for concrete (secant modulus at $0.40f_{cu}$)
E_{ce}	Effective elastic modulus for concrete
E_{it}	Initial tangent modulus of concrete
E_s	Modulus of elasticity for steel
f_c	Compressive stress of concrete

f_{cu}	Measured uniaxial compressive strength of concrete
f_{cue}	Effective uniaxial compressive strength of concrete
f_t	Tensile stress of concrete
f_{tu}	Uniaxial tensile strength of concrete
F_s	Yield strength of steel plate
F_{sh}	Stress at the onset of strain hardening of steel
F_u	Ultimate strength of steel plate
F_{yr}	Yield strength of additional reinforcing steel bars
k	Plate buckling coefficient
k_1 and k_2	Factors used to define the post-peak descending branch of the stress-strain curve of high strength concrete
l_f	Length of the steel fibre
L	Column Length
L/d	Overall column slenderness ratio
M_u	Column Length
n	Empirical factor used to relate effective flange width to actual flange width
P_{exp}	Experimental peak load
P_{num}	Numerical peak load
P_u	Peak load of the parametric column
M_u	Moment at the peak load of the parametric column
p and q	Factors used to define the compressive stress-strain curve of steel fibre reinforced concrete
s	Link spacing
s/d	Link spacing-to-depth ratio
t	Plate thickness
U_2	Axial Displacement
$U_{3,u}$	Maximum lateral displacement for strong axis bending
V_f	Volumetric ratio of steel fibres in concrete
w	Crack width of concrete in tension
w_f	Final crack width of concrete in tension

α	Factor used in the double-exponential model for concrete defined as c_3/c_2
α_1	Ratio of average stress in rectangular concrete compression block to concrete strength (CSA 2004c)
β	Parameter to control the shape of the compressive stress-strain curve of concrete
β_1	Ratio of depth of rectangular concrete compression block to depth to the neutral axis (CSA 2004c)
ε_a	Ratio of depth of rectangular concrete compression block to depth to the neutral axis (CSA 2004c)
$\varepsilon_{a,u}$	Average axial strain at peak load
ε_c	Compressive strain of concrete
ε_{cu}	Axial strain of concrete at f_{cu}
$\varepsilon_{0.2f_{cu}}$	Axial strain of concrete at $0.2\,f_{cu}$
$\varepsilon_c^{\sim pl}$	Effective plastic strain in compression
$\varepsilon_t^{\sim pl}$	Effective plastic strain in tension
ε_{exp}	Experimental peak axial strain
ε_{num}	Numerical peak axial strain
$\varepsilon_{\ln}^{pl}$	Logarithmic plastic strain of steel
ε_{sh}	Strain at the onset of strain hardening of steel
ε_u	Strain at the ultimate strength of steel
ε_y	Yield strain of steel
λ_p	Column slenderness parameter
ν	Poisson's ratio for concrete
ν_s	Poisson's ratio for steel
σ_L	Lateral confining pressure of concrete
ϕ	Transverse link diameter
Ψ	Parameter to account for size effects on PEC columns
δ_m	Maximum amplitude of local imperfection

LIST OF ABBREVIATIONS

CFT	Concrete filled tubes
FEC	Fully encased composite
FEM	Finite element method
PEC	Partially encased composite
NSC	Normal strength concrete
HSC	High strength concrete
HSFRC	Steel fibre reinforced high strength concrete

1. INTRODUCTION

1.1 Foreword

The effective use of a combination of steel with materials such as concrete can substantially improve the behaviour and cost efficiency of columns used in the construction of mid-rise and high-rise buildings, as compared to using steel-only columns. Two types of composite columns commonly used in North America are: concrete filled tubes (CFT) and fully encased composite (FEC) columns (Figure 1.1). Both of these composite systems have limitations such as limited cross-sectional dimensions of standard shapes (CFT), although large diameter tubes have occasionally been used, requirement of extensive formwork and additional reinforcing steel (FEC columns) and complex beam-to-column connections. These limitations have indirectly imposed restrictions on the use of composite columns.

In 1996, the Canam Group in Canada took the initiative to propose a new type of composite column consisting of a thin-walled, welded H-shaped steel section, built-up from hot-rolled steel plate, with concrete infill cast between the flanges, as shown in Figure 1.2. Transverse links are provided between the flanges at regular intervals to improve the resistance to local buckling. This new system has been termed the "partially encased composite (PEC) column," since the steel section is only partially encased by the concrete. Additional reinforcement consisting of longitudinal rebars and transverse U-shaped stirrups can be provided to improve the ductility of these columns somewhat under cyclic loading, but in general additional reinforcement is not required. The intent is that the steel column alone is used for erection of the building and resisting all construction loads and the concrete is provided to assist in resisting the service loads. The concrete is simply cast with the floor slab above, resulting in significant economies related to the construction schedule and, therefore, project financing.

Although apparently similar, the new PEC column is significantly different from that developed in Europe in the early 1980s, which was constructed with hot-rolled standard

1

wide flange shapes (Figure 1.3), not susceptible to local buckling. The cross-sectional size can exceed the outer dimensions of standard rolled W-shapes and can easily be customized to the needs of the project. Moreover, the steel sections are relatively light, easing handling considerations. On the other hand, the steel section of the Canam-type of PEC column features very slender plates that exceed the width-to-thickness ratio limits for Class 3 sections where local instability is one of the governing failure criteria. This requires the addition of links between the flanges.

As explored by Vincent (2000), this new PEC column system takes advantage of:

- In-plant prefabrication of steel;
- Economic compressive load carrying capacity of concrete;
- Standard connections to the steel flanges;
- Fire resistance improved due to the presence of the concrete;
- Simple installation and removal techniques of the formwork for concrete;
- Speed of erection of steel structures; and
- Less crane capacity required to erect the columns due to a much lighter steel section.

Extensive experimental research has been performed in Ecole Polytechnique de Montréal (Tremblay et al. 1998; Chicoine et al. 2000, 2003; Bouchereau and Toupin 2003) on small- and large-scale PEC column specimens under various conditions of loading. The influences of high performance materials on the behaviour of these columns have also been investigated experimentally by Prickett and Driver (2006) at the University of Alberta. Additional experimental research is currently being conducted to study the behaviour of this new composite system as a part of lateral load resisting systems such as braced steel frames and steel plate shear walls. A finite element model capable of reproducing the test results of concentrically loaded short column specimens was developed by Chicoine et al. (2001). The researchers identified significant challenges in modelling the triaxial behaviour and the rapid volumetric expansion of the encased concrete near and beyond the peak load. As a result, the model did not trace the post-peak behaviour or predict the residual capacities after buckling of the steel and crushing of the concrete had taken place. The researchers recommended that additional research be

performed to capture the complex behaviour near and beyond the peak capacity (Chicoine et al. 2001). Moreover, the effect of initial imperfections on the capacity of these columns has not been studied in detail. As a part of a lateral load resisting system, these columns will be subjected to the combined effect of axial and bending stresses. The behaviour under the combination of bending moment and axial load has not yet been explored numerically for this new composite system.

1.2 Objectives and Scope of the Study

The primary objective of this study was to develop a complete finite element model that can be applied for a variety of geometries of PEC columns, subjected to various loading conditions, and provide accurate simulations of behaviour without numerical difficulties well into the post-peak regime. The model, therefore, is to be capable of simulating numerically the full behavioural history including the peak and residual post-peak capacities and the failure mode caused by local buckling of the steel plates and/or crushing of the concrete. A concrete damage plasticity model and dynamic explicit solution strategy were chosen to model the behaviour using the ABAQUS/Explicit (HKS 2003) finite element software. The performance of the damage model needed to be verified for its ability to predict the concrete behaviour under uniaxial, biaxial and triaxial stress conditions with various levels of lateral confinement.

To evaluate the accuracy of the finite element model in predicting the overall behaviour of PEC columns, simulations were carried out on tests of 31 short and three long (i.e., slender) PEC specimens, as reported in the literature. The short columns, having lengths equal to five times the total depth, d, of the column cross-section, varied in cross-sectional size from 300 mm × 300 mm to 600 mm × 600 mm. The long PEC column test specimens, with a 450 mm × 450 mm cross-section, had lengths equal to 20d. The test specimens had a variety of link spacings (0.3d to 1.0d) and link diameters and a range of flange plate slenderness ratios, b/t, (from 23 to 35). (Note that the standard notation for the cross-sectional geometric properties of PEC columns is shown in Figure. 1.2 (a).) Three different types of concrete were used in the test columns: normal strength concrete,

3

high strength concrete and steel fibre reinforced high strength concrete. The columns simulated using the finite element model were tested under either monotonic concentric axial loading or monotonic eccentric axial loading with a variety of eccentricities.

This study also aimed to investigate the effects of local flange imperfections and residual stresses on the capacity of PEC columns. This would help to identify the importance of including these features, which add to the modelling complexity, in numerical simulations of PEC column behaviour.

Another objective of this study was to conduct a parametric analysis with a view to investigating the effect of a range of parameters on the behaviour of PEC columns, particularly when loaded eccentrically. The variables include the overall column slenderness ratio, L/d, where L is the overall length of the column, load eccentricity, e, link spacing, s, flange plate slenderness ratio, b/t, and compressive strength of concrete. The effects of these parameters were studied on 450 mm × 450 mm cross-section. The parametric columns were analysed under monotonic loading conditions with bending about the strong axis.

1.3 Organization of the Thesis

The thesis consists of seven chapters. Chapter 1 introduces the type of composite column studied herein and presents the objectives and scope of the research work. Chapter 2 presents a short review on the literature related to PEC columns with standard steel sections and explores in relative detail the experimental and numerical research works carried out on PEC columns with thin-walled built-up steel sections. The PEC column design requirements included in CSA standard S16–01 (CSA 2001) are also presented in this chapter. Chapter 3 includes the description of the concrete constitutive behaviour and discusses the performance of the damage plasticity model in predicting the compressive behaviour of concrete under different levels of confinement.

The detailed description of the finite element model for the PEC column, along with the properties of the reference test specimens, are given in Chapter 4. The selected element types, mesh configuration, material mechanical properties for steel and concrete, modelling of steel–concrete interactions at their common interfaces and the solution strategy implemented in the finite element model are presented. This chapter also describes the technique of modelling local and global imperfections in the numerical model for PEC columns.

The results of the numerical simulations of the test specimens used to validate the developed finite element model under concentric and eccentric loading conditions are presented in Chapter 5. Discussions are included on the comparison between the experimental and numerical failure modes, peak axial loads, average axial strains at peak load, load versus average axial strain curves, and load versus moment curves for different test groups. The effects of local imperfections and residual stresses on the column behaviour are also presented. In addition, the effects of link spacing on the column behaviour and the contributions of steel and concrete individually on the overall load carrying capacity of this composite system are demonstrated.

Chapter 6 presents the detailed parametric study conducted with the developed finite element model to cover the range of several geometric and material parameters on the behaviour of PEC columns. The findings of this parametric study are demonstrated and discussed.

A summary of the methodology and conclusions regarding the achievements of this research work are included in Chapter 7, along with recommendations for future research.

(a)

(b)
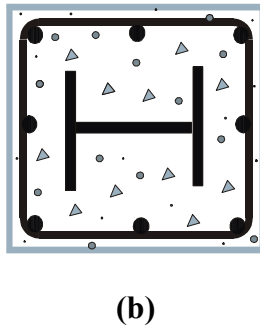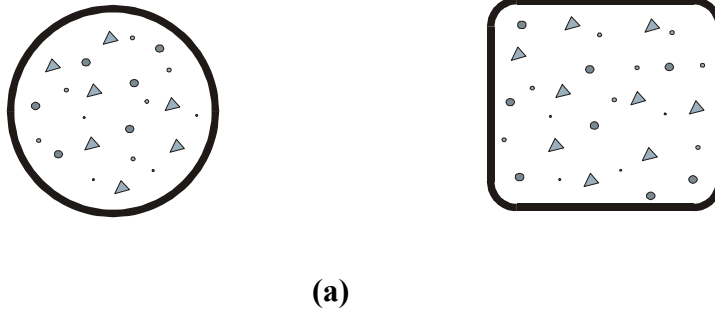
Figure 1.1 Common types of Composite Columns,
(a) Concrete Filled Tubes, (b) Fully Encased Composite Column

Welded H
steel shape
t

d

b

b_f

Link

Concrete

(a)

(b)
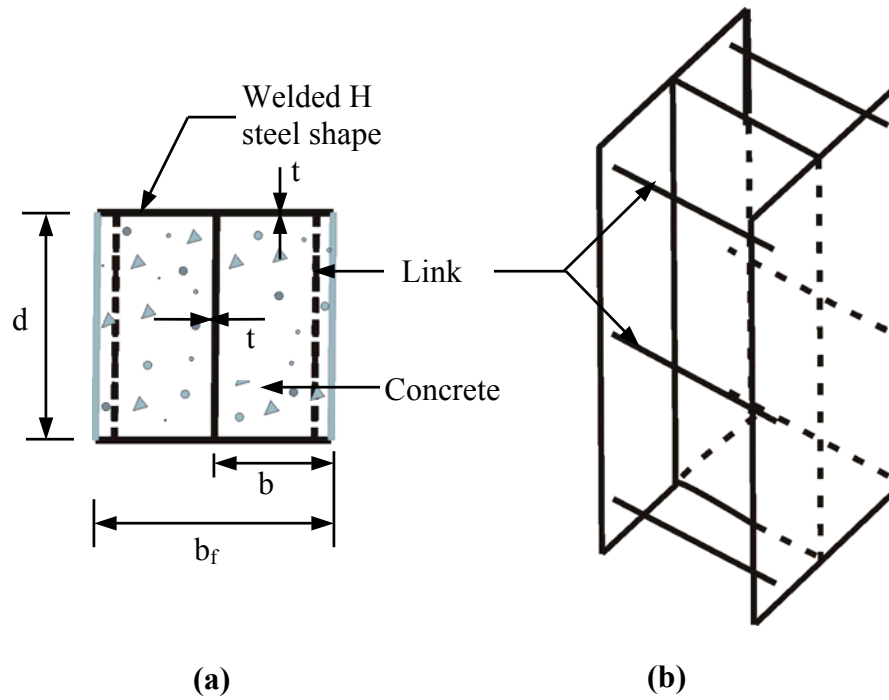
Figure 1.2 Partially Encased Composite Column with Thin-Walled Built-Up Steel Section, (a) Column Cross-Section and (b) 3D view of the Steel Configuration
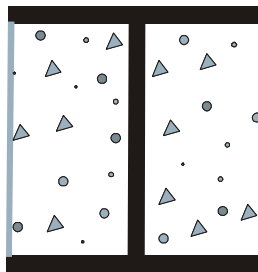
Figure 1.3 Partially Encased Composite Column with Compact Standard Steel Section

2. LITERATURE REVIEW

2.1 Introduction

A partially encased composite (PEC) section refers to an H–shaped steel section with concrete infill between the flanges. In Europe, in the early 1980s, PEC columns and beams were introduced using standard-sized rolled steel sections. In 1996, the Canam Group in North America proposed a PEC column section constructed from a thin–walled built–up steel shape with transverse links provided at regular intervals to restrain local buckling. Using a built–up steel section instead of a standard shape provides the designer with more flexibility when sizing the column cross-section. Moreover, thin steel plates were intentionally specified to obtain a more cost effective column by increasing the contribution of concrete in the load carrying capacity of the column. These factors have made PEC columns constructed with built-up shapes more attractive than those constructed with standard sections. However, thin–walled steel sections are susceptible to local buckling of the flanges and this needs to be accounted for in the design of these columns. To better understand the behaviour of the PEC column with a thin–walled steel section, on which the current study is being conducted, a review of the experimental and analytical investigations related to this composite system is presented in this chapter. A brief review on the literature on PEC columns with standard shapes is also included to compose a complete picture of the works on this type of composite section.

2.2 PEC Columns Fabricated with Standard Steel Sections

Several experimental investigations have been carried out on PEC beam-columns with fabricated shapes, typically used in Europe, subjected to static, cyclic and earthquake loading. The conventional form of this composite column consists of a compact steel section with longitudinal and tie reinforcements in the encased concrete. Elnashai et al. (1991) modified the conventional section by adding transverse bars linking the two flanges to prevent local buckling at large displacements and to increase the interaction between steel and concrete. From experimental investigations, the researchers reported

8

significant improvements in the seismic behaviour of these columns due to the addition of these bars. Elnashai and Elghazouli (1993) proposed a numerical model for this type of PEC column using the nonlinear static and dynamic analysis program ADAPTIC. The numerical model was calibrated against and compared with the experimental results (Elnashai et al. 1991). Elasto–plastic cubic elements were used to represent the test specimen and a uniaxial cyclic material model was employed to represent the concrete material behaviour. This model allowed for variable confinement across the cross-section, including concrete that is unconfined between the open face and the transverse links, fully-confined near the web of the steel shape, and partially confined between the two other confinement regions. The local imperfections in the steel section and the effect of residual stresses were not accounted for in the numerical model. Elghazouli and Elnashai (1993) carried out a detailed parametric study using the analytical model on the modified configuration of PEC columns with standard sections developed and tested by Elnashai et al. (1991). The main purpose of the study was to asses the capacity and ductility of PEC members and their sensitivity to a number of parameters such as axial load, steel characteristics, concrete confinement, flange slenderness and member slenderness. The study was limited to flexural members subjected to uniaxial bending and axial loads. They found that concrete confinement had no effect on the yield moment, but the ultimate moment was affected to some extent. It was demonstrated that substantial ductility could be attained by properly detailed members, particularly the modified section that includes transverse links. Later on, this modified PEC column was improved by removing the longitudinal and tie rebars in the concrete, with a view to easing the construction process and minimizing the cost.

Elnashai and Broderick (1994) carried out an experimental investigation on the improved section consisting of a compact steel shape and transverse links, in a context of seismic resistance. The tests included severe cyclic and pseudo-dynamic loading with varying levels of axial force. The results demonstrated that the link-only PEC columns were able to retain the earthquake–resistant capabilities of the modified section (PEC columns with links and additional rebars), thus making it a more attractive alternative. An analytical study was carried out by Broderick and Elnashai (1994) on this type of PEC column

using the program ADAPTIC. Most of the features of the numerical model were similar to those used by Elnashai and Elghazouli (1993) in their analytical models for the modified section of PEC columns. The model was able to predict the displacement and rotation ductility and the ultimate moment of the test specimens of Elnashai and Broderick (1994) with good accuracy. The superior earthquake–resistant capabilities of this composite system were also revealed from the analytical study.

Hunaiti and Fattah (1994) investigated the load carrying capacity of PEC columns subjected to monotonic eccentric axial load. Instead of using transverse links in the steel section, they used intermittent batten plates welded at the flange tips of the column. They also studied the effect of shear connectors to evaluate the effect of improving bond on the behaviour of these columns. The variables studied included eccentricity of the applied load with equal and unequal eccentricities at the column ends and concrete strength. The results demonstrated that the columns failed by yielding of steel and crushing of concrete, accompanied by large deflections. No signs of local or overall buckling were reported, which indicates that the columns tested developed the full flexural strength of the section (Hunaiti and Fattah 1994). All of the test columns—with and without batten plates and with shear connectors—behaved in a somewhat similar manner. Therefore, the researchers concluded that batten plates and shear connectors are not required for this type PEC column to achieve full composite behaviour between the infilled concrete and the steel section. However, to account for the effect of several factors in a real structure that could cause deterioration of the bond between the steel and concrete, they recommended that the mechanical shear connectors be included in the composite section.

2.3 PEC Columns Fabricated with Thin-Walled Built-Up Sections

2.3.1 Experimental Investigations

Extensive experimental research has been conducted on thin-walled PEC columns with built–up sections by several research groups (Fillion 1998; Tremblay et al. 1998; Chicoine et al. 2000; 2003; Muise 2000; Bouchereau and Toupin 2003; Prickett and Driver 2006) to investigate the behaviour of this type of PEC column under various

loading conditions. A large number of tests have been performed on short PEC columns constructed with normal strength concrete subjected to concentric and eccentric axial loads, including static and cyclic conditions. Short PEC columns with high performance concrete have also been tested under pure axial compression as well as combined axial and flexural compression. A few long column tests were carried out using normal strength concrete under static loading. Furthermore, tests of beam–to–column connections were performed for beams framing into the weak axis of the composite column. Descriptions of these experimental investigations along with the findings are presented in the following sections.

2.3.1.1 *Short Columns Constructed with Normal Strength Concrete*

2.3.1.1.1 *Columns Under Concentric Axial Loading*

The first series of tests on short PEC columns was performed by Fillion (1998) and Tremblay et al. (1998) on specimens with 300 mm × 300 mm and 450 mm × 450 mm cross–sections. The specimens had a length of five times the cross-section dimension and were loaded under axial compression. The test program included ten tests on bare steel columns and seven tests on composite columns with different transverse link spacings and flange slenderness ratios. The bare steel columns were examined to study the behaviour of the column under construction loading, prior to the composite action. To study the possible size effect on the behaviour of short PEC columns, Chicoine et al. (2000) tested five 600 mm×600 mm concentrically loaded columns and compared them with the first series of tests on short PEC specimens. They also varied the transverse link spacing and the flange slenderness ratio to study their influences on the column behaviour. One of the five composite specimens had additional reinforcements in the form of longitudinal and transverse rebars in the concrete. Local flange imperfections between the transverse links (out of the plane of the flange) were measured on the steel section of these test specimens. It was observed that the inward imperfection measurements outnumbered the outward ones with a ratio of 18:1 on the 600 mm specimens and no outward imperfections were found on the 300 mm and 450 mm specimens (Tremblay et al. 1998; Chicoine et al. 2000). The tendency of the flange to

11

bow inward was attributed to the fabrication process used for the specimens, which is influenced by the shrinkage of the web-to-flange welds. The maximum amplitude of the measured local imperfections in these test specimens varied from 0.39 mm (s/870) to 2.02 mm (s/335). The residual stresses in the steel plates of these test specimens were also measured before the tests.

The results of these tests showed that the bare steel PEC columns failed due to local buckling in the flanges and the web, while the failure of the composite columns occurred by a combination local buckling of the steel flanges between the transverse links, yielding of the steel and crushing of the concrete. Usually local buckling occurred at or near the peak load, depending on the slenderness of the flange plates and the link spacing. For columns with relatively wider link spacings (e.g., s = d), local buckling was observed to occur between 75% and 80% of their ultimate loads.

The load versus deformation response was studied for the test specimens to evaluate the influence of column size, plate slenderness ratio, link spacing and additional reinforcements. The test results on 300 mm, 450 mm and 600 mm short column specimens with equal plate slenderness and link spacing, demonstrated that the 450 mm and 600 mm specimens behaved in a similar manner while the 300 mm specimens exhibited a more gradual failure with the same post-peak response (Chicoine et al. 2002a). It was also reported that the specimens with higher b/t and s/d ratios exhibited a faster degradation of post-peak strength than columns with lower b/t ratios and smaller link spacings. However, the load versus deformation response before the ultimate load did not vary much from one specimen to another since it remained elastic until near the peak. The additional rebars had a negligible impact on the ultimate capacity of the column, but significant improvements were observed in the ductility of the post-peak response (Chicoine et al. 2002a). During the tests, the longitudinal and transverse strains in the steel shape and transverse links were measured from which the corresponding stresses were calculated. The strain measurements in the flanges indicated that the flanges were bending outwards slightly between the links and the web. However, the transverse stresses in the flanges and web of the steel shape due to the lateral expansion of concrete

12

were found to be small and did not affect the axial capacity of the column. On the other hand, the lateral expansion of concrete was observed to induce high tensile stresses in the transverse links. The stresses in the links were observed to be doubled when the link spacing was halved, as a result of better confinement of the concrete near the exposed face. Chicoine et al. (2000) reported weld failure between the transverse links and the flanges in three of the composite test specimens. It was recommended that the links be welded to the flanges to develop their full yield capacity.

Chicoine et al. (2003) investigated the effects construction loading sequence and long-term loading (such as the effects of shrinkage and creep of concrete) on the behaviour of PEC columns by testing seven short composite columns with 300 mm × 300 mm and 450 mm × 450 mm cross–sections. Four of these specimens were loaded for 150 days, following a typical construction sequence. The rest were without any long-term loading since they were used to assess the effect of shrinkage strains in the steel and the concrete. The specimens under long-term loading showed similar behaviour to that observed in the short-term loading tests (Chicoine et al. 2000; Tremblay et al 1998). The stress conditions before loading to failure were observed to have no influence on the ultimate capacity and failure mode of these columns.

2.3.1.1.2 Columns Under Combined Axial and Flexural Loading

Bouchereau and Toupin (2003) conducted tests to investigate the behaviour of short PEC columns subjected to axial compression and bending under monotonic and cyclic loading conditions. A total of 22 tests on 2250 mm long columns and two tests on 5000 mm long beams (as an upper bound to the moment-to-axial-force ratio) were performed. Two types of specimens were used, one without additional reinforcement and the other with reinforcing steel in the form of longitudinal (0.06%) and transverse rebars. Both types had a square cross-section of 450 mm × 450 mm × 9.53 mm where the first two numbers indicate the depth and width of the cross-section and the third number is the thickness of the steel plates. A link spacing of 300 mm was used in all the test columns. The loading conditions imposed in the tests were selected based on the flexural demand on PEC columns when used in concentrically braced structures subjected to design level

earthquake motions. To evaluate this demand, a nonlinear seismic dynamic analysis was carried out by the researchers on a 16- and a 24-storey braced frame building. The results of this study revealed limited flexural demand on gravity columns with considerably larger bending moments on the columns of the bracing bents (Tremblay 2003). The test program (Bouchereau and Toupin 2003) was mainly designed to simulate the conditions of a column of the bracing bents subjected to monotonic and cyclic eccentric axial loads. In each case the effect of strong and weak axis bending was investigated for two different values of load eccentricity. The effect of cyclic lateral loading with monotonic axial load on PEC columns was also explored for both strong and weak axis. In addition, two columns were tested under monotonic concentric loading only, the results of which were used as reference values for other tests performed by Bouchereau and Toupin (2003).

The short PEC columns with normal strength concrete subjected to both monotonic and cyclic eccentric loading demonstrated similar failure modes to those observed by Tremblay et al. (1998) in similar columns under concentric axial loading only. However, Bouchereau and Toupin (2003) reported that the occurrence of local buckling and concrete crushing was essentially simultaneous in all of the eccentrically loaded test specimens. The specimens with weak axis bending exhibited brittle and explosive failures as compared to other specimens. However, the presence of additional reinforcement in the specimens under weak axis bending was observed to improve the behaviour of these columns significantly. The additional reinforcements also increased the ultimate capacity of the PEC columns by an average of 8%, as observed by Bouchereau and Toupin (2003).

Comparing the results of the cyclic tests to corresponding monotonic tests, no significant differences in the column behaviour were observed. Bouchereau and Toupin (2003) reported that the cycles of loading did not have a deleterious effect on the ultimate capacity; rather, it improved the capacity obtained under monotonic loading conditions by about 4%. No significant difference was observed in the post-peak load versus displacement response between cyclically and statically loaded PEC columns. Bouchereau and Toupin (2003) also constructed load–moment interaction diagrams for PEC columns with normal strength concrete and validated the curves against the test

results. The interaction diagrams were developed using the methods typically adopted for reinforced concrete columns, assuming a linear strain distribution across the cross-section. Bouchereau and Toupin (2003) did not include the effect of local flange buckling, residual stresses in the steel section or confinement of concrete in calculating the load–moment interaction diagrams for PEC columns with normal strength concrete. Very good agreement was observed between the test and predicted capacities. However, the capacities of the two test columns with weak axis bending without additional rebars were lower than that predicted from the interaction diagram by 10 to 15%. Bouchereau and Toupin (2003) explained this inconsistency by noting the sensitivity of these columns to unexpected test conditions such as accidental eccentricity, improper installation or defects during the fabrication process. However, the researchers recommended that modifications to the load–moment interaction diagram be developed that consider the local buckling of the flanges, residual stresses, concrete confinement and transverse stresses in the steel.

2.3.1.2   *Short Columns Constructed with High Performance Concrete*

Prickett and Driver (2006) conducted a comprehensive experimental research project to study the behaviour of thin-walled PEC columns made with high performance concrete. The study included 11 short PEC columns measuring 400 mm × 400 mm × 2000 mm, with the primary variables being the concrete type, link spacing and load eccentricity. The plate slenderness ratio was kept constant (b/t = 25) for all of the test columns. The specimens were divided into two groups. The first group consisted of seven specimens subjected to axial compression only. Three different link spacings and three types of concrete (normal strength, high strength and high strength steel fibre reinforced concrete) were used in these specimens. Two normal strength concrete columns with different link spacings were used as reference specimens. Steel fibres were used to observe potential improvement in the failure mode of PEC columns with high strength concrete. Four identical PEC columns constructed with high strength concrete and subjected to axial compression and bending were tested in the second group of specimens by Prickett and Driver (2006). Bending axis and the amount of load eccentricity were varied to determine

the effects of these parameters on the column behaviour. Initial local imperfections in the flange plate were measured at several locations in the steel section for all 11 test specimens. The local imperfections in the flanges were observed to be inwards in most locations, with an average maximum amplitude of approximately 1.5 mm (s/375). Additional measurements of the local flange imperfections were performed after the columns had been cast and no significant differences were observed.

The column behaviour was examined by considering the failure mode, load versus strain response and the transverse stresses in the steel plates. The high strength concrete PEC columns failed in a similar manner to the PEC columns with normal strength concrete: concrete crushing combined with local flange buckling. However, the failure of a high strength concrete column was observed to be sudden as compared to an equivalent PEC column with normal strength concrete. Addition of steel fibres in the high strength concrete was found to improve the failure mode of the columns somewhat. Prickett and Driver (2006) reported no local buckling prior to the peak load in any of the concentrically loaded test specimens, even for the specimen with a link spacing equal to the depth of the column. However, one of the eccentrically loaded specimens experienced local buckling at 90% of the peak load. The effect of confinement, as revealed by transverse stresses in the steel section, on the capacity of the high strength concrete PEC columns was similar to that observed for the normal strength concrete PEC columns. However, the steel section of columns with high strength concrete yielded sooner relative to the peak load as compared to the steel section of the columns with normal strength concrete. The axial capacity of the high strength concrete PEC columns was not significantly affected by the confinement of the concrete and therefore Prickett and Driver (2006) recommend that confinement not be accounted for in the design of these columns. The maximum stresses in the links were well below the yield stress and therefore it was recommended by the researchers that the current design requirements for link cross-sectional area and welding in CSA standard S16-01 (CSA 2001) are satisfactory for high strength concrete PEC columns under concentric and eccentric loading conditions.

Prickett and Driver (2006) also studied the moment versus curvature response and developed load versus moment interaction diagrams for the eccentrically loaded specimens. The moment versus curvature curves for specimens with strong axis bending showed a gradual decline of the peak moment as compared to the sudden decline observed in the specimens with weak axis bending. To predict the capacity of the eccentrically loaded columns, the load versus moment interaction diagrams were developed using the methods used for reinforced concrete columns. The effect of local flange buckling was included by using an effective area of the steel flange in the compression zone. In general, the interaction curves provided a good and conservative estimate of the ultimate cross-sectional capacities of the eccentrically loaded PEC columns obtained from the tests. For columns with strong axis bending the capacities obtained from the test exceeded the predicted capacities by 17 to 27%, whereas for columns with weak axis bending the predicted capacities were exceeded by only 4 to 9%. Prickett and Driver (2006) attributed this discrepancy to the fact that the concrete confinement, which was neglected in predicting the column capacities, had a more pronounced effect on the columns under strong axis bending than on those under weak axis bending. The presence of a steel flange on the face that experiences maximum compression, provides more favourable confinement conditions than either columns under weak axis bending or those loaded concentrically.

2.3.1.3 Long Columns Constructed with Normal Strength Concrete

Four long PEC columns with a length-to-depth ratio of 20 were tested to study the overall buckling behaviour of these columns under monotonic loading (Chicoine et al 2000). In this test program, one bare steel column and three composite columns were tested with two different link spacings. All columns had a square cross-section of 450 mm × 450 mm and a flange slenderness ratio of 23. Additional reinforcements in the form of longitudinal and tie bars were provided in one of the composite specimens. Both local and global geometric imperfections were measured in all specimens before the tests took place. The flanges of these specimens were observed to have outward local imperfections (between links), with maximum amplitudes less than 1 mm (s/600). The global out-of-straightness was measured about the weak axis and was also found to be small,

representing typically about 1/3000 of the total height of the columns. The long columns were tested under concentric loading, except for one, which was tested with an eccentricity of 0.06d about the weak axis. However, Chicoine et al. (2000) reported the presence of significant bending moment in all specimens about both the strong and weak axes caused by accidental eccentricity or uneven end bearing. Equivalent strong and weak axis eccentricities were, therefore, calculated for each specimen at the bottom, mid-height and top elevations using elastic theory. Chicoine et al. (2000) recommended that these computed values of eccentricity be included in the finite element analysis of these test specimens.

The test results demonstrated the brittle and explosive failure modes of the long composite specimens that consisted of global flexural buckling along with local buckling and concrete crushing between two links. The steel-only specimen was observed to fail by global buckling followed by local buckling at several link intervals. As reported by Chicoine et al (2000), no welds of the transverse links failed during the tests. The ultimate capacities of the slender columns were observed to be about 80% of those of short columns with similar cross–sections and link spacings. The initial weak axis eccentricity of 0.06d applied in one of the tests decreased the column capacity by 20% when compared with the specimen having similar geometric and material properties. The transverse stresses on the flange plates were observed to be higher on the compression side and lower on the tension side, with intermediate values in the web. The additional reinforcement was observed to provide no improvement in the ductility of the long composite column, as opposed to the beneficial effect observed in the short composite columns. However, a direct comparison between the two long specimens with and without additional reinforcements was not possible due to the presence of accidental eccentricity in the test specimens.

2.3.1.4   Beam-to-Column Connections

In structures with PEC columns, beams framing into the column flange faces would typically be connected using standard shear connection details. On the other hand, the weak axis connection is made to a plate spanning between the flange tips rather than

connecting the beam directly to the column web as would normally be done in conventional steel construction. Muise (2000) examined the behaviour of beam-to-column connections to the weak axis of thin-walled PEC columns by conducting 14 full-scale tests under both bare steel and composite conditions. The columns were loaded through floor beams connected to flange tip connection plates. The column sizes varied between 450 mm and 600 mm. The variables included the length of the flange tip connection plate as well as its thickness. Different types of floor beam connections welded to the connection plates were also studied, including short and long double angle connections, one sided shear plates and stiffened and unstiffened seat angles. Shear studs were added to the back of some connection plates to assess their contribution.

Muise (2000) reported that the predicted capacity was exceeded in all the connection tests, with yielding being observed in several of the connections within the range of the design load. The connection type was observed to influence the rotational stiffness. Larger rotational flexibility was observed in double angle connections as compared to the other connections investigated. The one-sided shear plates were found to provide higher stiffness by enhancing the force transfer between steel and concrete. The length of the connection plate was also observed to have a significant effect on the force transfer, with longer connections resulting in a more uniform stress gradient below the connections. The presence of shear studs was found to improve the force transfer to the concrete, however it was recommended that the pullout forces that can develop at the shear studs be considered in connection design.

In the testing of the steel connections, the unbalanced connection load was observed to have a pronounced effect on the axial load carrying capacity of the column. As reported by Muise (2000), the connection load introduced at a single side of the column created a stress gradient in the column and initiated buckling in the column flange, immediately under the loaded endplate, at total axial loads less than those experienced in the concentric tests by Tremblay et al. (1998).

2.3.2 Numerical Investigations

A finite element model of PEC columns with thin–walled built–up sections was first developed by Maranda (1998), using the computer program MEF, to simulate the series of tests on PEC stub columns performed by Tremblay et al. (1998). Only a quarter cross–section was modelled using shell elements for the steel plate, solid elements for the concrete and beam elements for the transverse links. Contact elements were used at the steel–concrete interface to represent interaction between these two materials. The model included local imperfections of the steel flange by scaling the displacements obtained from the buckled elastic shape. The yield plateau of the steel stress–strain curve was modified to include the effect of residual stresses in the steel plates. Good agreement was observed between the numerical and the experimental results, with an average ratio of experimental-to-numerical peak loads of 0.95 and a standard deviation of 0.03. However, the model developed by Maranda (1998) was not capable of predicting the post-peak responses of the test specimens. In some cases the model exhibited positive stiffness at the last converged solution point, indicating that the ultimate point had not been reached. Moreover, local imperfections were modelled outwards as opposed to the inward imperfections measured in the test specimens.

Chicoine et al. (2002b) performed a finite element analysis using ABAQUS/Standard (HKS 2003) to reproduce numerically the behaviour of the composite column near the peak load, modes of failure, and stresses in the web of the steel shape and in the transverse links. The model was verified and calibrated against the experiments performed on short term load tests on short PEC columns subjected to gravity loading only (Tremblay et al. 1998; Chicoine et al. 2002a). The researchers also studied the effects of loading sequence and long term loading on the PEC column using the numerical model by simulating the long-term tests on short PEC columns (Chicoine et al. 2003). Similar to the numerical study performed by Maranda (1998), Chicoine et al (2002b) also modelled a quarter of the column cross–section with a length of one link spacing. The finite element model was developed using S8R shell elements for the steel section, C3D20R brick elements for concrete and B32 beam elements for the transverse links. Two node spring elements were used to represent the interaction between steel and

concrete at their common interface. The stiffness of these elements were adjusted to simulate the local buckling of the flange and the separation between steel and concrete as the load progresses. Very high compressive stiffness was defined for the springs to prevent inward buckling of the flange plate due to the presence of the concrete. On the other hand, very low tensile stiffness was given to allow the flange to buckle freely in the outward direction. To simulate perfect bond between the transverse link and concrete, all nodes of the link were coupled to the adjacent concrete nodes in the axial direction of the link.

Steel material behaviour was represented by a bilinear stress–strain curve based on the typical stress–strain curves obtained from tension coupon tests of the plates used in the column specimens (Chicoine et al 2000). The mechanical properties of concrete were defined using an effective compressive strength, f_{cue} and an effective elastic modulus, E_{ce} , given by:

$$f_{cue} = 0.92\psi f_{cu} \tag{2.1}$$

$$E_{ce} = \sqrt{0.92\psi}\, E_c \tag{2.2}$$

where f_{cu} and E_c are the compressive strength and elastic modulus obtained from cylinder tests at the day of column testing. The strength reduction factor 0.92ψ was proposed by Chicoine et al (2002a; 2002b), where 0.92 accounts for the lower quality of structural concrete in the test specimens as compared to the test cylinders and was selected to obtain a better fit between the experimental data and the results obtained from the numerical analysis by Chicoine et al (2002b). The factor ψ accounts for the size effect on cross-sectional strength and is expressed as:

$$\psi = 0.85\left(0.96 + \frac{22}{b}\right)\begin{cases} \geq 0.85 \\ \leq 0.97 \end{cases} \tag{2.3}$$

Here, b is half of the flange width of the column in mm.

The cracking model in ABAQUS/Standard was used by Chicoine et al (2002b) to represent the concrete material behaviour in PEC columns. The local imperfections were included by applying a deformed shape corresponding to the first buckling mode obtained from an eigenvalue buckling analysis on the bare steel section with a length of one link spacing. The model also includes the residual stresses defined as initial conditions in the steel plates. Chicoine et al. (2002b) used the Riks displacement control technique to simulate the applied loading conditions in the test specimens. Therefore, an implicit solution strategy was implemented to trace the overall column behaviour throughout the applied displacement history. To model the sequence of loading in the long-term test series (Chicoine et al 2003), the entire composite section was defined initially. The concrete elements were then removed and the steel section was loaded to match the construction-induced stresses. Finally, the concrete elements were reinstated and the load was applied to the composite section. The long-term deformations were included by adding the increase in stress measured in the steel during the tests by Chicoine et al. (2003).

The finite element model developed by Chicoine et al. (2002b) provided a very good representation of the ultimate capacity and load versus displacement response of short PEC test specimens up to the ultimate load. The mean experimental-to-numerical peak load ratio was observed to be 1.0 with a standard deviation of 0.03. The numerical model overestimated the experimental strain at peak load by about 5% on average. The post-peak response of the columns was obtained only over a short deformation range due to convergence problems experienced by the numerical model. This can be attributed to the inadequacy of the implicit solution method for representing the highly nonlinear post-peak behaviour. However, the ultimate point was observed to be passed successfully since the post-peak stiffness in all the analyses was negative (Chicoine et al. 2002b). The numerical failure mode in axial compression was identical to the experimental one, with local buckling of the flange occurring outwards in a single wave between links. However, the model was incapable of predicting the proper failure mode with the inwards imperfection. Chicoine et al. (2002b) reported that if the imperfections were modelled

inwards as measured in the tests, the mode of failure of the numerical model showed the flange buckling occurring in two waves between the transverse links. This failure mode was not observed experimentally. Moreover, inwards imperfections also tend to give higher values of the ultimate loads (Chicoine et al. 2002b). For these reasons, Chicoine et al. (2002b) included outwards local imperfections (which is contradictory to experimental observations) in the finite element model of the test specimens.

Chicoine et al. (2002b) also studied the stresses in the steel plates and concrete of this composite system at the peak load using the numerical model. The average stresses carried by the flanges and the web at the peak load point were reported to be $0.88F_y$ and $0.93F_y$, respectively. Buckling, along with initial imperfections and high tensile residual stresses near the welds, were responsible for the reduction in the flange capacity (Chicoine et al. 2002b). The reduction of the web capacity was attributed to the combined effects of tensile residual stresses near the welds and the tensile transverse stresses that developed due to the rapid expansion of concrete near the ultimate load. Chicoine et al. (2002b) also reported that the increase in concrete strength due to confinement effects is 1% of its uniaxial compressive strength and, therefore, can be neglected in design. The numerical model was also used to represent the stresses in the transverse links and transverse stresses in the web plate. A good representation of the link stresses was obtained which was found to be affected by the transverse expansion of concrete. At peak load, the numerical model generally underestimated the link stress due to the limitations of the concrete model used by Chicoine et al (2002b) in representing the concrete material behaviour. The numerical transverse stresses in the web were observed to be compressive at the beginning of the analysis and tensile at peak load due to the variation of the concrete Poisson's ratio. Similar observations were found in the experiments (Chicoine et al. 2000).

2.3.3 Prediction of PEC Column Capacity

2.3.3.1 Columns Under Concentric Axial Loading

The experimental and numerical investigations on PEC columns with built-up sections led to the development of a capacity prediction model for these columns. In this model the compressive cross-sectional strength of the PEC column is calculated using the following expression proposed by Tremblay et al. (2000a), with modifications from the work of Chicoine et al. (2002a; 2002b):

$$C_r = \left(A_{se}F_y + 0.92\psi A_c f_{cu} + A_r F_{yr}\right) \tag{2.4}$$

where A_{se} is the effective area of the steel shape as defined by Equation (2.5), F_y is the yield strength of the steel plate, A_c is the cross-sectional area of concrete, f_{cu} is the concrete cylinder strength and A_r and F_{yr} are the area and yield strength of the longitudinal rebars.

The effective steel area, A_{se}, in Equation (2.4) is determined as:

$$A_{se} = (d - 2t + 2b_e)t \tag{2.5}$$

where d is the overall depth of the cross-section, t is the thickness of the steel plates and b_e is the total effective width of the flange. To account for the effect of local buckling in the column capacity, b_e is expressed as a function of flange slenderness ratio (b/t) and the aspect ratio of the unsupported flange panel (s/b):

$$b_e = \frac{b_f}{\left(1 + \lambda_p^{2n}\right)^{1/n}} \leq b_f \tag{2.6}$$

$$\lambda_p = \frac{b}{t}\sqrt{\frac{12\left(1 - v_s^2\right)F_y}{\pi^2 E_s k}} \tag{2.7}$$

$$k = \frac{4}{(s/b)^2} + \frac{15}{\pi^4}(s/b)^2 + \frac{20}{3\pi^2}(2 - 3v_s) \qquad (2.8)$$

Equation (2.6) was adapted from the column design curve expression proposed by Loov (1996). In this equation, b_f is the full width of a flange plate and λ_p is a slenderness parameter calculated using Equation (2.7). E_s and v_s in Equation (2.7) are the elastic modulus and Poisson's ratio, respectively, of steel. The plate buckling coefficient, k, in Equation (2.7) was originally to be calculated using Equation (2.8), as proposed by Tremblay et al (2000) based on energy conservation methods, to represent the local buckling capacity of the flange panel between adjacent links. However, Chicoine et al (2001) reported that Equation (2.8) does not give capacities consistent with the experimental and numerical results and therefore proposed that it be modified to (and recast in terms of the full flange width, b_f for convenience):

$$k = \frac{0.9}{(s/b_f)^2} + 0.2(s/b_f)^2 + 0.75, \qquad (0.5 \le s/b_f \le 1) \qquad (2.9)$$

Equation (2.9) was derived empirically from a series of elastic buckling analyses of the unsupported steel flange panel of the column using the finite element method and it resulted in a better fit with the existing pool of PEC column data.

The value of the factor n in Equation (2.6) is taken as 1.5, as proposed by Chicoine et al (2002b). (Initially, a value of n = 1.0 was used by Tremblay et al. (2000a), which resulted in a good fit for the experimental data on small and large scale specimens under short term loading. Later, Chicoine et al (2002b) obtained an average value of test-to-predicted ratio of 1.00, with a standard deviation of 0.03, using n = 2.0 for the ultimate capacity of all columns including those under long term loading. However, in order to account for the likelihood that flange imperfections in actual columns would be closer to the fabrication tolerances permitted by CSA G40.21 (CSA 2004b) than those measured in the reference test columns, a value of n = 1.5 was recommended for design.) The use of n = 1.5 results

in a mean test-to-predicted load ratio of 1.03, with a standard deviation of 0.03, and provides a margin to account for the imperfect conditions in a real column.

Equations (2.4) to (2.7) and (2.9, but without the restrictions on s/b$_f$) are included in CSA S16-01 (CSA 2001) for determining the design capacity of axially loaded PEC columns with built-up thin-walled shapes, but with a slight modification in the concrete strength reduction factor. For simplicity, the strength reduction factor 0.92ψ in Equation (2.4) was replaced by 0.8 in CSA S16–01. However, these design equations are subjected to certain limitations on geometric and material parameters imposed by the scope of the experimental and numerical programs performed by Tremblay et al. (1998) and Chicoine et al (2002a, 2002b). The yield strength of the steel plate and reinforcing bars is limited to no greater than 350 MPa and 400 MPa, respectively, and concrete strengths only up to 40 MPa are allowed (normal density). The flange width, b$_f$, must be within 0.9 to 1.1 times the section depth, d, and have a slenderness ratio, b$_f$/2t, not greater than 32. The thickness of the web plate must be equal to the thickness of the flanges and the connections between them must be provided by continuous fillet welds designed to develop the shear yield capacity of the web. The spacing of the transverse links is limited to the lesser of 500 mm or 0.67d and the area of a link must be at least the greatest of 63 mm^2, 0.01b$_f$t and 0.5 mm^2 per mm of link spacing. The maximum amplitude of local flange imperfection should not exceed 0.5% of the link spacing. Finally, the equations are applicable only to concentrically loaded columns with a clear height-to-depth ratio less than 14.

As reported by Prickett and Driver (2006), the design equations for concentrically loaded columns provide conservative estimations of the axial capacity of PEC columns with high strength concrete. Therefore, it was recommended that the current upper limit for the strength of concrete be increased from 40 to 70 MPa. Although Prickett and Driver (2006) obtained good estimates of the axial capacity of these columns using the methods of CSA S16–01 along with the full steel area (consistent with the observed occurrence of local buckling after the peak load), they proposed that the use of a reduced steel area, as given in the design standard (Equation 2.5), be retained until additional tests are

completed on high strength concrete PEC columns with a $b_f/2t$ ratio greater than 25, which was used in their test specimens. They also suggested using a concrete strength reduction factor of 0.9 for high strength concrete, instead of the factor 0.8 used in CSA S16–01 (CSA 2001) for normal strength concrete, since the coefficient 0.8 resulted in overly conservative predictions of the column capacity of the test specimens constructed with high strength concrete.

2.3.3.2 Columns Under Combined Axial and Flexural Loading

Bouchereau and Toupin (2002) and Prickett and Driver (2006) predicted the capacity of eccentrically loaded columns from load–moment interaction diagrams constructed using a procedure commonly adopted for reinforced concrete columns. However, Prickett and Driver (2006) used the reduced steel area in calculating the design capacity to account for the local buckling of the flanges, since local buckling was observed in a few eccentrically loaded columns shortly before the peak load. A linear strain distribution along the cross-section, based on observations from the strain measurements taken during the test, was implemented for the construction of this diagram. The extreme compressive strain was set at 3500 $\mu\varepsilon$ (considered to be the crushing strain of concrete), whereas the extreme tensile strain was varied from 0 to 10 times the yield strain of the steel. For each strain gradient the ultimate load and moment capacities were calculated from the material and geometric properties of the composite cross-section. The compressive force in the concrete, C_c, was calculated using the following expression, assuming a rectangular stress block:

$$C_c = \alpha_1 f_{cu} b_c \beta_1 c \tag{2.10}$$

where b_c is the net width of the concrete block (i.e., excluding the web thickness for strong axis bending and excluding the flanges for weak axis bending), c is the distance between the extreme compression fibre and the neutral axis and the factors α_1 and β_1 are expressed as (CSA 2004b),

$$\alpha_1 = 0.85 - 0.0015 f_{cu} \geq 0.67 \qquad\qquad (2.11)$$

$$\beta_1 = 0.97 - 0.0025 f_{cu} \geq 0.67 \qquad\qquad (2.12)$$

To calculate the contribution of the steel to the capacity of the composite column, the section was discretised in such a way as to have effectively uniform strain in each individual piece. For strong axis bending, the flanges were considered to be one piece, whereas the web was divided into ten pieces. On the other hand, for weak axis bending the web was considered as one piece and each flange was discretised into ten pieces (Prickett and Driver 2006). The resultant force for each individual piece was calculated by multiplying the area of the piece by its average strain and by the elastic modulus of steel. (However, if the strain in the individual piece exceeded the yield strain the force resultant is determined by multiplying the area of that piece by the yield stress.) In calculating the area of a flange piece in compression, the effective width (using Equation (2.6) with n = 1.5) was used by Prickett and Driver (2006). Finally, the total load capacity of the composite column was determined by adding the force resultants for concrete and steel and the moment capacity were obtained from the summation of each force multiplied by its distance from the centreline of the column cross-section.

2.4 Conclusions

The research on PEC columns with thin-walled sections reviewed in this chapter reveals that the behaviour of this composite system with normal and high performance materials have become relatively well understood from the full scale experimental investigations for monotonic concentric and eccentric axial loading conditions. However, it is not possible to obtain a complete understanding of the influences of various components from experimental investigations only due to the high cost and time requirement for full scale testing. The finite element model developed thus far for this new composite system, modelling only a small segment of the column, can adequately represent the local buckling behaviour and ultimate loads for axially loaded short columns, although post-peak behaviour could not be reproduced. The effect of initial imperfections on the capacity of these columns has not been studied as the existing model failed to predict the

actual failure mode with inward local imperfections of the thin flange plates. No finite element study has yet been performed to explore the behaviour of these columns under the combined action of axial and flexural loads. In this regard, a finite element model including the complete cross-section needs to be formulated that can accurately represent the peak and post-peak behaviour of these columns, as well as simulating the proper failure modes, even with inwards initial imperfections, under various loading conditions. Moreover, the influences of several key parameters, which could not be covered by the experimental programs, on the behaviour of these columns under axial compression and bending, need to be investigated using the finite element model.

3. CONCRETE MATERIAL MODEL

3.1 Introduction

In partially encased composite (PEC) columns the concrete blocks are surrounded by the steel plates on three sides and partially supported by the transverse links on one side. This system is expected to provide low levels of passive confinement to the concrete. Previous research work on numerical modelling of PEC columns (Chicoine et al. 2001), although able to simulate the pre-peak behaviour relatively well, was unsuccessful in representing the triaxial behaviour of concrete in these columns near and beyond the ultimate load. An attempt has been made in the current study to eliminate this limitation of the finite element model by using the damage plasticity model that is implemented within ABAQUS to represent the concrete material behaviour in this composite system. A brief description of the damage plasticity model and its ability to predict the uniaxial, biaxial and triaxial behaviour of concrete under various levels of lateral confinement is included in this chapter. Also presented are the uniaxial compressive and tensile stress–strain relationships of plain and steel fibre reinforced concrete used in the PEC test specimens. Complete stress–strain curves for concrete under uniaxial compression and tension are necessary to predict the structural response of the composite column from the nonlinear finite element analysis using the damage plasticity model for concrete.

3.2 Stress–Strain Relationship of Concrete in Compression

3.2.1 Plain Concrete

There have been many attempts (Desayi and Krishnan 1964; Popovics 1973; Wang et al. 1978; Carreira and Chu 1985; Tsai 1988; CEB 1990; Hsu and Hsu 1994a; Almusallam and Alsayed 1995; Gysel and Taerwe 1996; Wee et al. 1996; Barr and Lee 2003) to develop analytical formulations to represent the stress–strain relationships for normal and high strength concrete in uniaxial compression. A review of these models is performed to select a simple formulation that can adequately represent the strain-softening behaviour

of normal and high strength concrete in uniaxial compression. Some of these models are complex (CEB 1990; Almusallam and Alsayed 1995) or require cumbersome computations (e.g., Wang et al. 1978) to evaluate the key parameters used in the formulation. A number of models use two separate expressions (e.g., CEB 1990; Hsu and Hsu 1994a; Gysel and Taerwe 1996) to represent the complete stress–strain curve, which adds to the complexity of the model. Some models require fitting parameters (e.g., Hsu and Hsu 1994a; Almusallam and Alsayed 1995; Gysel and Taerwe 1996) derived via curve fitting methods, which make them dependent upon testing conditions such as the rate and duration of loading, type of testing machine, size and shape of specimen, size and location of strain gages, number of load repetitions, boundary conditions, etc. (Popovics 1970; Gysel and Taerwe 1996; Wee et al. 1996). Since the strain softening behaviour of plain concrete is greatly affected by these factors, the analytical models developed primarily on the basis of curve fitting sometimes give conflicting results for the descending branch of the curve, particularly for high strength concrete.

Most common stress–strain models (Hognestad 1951; Desayi and Krishnan 1964; Popovics 1973; Carreira and Chu 1985; Tsai 1988; CEB 1990; Gysel and Taerwe 1996; Barr and Lee 2003) cannot adequately represent the strain softening behaviour and the post–peak residual strength for high strength concrete, with the exception of the model proposed by Wee et al. (1996). However, the Barr and Lee (2003) formulation can adequately predict the strain softening behaviour of normal strength concrete with an ability to control the steepness of the descending branch (i.e., level of brittleness) with a single parameter. In the numerical model for PEC columns the stress–strain relationships for normal strength and high strength concrete are generated using the formulations proposed by Barr and Lee (2003) and Wee et al. (1996), respectively, because of their simplicity, computational efficiency and adequacy in representing the strain softening behaviour of concrete in uniaxial compression. At the initial stage of the study, while verifying the suitability of the damage plasticity model itself in predicting the concrete material behaviour, the model of Tsai (1988) was implemented primarily because of its simplicity. The stress–strain curves generated by all three of the models used in this research are based on the values of uniaxial compressive strength, f_{cu}, strain at ultimate

strength, ε_{cu}, and modulus of elasticity of concrete, E_c. Stress–strain curves for normal and high strength concrete used in the numerical analyses of PEC columns included in the parametric study (presented in Chapter 6) are shown in Figure 3.1. A brief description of the formulations used in this study are presented in the following sections.

3.2.1.1 *Formulation Proposed by Tsai (1988)*

Tsai (1988) proposed the following stress–strain relationship for concrete under uniaxial compression:

$$f_c(\varepsilon) = \left[\frac{m\left(\dfrac{\varepsilon}{\varepsilon_{cu}}\right)}{1 + \left(m - \dfrac{n}{n-1}\right)\dfrac{\varepsilon}{\varepsilon_{cu}} + \dfrac{\varepsilon^n}{n-1}} \right] f_{cu} \qquad (3.1)$$

where m is the ratio of the initial tangent modulus to the scant modulus at f_{cu} and n is a factor to control the steepness of the descending portion of the stress–strain curve. The slope of the ascending portion is controlled by the parameter m. The values of m and n can be calculated using the following expressions (Tsai 1988):

$$m = 1 + \frac{17.9}{f_{cu}} \qquad (f_{cu} \text{ in MPa}) \qquad (3.2)$$

$$n = \frac{f_{cu}}{6.68} - 1.85 > 1 \qquad (f_{cu} \text{ in MPa}) \qquad (3.3)$$

The proposed stress–strain formulation was verified against the test results of Wang et al. (1978) and was observed to fit the test results well for normal strength concrete. However, for high strength concrete this model underestimates the residual strength in the post-peak region of the stress–strain curve.

3.2.1.2 Formulation Proposed by Barr and Lee (2003)

Barr and Lee (2003) developed a simple descriptive formulation for the constitutive behaviour of plain concrete using a single continuous function. The formulation is called a "double exponential model" since it results from the superposition of two exponential functions as follows:

$$f_c(\varepsilon) = c_1(e^{-c_2\varepsilon} - e^{-c_3\varepsilon}) \tag{3.4}$$

where c_1, c_2 and c_3 are constants controlling the shape of the stress–strain curve. The first exponential term in this expression controls the descending branch of the stress–strain curve, whereas the initial part of the curve is influenced by the second exponential expression. The relative values of the two components determine the overall shape of the curve.

Barr and Lee (2003) observed that by varying the three model parameters—c_1, c_2 and c_3—a wide range of stress–strain curves can be developed. It was also reported that the model parameter c_1 accounts for the nominal strength of plain concrete, whereas the parameters c_2 and c_3 influence the post-peak region and the initial part, respectively, of the stress–strain curve. A parametric analysis was carried out by Barr and Lee (2003) to investigate the sensitivity of the model to these parameters, which led to the following relationships between the parameters and the values of stress and strain at the ultimate stress, f_{cu} and ε_{cu}:

$$\varepsilon_{cu} = \frac{1}{c_3 - c_2} \ln\left(\frac{c_3}{c_2}\right) \tag{3.5}$$

$$c_1 = \frac{f_{cu}}{\left(\alpha^{\frac{1}{1-\alpha}} - \alpha^{\frac{\alpha}{1-\alpha}}\right)} \tag{3.6}$$

$$c_2 = \frac{\ln\alpha}{\varepsilon_{cu}(\alpha - 1)} \tag{3.7}$$

33

Here, $\alpha = c_3/c_2$ and can be calculated using the following equations:

$$\alpha = \begin{cases} 10^4 & for & \left(\dfrac{\varepsilon_{cu}}{\varepsilon_{0.2f_{cu}}}\right) \leq 0.000572 \\[2em] 1.67\left(\dfrac{\varepsilon_{cu}}{\varepsilon_{0.2f_{cu}}}\right)^{-1.17} & for & 0.000572 \leq \left(\dfrac{\varepsilon_{cu}}{\varepsilon_{0.2f_{cu}}}\right) \leq 0.026 \\[2em] \sum\limits_{i=0}^{6} \chi_i \left(\dfrac{\varepsilon_{cu}}{\varepsilon_{0.2f_{cu}}}\right)^i & for & 0.026 \leq \left(\dfrac{\varepsilon_{cu}}{\varepsilon_{0.2f_{cu}}}\right) \leq 0.262 \\[2em] 1.0001 & for & \left(\dfrac{\varepsilon_{cu}}{\varepsilon_{0.2f_{cu}}}\right) \geq 0.262 \end{cases} \qquad (3.8)$$

where, $\varepsilon_{0.2f_{cu}}$ is the strain corresponding to a stress of 20% of uniaxial compressive strength, f_{cu}, in the post–peak regime of the stress–strain curve. Barr and Lee (2003) showed that for a given uniaxial compressive strength, f_{cu}, and corresponding strain, ε_{cu}, the ratio α ($=c_3/c_2$) can be varied in the model to represent a range of responses varying from a brittle to an elastic–plastic material behaviour. (An elastic–plastic response is obtained as $\alpha \to \infty$ and the model exhibits a very steep post–peak softening as $\alpha \to 1$.) Therefore, the level of brittleness, i.e., the slope of the post–peak descending branch of the stress–strain curve, of plain concrete can be controlled by this single parameter.

To calculate the parameter α using Equation (3.8), the strain value at 20% of the ultimate strength after failure, $\varepsilon_{0.2f_{cu}}$, is required, which cannot easily be obtained from a uniaxial compressive test on concrete cylinders. Therefore, for simplicity, this study assumes a value of α rather than assuming the value of $\varepsilon_{0.2f_{cu}}$. Several numerical analyses were performed on ten PEC test specimens (Tremblay et al 1998 and Chicoine et al 2002a) to determine a suitable value of this parameter that provides the best

representation of the experimental post-peak response of the test columns. The value used in this study is 10, which is applied for all PEC test specimens constructed with normal strength concrete.

Barr and Lee (2003) verified the model against experimentally obtained load–deformation responses for normal strength and high strength concrete. Satisfactory results were obtained from this model in predicting the behaviour of normal strength concrete. However, it was less successful in modelling the brittle response of high strength concrete. Therefore, the double exponential model is more appropriate for materials that do not exhibit significantly brittle behaviour and was therefore used only for normal strength concrete in the current research.

3.2.1.3   *Formulation Proposed by Wee et al. (1996)*

Wee et al. (1996) proposed a simple model to generate the complete stress–strain relationships particularly for high strength concrete (ranging from 50 to 120 MPa). They used the equation proposed by Carreira and Chu (1985) with two correction factors to better represent the post-peak descending branch for high strength concrete. The ascending branch of the stress versus strain response is represented by the following equation (Carreira and Chu 1985):

$$f_c = f_{cu} \left[\frac{\beta \left(\dfrac{\varepsilon}{\varepsilon_{cu}} \right)}{\beta - 1 + \left(\dfrac{\varepsilon}{\varepsilon_{cu}} \right)^{\beta}} \right] \tag{3.9}$$

where β is a material parameter that depends on the shape of the stress–strain diagram. It is given by:

$$\beta = \cfrac{1}{1 - \left(\cfrac{f_{cu}}{\varepsilon_{cu} E_{it}} \right)} \tag{3.10}$$

Here, E_{it} is the initial tangent modulus of concrete. Several researchers (Wee et al. 1996; CEB 1990; Carriera and Chu 1985) proposed relationships between E_{it} and f_{cu} based on experimental investigations of uniaxial compressive behaviour of concrete. The initial tangent modulus, E_{it}, is not normally available from standard tests. Therefore, a simplified expression for β as a function of f_{cu} only, proposed by Popovics (1973), is used:

$$\beta = 0.058 f_{cu} + 1.0 \qquad (f_{cu} \text{ in MPa}) \tag{3.11}$$

The residual strength of high strength concrete at high strains becomes nearly zero if the same β (calculated from Equation (3.11)) is used for the descending branch of the stress–strain curve. Therefore, a value of $\beta = 3$, which was also used by Tulin and Gerstle (1964), is assumed to define the descending branch of the stress–strain curve for high strength concrete in the current research.

Wee et al. (1996) reported that Equations (3.9) to (3.11) give good prediction of the ascending portion of the stress–strain curves for normal and high strength concretes. However, for high strength concrete the descending branch and the post-peak residual strength at high strains are not adequately represented by the Carreira and Chu model. Therefore, two modification factors, k_1 and k_2, were introduced into Equation (3.9) by Wee et al. (1996) for modelling the descending branch of the stress–strain response. The expression for the descending branch becomes:

$$f_c = f_{cu} \left[\cfrac{k_1 \beta \left(\cfrac{\varepsilon}{\varepsilon_{cu}} \right)}{k_1 \beta - 1 + \left(\cfrac{\varepsilon}{\varepsilon_{cu}} \right)^{k_2 \beta}} \right] \tag{3.12}$$

The factors k_1 and k_2 were determined empirically by Wee et al (1996) based on their experimental investigations of high strength concrete behaviour (with f_{cu} ranging from 50 to 120 MPa):

$$k_1 = \left(\frac{50}{f_{cu}} \right)^{3.0}$$

$$k_2 = \left(\frac{50}{f_{cu}} \right)^{1.3}$$

$$(3.13)$$

Therefore, for a given concrete strength, f_{cu}, and corresponding strain, ε_{cu}, the complete stress–strain curve for high strength concrete can be generated by Equations (3.9) to (3.13).

3.2.2 Steel Fibre Reinforced High Strength Concrete

The stress–strain models developed to predict the compressive behaviour of plain concrete are, in general, not suitable for steel fibre reinforced concrete because the addition of steel fibres improves the post-cracking behaviour of plain concrete leading to increased ductility and toughness of the material. Based on uniaxial compression tests on steel fibre reinforced high strength concrete, Fanella and Naaman (1985), Taerwe (1992), Hsu and Hsu (1994b), Mansur et al (1999) and Neves and Almeida (2005) reported a less steep descending branch in the stress–strain curve of steel fibre reinforced high strength concrete than plain concrete. These researchers also proposed formulations to generate the complete stress–strain response curve of steel fibre reinforced concrete. Among these models, the one proposed by Neves and Almeida (2005) is implemented in the current study to generate the stress–strain curve (as shown in Figure 3.1) of steel fibre reinforced high strength concrete.

Neves and Almeida (2005) used the following expression, which was originally proposed by Vipulanandan and Paul (1990) for polymer concrete behaviour, to represent the stress–strain curve of fibre reinforced high strength concrete:

$$f_c = f_{cu} \left[\frac{\dfrac{\varepsilon}{\varepsilon_{cu}}}{(1-p-q) + q\left(\dfrac{\varepsilon}{\varepsilon_{cu}}\right) + p\left(\dfrac{\varepsilon}{\varepsilon_{cu}}\right)^{1-q/p}} \right] \quad (3.14)$$

in which the parameters p and q are related to material deformability and can be determined from the following equations (Neves and Almeida 2005):

$$p = 1 - 0.85 \times f_{cu}^{\left[-0.0013 \times \left(V_f l_f / d_f\right)^2\right]} \quad (3.15)$$

$$p + q = 1 - \frac{f_{cu}}{E_c \varepsilon_{cu}} \quad (3.16)$$

Here, V_f is the volumetric ratio of steel fibres in percentage, and l_f and d_f are the fibre length and diameter, respectively, in mm. The proposed model is suitable for predicting the compressive behaviour of plain and steel fibre reinforced concrete with strengths and fibre volumes up to 60 MPa and 1.5%, respectively. The stress–strain curve for steel fibre reinforced concrete shown in Figure 3.1 has a strength of 60 MPa with 1% steel fibres by volume.

3.3 Stress–Displacement Relationship of Plain and Steel Fibre Reinforced Concrete in Tension

For nonlinear finite element analysis, the stress–displacement relationship for concrete members in the cracked state under uniaxial tension is required. In an uncracked state, the stress–strain relationship under uniaxial tension can be expressed with a linear function (Hillerborg et al. 1976; Foote et al. 1986). After cracking, the stress versus crack width response is more appropriate for representing the material behaviour under uniaxial tension, since no unique stress-strain relationship exists in the post-peak softening region (Gopalaratnam and Shah 1985).

Numerous expressions are available in the literature (e.g. Hillerborg et al. 1976; Gopalaratnam and Shah 1985; Foote et al. 1986; Zhen-hai and Xiu-qin 1987; Liaw et al. 1990; Du et al. 1992; Marzouk and Chen 1995; Li and Ansari 2000; Li et al 2002) to represent the stress versus crack width relationship of concrete in uniaxial tension. These expressions vary from simple linear functions (Hillerborg et al. 1976) to sophisticated trilinear models (Liaw et al. 1990). However, most researchers (Gopalaratnam and Shah 1985; Foote et al. 1986; Du et al. 1992; Li and Ansari 2000; Li et al. 2002) used exponential functions to represent the post-cracking behaviour of concrete.

The current study uses the model proposed by Li et al. (2002), Equation (3.17), for normal strength concrete and that proposed by Li and Ansari (2000), Equation (3.18), for high strength concrete. In each model the post-peak response is represented as an exponential function of the ratio of crack width, w, to final crack width, w_f:

$$f_t = f_{tu}\left\{1 - \exp\left[\frac{0.05}{\dfrac{w}{w_f}}\right]^{1.3}\right\} \quad \text{(Li et al. 2002)} \quad (3.17)$$

$$f_t = f_{tu}\left\{1 - \exp\left[\frac{0.03}{\dfrac{w}{w_f}}\right]^{0.9}\right\} \quad \text{(Li and Ansari 2000)} \quad (3.18)$$

These two expressions were developed through regression analyses to best fit the results of uniaxial tension tests performed on normal and high strength concrete test specimens, respectively. While modelling the PEC columns in the current research, the values of final crack width are chosen in such a way that consistent fracture energy values for concrete as reported in the literature (Gopalaratnam and Shah 1985; Zhen-hai and Xiu-qin 1987; Marzouk and Chen 1995; Li and Ansari 2000; Li et al. 2002) are obtained. The resulting tensile relationships are shown in Figure 3.2.

Addition of steel fibres to plain concrete can significantly improve its tensile behaviour, as observed by several researchers (Song and Hwang 2004; Lee and Barr 2004; Kützing and König 1999). Fibres act to inhibit crack growth, thus increasing the required energy for crack propagation. In the current study, two out of 34 test columns modelled numerically were constructed with steel fibre reinforced high strength concrete. To represent the tensile stress versus crack width response for this concrete a simple trilinear curve is assumed, as shown in Figure 3.2. The points on the curve are defined based on the results of uniaxial tension tests performed on concrete with a design strength of 60 MPa and with 80 kg/m^3 of steel fibres in the mix (Kützing and König 1999), parameters that are nominally identical to those of the fibre reinforced high strength concrete of the PEC columns modelled. For other concrete mixes with steel fibres, more sophisticated expressions (Lee and Barr 2004) are available.

3.4 Concrete Damage Plasticity Model

3.4.1 Description of the Model

The damage plasticity model in ABAQUS/Explicit (HKS 2003) provides a general capability for modelling concrete and other quasi-brittle materials in all types of structures. The model is a continuum, plasticity-based damage model (Lubliner et al. 1989) that can predict both compressive and tensile behaviour of concrete under low confining pressures, i.e., less than four or five times the uniaxial compressive strength of concrete (HKS 2003). The model is capable of taking into consideration the degradation of elastic stiffness (or "damage") induced by reversible cycles as well as high temperatures both in tension and compression. The concrete damage plasticity model uses a non-associated plastic flow rule in combination with isotropic damage elasticity. The Drucker–Prager hyperbolic function is used to define the plastic flow potential. The dilation angle defines the plastic strain direction with respect to the deviatoric stress axis in the meridian plane. The volumetric expansion of concrete can be controlled by varying the dilation angle. In this study, a value of 15 degrees is used for the dilation angle, as recommended by Lubliner et al. (1989) for low-confined concrete material modelling.

The model uses the yield function of Lubliner et al. (1989), with modifications proposed by Lee and Fenves (1998) to account for a different evolution of strength under tension and compression using multiple hardening variables. The two hardening variables used to trace the evolution of the yield surface are the effective plastic strains in compression and in tension, $\varepsilon_c^{\sim pl}$ and $\varepsilon_t^{\sim pl}$, respectively. The start of compressive yield in a numerical analysis using this model occurs when $\varepsilon_c^{\sim pl} > 0$, whereas when $\varepsilon_t^{\sim pl} > 0$ and the principal plastic strain is positive, it indicates the onset of tensile cracking.

The uniaxial compressive and tensile responses (Figures 3.3(a) and 3.3(b), respectively) of concrete used in this model are somewhat simplified to capture the main features of the response. Under uniaxial compression, the stress–strain response (as shown in Figure 3.3(a)) is assumed to be linear up to the initial yield stress, which is assumed to be $0.30 f_{cu}$ in the current study. The plastic region is characterized by stress hardening, followed by strain softening after reaching the ultimate strength, f_{cu}. The uniaxial compression hardening curve is defined in terms of the inelastic strain, $\varepsilon_c^{\sim in}$, which is calculated using Equation (3.19). The damage plasticity model automatically calculates the compressive plastic strains, $\varepsilon_c^{\sim pl}$, Equation (3.20), using a damage parameter, d_c, that represents the degradation of the elastic stiffness of the material in compression.

$$\varepsilon_c^{\sim in} = \varepsilon_c - \frac{f_c}{E_c} \tag{3.19}$$

$$\varepsilon_c^{\sim pl} = \varepsilon_c^{\sim in} - \frac{d_c}{\left(1 - d_c\right)} \frac{f_c}{E_c} \tag{3.20}$$

Since, the current study includes only monotonic loading conditions, no stiffness degradation or recovery is considered. Hence, the plastic strain expression becomes:

$$\varepsilon_c^{\sim pl} = \varepsilon_c^{\sim in} \tag{3.21}$$

Figure 3.3(b) shows the uniaxial tensile behaviour of concrete used in the damage plasticity model. The stress–strain curve in tension is assumed to be linearly elastic until the failure stress, f_{tu}, is reached. After this point strain softening represents the response of the cracked concrete that is expressed by a stress versus cracking displacement curve (as described in section 3.3). The values of the plastic displacements calculated by the damage model are equal to the cracking displacements since the tensile damage parameter, d_t, is zero for current study.

3.4.2 Performance of the Model in Predicting Compressive Behaviour of Concrete

Before implementing the damage plasticity model to represent the concrete material behaviour in the numerical model of PEC columns, a study was conducted to observe the performance of this model under three distinct conditions of loading: uniaxial, biaxial and triaxial compression. For uniaxial and biaxial compression the test results of Kupfer et al (1969) are reproduced using the damage model. The triaxial compression tests performed by Sfer et al (2002) under different levels of confining pressures (ranging from 0% to 30% of the uniaxial compressive strength) are simulated to observe the performance of this model in predicting the triaxial behaviour of concrete. In the numerical simulations of these tests, the uniaxial concrete compression hardening curves are calculated from the given uniaxial compressive strength of concrete using the material model developed by Tsai (1988) and described in Section *3.2.1.1*. The tension softening behaviour is defined in terms of the tensile stress as a function of the cracking displacement (Li et al. 2002).

3.4.2.1 *Uniaxial and Biaxial Compression*

Kupfer et al. (1969) tested square concrete plates of 200 mm × 200 mm × 50 mm under uniaxial and biaxial stresses, as shown in Figure 3.4. The uniaxial compressive strength of the concrete was 32.8 MPa at a strain of 2200 με, with an elastic modulus of 27 000 MPa. For biaxial compression, the ratios of the transverse to the longitudinal stresses, f_{22}/f_{11}, used were 0.52 and 1.00 and they were kept constant throughout the test.

The load was applied through brush-like bearing platens, instead of solid bearing platens of conventional testing machines, to minimize the effects of end restraint (tangent to the platen surfaces) on the stress–strain behaviour of the concrete. In the numerical simulations of these tests, the square concrete plate is modelled with eight-node C3D8R solid elements using a 4×4 mesh with one element through the thickness. In simulating the boundary conditions of the test specimens, free movement is permitted parallel to the loading surfaces. The load is applied through displacement control in two directions (directions 1 and 2, as shown in Figure 3.4) at f_{22}/f_{11} ratios of 0.0 (uniaxial loading in direction 1), 0.52 and 1.00.

The normalised longitudinal stress versus longitudinal (direction 1) and transverse (directions 2 and 3) mean strain curves from the numerical analyses are compared with the corresponding experimental curves in Figure 3.5. For uniaxial compression (Figure 3.5(a)), the normalized stress versus longitudinal and transverse strain curves obtained numerically coincide well with the corresponding experimental curves. Figures 3.5(b) and (c) represent the numerical and experimental responses for biaxial compression with f_{22}/f_{11} ratios of 0.52 and 1.00, respectively. In general, good agreement is obtained between the numerical and experimental curves, except in the longitudinal strain, ε_l, values near the ultimate point. The numerical strains at the ultimate longitudinal stress are 2130 $\mu\varepsilon$ and 1980 $\mu\varepsilon$ for $f_{22}/f_{11} = 0.52$ and 1.00, respectively, which underestimate the corresponding experimental strains by 29 % and 17 %, respectively. However, the numerical curves show accurate predictions of the experimental ultimate strength in both cases of biaxial compression. For $f_{22}/f_{11} = 0.52$, the uniaxial compressive strength of concrete is increased by 27%, which was obtained both experimentally (Kupfer et al 1969) and numerically. This increase in strength is approximately 16% for equal compressive stresses in the two loaded directions (i.e., $f_{22}/f_{11} = 1.0$).

3.4.2.2 Triaxial Compression

Sfer et al. (2002) studied the confined compression behaviour of concrete using standard $150\,\text{mm} \times 300\,\text{mm}$ cylindrical specimens subjected to hydrostatic pressure and axial load. Several levels of confining pressure were used in order to study the brittle–ductile transition of the response: 0.0, 1.5, 4.5, 9.0, 30.0 and 60.0 MPa. These pressures correspond approximately to lateral pressures, σ_L, of 0.0, $0.05f_{cu}$, $0.15f_{cu}$, $0.30f_{cu}$, $1.0f_{cu}$ and $2.0f_{cu}$, respectively, where f_{cu} is the ultimate strength of the concrete when loaded uniaxially. In these tests the prescribed hydrostatic pressure was applied first in a triaxial cell and then the axial load was increased monotonically. The damage plasticity model in ABAQUS/Explicit was used to simulate the concrete behaviour in these tests by modelling the cylindrical specimen using four-node axisymmetric solid elements. The test specimen and the 2D finite element mesh from which the axisymmetric elements are generated are shown in Figure 3.6.

In the actual specimens, the axial load was applied through steel loading platens placed at the flat ends. The boundary conditions were not well defined by Sfer et al. (2002), so for simplicity fixed boundary conditions were assumed at the end surfaces of the test cylinder. The load was applied in two steps: first the confining pressure was applied in the radial direction of the cylinder and in the second step the axial compression was applied through displacement control. Since it was reported (Chicoine et al. 2000; Prickett and Driver 2006) that the levels of concrete confinement in PEC columns are generally negligible, numerical simulations of the triaxial cylinder tests were performed for only four confining pressure levels ranging from 0 to $0.30f_{cu}$.

Figure 3.7 presents the numerical and corresponding experimental axial stress–strain responses for the specimens modelled. The numerically generated stresses are taken from the middle zone of the cylinder and for the tests themselves they are simply the axial load divided by the original cross-sectional area. The strains are taken from the middle zone in both cases, although in the tests after the peak they are derived from the overall shortening of the cylinder with a correction factor introduced to account for the different behaviour in the end regions, which introduces some uncertainty. For $\sigma_L = 0$ (i.e., the

uniaxial loading condition) and $0.05f_{cu}$, the numerical curves by and large coincide with the corresponding experimental curves. However, the numerical peak axial stress for $\sigma_L = 0.5f_{cu}$ is slightly lower than the experimental peak stress, with an experimental-to-numerical ratio of 1.08.

The numerical model accurately predicts the increase in axial compressive strength for $\sigma_L = 0.15f_{cu}$, as shown in Figure 3.7 (c). For this level of confining pressure the axial strains near the peak stress are observed to be underestimated by the model, with an experimental-to-numerical axial strain at the peak stress of 1.17. However, for $0.30f_{cu}$ the numerical stress–strain curve does not match well with the experimental one, as shown in Figure 3.7(d). The ratios of the experimental-to-numerical peak stress and corresponding strain are 0.83 and 1.73, respectively.

3.5   Summary

Stress–strain response models for concrete under uniaxial compression and tension that have been proposed by several researchers have been assessed critically, and the models that are both simple and able to predict the strain softening behaviour of concrete accurately have been implemented in the numerical model used for the analysis of PEC columns. The damage plasticity model in ABAQUS, which has been selected to represent the nonlinear material behaviour of concrete in PEC columns, is observed to predict the uniaxial, biaxial and triaxial response of concrete under low levels of lateral confinement with satisfactory performance. However, as the confining pressure increases, the accuracy of the model in predicting the axial strain near the ultimate point declines. In the triaxial state with hydrostatic pressure of $0.30f_{cu}$, the differences between the experimental and numerical results are significant. This level of passive confining pressure is, however, unlikely to develop within PEC columns, as observed by Chicoine et al. (2000) and Prickett and Driver (2006).
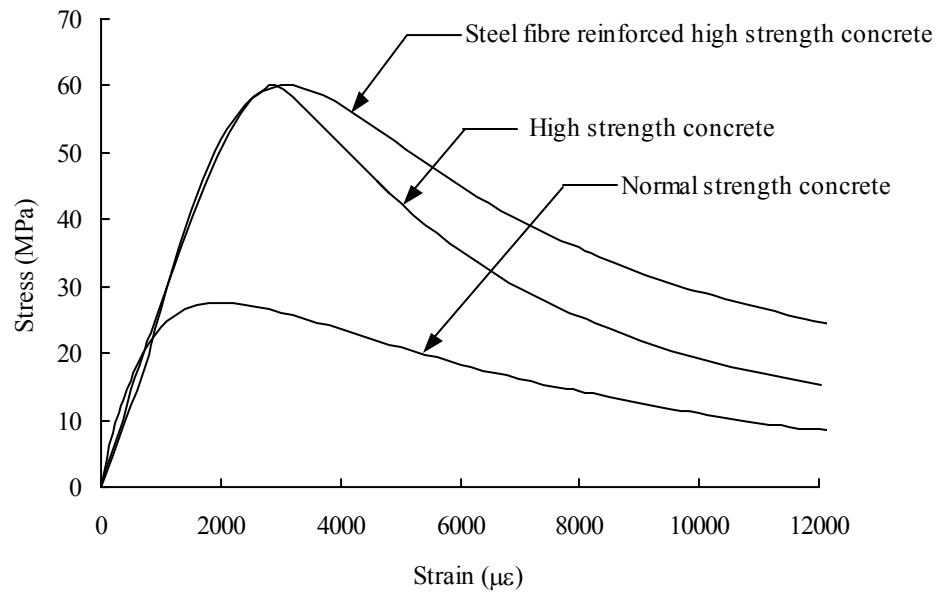
Figure 3.1 Stress–Strain Curves for Concrete in Uniaxial Compression
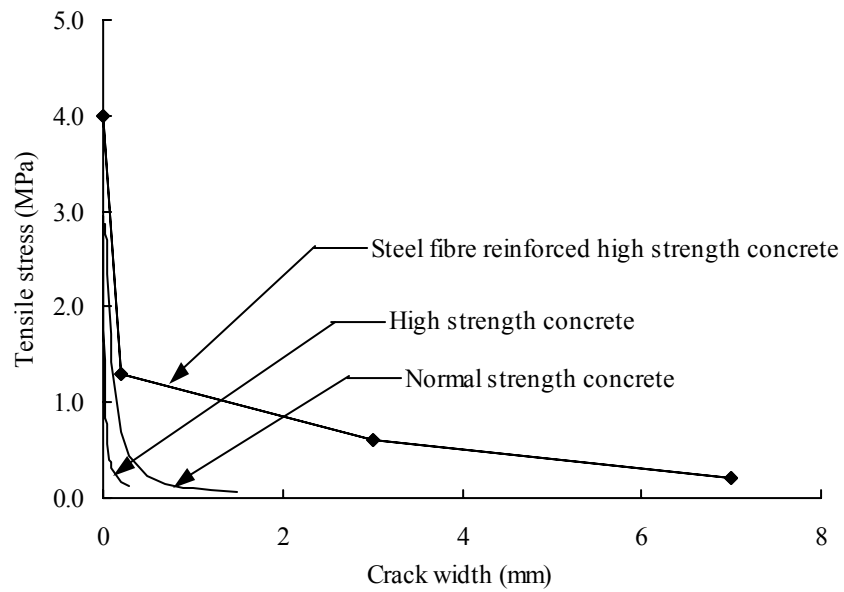
Figure 3.2 Stress–Crack Width Curves for Concrete in Uniaxial Tension

46
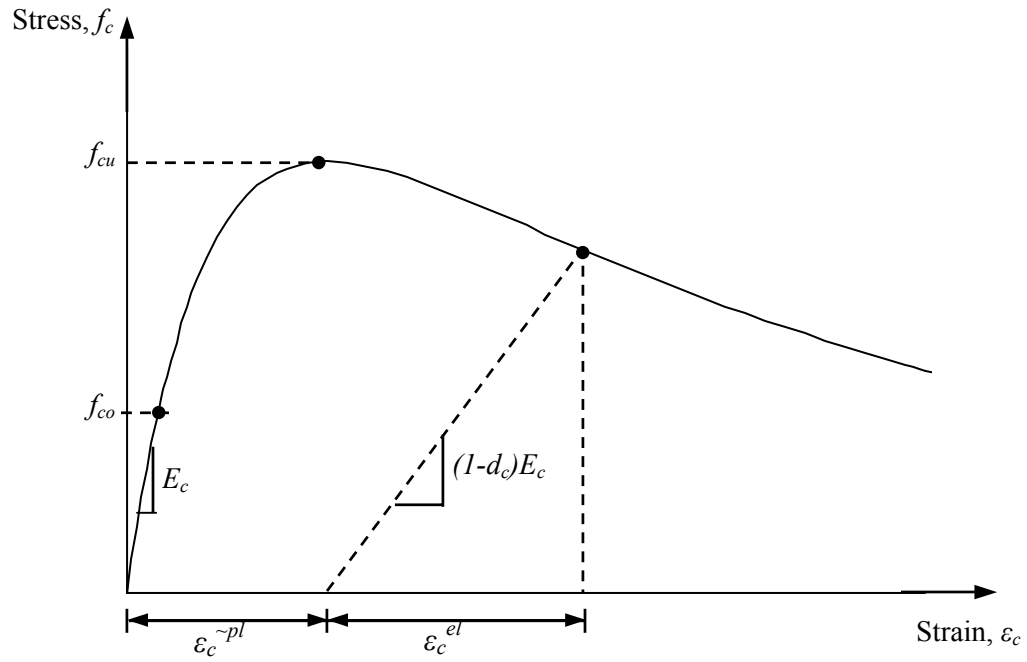
(a) Uniaxial Compression
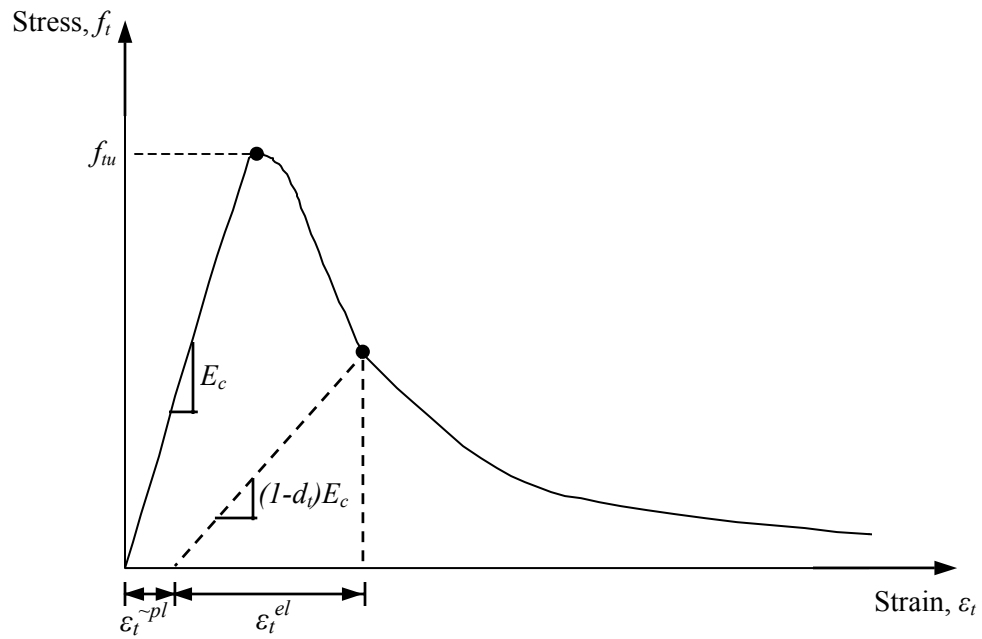
(b) Uniaxial Tension

Figure 3.3 Uniaxial Compressive and Tensile Behaviour of Concrete Used by Damage Plasticity Model in ABAQUS (after HKS 2003)
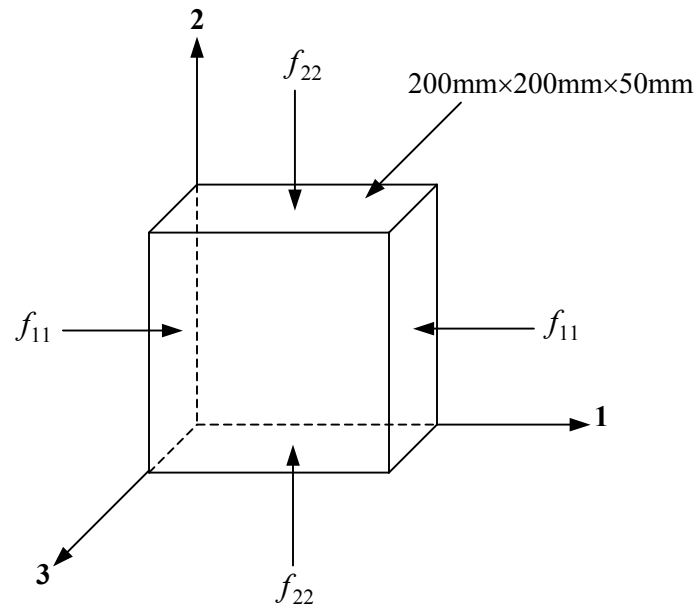
Figure 3.4 Square Concrete Plate Tested by Kupfer et al. (1969) in Uniaxial and Biaxial Compression
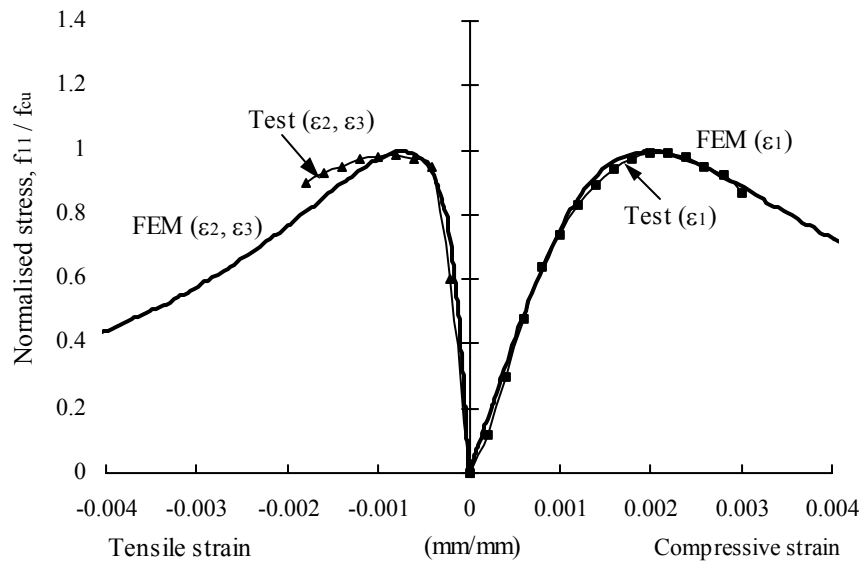
(a) Uniaxial Compression
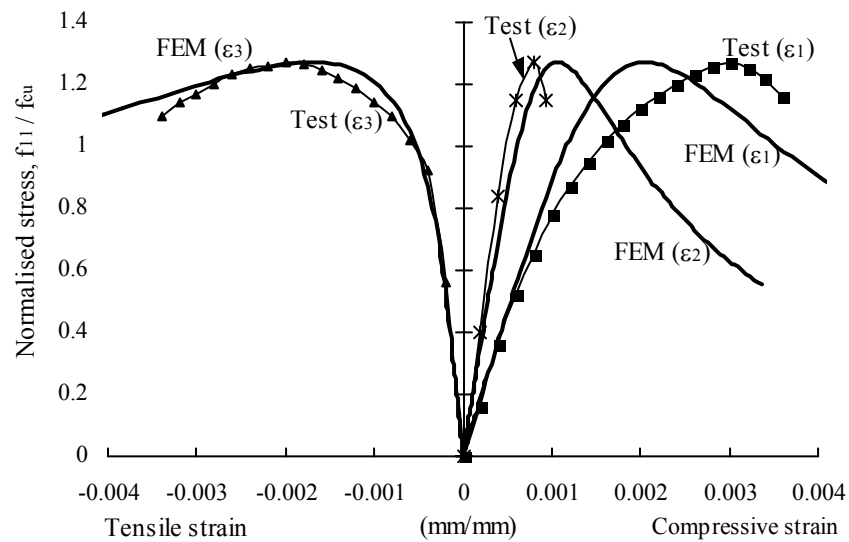
(b) Biaxial Compression ($f_{11} = 0.52f_{22}$)

Figure 3.5 Performance of Concrete Damage Plasticity Model in Uniaxial and Biaxial Compression (test data from Kupfer et al. 1969)
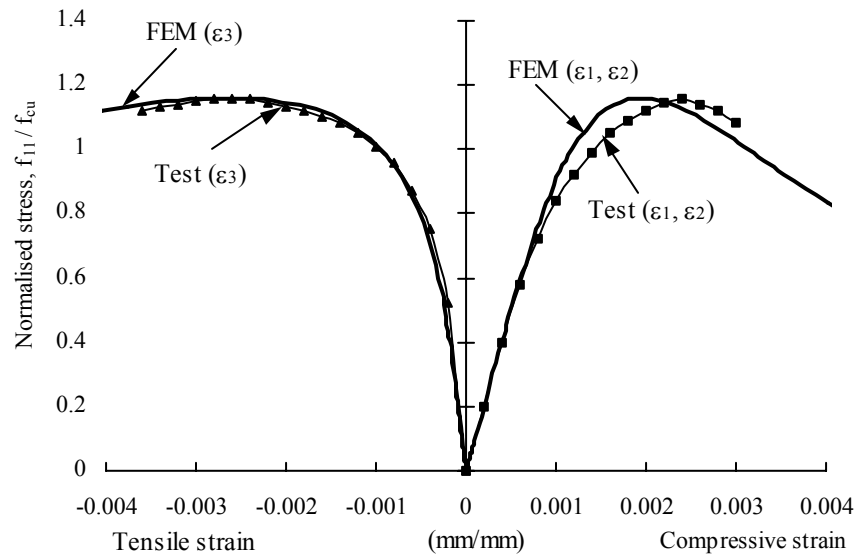
(c) Biaxial Compression ($f_{11} = 1.0f_{22}$)

Figure 3.5 (cont.) Performance of Concrete Damage Plasticity Model in Uniaxial and Biaxial Compression (test data from Kupfer et al. 1969)
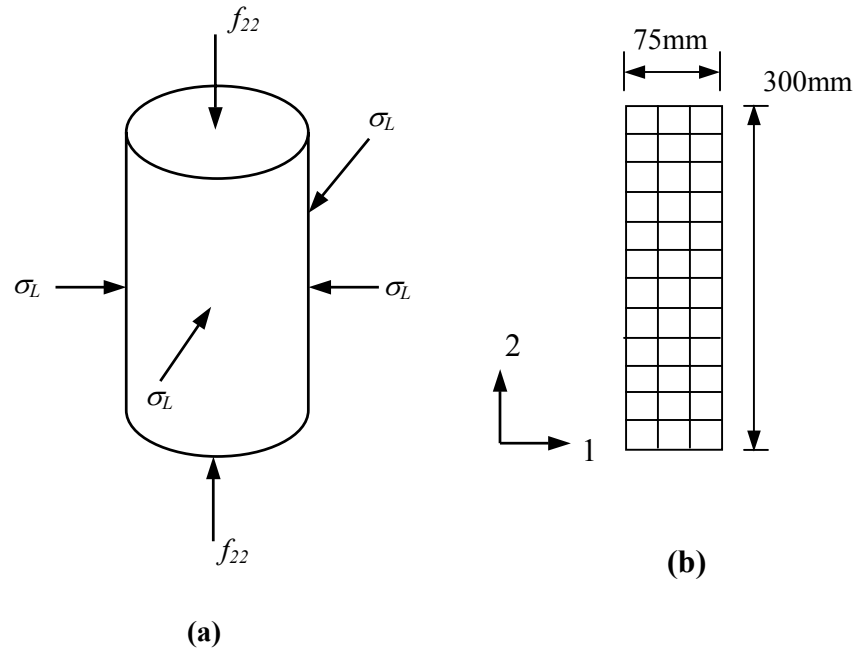
Figure 3.6 (a)Standard Concrete Cylinder (150 mm×300 mm) Tested by Sfer et al. (2002) under Triaxial Compression and (b)Finite Element Mesh using Axisymmetric Elements
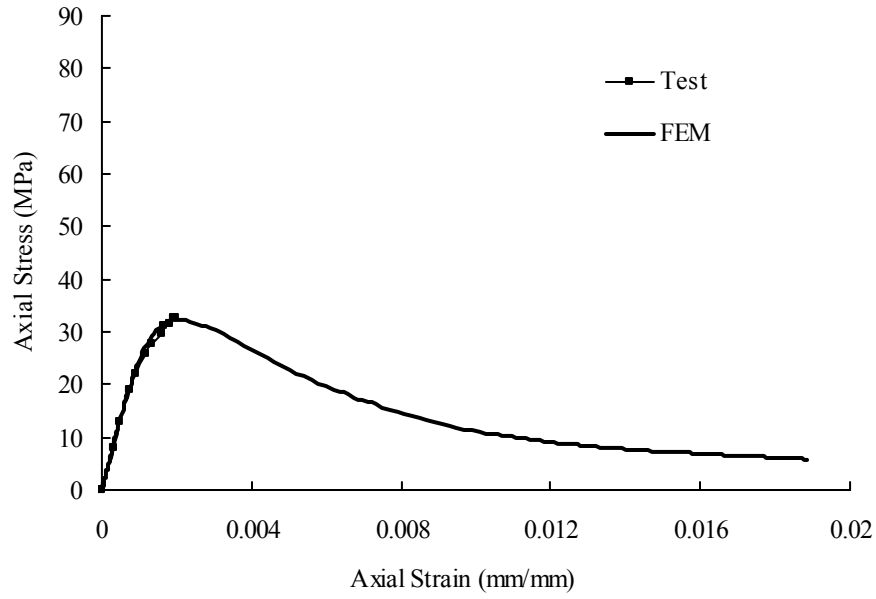
(a) $\sigma_L = 0.0$
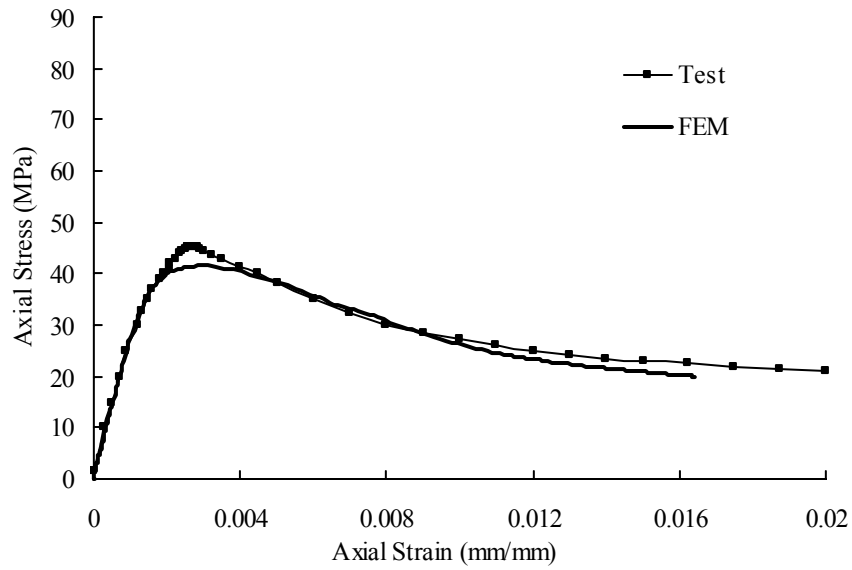
(b) $\sigma_L = 0.05f_{cu}$

Figure 3.7 Performance of Concrete Damage Plasticity Model under Triaxial Compression for Confining Pressures, σ_L, of: (a) 0; (b) 0.05f_{cu} ; (c) 0.15f_{cu} ; and (d) 0.30f_{cu} (test data from Sfer et al. 2002)
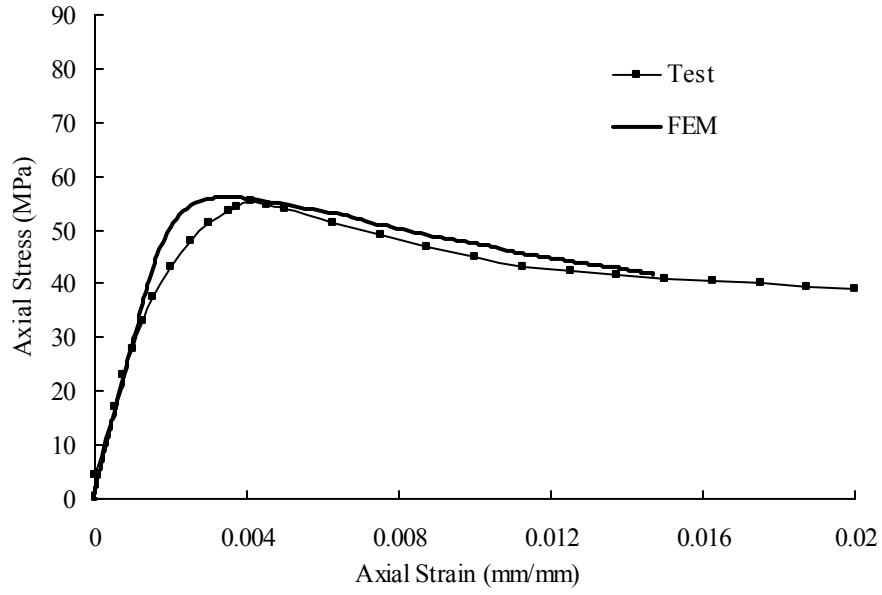
(c) $\sigma_L = 0.15f_{cu}$
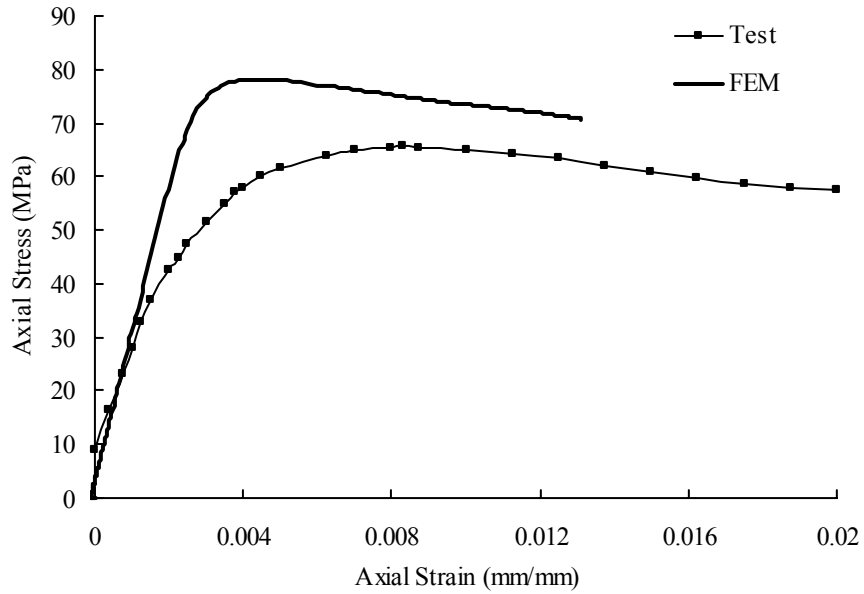
(d) $\sigma_L = 0.30f_{cu}$

Figure 3.7 (cont.) Performance of Concrete Damage Plasticity Model under Triaxial Compression for Confining Pressures, σ_L, of: (a) 0; (b) 0.05f_{cu} ; (c) 0.15 f_{cu} ; and (d) 0.30f_{cu} (test data from Sfer et al. 2002)

4. FINITE ELEMENT MODEL OF PEC COLUMNS

4.1 Introduction

Due to the relatively high cost of large-scale experimental research, a means of modelling PEC columns accurately using computer-aided methods is needed to broaden the current knowledge about the behaviour of these columns and improve the understanding of the influences of the various components. The primary objective of this chapter is to develop a complete finite element model that can be applied for a variety of geometries of PEC columns, subjected to various loading conditions, and provide accurate simulations of behaviour without numerical difficulties well into the post-peak regime. The model, therefore, is to be capable of simulating numerically the full behavioural history including the peak and residual post-peak capacities and the failure mode caused by local buckling of the steel plates and crushing of the concrete.

A concrete damage plasticity model (as described in Chapter 3), which is capable of predicting both compressive and tensile failures, is used to model the concrete material behaviour. The steel–concrete interface in the composite column is modelled using the contact pair algorithm in ABAQUS. A friction-type simple master–slave contact is assumed at the interface of the steel flange and concrete infill. Nonlinear material behaviour as well as the geometric nonlinearities due to large rotations are accounted for in the numerical model. A dynamic explicit solution strategy is used to trace a stable post-peak response of the composite system up to failure. To validate the model, simulations are conducted for both concentrically and eccentrically loaded column test specimens from five experimental programs, encompassing a wide variety of geometries and material properties. Detailed descriptions of the test specimens are provided in the following section. This is followed by a description of the finite element model geometry used to simulate the various tests, the material model parameters, as well as the loading program.

4.2   Properties of Reference Test Specimens

4.2.1   Short PEC Column Test Specimens with Normal Strength Concrete

A total of 22 short PEC columns constructed with normal strength concrete under different loading conditions are modelled for finite element analysis. The lists of these specimens, along with their geometric properties, are given in Table 4.1. (Plate thicknesses presented in the tables in this chapter are measured values where available; otherwise, nominal values have been used.) Figure 4.1 shows the cross-sections and steel side elevations of typical test columns. Specimens C-1 to C-7 were tested during the initial phase of the research program by Tremblay et al. (1998) to study the behaviour of these columns under concentric gravity loading. Specimen C-1 is not included in the numerical analysis because it is a prototype column having different characteristics. In this specimen, stiff bent bars were used as transverse links instead of straight bars that are usually used in Canam-type PEC columns. Specimens C-2 to C-7, which were modelled numerically, had square cross-sections of 300 mm × 300 mm and 450 mm × 450 mm, and a length equal to 5d, where d is the depth of the cross-section. The flange plate slenderness (b/t) ratio varied between 23 and 35. Round mild steel bars of 12.7 mm diameter were used as transverse links in these columns, except specimen C-5 had larger bars of 22.2 mm diameter. Three different link spacings—0.5d, 0.75d and 1.0d—were used in these columns. Specimens C-8 to C-11, tested by Chicoine et al. (2000), also under axial compression, were larger in their cross–sectional dimensions (600 mm×600 mm) as compared to the previous test specimens. As shown in Table 4.1, most of the geometric properties for these specimens were similar, except specimen C-10, which had a link spacing of 0.5d and specimen C-11, which had a b/t ratio of 31.

Bouchereau and Toupin (2003) performed 24 tests on 450 mm × 450 mm columns, with and without additional reinforcement, subjected to concentric, eccentric and lateral loading under both monotonic and cyclic conditions. Only the ten tests performed using an axial load only under static conditions from these researchers (as shown in Table 4.1) are selected for the analysis with the finite element model. All of these test columns were fabricated with 9.53 mm thick steel plates (b/t ratio of 23.6), a length of 2250 mm and

55

16 mm diameter links spaced at either 0.5d or 0.67d. Specimens with designations starting with B2 had additional longitudinal and transverse reinforcement (Figure 4.1 (b)) in the concrete.

Among these test columns, specimens B1-AX and B2-AX were tested under concentric gravity loading only. Four columns (B1-X1, B2-X1, B1-X3 and B2-X3) were loaded with an eccentricity that resulted in strong axis bending and the rest (B1–Y1, B2–Y1, B1–Y3 and B2–Y3) were subjected to weak axis bending. Two different values of eccentricity were applied relative to each axis of bending, as described in Table 4.1.

Specimens H1 and H2, described in Table 4.1, are from the series of tests performed by Prickett and Driver (2006). These columns were 2000 mm long and had a cross-section of 400 mm × 400 mm with a flange width to thickness (b/t) ratio of 25. Two different values of link spacing were used in these specimens: 0.5d in column H1 and 1.0 d in column H2. The link diameter was 12.7 mm in column H1 and 16 mm in column H2, both satisfying the requirements of CSA S16-01 Clause 18.3.1 (CSA 2001).

The material properties for steel and the test region concrete used in these PEC columns are given in Table 4.2. All these columns were fabricated with CSA-G40.21-350W grade steel plate, and were cast with normal strength concrete, ranging from 28 to 34 MPa. As shown in Figure 4.1 (c), the test region, where failure is forced to take place, is the central three–fifths region of the short PEC test specimens. High strength concrete and a closer link spacing were used at the end regions of the columns to avoid local failure in those regions. Tremblay et al. (1998), Chicoine et al. (2000) and Bouchereau and Toupin (2003) used 60MPa (nominal strength) and Prickett and Driver (2006) used 80MPa (nominal strength) concrete at the end regions.

4.2.2 Short PEC Column Test Specimens with High Strength Concrete

Nine short PEC columns, designated H3 to H11 as listed in Table 4.3, constructed with high strength concrete were tested by Prickett and Driver (2006) under concentric and

eccentric axial loading conditions. These columns had a cross-section of 400 mm × 400 mm with a b/t ratio of 25. Three different link spacing values—0.3d, 0.5d and 1.0d—were provided in columns H3 to H7, which were subjected to axial compression only. On the other hand, a link spacing of 0.6d was used in the eccentrically loaded columns (H8 through H11) to just meet the spacing requirement currently in S16. These four specimens were designed to have identical geometric properties. The parameters that varied for H8 through H11 were the load eccentricity and the column orientation. Columns H8 and H9 were loaded at 23 mm and 100 mm eccentricities, respectively, inducing bending about their strong axes. Columns H10 and H11 were loaded to have weak axis bending at 25 mm and 74 mm eccentricities, respectively.

Table 4.4 provides the mechanical properties for the steel section and the test region concrete in these specimens. The steel section was fabricated with CSA-G40.21-350W grade steel plate. High strength concrete of 60 MPa (nominal strength) was used in the test region of these specimens. However, two of the nine specimens (H6 and H7) had 1% steel fibres by volume (i.e., 80 kg/m^3 density) in the high strength concrete. The end regions of columns H3 to H11 had very high-strength concrete (nominally 80 MPa) to restrict failure to the test zones.

4.2.3 Long PEC Column Test Specimens with Normal Strength Concrete

Three 9.0 m long PEC columns with a cross–section of 450 mm × 450 mm × 9.75 mm tested by Chicoine et al. (2000) are selected for finite element simulation to study the ability of the current model to predict the global buckling behaviour. The geometric and material properties of these specimens are presented in Tables 4.5 and 4.6, respectively. An elevation of a typical long PEC test column is shown in Figure 4.1 (d). In the test region of these columns, two types of links spacings were used: 1.0d in specimens CL-1 and CL-2, and 0.5d in specimen CL-3. Additional reinforcements were provided only in specimen CL-3, as described in Table 4.5. Among these three specimens, one (specimen CL–2) was intended to have eccentric loading, where the load was applied at an eccentricity of 28 mm, resulting in bending about the weak axis. Though specimens CL-1

and CL-3 were loaded concentrically, Chicoine et al. (2000) reported the presence of bending moments in these tests, possibly caused by uneven end plates, alignment problems or accidental eccentricity. To represent these bending moments, both strong and weak axis equivalent eccentricities were calculated from the longitudinal strain gauge readings for all three specimens. Chicoine et al. (2000) proposed that these eccentricities should be included in the finite element analysis of long columns since the corresponding bending moments can significantly affect the global buckling behaviour of these columns. Two sets of numerical analyses were, therefore, performed for each of the long test columns, one using the applied eccentricity and the other using the measured eccentricity about the weak axis reported by Chicoine et al. (2000). The eccentricities listed in Table 4.5 for these long columns are the eccentricities applied at the beginning of the test. The deduced values of weak axis eccentricity used in the numerical analysis of specimen CL-1 were 20 mm at the top and 10 mm at the bottom end of the column. For specimen CL-2, these values were 45 mm and 35 mm at top and bottom end of the column, respectively, and 35 mm and -5 mm at top and bottom end, respectively, of column CL-3.

These columns were also fabricated from CSA-G40.21-350W grade steel plate. Normal strength concrete (nominally 30 MPa) was used in the test region of these columns. To strengthen the end regions of these test specimens, high strength concrete of 60 MPa nominal strength was used along with the closer link spacings provided in these zones.

4.3 Geometric Properties of the Finite Element Models

At the preliminary stage of this research, a segment of the column extending only from a link location to half way to the next link (as shown hatched in Figure 4.2 (a)) was modelled by Begum et al. (2004) to study the performance of the concrete damage plasticity model and contact algorithm in modelling the steel–concrete interface. This model is referred to herein as the "small" model (Figures 4.2 (b) and (c)). The height of this model was selected based on the observed failure mode in the experiments on concentrically loaded specimens.

In subsequent work (Begum et al. 2005) the "small" model was extended to half the total height of the column to include the effect of different geometric and material properties along the height of the test specimens. The segment of the column on the right hand side of line a-b-c in Figure 4.2 (a) defines this model. This "extended" model was used to capture the overall behaviour of the column. For both models, only one-quarter of the composite cross-section was included since the cross–section of a perfect PEC column can be considered as doubly symmetric. Comparisons between the small and extended models applied to ten concentrically loaded PEC column tests performed by Tremblay et al. (1998) and Chicoine et al. (2000) are presented in Chapter 6.

Finally, a "full" model including the entire length and cross–section of the column is developed to capture, as accurately as possible, the behaviour of PEC columns under the combined action of axial load and flexure, which is the primary objective of the current study. This model is verified against both concentrically and eccentrically loaded test specimens carried out by Bouchereau and Toupin (2003) and Prickett and Driver (2006). Three long PEC column specimens (Chicoine et al. 2000) are also simulated using the full model to study the ability of the model to capture the global buckling behaviour of long columns.

Descriptions of the mesh and elements used in the finite element models of the test specimens, along with the boundary conditions—including steel–concrete interactions—are presented in the subsequent sections.

4.3.1 Element Selection

The steel section in the PEC column is constructed with thin plates, which are susceptible to local buckling. As reported in Chapter 2, the stub PEC columns reach their ultimate capacity at the simultaneous occurrence of local buckling of the thin flanges and crushing of the encased concrete. In order to capture this behaviour, finite strain S4R shell elements were used to model the steel plates and eight-node solid elements were used to model the concrete.

Each node of the S4R shell element has six degrees of freedom—three translations and three rotations. This element uses one integration point on its mid-surface to form the element internal force vector. The default number of integration points through the thickness of this element is five, which is considered sufficient for modelling the nonlinear material behaviour of the current problem under monotonic loading. The C3D8R element selected to model the encased concrete blocks between the flange plates and the web of the composite section is an eight-node reduced integration brick element with three translational degrees of freedom at each node.

All continuum and plate elements in ABAQUS/Explicit are based on an updated Lagrangian formulation (HKS 2003). This formulation is useful for the current problem because the elements experience considerable shape changes resulting from large rotations due to local buckling of the flange plates. To account for the shape change, the nodal coordinates are updated at the beginning of each increment to reflect current positions in space and all the shape functions and derivatives are re-evaluated using the updated nodal coordinates.

Chicoine et al (2000) reported that the bending effect in the links of concentrically loaded PEC column test specimens were negligible. Prickett and Driver (2006) also observed negligible flexural effects in the links of both concentrically and eccentrically loaded PEC columns. Initially, therefore, T3D2 three dimensional truss elements were used to model the links. However, later in the study the truss elements in the links were replaced by B31 beam elements for ease of modelling the contact boundary conditions between the steel flanges and concrete. The B31 element is a two-node three-dimensional beam element, which has six degrees of freedom at each node: three translational and three rotational. The additional longitudinal and tie rebars in some PEC column specimens were modelled using T3D2 truss elements.

4.3.2 Mesh Description

The mesh configuration for the small model is shown in Figures 4.2(b) and (c) for two different link spacings, s: 1.0 d and 0.5 d. Seven elements are defined along the half-width of the web and flange plates of a specimen. Along the height of the small finite element model, six elements are used for specimens with s = 1.0d or 0.75d, whereas this number is reduced to three for specimens with s = 0.5d. A sensitivity analysis was performed with S4R elements to optimize the mesh in order to produce proper representations of local buckling of the steel flange, while maintaining reasonable computing economies. For all the elements except the elements defined at the web-flange corner, the aspect ratio was close to 1.0. At the corner where the plates meet, narrow elements with a width equal to one-half the thickness of the plates are defined to match the mesh of the steel plates with that of the concrete. The concrete infill is modelled with C3D8R solid elements using a 6 × 6 mesh over the quarter cross–section. The number of solid elements in the longitudinal direction is equal to the number chosen for the steel plates. The transverse steel link is meshed in such a way so as to match the nodes of the concrete elements of the column.

The extended model of the column is constructed initially in several parts, each with a unique link spacing and compressive strength of concrete. The parts are then assembled to produce the model in Figure 4.3 using the "part," "instance" and "assembly" options in ABAQUS. The mesh configuration in a typical part between two consecutive links in the test region of the column is similar to that of the small model. At the common interface between two adjacent parts in the model, the corresponding nodal degrees of freedom are linked using multi-point constraints to ensure compatibility. Figure 4.3 (a) shows the extended model, displaying the boundaries of the individual parts in the model and the positions of the transverse links. The entire model mesh is displayed in Figure 4.3 (b).

In the full finite element model the entire length and cross–section of the test specimens are modelled. Most of the features of this model are similar to those of the small and extended models. However, the number of elements is reduced in the full model to minimize the solution time, while maintaining a proper representation of local buckling

61

of the steel flange. Similar to the extended model, the full model is also constructed in individual parts between two successive transverse links. Figure 4.4 (a) shows the full model for a short PEC test column with s = 0.5d. This figure displays the boundaries of different parts of the column. The mesh description is shown in Figure 4.4 (b) for a typical part in the test region of the column. The end plates used in the test specimens are represented in the full model by rigid body surfaces and are fixed to the adjacent nodes of the end surfaces of the column. The additional rebars in five of the test columns are modelled using truss elements, the nodes of which are different than the nodes used for the concrete elements. Therefore, to ensure bonding between the concrete and the reinforcing bars, the rebars are defined as "embedded" reinforcement in the infill concrete blocks, which effectively couples the longitudinal behaviour of the rebar with that of the adjacent concrete.

4.3.3 Modelling of Steel–Concrete Interactions

One of the most challenging aspects of this study was to model successfully the steel–concrete interaction at their interfaces with a contact algorithm. Contact conditions are a special class of discontinuous constraint in a numerical analysis. They allow forces to be transmitted from one part of the model to another only when the surfaces are in contact. When the surfaces separate, no constraint is applied. ABAQUS/Explicit provides two algorithms for modelling contact: a general contact algorithm and a contact pair algorithm. The general contact algorithm is more powerful and allows for simpler contact definitions. However, the contact pair algorithm is useful in cases where more specialized contact features are required such as in the current problem.

In PEC columns, initially there is contact between the steel plates and the adjacent surfaces of the concrete infill. As the loading progresses, the flanges of the steel section between two consecutive links may experience local buckling resulting in a separation between the flange and the concrete blocks. However, neither local buckling of the web nor separation between the web plate and concrete block was observed (Tremblay et al.

1998, Chicoine et al. 2000, Bouchereau and Toupin 2003, Prickett and Driver 2006). Therefore, a contact algorithm was used only at the interior flange surfaces.

The contact pair algorithm in ABAQUS/Explicit was used to model the interaction between the flange and the adjacent concrete surface. First, the two contact surfaces are defined geometrically. The steel plate surface is defined as the master surface, whereas the concrete surface in contact is defined as the slave surface. As long as the two surfaces are in contact, they transmit shear and normal forces across the interface. However, the tensile bond between the contact surfaces is assumed to be zero. A mechanical interaction model, including friction, is defined to model this interaction between the steel and concrete surfaces. The basic Coulomb friction model is used in ABAQUS to formulate the tangential and normal forces using the coefficient of friction. The value of the frictional coefficient used in this study was 0.1 as recommended by Gorst et al. (2003) as the minimum value of static friction between steel and concrete surfaces. However, finite element analyses were performed for frictional coefficients ranging from 0.1 to 0.3 and the behaviour of the PEC columns were observed to be insensitive to this parameter. The following paragraphs describe the constraint enforcement method, the sliding formulation and contact surface weighting for the friction-type contact applied in the current problem.

The contact constraints in the contact pair algorithm can be enforced either using the kinematic method or the penalty method. The kinematic method uses a predictor/corrector contact algorithm to enforce contact constraints strictly (HKS 2003). The increment at first proceeds under the assumption that contact does not occur. If at the end of the increment there is an "overclosure" (overlap), the acceleration is modified to obtain a corrected configuration in which the contact constraints are enforced. On the other hand, the penalty method searches for node-into-face and edge-into-edge penetrations in the current configuration (HKS 2003). At the penetration points, equal and opposite contact forces with magnitudes equal to the penalty stiffness times the penetration distance are applied to the master and slave nodes. The kinematic constraint method was implemented initially in the current study for modelling the contact, primarily for its computational efficiency (Begum et al. 2004).

In developing the extended model (Begum et al. 2005) and the full model (Begum et al. 2007), geometric kinematic constraints (MPC option in ABAQUS) were used to ensure continuity between different parts in the model. When kinematic contact is used, some of the nodes at the bottom and top of each part are included in both the geometric kinematic constraints and the kinematic contact constraints. At such nodes the contact constraint most often overrides the geometric constraint. As a result, the continuity between parts of the extended and full models is lost. Therefore, the penalty method (though computationally less efficient) was chosen for the constraint enforcement at the steel–concrete interface of the PEC columns. The penalty contact algorithm introduces numerical softening through the use of penalty springs and does not interfere with geometric kinematic constraints.

To account for the relative motion of the two surfaces forming the contact pair, finite sliding is used, which is the most general and allows arbitrary motion of the surfaces forming the contact pair. Initially, a small sliding formulation was defined in the contact formulation (Begum et al. 2004) since there is relatively little sliding between the contact surfaces of the steel flange and concrete. Moreover, the small sliding formulation is computationally less expensive. However, penalty contact enforcement, which is implemented in the extended and full numerical models, only allows the finite sliding formulation.

Since geometric imperfections were not included in the finite element model for the PEC columns developed at the initial stage of the study, a pure master–slave surface weighting was successfully implemented in modelling the local buckling and separation of the steel flange from the concrete surface (Begum et al. 2004). However, while including inward local flange imperfections in the model, the steel surface (the master surface) was observed to penetrate the adjacent concrete surface (the slave surface) at the level of the transverse links (Begum et al. 2007). This might have occurred because in pure master–slave weighting, only penetrations of slave nodes (concrete nodes) into master facets (steel flange) are prevented while penetrations of master nodes into the slave surface can

go undetected. To avoid this situation, a balanced master–slave contact was used, which simply applies the pure master–slave approach twice, reversing the surfaces on the second pass (HKS 2003). The acceleration corrections or forces are obtained by taking a weighted average of the two calculations. Hence, the balanced approach minimizes the penetration of the contacting bodies and provides an appropriate simulation of the interaction between the steel flange and concrete of an imperfect PEC column.

Finite element analyses were performed without any constraint between the web and the adjacent concrete in the small and extended models. The results showed that the concrete elements expanded beyond the web plate, which is impossible in a real situation. The symmetry boundary conditions at the web plates did not provide constraint to the adjacent concrete nodes. Therefore, it is necessary in the small and extended models to fix the web plate with the adjacent concrete surfaces using geometric-type constraints. In the full model, no constraint is applied between the web and the adjacent concrete surfaces, as no separation was observed between the web plate and concrete in the test specimens.

4.3.4   End Boundary Conditions

Symmetry boundary conditions are applied along the planes of symmetry of the small and extended models. In addition, the rotations about axes 1 and 3 (Figure 4.2) are fixed at the top edge of the flange in the small model. Since the rigid end plates in the test specimens were not modelled in the small and extended models, the load is applied to the top surface of the model through a displacement control technique. In the extended model, no separation is permitted between the flange plate at the top segment of the column and the adjacent concrete surface to avoid local failure near the top of the column.

The boundary conditions applied in the "full" model to simulate the end conditions for concentrically and eccentrically loaded specimens are shown in Figure 4.5. In concentrically loaded column tests, translations and rotations at both ends were fixed except the vertical displacement at the top. The same condition was applied through

reference nodes at the top and bottom rigid surfaces of the finite element model. The axial load was applied through the top rigid body reference node, which was defined at the centre of the column cross–section, using a displacement control technique. In the finite element model for eccentrically loaded test specimens, pinned–pinned end conditions were applied at the end eccentric points located on the end rigid planes. For strong axis bending, rotations about the strong axis were released at these points. Similarly, rotations about the weak axis were released for weak axis eccentricity. A rigid beam was defined between the eccentric points and the rigid body reference nodes on the end rigid planes, as shown in Figure 4.5. This was done to constrain the displacements and rotations of the reference nodes at the rigid surfaces to those of the corresponding eccentric nodes at the two surfaces. A smooth amplitude displacement was applied through the top eccentric point to simulate the applied loading condition in the test.

4.3.5 Modelling of Residual Stresses

The residual stresses in a PEC column occur mainly because of the welding of the steel plates to form the steel section. Since these stresses might have a significant effect in reducing the buckling capacity of the thin flanges in the composite column, they were included in the numerical model for all 34 PEC test columns. In the finite element model, the residual stresses in the steel plate were modelled as initial stresses in each element of the flange and web. It was assumed to be constant along the height of the numerical model. The residual stress distributions across the cross–section of the PEC columns were obtained from Tremblay et al. (2000b) and Chicoine et al. (2001). The residual stresses for specimens H1 to H11 (Prickett and Driver 2006), which had a cross–section of 400 mm × 400 mm × 7.98 mm, were not measured during the tests. Therefore, the distribution of residual stresses applied in the numerical models for these specimens were adopted from that of specimen C-2 (450 mm × 450 mm × 9.5 mm) which had cross–sectional dimensions similar to those of specimens H1 to H11. Moreover, two sets of numerical analyses were performed on specimens H3 through H11 using the full column finite element model—including and excluding the residual stresses—to study the effect

of the residual stresses on the behaviour of PEC columns. The results are presented in Chapter 5.

4.3.6 Modelling of Geometric Imperfections

Initial geometric imperfections can play a significant role in the stability behaviour of PEC columns. The columns can have two types of geometric imperfections—local imperfections and global imperfections. Local imperfections are usually important for stub columns where local buckling is the governing failure mode. A study was performed using the numerical model to observe the sensitivity of the buckling behaviour of short PEC columns to local imperfections. The results of this study are presented in Chapter 5.

Since the behaviour of the long columns can be affected significantly by global imperfections, they were included in the numerical models of the three long test columns. The description of the measured imperfections in the test PEC columns, along with how they were implemented in the finite element model, is presented in the following sections.

4.3.6.1   Local Imperfections

Local imperfections in a PEC column are defined as the out-of-straightness of the steel flange between two consecutive transverse links. Extensive measurements of all test specimens revealed that with very few exceptions the imperfection in the flange plate between any two links was inward (as shown in Figure 4.6(a)) due to the fabrication process (Chicoine et al. 2000, Prickett and Driver 2006). The inward imperfection of the flange plate was expected to improve the resistance of these columns to local buckling. On the other hand, if the imperfection were outwards, it would be expected to decrease the local buckling capacity of the flange. The finite element model developed by Chicoine et al. (2001) did not predict the proper failure mode with inward initial imperfections. However, the study reported here made an attempt to overcome this limitation by using the contact algorithm to define the interaction between the steel flange and concrete. Moreover, the effects of inward and outward imperfections on the capacity

67

of PEC columns were studied to evaluate the necessity of including the local imperfections in the finite element model.

The imperfection sensitivity study was performed using the full model on specimen C-2 (450mm×450mm×9.5 mm, with s = 0.5d), specimen C-8 (600mm×600mm×12.7 mm, with s = 1.0d) and specimen C-11 (600mm×600mm×6.35 mm, with s = 1.0d). These three specimens were selected to cover a range of flange thicknesses and link spacings, as well as including two different flange widths. The imperfection was applied by shifting the steel flange and the adjacent concrete nodes according to the idealized imperfect shape shown in Figure 4.6(b). The failure modes obtained for inward and outward imperfections for all three columns were consistent with those observed in the corresponding test specimens and, therefore, the imperfection shape was considered suitable for this study. The maximum (inward) amplitude of the measured initial imperfections in all the test specimens varied from 0.39 mm (C-2 and C-5) to 2.02 mm (C-9) and, as expected, tended to be larger for larger link spacings (Chicoine et al. 2001). In this study, imperfections with maximum amplitudes of ±2 mm and ±6 mm, as well as no imperfections, were modelled for specimen C-8 and C-11. The values used for specimen C-2, with the closer link spacing, were 0 mm, ±1 mm and ±3 mm. The imperfections are applied only at the middle segment of the column in between two links.

4.3.6.2   Global Imperfections

Global imperfections refer to the overall out-of-straightness of the column and can significantly affect the behaviour of slender columns. In this study, the global imperfection was modelled only for the slender test specimens performed by Chicoine et al. (2000). In the test the imperfections (as given in Table 4.5) were measured only in the direction of expected buckling, which was about the weak axis of the composite section. In the finite element analysis the imperfect shape of the column was assumed to be parabolic. The maximum amplitude of the global imperfection obtained from the experimental data was assumed to occur at the mid-height of the column. The

imperfection was defined by perturbation in the nodal coordinates of the perfect column using the "imperfection" option in ABAQUS/Explicit.

4.4 Material Properties

4.4.1 Steel

The steel material properties for the plate and link were modelled with an elasto-plastic J2 model. The stress–strain relationship for steel is defined as a trilinear curve, as shown in Figure 4.7. Point A in the stress–strain curve is the yield point, point B refers to the onset of strain hardening and point C is the ultimate stress point. The material data used to define this trilinear curve for the steel plate material in the finite element analysis are listed in Tables 4.2, 4.4 and 4.6. These values are obtained from tensile tests on steel coupons from the test specimens (Tremblay et al. 1998; Chicoine et al. 2000; Bouchereau and Toupin 2003; Prickett and Driver 2006).

Since the model formulation is based on the updated Lagrangian description, the true (Cauchy) stress and logarithmic strain are needed to describe the effective stress–effective plastic strain. The stress and strain data obtained from the uniaxial tension tests are converted to true stress, σ_{true}, and logarithmic plastic strain, $\varepsilon_{\ln}^{pl}$, using the following relationships (Lubliner 1990):

$$\sigma_{true} = \sigma_{nom}(1 + \varepsilon_{nom}) \tag{4.1}$$

$$\varepsilon_{\ln}^{pl} = \ln(1 + \varepsilon_{nom}) - \frac{\sigma_{true}}{E_s} \tag{4.2}$$

where, E_s is the modulus of elasticity of steel, σ_{nom} is the nominal, or engineering, stress and ε_{nom} is the nominal, or engineering, strain obtained from material tests. The value of Poisson's ratio for steel used in the numerical analysis is 0.3.

4.4.2 Concrete

The damage plasticity model in ABAQUS was used to simulate the concrete material behaviour in the composite columns. The model was verified (Chapter 3) against published uniaxial, biaxial and triaxial compressive test results (Sfer et al. 2002) for normal strength concrete under various levels of lateral confinement and was observed to provide satisfactory results for low levels of confinement. The uniaxial compressive stress–strain response of both normal and high strength concrete was assumed to be linear up to 30% of its compressive strength. In the plastic regime, the effective stress–plastic strain function was described through a stress–strain function (compression hardening function) in uniaxial compression using the models described in Chapter 3. The material properties used to generate the concrete stress–strain curve for the test specimens are listed in Tables 4.2, 4.4 and 4.6. These data were obtained from standard cylinder tests performed at the test day on concrete in each test specimen.

The compressive concrete strength, used to define the uniaxial compression curve for normal strength concrete in the numerical analysis, was reduced to its effective value, f_{cue}. by multiplying the cylinder compressive strength, f_{cu}, at test day by the factor 0.92ψ, as described in Section *2.3.3.1* of Chapter 2.

In the numerical analysis of high strength concrete PEC columns, no reduction factor is applied to the compressive strength of the concrete. Analyses were initially performed with $f_{cue} = 0.92\,\psi f_{cu}$ and $0.92 f_{cu}$. In both cases the numerical compressive strengths of the PEC columns were observed to be 10 to 15% lower than the experimentally obtained strengths. Hence, it was decided that since the reduction factor was in fact based on results of column tests using normal strength concrete and may therefore not apply to these columns, the actual compressive strength obtained from the standard cylinder test at the test day would be used to generate the stress–strain curve of high strength concrete with and without steel fibres.

The uniaxial tensile strength of concrete, f_{tu}, was set at 10% of the effective uniaxial compressive strength for the normal strength concrete and 5% for the high strength

concrete following the recommendations of Marzouk and Chen (1995). For steel fibre reinforced high strength concrete, the tensile strength was calculated according to an equation developed by Kützing and König (1999):

$$f_{tu} = 2.12 \times \ln\left(1 + \frac{f_{cu}}{10}\right)$$ (4.3)

In the damage model, the stress–strain response under uniaxial tension follows a linear elastic relationship until the tensile strength is reached. The post-cracking tensile properties for the concrete model are defined as a stress–displacement curve following the relationships described in Chapter 3.

4.5 Dynamic Explicit Solution Strategy

4.5.1 Advantages of Explicit Solution Method over Implicit Method

The commercial finite element software ABAQUS has two analysis modules—ABAQUS/Standard and ABAQUS/Explicit—that use different solution strategies for solving nonlinear quasi-static and dynamic problems. The ABAQUS/Explicit module determines the solution without iteration by explicitly advancing the kinematic state over small time increments, whereas ABAQUS/Standard uses an implicit strategy and must iterate to establish equilibrium in a nonlinear problem (HKS 2003). Each iteration in an implicit analysis requires solving a large system of linear equations and requires considerable computation effort, disk space, and memory. In some complex problems such as the current study, which exhibits highly nonlinear behaviour containing contact and frictional sliding features, convergence may not be possible using the implicit method, especially after the limit point.

ABAQUS/Explicit uses the central difference rule to integrate the equations of motion explicitly through time. The kinematic conditions at the beginning of one increment are used to calculate those at the beginning of the next increment. The term "explicit" refers to the fact that the state at the end of the increment is based solely on the displacements,

71

velocities, and accelerations at the beginning of the increment. No iterations are necessary; hence, the convergence problems associated with implicit strategies do not apply.

ABAQUS/Explicit contains extensive capabilities for modelling contact and surface interactions that are not available in ABAQUS/Standard. Contact conditions and other extremely discontinuous events are readily formulated in the explicit method and can be enforced on a node-by-node basis without iteration.

Material degradation and failure often lead to severe convergence difficulties in implicit analysis programs. On the other hand, ABAQUS/Explicit allows the modelling of material degradation and failure, avoiding these difficulties by explicitly advancing the kinematic state.

For the explicit method to produce accurate results, the time increments must be quite small so that the accelerations are nearly constant during an increment. As a result, analyses typically require many thousands of increments. Nevertheless, the analysis can still be more efficient in ABAQUS/Explicit if the same analysis in ABAQUS/Standard requires many iterations.

4.5.2   Simulation of Quasi-Static Response with Explicit Dynamic Solution Strategy

The explicit solution method was originally developed for dynamic problems in which inertia plays a prominent role in the solution. This method can be applied to quasi-static problems with some special considerations in the applied loading history. An accurate and efficient quasi-static analysis requires the loading to be as smooth as possible. ABAQUS/Explicit has a simple, built-in type of amplitude function, called "smooth step" that automatically limits spurious oscillations. Defining the time–amplitude data pairs using this function allows ABAQUS/Explicit to connect each of the data pairs with curves, as shown in Figure 4.8(a). The first and second derivatives of this amplitude

curve are smooth with zero slopes at each data point. Hence, this type of loading amplitude allows a quasi-static analysis to be performed without generating waves due to discontinuities in the rate of applied loading.

The central difference method, which is used in the explicit method to integrate the equations in time, is conditionally stable. The stable time increment is smaller than the time required for a sound wave to travel through the smallest element in the analysis. Since a static solution is, by definition, a long-time solution, it is often computationally impractical to analyze the simulation in its natural time scale, which would require an excessive number of small time increments (HKS 2003). To obtain an economical solution, the event must be accelerated in some way without affecting the state of static equilibrium; i.e., the inertial forces must remain insignificant. This can be achieved either by reducing the time period of the analysis (which in turn increases the loading rate) or by increasing the mass density of the whole or part of the model artificially, a method called "mass scaling." An artificial increase in the material density decreases the wave speed, resulting in an increase in the stable time increment. As a consequence, fewer increments are required to perform the same analysis for the same time period resulting in less computing time to achieve the solution. However, it should be ensured that changes in the loading rate or mass density, and consequent increases in the inertial forces, do not alter the solution significantly.

In this study, the load was applied using a smooth amplitude displacement history at rates that rendered the inertial effects negligible. The "small" model used a displacement rate of 1 mm/sec, whereas the "extended" model used a rate of 18 mm/sec. In the "full" model analysis, the displacement was applied at a rate of 8 mm/sec for both concentrically and eccentrically loaded specimens.

Due to its complexity, a mass-scaling factor of 100 was applied to the full model to improve the efficiency of the solution time. The applied loading rates and the value of the mass-scaling factor for the numerical models were chosen through an iterative process to obtain a quasi-static response, as well as an economical solution time. To evaluate the

quality of quasi-static responses, the energy history was examined. In a quasi-static system, the work applied by the external forces should be nearly equal to the internal energy of the system, while the kinematic energy remains bounded and small. Both of these criteria were observed to be satisfied. The energy history of a typical explicit test specimen analysis is shown in Figure 4.8(b).

Table 4.1 Geometric Properties of Reference Test Specimens with Normal Strength Concrete

Reference	Specimen designation	Plate size b_f x d x t (mm)	Length L (mm)	Plate slenderness ratio b/t	Link Spacing s (mm)	Link Spacing s/d	Diameter ϕ (mm)	Additional reinforcement Longitudinal rebars (mm)	Additional reinforcement Tie rebars (mm)	e_x (mm)	e_y (mm)
	C-2	450 x 450 x 9.70	2250	23.2	225	0.5	12.7	-	-		
	C-3	450 x 450 x 9.70	2250	23.2	337.5	0.75	12.7	-	-		
Tremblay	C-4	450 x 450 x 9.70	2250	23.2	450	1.0	12.7	-	-		
et al. 1998	C-5	450 x 450 x 9.70	2250	23.2	225	0.5	22.2	-	-		
	C-6	450 x 450 x 6.35	2250	35.4	337.5	0.75	12.7	-	-		
	C-7	300 x 300 x 6.35	1500	23.6	300	1.0	12.7	-	-		
	C-8	600 x 600 x 12.90	3000	23.2	600	1.0	15.9	-	-		
Chicoine	C-9	600 x 600 x 12.90	3000	23.2	600	1.0	15.9	-	-		
et al. 2002	C-10	600 x 600 x 12.80	3000	23.2	300	0.5	15.9	-	-		
	C-11	600 x 600 x 9.70	3000	30.9	600	1.0	15.9	-	-		
	B1-AX	450 x 450 x 9.53	2250	23.6	300	0.5	15.9	-	-		
	B2-AX	450 x 450 x 9.53	2250	23.6	300	0.5	15.9	#20	#10		
	B1-X1	450 x 450 x 9.53	2250	23.6	300	0.67	15.9	-	-	142	-
Bouchereau	B2-X1	450 x 450 x 9.53	2250	23.6	300	0.67	15.9	#20	#10	143	-
and	B1-X3	450 x 450 x 9.53	2250	23.6	300	0.67	15.9	-	-	33	-
Toupin 2003	B2-X3	450 x 450 x 9.53	2250	23.6	300	0.67	15.9	#20	#10	33	-
	B1-Y1	450 x 450 x 9.53	2250	23.6	300	0.67	15.9	-	-	-	84
	B2-Y1	450 x 450 x 9.53	2250	23.6	300	0.67	15.9	#20	#10	-	91
	B1-Y3	450 x 450 x 9.53	2250	23.6	300	0.67	15.9	-	-	-	23
	B2-Y3	450 x 450 x 9.53	2250	23.6	300	0.67	15.9	#20	#10	-	23
Prickett and	H1	400 x 400 x 7.98	2000	25	200	0.5	12.8	-	-	-	-
Driver 2006	H2	400 x 400 x 8.00	2000	25	400	1.0	15.9	-	-	-	-

Table 4.2 Material Properties of Reference Test Specimens with Normal Strength Concrete

Reference	Specimen designation	Properties of concrete in test region				Properties of steel plate					
		f_{cu} (MPa)	E_c (MPa)	ε_{cu} (µε)	ν	F_y (MPa)	F_{sh} (MPa)	F_u (MPa)	ε_y (%)	ε_{sh} (%)	ε_u (%)
Tremblay et al.1998	C-2	32.7	28000	2250	0.18	370	370	519	0.19	1.87	15.20
	C-3	32.4	27800	2250	0.18	370	370	519	0.19	1.87	15.20
	C-4	31.9	28000	2250	0.18	370	370	519	0.19	1.87	15.20
	C-5	34.3	28800	2250	0.18	370	370	519	0.19	1.87	15.20
	C-6	33.1	28200	2250	0.18	374	374	519	0.19	1.87	15.20
	C-7	31.9	31500	2250	0.18	374	374	519	0.19	1.87	15.20
Chicoine et al. 2002	C-8	34.2	27300	2000	0.18	360	360	519	0.19	1.87	15.20
	C-9	34.2	27300	2000	0.18	360	360	519	0.19	1.87	15.20
	C-10	34.2	27300	2000	0.18	360	360	519	0.19	1.87	15.20
	C-11	34.2	27300	2000	0.18	345	345	529	0.18	1.95	30.10
Bouchereau and Toupin 2003	B1-AX	33.8	28500	2250	0.18	358	358	549	0.27	1.15	9.15
	B2-AX	33.8	28500	2250	0.18	358	358	549	0.27	1.15	9.15
	B1-X1	34.1	28500	2250	0.18	358	358	549	0.27	1.15	9.15
	B2-X1	34.1	28500	2250	0.18	357	357	552	0.24	1.11	12.06
	B1-X3	34.1	28500	2250	0.18	358	358	549	0.27	1.15	9.15
	B2-X3	34.1	28500	2250	0.18	357	357	552	0.24	1.11	12.06
	B1-Y1	33.8	28500	2250	0.18	358	358	549	0.27	1.15	9.15
	B2-Y1	33.8	28500	2250	0.18	357	357	552	0.24	1.11	12.06
	B1-Y3	33.8	28500	2250	0.18	358	358	549	0.27	1.15	9.15
	B2-Y3	33.8	28500	2250	0.18	357	357	552	0.24	1.11	12.06
Prickett and Driver 2006	H1	28.7	23300	2220	0.13	394	394	528	0.19	1.67	15.80
	H2	29.7	23300	2230	0.13	394	394	528	0.19	1.67	15.80

Table 4.3 Geometric Properties of Reference Test Specimens with High Strength Concrete

Reference	Specimen designation	Plate size b_f x d x t	Length L	Plate slenderness ratio b/t	Link Spacing s	s/d	Diameter ϕ	Additional reinforcement Longitudinal rebars	Tie rebars	Eccentricity e_x	e_y
		(mm)	(mm)		(mm)		(mm)	(mm)	(mm)	(mm)	(mm)
	H3	400 x 400 x 7.99	2000	25	120	0.3	12.8	-	-	-	-
	H4	400 x 400 x 8.01	2000	25	200	0.5	12.8	-	-	-	-
Prickett and	H5	400 x 400 x 8.02	2000	25	400	1.0	15.9	-	-	-	-
Driver 2006	H6	400 x 400 x 8.02	2000	25	200	0.5	12.8	-	-	-	-
	H7	400 x 400 x 8.02	2000	25	400	1.0	15.8	-	-	-	-
	H8	400 x 400 x 7.95	2000	25	240	0.6	12.8	-	-	23	-
	H9	400 x 400 x 7.98	2000	25	240	0.6	12.8	-	-	100	-
	H10	400 x 400 x 8.01	2000	25	240	0.6	12.7	-	-	-	25
	H11	400 x 400 x 7.95	2000	25	240	0.6	12.7	-	-	-	74

Table 4.4 Material properties of Reference Test Specimens with High Strength Concrete

Reference	Specimen. designation.	Properties of concrete in test region				Properties of steel plate					
		f_{cu} (MPa)	E_c (MPa)	ε_{cu} (µε)	v	F_y (MPa)	F_{sh} (MPa)	F_u (MPa)	ε_y (%)	ε_{sh} (%)	ε_u (%)
	H3	60.0	28000	2880	0.16	394	394	528	0.19	1.67	15.80
	H4	58.9	28800	2995	0.16	394	394	528	0.19	1.67	15.80
	H5	61.7	28500	3165	0.16	394	394	528	0.19	1.67	15.80
Prickett and Driver 2006	H6	49.3	24800	2490	0.15	394	394	528	0.19	1.67	15.80
	H7	52.9	24800	2850	0.15	394	394	528	0.19	1.67	15.80
	H8	62.4	29800	2900	0.17	394	394	528	0.19	1.67	15.80
	H9	64.5	28600	3040	0.15	394	394	528	0.19	1.67	15.80
	H10	65.7	29000	2745	0.15	394	394	528	0.19	1.67	15.80
	H11	65.1	28700	3225	0.16	394	394	528	0.19	1.67	15.80

Table 4.5 Geometric Properties of Reference Long Test Specimens

Reference	Specimen designation	Plate size $b_f \times d \times t$ (mm)	Length L (mm)	Global imperfection δ_ψ	Plate slenderness ratio b/t	Link Spacing s (mm)	Link Spacing s/d	Link Diameter ϕ (mm)	Additional reinforcement Longitudinal rebars (mm)	Additional reinforcement Tie rebars (mm)	Eccentricity e_x (mm)	Eccentricity e_y (mm)
Chicoine et al. 2002	CL-1	450 x 450 x 9.78	9000	1.46	23	450	1.0	12.7	-	-	-	-
	CL-2	450 x 450 x 9.78	9000	2.70	23	450	1.0	12.7	-	-	-	28
	CL-3	450 x 450 x 9.78	9000	1.01	23	225	0.5	12.7	#15	#10	-	-

Table 4.6 Material Properties of Reference Long Test Specimens

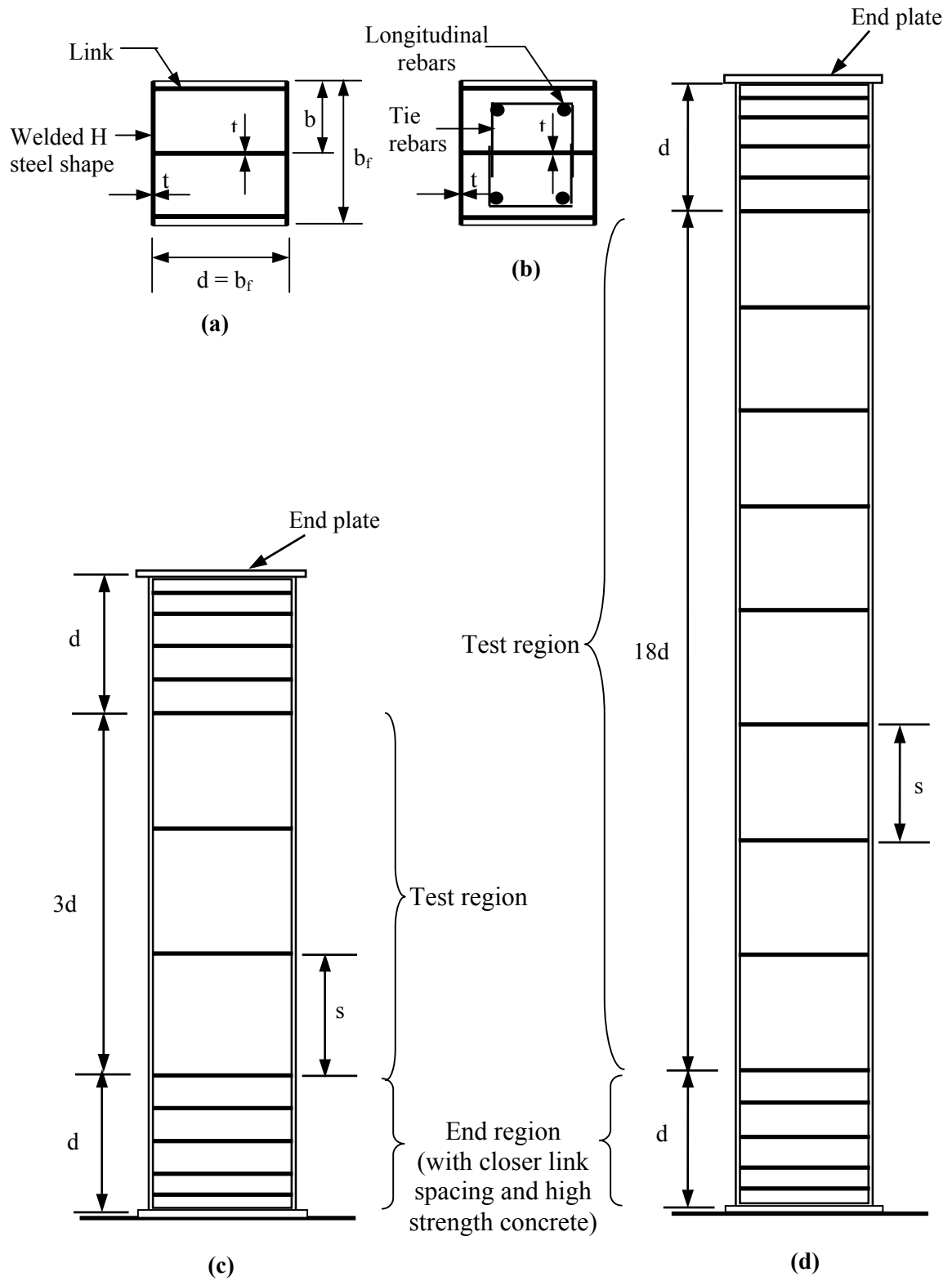| Reference	Specimen designation	Properties of concrete in test region f_{cu} (MPa)	E_c (MPa)	ε_{cu} (με)	ν	Properties of steel plate F_y (MPa)	F_{sh} (MPa)	F_u (MPa)	ε_y (%)	ε_{sh} (%)	ε_u (%)
Chicoine et al. 2002	CL-1	34.6	27900	2050	0.18	345	345	529	0.18	1.95	30.10
	CL-2	34.6	27900	2050	0.18	345	345	529	0.18	1.95	30.10
	CL-3	34.6	27900	2050	0.18	345	345	529	0.18	1.95	30.10

Figure 4.1 Geometry of Typical PEC Test Columns,

(a) Cross-section, (b) Cross-section with Additional Rebars, (c) Elevation
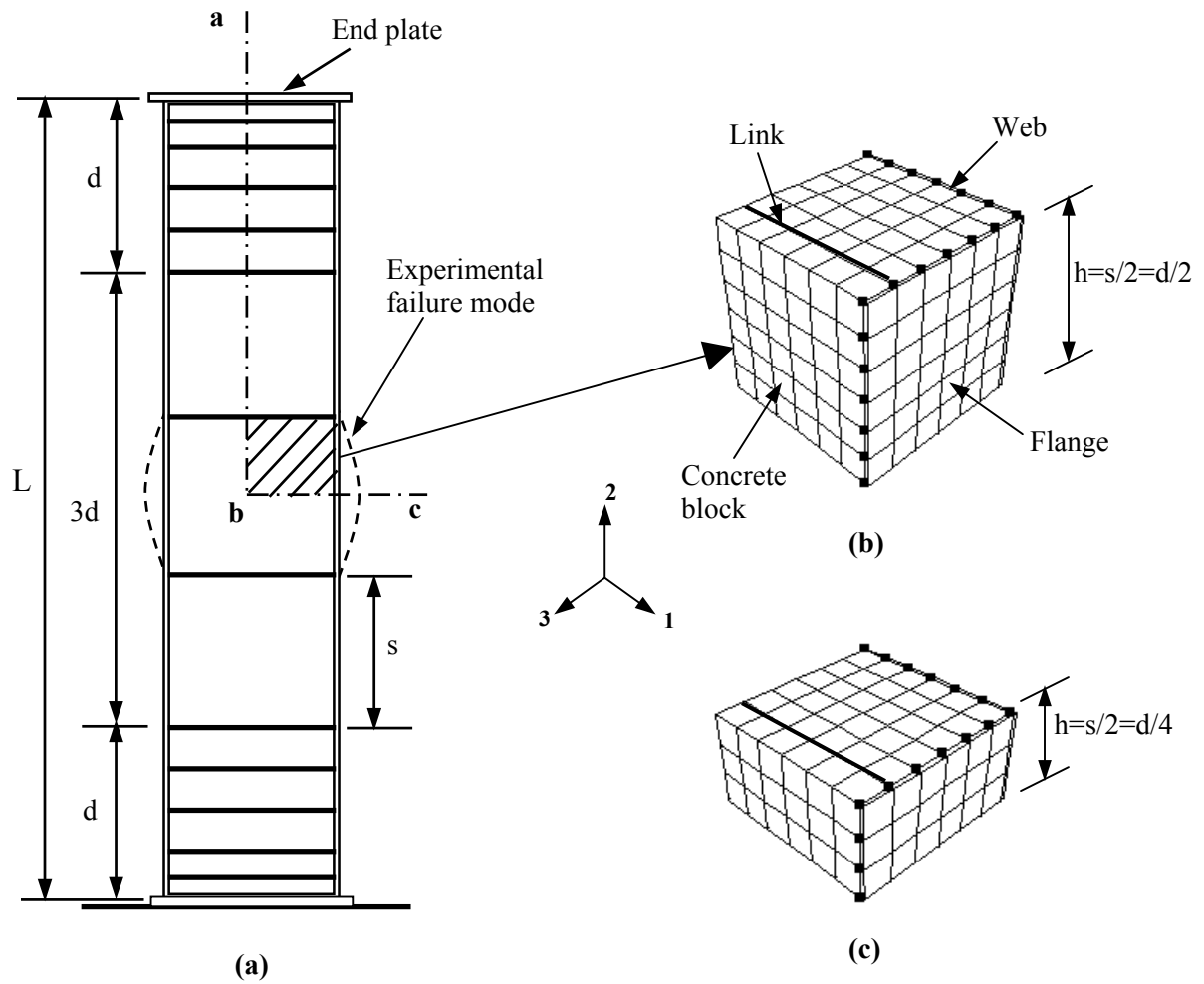
of a Short Column, and (d) Elevation of a Long Column

Figure 4.2 "Small Models", (a) A Typical Column, (b) Mesh for s = d, and
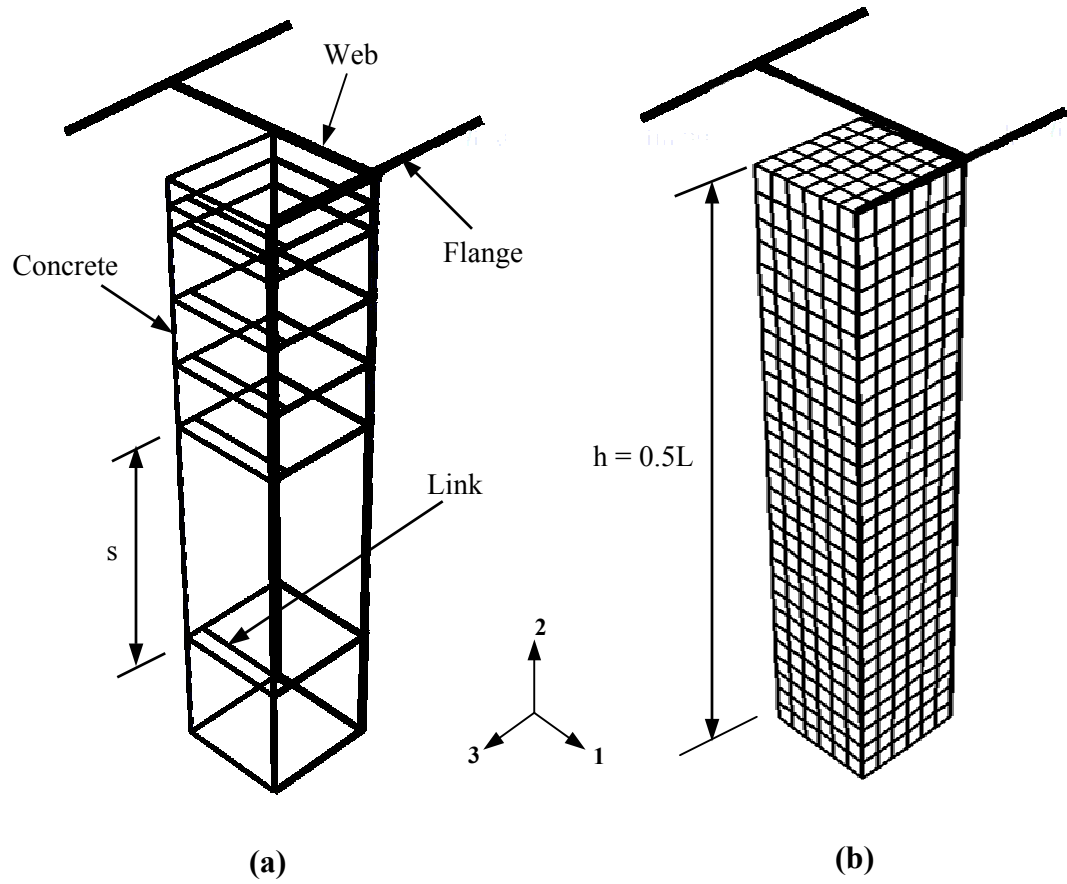(c) Mesh for s = 0.5 d

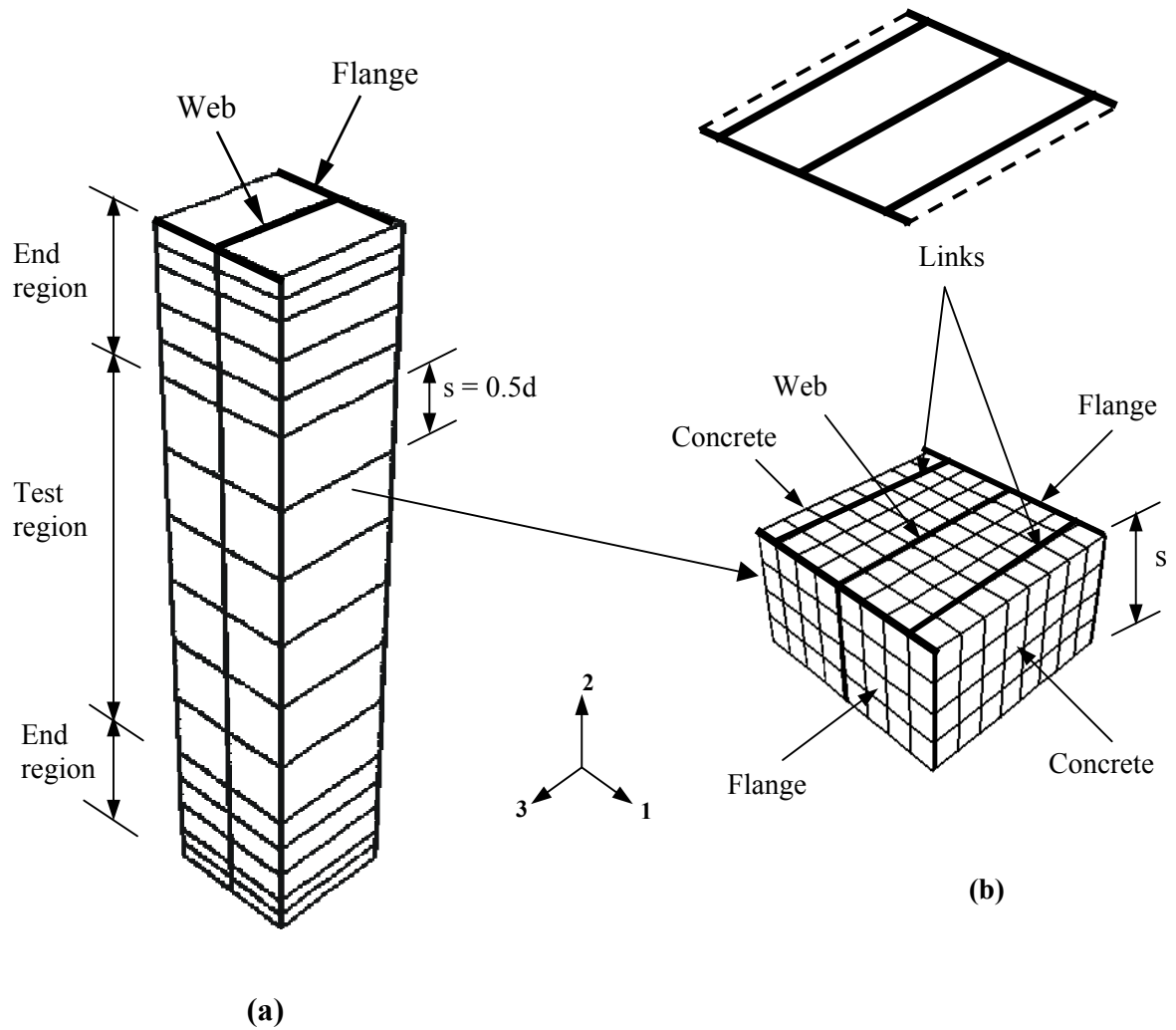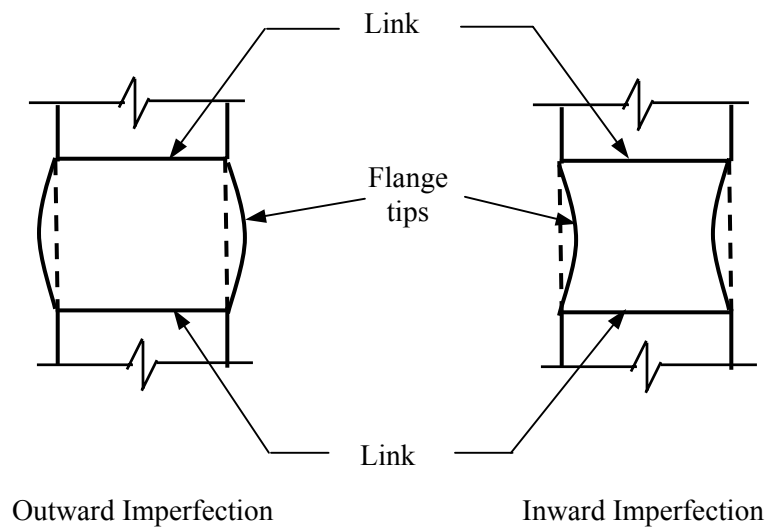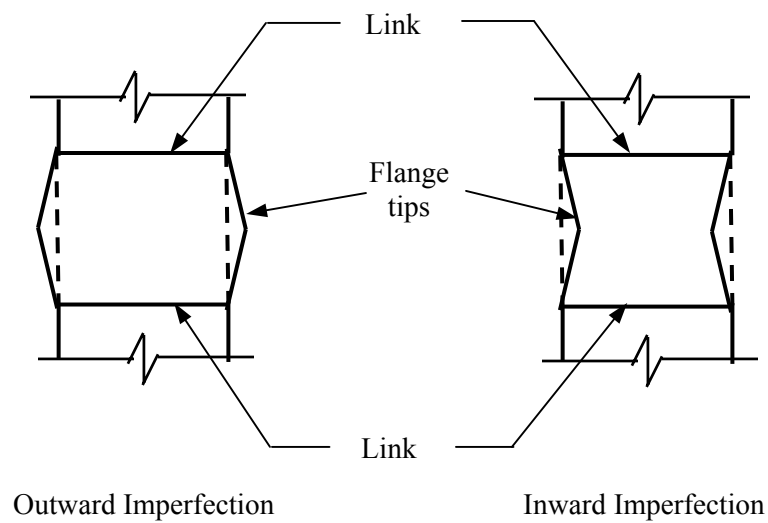**Figure 4.3 "Extended" Model, (a) Parts between Consecutive Links, and (b) Entire Model Mesh**

Figure 4.4 Finite Element Mesh for Full Model,

(a) Typical Short Column Displaying the Parts between Consecutive Links, and

(b) Mesh Configuration of a Typical Part in the Test Region of the Column

**Figure 4.5 End Boundary Conditions in Full Finite Element Model
for Concentrically and Eccentrically Loaded PEC Test Columns**

Link

Flange
tips

Link

Outward Imperfection   Inward Imperfection

(a) Actual shape

Link

Flange
tips

Link

Outward Imperfection   Inward Imperfection

(b) Idealized shape

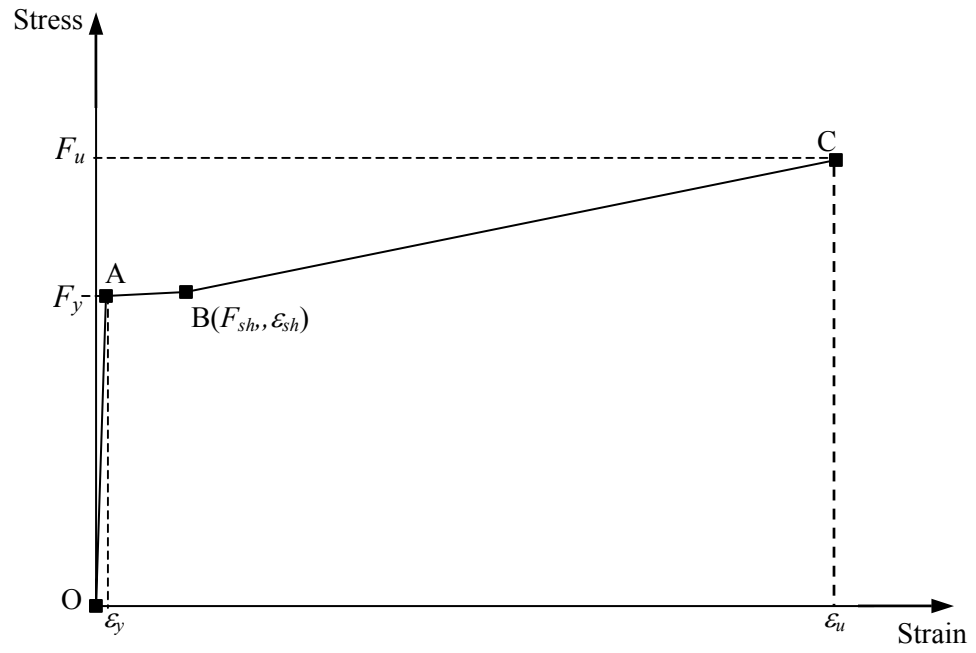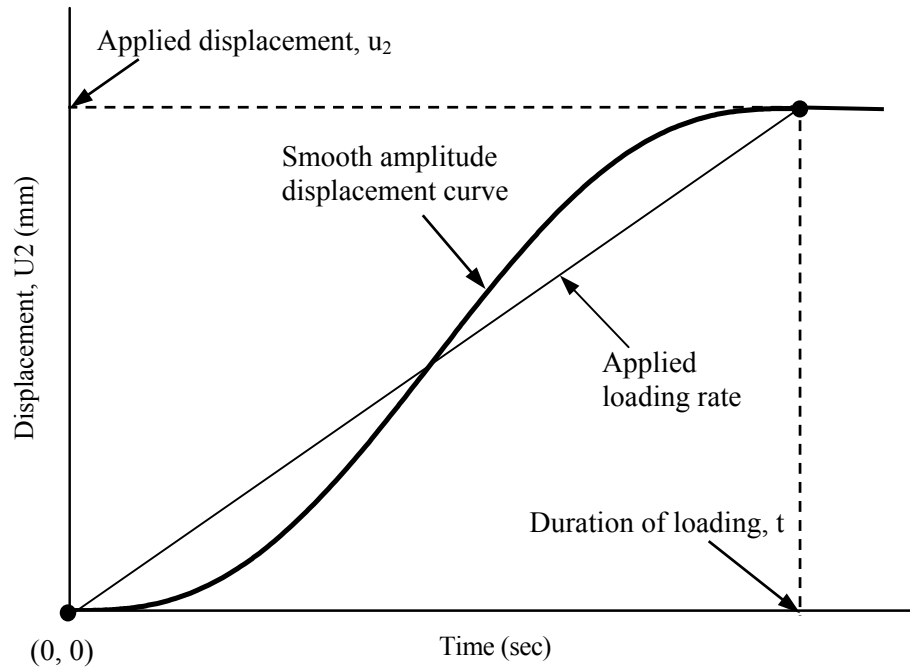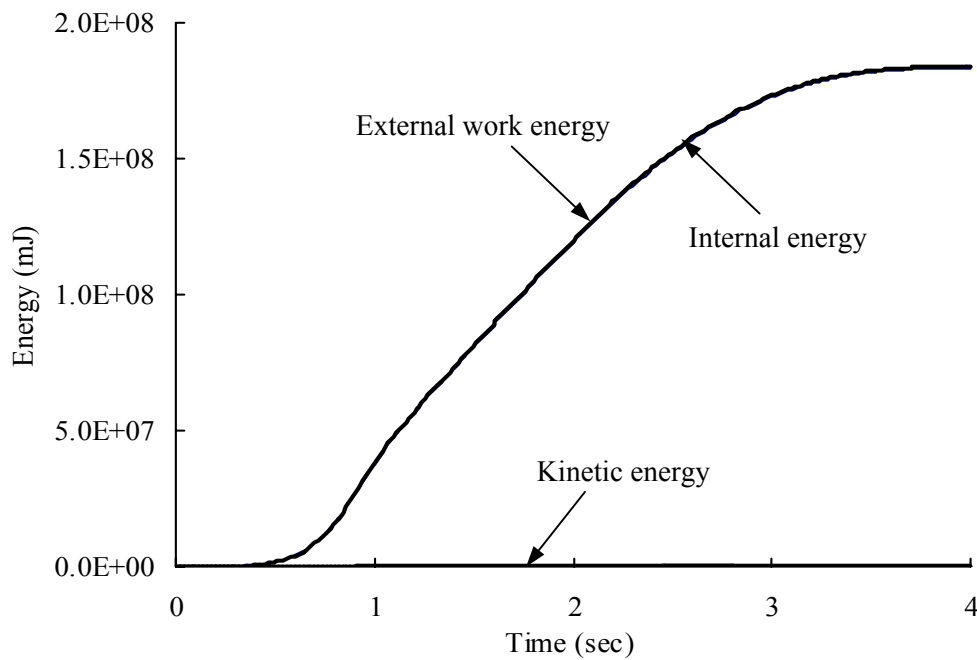**Figure 4.6 Modelling of Local Imperfections (side elevation—exaggerated)**

Figure 4.7 Stress–Strain Curve for Steel used in the Numerical Analysis

(a) Applied loading and smooth amplitude displacement curve

(b) Energy history of a typical column

Figure 4.8 Simulation of Quasi-static Response of PEC Columns using Explicit Dynamic Solution Strategy

5. PERFORMANCE OF FINITE ELEMENT MODELS

5.1 Introduction

The finite element models developed in Chapters 3 and 4 are validated using simulations of 34 PEC column tests reported in the literature (Tremblay et al. 1998; Chicoine et al. 2000; Bouchereau and Toupin 2003; Prickett and Driver 2006). The tests were performed on a wide variety of PEC columns with different geometric and material properties. The descriptions of the geometric and material properties of these test specimens have been presented in Chapter 4. From the finite element analysis of each of these test columns, the predicted load versus deformation response, peak load, peak axial strain and failure mode are obtained and compared with the corresponding experimental results. Moreover, for the eccentrically loaded short columns, comparisons are made between the numerical and experimental load versus second-order bending moment diagram. The axial and transverse stresses in the steel sections of the composite columns at failure are also investigated using the numerical model. In addition, a prediction of the individual contributions of steel and concrete to the total load carrying capacity of the PEC column throughout the loading history is presented for ten of the concentrically loaded test specimens. The finite element model is also used to study the effect of initial local imperfections, link spacing and residual stresses on the column behaviour and thus the sensitivity of the finite element results to these parameters.

5.2 Performance of Small and Extended Models

The small model, described in Chapter 4, was developed at the initial stage of this research with a view to studying the suitability of the concrete material model and contact boundary conditions in predicting the behaviour of these columns under concentric loading. Ten concentrically loaded specimens (C-2 to C-11) tested by Tremblay et al. (1998) and Chicoine et al. (2000) were analyzed using the small model. Among these test columns, specimens C-8 and C-9 had nominally identical size and link spacing, which was intended to check the test reproducibility; hence, a single numerical analysis was

performed for this configuration. The specimens (C-2 to C-11) were also analyzed using the extended model, also described in Chapter 4, which includes one-eighth of the volume of the PEC column. This model was developed to overcome the discrepancy in the peak and post-peak axial strain values in the load versus axial strain response obtained from the numerical analysis using the small model. In the subsequent sections, ultimate capacities and the strains at the peak load, overall axial load versus axial strain behaviours, and failure modes from both analyses are compared with the experimental results. The extended model is further used to study the contributions of steel and concrete to the load carrying capacity of these columns.

5.2.1   Ultimate Capacity and Strain at Peak Load

The ultimate capacities obtained from both the small and extended numerical models are compared with those obtained from the experiments in Table 5.1. For both models, the axial loads at the ultimate point are found to be very close to those observed in the experiments, except in the case of specimen C-10. However, this specimen behaved atypically during the test. Because the link spacing was half that of C-8 and C-9, the specimen should have failed at a load greater than that achieved by C-8 and C-9, as predicted by the numerical model. Instead, the specimen failed prematurely during the test. Excluding specimen C-10, the mean value of the experimental-to-numerical load ratios is 0.98, with a standard deviation of 0.02, from the analyses using the small model and 1.00, with a standard deviation of 0.03, from the analyses performed using the extended model.

Table 5.1 also shows the axial strain values at the ultimate load for both models, along with the ratios of the experimental-to-numerical peak strains. For the small model, the numerically predicted strains at peak loads are found to be higher compared to the experimental values, with an average experimental-to-numerical ratio of 0.73. This low ratio is expected, and it occurs because the strains obtained from the small model are taken only in the failure zone over a height of one-half of the link spacing, whereas in the experiments the average strains were calculated over a gauge length of 2600 mm,

including parts of the end zones constructed with high strength concrete and a closer link spacing. Since these end zones are included in the extended model, numerically predicted axial strains at the ultimate load from this model become very close to the experimental values, with a mean experimental-to-numerical ratio of 1.01. However, the strains predicted using the small model are the actual localized strains at the failure zone of the column.

5.2.2   Load versus Axial Strain Response

Figure 5.1 shows the numerically and experimentally obtained axial loads plotted against the average longitudinal strain for ten of the concentrically loaded specimens (specimens C-2 to C-11). The numerical results obtained from both the small and the extended models are plotted. In general, for both models the initial portions of the numerical load versus strain curves match very well with the experimental ones, though a slight underestimation of the axial stiffness is observed in within the initial portions of the numerical curves for specimens C–3 to C–7. The small model also predicts strains significantly higher than those obtained experimentally, near and after the ultimate point on the load versus strain curve. The reason behind this is the exclusion of the end regions of the test specimens in the small model, as explained in the previous section. However, the finite element analyses using the extended model provide a better representation of the axial strains at the peak as well as in the post-peak descending branch of the experimental load verses axial strain curve. Moreover, in general this model gives a reasonable prediction of the residual capacities after buckling of the steel and crushing of the concrete have taken place, without any numerical difficulties.

The post-peak descending branch of the numerical load versus strain curve obtained from the extended model is observed to be in good agreement with the experimental load versus strain response except for specimen C–6. The experimental response of specimen C–6 after the peak load was significantly different than that observed in other short PEC test specimens. However, this specimen had similar geometric properties to specimen C–3, except for the flange slenderness ratio. Specimen C–6 had the highest b/t

ratio, with a value of 35.4, among the PEC columns selected herein for the finite element investigation. No explanation regarding the dissimilar behaviour of specimen C-6 was reported by Tremblay et al. (1998); however, they reported an explosive failure mode in specimen C–6 as compared to the failures observed in other test specimens, which might have an effect on the deformation readings provided by the instrumentations at the test region of the column after failure.

The ultimate capacities in the PEC columns coincide generally with the occurrences of local buckling and concrete crushing. Near the ultimate point, some fluctuations are observed both in the numerical and experimental responses. This is mainly due to the local buckling of the thin flanges followed by separation of the concrete and steel surfaces. This behaviour is more pronounced in specimens with larger link spacings and higher b/t ratios (e.g., specimens C-6 and C-11). In these specimens, local buckling was observed before the peak load was reached and failure was brittle and explosive, as reported by Chicoine et al. (2000).

5.2.3 Contribution of Steel and Concrete to Load Carrying Capacity

The finite element model is able to isolate the contributions of the steel and concrete in the total load carrying capacity of the PEC columns. The axial load versus strain behaviour of each of these materials in the composite section is shown in Figure 5.1 for specimens C-2 to C-11 (extended model only). In most of the specimens, the loads carried by the steel and concrete are nearly equal up to about the peak load except for the specimens with very thin plates such as specimens C-6 and C-11. These specimens had a b/t ratio greater than 30, which resulted in a reduced contribution of the steel plates to the load carrying capacity as compared to that of concrete. The steel sections of these two specimens also showed lower axial stiffness than the concrete sections in the ascending branch of the load versus average axial strain curves. For all specimens, after the ultimate load point the steel plates carry most of the load as the concrete softens quickly after reaching the crushing strength. However, the post-peak strength decline of the load versus axial strain curve for the PEC column is similar to that of the concrete material.

5.2.4 Failure Mode

The observed failure modes in the numerical analyses with the small and extended models are shown in Figure 5.2. In the numerical analyses, the ultimate capacity was reached through local buckling between two transverse links followed by crushing of the adjacent concrete. In most cases, local buckling and concrete crushing occurred almost simultaneously. However, specimens C-6 and C-11 experienced local buckling before concrete crushing since they had higher b/t ratios and large link spacings. Similar behaviour was observed in the experiments. Figures 5.2 (a) and (b) show the local flange buckling for typical specimens with $s = 1.0d$ (C-4) and $s = 0.5d$ (C-2), respectively. Figures 5.2 (c) and (d) show the local buckling in a typical specimen (C-8) using the extended model with and without the mesh configuration, respectively. The accurate prediction of the failure mode by both finite element models indicates that the defined master–slave contact algorithm with frictional sliding features (as described in Chapter 4) at the interfaces of the steel flange and concrete infill were able to model successfully the separation of the flange and concrete block due to local buckling of the flange plate. However, in the numerical analyses using the small and extended models, no local buckling is observed to occur in the web plate since it is fixed with the adjacent concrete nodes using a tie type of surface constraint. This method of modelling was employed because in the experiments no local buckling was reported in the web plate (Tremblay et al. 1998; Chicoine et al. 2000).

5.3 Performance of Full Model

The full finite element model, including the entire length and cross-section of the column, was developed to predict the column behaviour under compression and bending. The full model has similar characteristics to the extended model. The only difference between them is in the end conditions. The end plates used in the test columns were not modelled in the extended model. They were included in the full model to simplify the load application technique for the eccentrically loaded test columns. The performance of the full model is studied through the reproduction of nine concentrically and 12 eccentrically loaded short PEC columns tested by Chicoine et al. (2000), Bouchereau and Toupin

(2003) and Prickett and Driver (2006). Three long (i.e., slender) PEC test specimens (Chicoine et al. 2000) are also analysed using this model. The results of all these analyses along with the experimental results are presented in the following sections.

5.3.1 Ultimate Capacity and Strain at Peak Load

The performance of the full model in predicting the peak axial load and the corresponding axial strain of the test columns is presented in Tables 5.2 to 5.4. The ratios between the experimental and numerical values for short PEC columns with normal strength concrete (under concentric and eccentric loading) are shown in Table 5.2. The numerical model provides a very good estimation of the peak axial load with experimental-to-numerical ratios ranging from 0.90 (specimen B1-AX) to 1.06 (specimens B1-X1; B2-X1 and B2-Y1), with a mean value of 1.01 and a standard deviation of 0.05. The lower value of the experimental-to-numerical load ratio for specimen B1-AX can be attributed to the premature test failure, as reported by Bouchereau and Toupin (2003). Specimens B1-AX and B2-AX had more than 40 strain gauges embedded in the concrete in the test region of the column. The presence of the gauges and their connecting wires caused discontinuities in the column concrete resulting in premature failure at the location where the wires emerged from the concrete. In spite of the presence of the large number of strain gauges, specimen B2-AX behaved somewhat better than specimen B1-AX in the experiment because of the presence of the additional reinforcements in this specimen.

Although the numerical axial capacity for specimen B2-AX matched very well with its experimental capacity (with experimental-to-numerical peak load ratio of 0.97), the experimental average axial strain at the peak load is underestimated by the numerical model (with experimental-to-numerical ratio of 1.31). The numerical model also underestimates the experimental axial strain at peak axial load for specimen B2-X1 that also had additional reinforcements in the concrete. This discrepancy in strain values may be attributed to the inability of the numerical model to predict the effect of additional longitudinal and tie reinforcements on the axial deformation of these columns. (In spite of

93

this, the model can accurately predict the increase in the ultimate capacity of these columns due to the addition of longitudinal and tie rebars.) On the other hand, the numerical model overestimated the average axial strain at peak axial load for specimens B1–Y1 and B1–Y3. The experimental-to-numerical strain ratios at peak load for these specimens are 0.52 (specimen B1–Y1) and 0.73 (specimen B1–Y3). These two specimens were loaded eccentrically with bending about the weak axis and did not have additional rebars. Bouchereau and Toupin (2003) reported brittle and explosive failure in these specimens during the tests as compared to that observed in identical specimens with additional rebars (i.e., specimens B2–Y1 and B2–Y3, respectively). Hence, the experimental results for these specimens are highly sensitive to imperfect test conditions, as indicated by Bouchereau and Toupin (2003), such as the presence of a slight error on the eccentricity, a manufacturing defect or an error in the installation technique. However, the mean ratio of the experimental-to-numerical average axial strain at peak load for all 12 specimens with normal strength concrete is 0.97, with a standard deviation of 0.20. The relatively high value of standard deviation results from the differences between the numerical and experimental strains for specimens B2-AX, B1-Y1 and B1-Y3 as addressed in this section.

The values of experimental and numerical peak loads and peak strains along with their ratios for PEC columns with high strength concrete are shown in Table 5.3. The results of specimens H6 and H7, which had steel fibre reinforced concrete in the test-region of the column, are included in this table for completeness but are excluded from the mean and standard deviation of the peak load and average strain ratios. The mean value of the peak load for the high strength concrete PEC columns is 0.99, with a standard deviation of 0.03. This indicates the excellent performance of the finite element model in predicting the ultimate capacity of PEC columns with high strength concrete without applying any strength reduction factor to the material capacities obtained from standard cylinder tests, as discussed in Chapter 4.

As shown in Table 5.3 the ratio of the experimental-to-numerical average axial strain at peak load ranged from 0.97 (specimen H11) to 1.28 (specimen H9), with a mean value of

1.09 and a standard deviation of 0.12. Although providing excellent estimates of the peak load, the numerical model is observed to underestimate the axial deformation at peak load by 18, 16 and 28%, respectively, for specimens H3, H8 and H9 with high strength concrete without steel fibres. The possible reason behind this could be the presence of larger confining pressures to the concrete as compared to the other specimens, exerted by closer link spacings in specimen H3 and by the compression flange of specimens H8 and H9, which had bending about the strong axis. This issue is discussed further in Section *5.3.2.1* while describing the load versus axial strain response for the test specimens.

Table 5.4 shows the comparisons between the experimental and numerical results for the three long column specimens. The peak load and corresponding axial strain for each column for the two sets of numerical analyses (one using the applied eccentricity and the other using individual top and bottom eccentricities deduced through measured strain data) are presented. The axial capacities obtained from the numerical analyses of the long PEC test columns with the applied eccentricity were observed to greatly overestimate the experimentally obtained capacities for these specimens. The ratios of the experimental-to-numerical peak load for the applied values of eccentricity for specimens CL-1 and CL-2 are 0.77 and 0.86, respectively. However, these values become close to unity (0.95 for CL-1 and 0.99 for CL-2) when the specimens are analysed with eccentricities deduced from measured strains. In the case of specimen CL-3, both of the numerical analyses were observed to give higher peak loads than that obtained experimentally, although the estimate was improved somewhat using the deduced eccentricities. Specimens CL-3 and CL-1 had the same cross-section and were subjected to nominally concentric loading. However, these two specimens differed in their link spacings—CL-1 had a link spacing of s = 1.0d and CL-3 had s = 0.5d—and specimen CL-3 had additional reinforcement that was not present in CL-1. Therefore, specimen CL-3 would be expected to have a higher capacity than CL-1, but this was not observed in the test. Chicoine et al (2000) reported a premature failure in specimen CL-3 due to the presence of the accidental eccentricities about the weak axis resulting from the misalignment of the specimen prior to the test.

Had this not occurred, the experimental-to-nominal capacity ratio for this specimen would likely have been closer to unity.

The axial strains at peak load for the long PEC columns (Table 5.4) were overestimated by the numerical model in both sets of analyses, with better prediction in the analyses including eccentricities deduced from measured strain data. The sudden and explosive failure mode observed for these specimens that occurs at a strain that is considered sensitive to any imperfect test conditions can result in lower values of experimental strains at failure.

5.3.2   Load versus Axial Strain Response

5.3.2.1   Short PEC Columns with Normal Strength Concrete

Figure 5.3 shows the comparison between the experimental and numerical load versus average axial strain behaviours for four short, concentrically loaded PEC test columns (H1, H2, B1-AX and B2-AX) constructed with normal strength concrete (NSC). The numerical load versus average axial strain curves for specimens H1 and H2 are in excellent agreement with the experimental curves up to the peak load, and the prediction of the post-peak curve for specimen H2 is also excellent. The slight difference between the experimental and numerical peak regions of the load versus strain plot for specimen H2 (Figure 5.3 (b)) is attributed to the presence of a significant inward local flange imperfection, with a maximum amplitude of 1.20 mm, at the middle segment (between two consecutive links) of the column, as reported by Prickett and Driver (2006). As discussed in Chapter 4, the inward local imperfection is expected to improve the capacity of these columns by delaying the occurrence of local buckling. The differences between the experimental and numerical peaks and post-peak responses of specimen B1-AX (Figure 5.3 (c)) are due to the premature test failure, as discussed in Section 5.3.1. For specimen B2–AX, the numerical load versus strain curve, shown in Figure 5.6 (d), is observed to predict lower strains around and after the peak axial load, as compared to the test curve. This discrepancy could be due to the inability of the model to

simulate the confinement effect in the concrete due to the presence of additional reinforcements, also mentioned in Section 5.3.1.

The results of the numerical analysis of eight eccentrically loaded short PEC columns with normal strength concrete are compared with the corresponding experimental results in Figure 5.4. The load versus strain curves for compressive, tensile and average strains are plotted. The numerical behaviours of the specimens subjected to strong axis bending (Figures 5.4 (a) to (d)) are observed to be in good agreement with the experimental responses, but often with somewhat lower strains at the corresponding load near and after the peak load. This difference is amplified in specimens with additional reinforcement (B2-X1 and B2-X3). Since the flanges in columns under strong axis bending undergo the maximum compression, the concrete in these columns is subjected to higher confinement from the surrounding steel section as compared to the concrete in columns under weak axis bending. The presence of additional rebars may also improve the confinement conditions. The study presented in Chapter 3 showed that the damage plasticity model implemented in the current research for modelling the concrete material behaviour can predict the axial deformation of concrete under triaxial compression very well under low confining pressures (0 to 5% of the uniaxial compressive strength). However, the model was found to underestimate the experimental strains near the ultimate point of the stress versus axial strain curve obtained from triaxial compression tests on concrete cylinders for a lateral pressure of 15% of the uniaxial compressive strength of concrete (see Figure 3.7 (c)). The results of Figures 5.4 (a) to (d) tend to indicate that pressures greater than 5% of the concrete strength may have been present. Negligible confining pressure in the concrete of PEC test specimens were reported by Chicoine et al (2000) and Prickett and Driver (2006), based on the transverse strain measurements on the steel flanges and web of the column. The researchers did not provide any value to quantify the confining pressure in the encased concrete of PEC columns based on their experimental investigations. Though the lateral pressure was not quantified in the numerical analysis, the increase in the uniaxial compressive strength of concrete was obtained. For concentrically loaded columns, the increase in the uniaxial compressive strength of concrete was found to be 4% and 1.4%, respectively, for column H1 (s = 0.5d) and

column H2 (s = 1.0d). On the other hand, for eccentrically loaded columns with strong axis bending, the increase in concrete strength ranged from a minimum of 6% (column B1-X3) to a maximum of 15% (column B2-X1), with a mean value of 11%, indicating a more highly confined environment for the concrete, particularly when rebars are added.

The specimens subjected to weak axis bending showed very good agreement between the numerical and the experimental load versus strain responses, as shown in Figures 5.4 (e) to 5.4 (h). In these specimens the concrete on one side is subjected to maximum compression resulting in brittle failure responses, as observed in the tests. The slight differences between the numerical and experimental load versus axial strain curves for these specimens observed around the peak zone can be attributed to the high sensitivity of these tests to any imperfect test conditions, as mentioned in Section 5.3.1.

5.3.2.2   *Short PEC Columns with High Strength Concrete*

The experimental and numerical load versus strain responses for high strength concrete PEC columns (specimens H3, H4 and H5) subjected to axial compression are shown in Figure 5.5. The numerical models for specimen H4 and H5 predicted the experimental response with good accuracy both in the pre-peak and post-peak regions of the load versus average axial strain curves. These two specimens had transverse links of 12.8 mm diameter spaced at s = 0.5d and 15.8 mm diameter spaced at s = 1.0d, respectively. On the other hand, the numerical curve for specimen H3, which had 12.8 mm diameter links spaced at s = 0.3d, did not match well with the experimental curve around and after the peak. One possible explanation for this discrepancy is the less accurate performance of the material model in predicting axial strains of concrete confined under lateral pressures greater than 5% of the uniaxial strength of concrete as mentioned before. Among all the tests performed on PEC columns published in the literature, specimen H3 was the only column that had a link spacing of s < 0.5d. More tests on PEC columns with link spacings less than 0.5d are, therefore, required to propose a proper explanation of the disagreement between the numerical and experimental behaviours for specimen H3.

98

Figure 5.6 represents the performance of the finite element model in predicting the load versus strain behaviour for high strength concrete PEC columns (specimens H8 to H11) subjected to axial compression and bending. For all specimens, in general good agreement is obtained between the numerical and the experimental load versus strain behaviours. However, the axial strains around and after the peak of the load versus axial strain curves for specimens H8 and H9 are underestimated somewhat by the numerical model, which could be due to the reasons discussed in Section *5.3.2.1* for PEC columns with normal strength concrete under strong axis bending.

5.3.2.3   *Short PEC Columns with Steel Fibre Reinforced High Strength Concrete*

The numerical and experimental load versus average axial strain responses for specimens H6 and H7, which were constructed with high strength fibre reinforced concrete, are presented in Figure 5.7. The numerical behaviour for these two specimens is observed to coincide with the experimental behaviour in the pre-peak region of the load versus axial strain curve. Specimen H7 also shows excellent agreement in the post-peak descending branches of the numerical and experimental load versus axial strain plot (Figure 5.7 (b)). However, a slight underestimation of the experimental peak axial load along with a slight overestimation of the experimental residual strength is observed in the numerical behaviour for this specimen. On the other hand, for specimen H6, significant differences are found between the numerical and experimental peak load and the post-peak strength decline zone (Figure 5.7 (a)). The strengths of the test-region concrete used in the numerical analyses for these columns are 49.3 MPa (H6) and 52.9 MPa (H7), which are the test day strengths of the concrete used in these specimens (Prickett and Driver 2006). These values were observed to be lower than the 28-day strength values for the same concrete. In other high strength concrete PEC test specimens (H3 to H5 and H8 to H11), the test day strength was observed to be higher than the 28-day strength by an average of 3.4%. Prickett and Driver (2006) reported that if a similar strength gain were observed in the concrete of specimens H6 and H7, the concrete strength values for these specimens would have been 55.4 MPa and 60.2 MPa, respectively. If the finite element analyses

were conducted with these speculated values it would result in a somewhat better representation of the peak zone in the curves shown in Figure 5.7, especially for specimen H6. However, more tests on PEC columns with high strength fibre reinforced concrete would be helpful to judge the suitability of the concrete model used in the numerical analysis in predicting the behaviour of these columns.

5.3.2.4   *Long PEC Columns with Normal Strength Concrete*

The numerical results of three long PEC column test specimens along with their experimental responses are shown in Figure 5.8. Normal strength concrete was used in the test region of these columns. As mentioned before, two sets of numerical analyses were performed for each of the long test columns, one using the applied eccentricity and the other using the eccentricities deduced from strains measured during the test. For specimens CL-1 and CL-2, the test load versus strain response is observed to be close to the numerical response using the deduced eccentricities. On the other hand, in case of specimen CL-3, neither of the two numerical analyses is observed to predict the experimental behaviour well, yet the response with the deduced eccentricities is much closer to the experimental response. However, for all three long columns the numerical model gave an accurate prediction of the initial axial stiffness observed in the experimental load versus strain curve. For all three specimens the axial strains at and after the peak load point are observed to be higher in the numerical models as compared to those obtained experimentally. The behaviour of the slender columns tends to be sensitive to loading and geometric imperfections present in the test. More tests on slender PEC columns are, therefore, required to explain the differences between the numerical and experimental results shown in Figure 5.8.

5.3.3   Failure Mode

In general the failure of all of the short PEC column specimens in the numerical analyses using the full model occurred due to concrete crushing combined with local buckling of the steel flanges between two transverse links. Figure 5.9 shows the failure modes for typical concentrically and eccentrically loaded specimens with strong and weak axis

bending. Since the column cross-section in the numerical model is perfectly symmetric, local buckling in a concentrically loaded column is observed to occur on all four sides of the unsupported flange (i.e., between two consecutive links) in the middle segment of the column. On the other hand, local buckling is observed in the flange plates on the compression side only of the eccentrically loaded columns. In all cases the failure mode matched well with that observed in the experiments, as shown in Figure 5.10.

The occurrence of local buckling with respect to the peak load point is also studied with the numerical model for the test columns and compared with the experimental observations. Specimens H1, H2, B1–AX and B2–AX, which were all constructed with normal strength concrete and loaded under concentric axial compression, experienced local buckling at the peak axial load along with crushing of the concrete. Neither in the numerical analyses nor in the tests conducted on these specimens did local buckling occur before the peak load had been reached. The eccentrically loaded normal strength concrete PEC columns showed behaviour similar to the concentrically loaded columns both numerically and experimentally in that both local buckling and crushing of the concrete occurred at the peak axial load.

The numerical model for concentrically loaded high strength concrete PEC test specimens (column H3 to H7, with b/t = 25 and link spacings ranging from 0.3d to 1.0d) tested by Prickett and Driver (2006) exhibited concrete crushing at the peak load followed by local buckling of the flanges. However, specimen H5, which had a link spacing of 1.0d experienced local buckling and concrete crushing simultaneously at the peak load. On the other hand, the peak load of the eccentrically loaded high strength concrete PEC columns was attained through crushing of concrete and local buckling took place after the peak load.

In the numerical analyses using the full model, the web plate was also observed to experience local buckling eventually, which was not reported in the tests. However, in the test specimens it is not possible to see the web buckling unless all the concrete has been removed to expose the web plate. In all of the numerical analyses conducted on short

columns, local buckling in the web plate occurred only after the capacity had dropped to its residual strength. In the full model no constraint was imposed on the nodes in the web plate; the movement of the web plate is therefore restrained only by the adjacent concrete elements. However, after undergoing substantial crushing the concrete elements have insufficient stiffness to prevent the web plate from buckling locally in the numerical simulation. To examine the impact of this, additional finite element analyses were performed by fixing the web plate with the concrete in a similar way as applied in the small and extended models. This prevented the web from buckling locally but increased the capacity of the composite section significantly (around 10% of the strength obtained without applying the constraint). Again, contact constraints could have been defined at the interfaces of web and concrete, but this would make the model computationally very expensive. Since the local buckling of the web plate is not governing the behaviour of these columns at failure it was decided that no constraint would be applied to the web plate.

In the numerical analysis of slender columns, failure occurred due to global bending of the column about the weak axis accompanied by local flange buckling and concrete crushing (see Figure 5.11 (a)). Similar behaviour, as shown in Figure 5.11 (b), was observed in the experiments. Moreover, in the test the failure was brittle and explosive as reported by Chicoine et al. (2000). The numerical model also experienced brittle failure as observed in the post-peak descending branch of the load versus strain curves (see Figure 5.8).

5.3.4 Load versus Moment Response

For the eccentrically loaded test columns the load versus moment diagrams are plotted from the numerical results and compared with the corresponding diagrams obtained from the experiments. Figure 5.12 shows the numerical load versus moment curves along with the experimental load capacity and concurrent moment for the eight columns (with normal strength concrete) tested by Bouchereau and Toupin (2003) under monotonic eccentric axial loading. The numerical moments are the applied load multiplied by the

102

sum of the initial load eccentricity and the lateral displacement at the column mid-height. However, this direct calculation could not be performed to determine the associated experimental moments for these columns. Bouchereau and Toupin (2003) measured the lateral displacements of only two test specimens out of the 22 tests performed on eccentrically loaded PEC columns. Of these, one (specimen B2–X2) had additional reinforcement and was subjected to eccentric cyclic loading with strong axis bending, and the other, (specimen B1–Y2) was subjected to eccentric cyclic loading with weak axis bending and did not have any additional reinforcements. However, these specimens were not analysed since the current study is confined to monotonic loading conditions only. Based on the lateral displacements obtained from those two test specimens, Bouchereau and Toupin (2003) reported that the lateral displacement at the mid-height of the column at the peak load corresponds to 6% of the initial load eccentricity. Since all the columns tested by Bouchereau and Toupin (2003) had nominally identical cross-sections and nearly identical material properties, they suggested using a lateral displacement of 0.06 times the initial eccentricity to obtain the second order moment at the peak load for all test columns, as shown in Figures 5.12(a) to (d). Bouchereau and Toupin (2003) also considered a linear relationship between the load and the bending moment. If the actual lateral displacements at each load level were known the expected curvature in the experimental load versus moment responses would have been very similar to the numerical curves shown in Figure 5.12.

Figure 5.13 presents the numerical and experimental load versus moment curves for short eccentrically loaded PEC columns with high strength concrete (specimens H8 to H11) tested by Prickett and Driver (2006) for both strong and weak axis bending. The lateral displacements of these test specimens were measured during the test and were added to the initial eccentricity to calculate the second order bending moment at each load level. The numerical moments also include the second order effects resulting from the lateral displacements at the column mid-height. For all four specimens, excellent agreement was observed between the numerical and the experimental load versus moment curves over the entire loading histories. This demonstrates the ability of the numerical model to

predict the behaviour of PEC columns accurately when they are subjected to both axial compression and flexure.

5.4 Axial and Transverse Stresses in the Steel Section

The axial stresses in the flanges and web plates and the transverse links, along with the transverse stresses in the steel plates, at or near the peak load are studied for the test specimens using the finite element model. In general, the flanges and web plate reached the yield strength at or shortly before reaching the peak load. The PEC test columns with larger link spacings or thinner flanges were observed to experience yielding of the steel plates earlier as compared to the columns with closer links or thicker flanges. No yielding of the transverse links was observed before the peak load had been reached. In the concentrically loaded columns, at the peak axial load, axial stress in the transverse links ranged from 51% (specimen C-8) to 79% (specimen H-7) of the yield stress. The link stresses in the eccentrically loaded columns where generally higher than those found in the concentrically loaded columns but were still observed to be less than 85% of the yield strength. The transverse stresses in the steel plates were negligible (less than 8% of the yield strength). All these findings are consistent with observations from the experimental investigations by Chicoine et al. (2000) and Prickett and Driver (2006). However, a detailed study of the stress history and stress distribution in the composite cross-section was not performed in the current study since the main interest was to examine the global behaviour of PEC columns with normal and high performance materials under various loading conditions.

5.5 Effect of Local Flange Imperfections on Ultimate Capacity

Numerical analyses using the full column model were performed on three test specimens (C-2, C-8 and C-11) to study the effect of both inward and outward local imperfections in the flange plates (described in Chapter 4) on the axial capacity of these columns. These three specimens were selected to observe this effect for different link spacings and flange slenderness ratios. The results are presented in Table 5.5. As observed for specimen C-2 (b/t =23, s = 0.5d), inward imperfections with a maximum amplitude, δ_m, of 1 mm

increase the capacity by only 0.69 %, whereas the same amplitude of outward imperfection results in a 1.19 % reduction in the ultimate capacity. For specimen C-8, which has the same flange slenderness ratio as specimen C-2 but a link spacing of s = 1.0d, inward imperfections of 2 mm (which is analogous to 1 mm for the s = 0.5d spacing) results in a 0.36 % increase in capacity and the same amplitude of outward imperfection decreases the capacity by 2.03 %. The ultimate capacity of specimen C-11, which has the same link spacing as specimen C-8 but a higher flange slenderness ratio (b/t = 31), is decreased by 3.78 % for an outward imperfection of 2 mm. On the other hand, the same amount of inward imperfection increases the capacity of this specimen by only 0.53 %. The results using larger amplitudes of imperfection are also shown in Table 5.5 for comparison, although these are generally much larger than those measured on the test specimens. Specimens with a link spacing equal to the depth of the column and higher flange slenderness ratios are, therefore, more vulnerable to the effects of outward local imperfections.

For all the three specimens, the increase in capacity arising from any reasonable inward imperfection is considered negligible. Moreover, since the local flange imperfections observed in the test specimens considered in this study (Chicoine et al. 2002), as well as those of other specimens (Prickett and Driver 2006), were nearly all inward, it is reasonable to exclude the modelling of these local imperfections from the finite element model of PEC columns.

5.6 Effect of Link Spacing

The spacing of the transverse links, which is also the unsupported length of the flange plates, has a significant effect on the behaviour of PEC columns, as reported by all PEC column researchers. It has been found from the experiments that the specimens with a link spacing equal to half of the column depth exhibited gradual failure as compared to those with a link spacing equal to the column depth. The same behaviour, as shown in Figure 5.14, is observed in the numerical analyses for concentrically loaded specimens with 1.0d and 0.5d link spacings. The comparisons between axial load versus strain

behaviour for specimens C-2 and C-4 and for specimens C-8 and C-10 are shown in Figures 5.14 (a) and (b), respectively. All the geometric and material properties for the specimens in each set are nominally identical except the link spacing. The link spacings in specimens C-2 and C-10 are half of those in specimens C-4 and C-8, respectively.

The concrete behaviour near the peak load is slightly affected by link spacing, as shown in Figure 5.14. The strains in specimens C-4 and C-8 at the ultimate concrete load are lower than those in specimens C-2 and C-10 by 13% and 15%, respectively. This in an indication of a somewhat greater loss in confinement in the encased concrete (after the occurrence of local buckling in the thin plates) in PEC columns with $s = 1.0d$ as compared to columns with $s = 0.5d$. The effect of link spacing is more apparent in the load versus axial strain plots for the steel sections of the composite columns. The steel sections for specimens C-2 and C-10 show a gradual drop in capacity as compared to the sudden loss observed in specimens C-4 and C-8.

5.7 Effect of Residual Stresses

The effect of residual stresses in the steel plates on the peak load and average axial strain at peak load is presented in Table 5.6 for nine test specimens (H3 to H11). Two sets of analyses were performed on these specimens using the full column finite element model: including and excluding the residual stresses. The residual stress distribution implemented in the numerical model for these specimens (400 mm×400 mm×7.95 mm sections) was that of specimen C-2 (450 mm×450 mm×9.5 mm section) tested by Tremblay et al. (2000b). No significant change is observed in the ultimate axial capacity and axial strain at the ultimate point of these specimens due to the presence of residual stresses. The load versus axial strain behaviour is also unaffected by these stresses as shown in Figure 5.15 for two typical specimens (H4 and H7). Since local buckling of the thin plates and the load carrying capacity of the concrete infill mainly govern the behaviour of PEC columns, the residual stresses do not significantly affect the load versus deformation response. For this reason, residual stresses do not need to be included in the model to obtain accurate numerical simulations.

106

5.8 Summary

The performance of the finite element models in predicting the behaviour of a variety of PEC columns tested under concentric and eccentric loading can be summarised as follows:

- The small model, developed at the initial stage of the study was observed to predict the ultimate axial capacity and the failure mode of short PEC columns accurately. However, since the model only includes the failure zone of the test specimen, it overestimates the experimental peak and post-peak response of the load versus axial strain curve. The extended model was able to eliminate this discrepancy and was able to trace a stable, complete and fairly accurate load–strain history for this column under uniaxial compression.

- The full finite element model, used to reproduce both concentrically and eccentrically loaded PEC test specimens, was able to reproduce the experimental behaviour with good accuracy. The peak load, axial deformation at the peak load, post-peak behaviour, axial load versus moment relationship and the failure mode observed in the tests are all predicted very well by this model.

- The dynamic explicit solution strategy used in the finite element models made it possible to trace the full behavioural history of this composite column without any numerical difficulties.

- The interaction between the steel and concrete and their separation at the common interface due to the local instability of the flange is successfully modelled with the contact pair algorithm.

- The stress versus strain relationships used for normal and high strength concrete can satisfactorily predict the behaviour of short PEC columns under both concentric and eccentric loading.

- No concrete strength reduction factor is required in the numerical material model for high strength concrete PEC columns and the factor recommended by Chicoine et al. (2000) provides good results for PEC columns with normal strength concrete.

- The effects of different link spacings on the behaviour of these columns are captured adequately in the finite element model.

- The ultimate capacity of the column is not affected significantly by the presence of inward local imperfections. Since the measured imperfections were inward and small, they can be omitted from finite element models of these columns.

- Residual stresses in the steel section of the composite column have a negligible effect on the column behaviour and can therefore be omitted from finite element models of these columns.

Table 5.1 Performance of Small and Extended Models

Specimen designation	Peak axial load			P_{exp}/P_{num}		Axial strain at peak load			$\varepsilon_{exp}/\varepsilon_{num}$	
	Numerical		Exp.			Numerical		Exp.		
	Small model	Extended model		Small model	Extended model	Small model	Extended model		Small model	Extended model
	P_{num} (kN)	P_{num} (kN)	P_{exp} (kN)			ε_{num} ($\mu\varepsilon$)	ε_{num} ($\mu\varepsilon$)	ε_{exp} ($\mu\varepsilon$)		
C-2	10300	10230	10100	0.98	0.99	2930	2270	2305	0.79	1.02
C-3	9970	9920	9650	0.97	0.97	2620	1985	1920	0.73	0.97
C-4	9490	9190	9390	0.99	1.02	2545	1650	1695	0.67	1.03
C-5	10600	10350	10000	0.94	0.97	2935	2265	2330	0.79	1.03
C-6	8020	8100	7650	0.95	0.94	2330	1810	1765	0.76	0.97
C-7	4260	4110	4280	1.00	1.04	2790	2210	2140	0.77	0.97
C-8	17150	16540	16470	0.96	1.00	2655	1685	1845	0.70	1.10
C-9	17150	16540	16610	0.97	1.00	2655	1685	1770	0.67	1.05
C-10	18160	18030	16240	0.89	0.90	2630	2360	2255	0.86	0.96
C-11	14670	14280	14930	1.02	1.05	2655	1870	1810	0.68	0.97
Mean[a]				0.98	1.00				0.73	1.01
SD[a]				0.02	0.03				0.05	0.05

[a] Excluding specimen C-10 which failed prematurely

Table 5.2 Comparison of Numerical and Experimental Results of Columns with Normal Strength Concrete

Specimen design.	Eccentricity		Peak axial load		P_{exp}/P_{num}	Avg. axial strain at peak load		$\varepsilon_{exp}/\varepsilon_{num}$
			Num.	Exp.		Num.	Exp.	
	e_x	e_y	P_{num}	P_{exp}		ε_{num}	ε_{exp}	
	(mm)	(mm)	(kN)	(kN)		($\mu\varepsilon$)	($\mu\varepsilon$)	
H1	---	---	7290	7383	1.01	2510	2770	1.10
H2	---	---	7355	7573	1.03	2013	2081	1.03
B1-AX	---	---	9740	8800	0.90	2150	2000	0.93
B2-AX	---	---	10350	10064	0.97	2335	3056	1.31
B1-X1	142	---	5350	5650	1.06	1840	1789	0.97
B2-X1	143	---	5560	5920	1.06	1920	2233	1.16
B1-X3	33	---	8320	8280	1.00	1862	1856	1.00
B2-X3	33	---	8730	9040	1.04	2075	2111	1.02
B1-Y1	---	84	5150	5130	1.00	1370	717	0.52
B2-Y1	---	91	5150	5460	1.06	1389	1300	0.94
B1-Y3	---	23	7970	7460	0.94	1840	1348	0.73
B2-Y3	---	23	8400	8710	1.04	1911	1856	0.97
Mean					1.01			0.97
SD					0.05			0.20

Table 5.3 Comparison of Numerical and Experimental Results of Columns with High Strength Concrete

Specimen design.	Eccentricity		Peak axial load		P_{exp}/P_{num}	Avg. axial strain at peak load		$\varepsilon_{exp}/\varepsilon_{num}$
			Num.	Exp.		Num.	Exp.	
	e_x	e_y	P_{num}	P_{exp}		ε_{num}	ε_{exp}	
	(mm)	(mm)	(kN)	(kN)		($\mu\varepsilon$)	($\mu\varepsilon$)	
H3	---	---	12450	12340	0.99	2890	3420	1.18
H4	---	---	12150	11860	0.98	2810	2835	1.01
H5	---	---	12160	12390	1.02	2890	2905	1.00
H6	---	---	11000	12180	1.11	2590	3005	1.16
H7	---	---	11200	11890	1.06	2700	2830	1.05
H8	23	---	10700	10920	1.02	2290	2650	1.16
H9	100	---	7160	7260	1.01	1590	2040	1.28
H10	---	25	10100	9740	0.96	1820	1895	1.04
H11	---	74	6840	6370	0.93	1330	1290	0.97
Mean[b]					0.99			1.09
SD[b]					0.03			0.12

[b] Excluding specimens H6 and H7 with steel fibre reinforced concrete

Table 5.4 Comparison of Numerical and Experimental Results for Long Columns

Specimen design.	Eccentricity[c]		Peak axial load		P_{exp}/P_{num}	Avg. axial strain at peak load		$\varepsilon_{exp}/\varepsilon_{num}$
	(about weak axis)		Num.	Exp.		Num.	Exp.	
	e_{top}	e_{bottom}	P_{num}	P_{exp}		ε_{num}	ε_{exp}	
	(mm)	(mm)	(kN)	(kN)		($\mu\varepsilon$)	($\mu\varepsilon$)	
CL-1	0	0	9650	7440	0.77	1770	1187	0.67
	20	10	7840		0.95	1390		0.85
CL-2	28	28	6610	5700	0.86	1150	904	0.79
	45	35	5770		0.99	1020		0.89
CL-3	0	0	10300	6670	0.65	1962	1060	0.54
	35	-5	7770		0.86	1590		0.67

[c] Applied eccentricities listed first

Table 5.5 Effect of Local Imperfections on Ultimate Capacity

Specimen designation	δ_m [(d)]	P_{num}	Increase in strength
	mm	kN	%
	-3	10000	1.01
C-2	-1	9970	0.69
b/t=23	0	9900	0
s=d/2=225 mm	1	9780	-1.19
	3	9660	-2.48
	-6	17360	0.59
C-8	-2	17330	0.36
b/t=23	0	17260	0
s=d=600 mm	2	16910	-2.03
	6	16570	-4.04
	-6	15270	1.04
C-11	-2	15190	0.53
b/t=31	0	15110	0
s=d=600 mm	2	14540	-3.78
	6	14360	-4.96

[(d)] Negative values indicate inward imperfections

Table 5.6 Effect of Residual Stress on Peak Axial Load and Average Axial Strain at Peak Load

Specimen design.	Peak axial load			P_{exp}/P_{num}		Average axial strain at peak load			$\varepsilon_{exp}/\varepsilon_{num}$	
	Numerical		Exp.	with residual stress	without residual stress	Numerical		Exp.	with residual stress	without residual stress
	with residual stress	without residual stress				with residual stress	without residual stress			
	P_{num} (kN)	P_{num} (kN)	P_{exp} (kN)			ε_{num} (με)	ε_{num} (με)	ε_{exp} (με)		
H3	12450	12475	12335	0.99	0.99	2890	2840	3420	1.18	1.20
H4	12155	12180	11863	0.98	0.97	2810	2800	2835	1.01	1.01
H5	12160	12016	12388	1.02	1.03	2890	2730	2903	1.00	1.06
H6	10995	11040	12183	1.11	1.10	2590	2610	3003	1.16	1.15
H7	11200	11190	11891	1.06	1.06	2700	2600	2828	1.05	1.09
H8	10700	10790	10924	1.02	1.01	2290	2280	2652	1.16	1.16
H9	7160	7120	7259	1.01	1.02	1590	1540	2041	1.28	1.33
H10	10100	10400	9736	0.96	0.94	1820	1805	1893	1.04	1.05
H11	6840	6930	6369	0.93	0.92	1330	1330	1292	0.97	0.97
Mean				1.01	1.01				1.10	1.11
SD				0.05	0.06				0.10	0.11
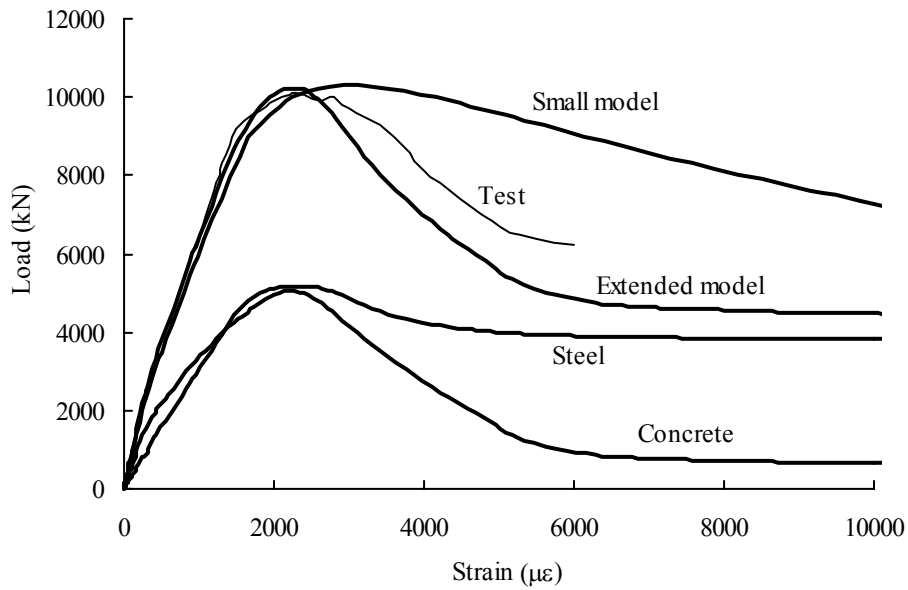
(a) Specimen C-2 (Tremblay et al. 1998)
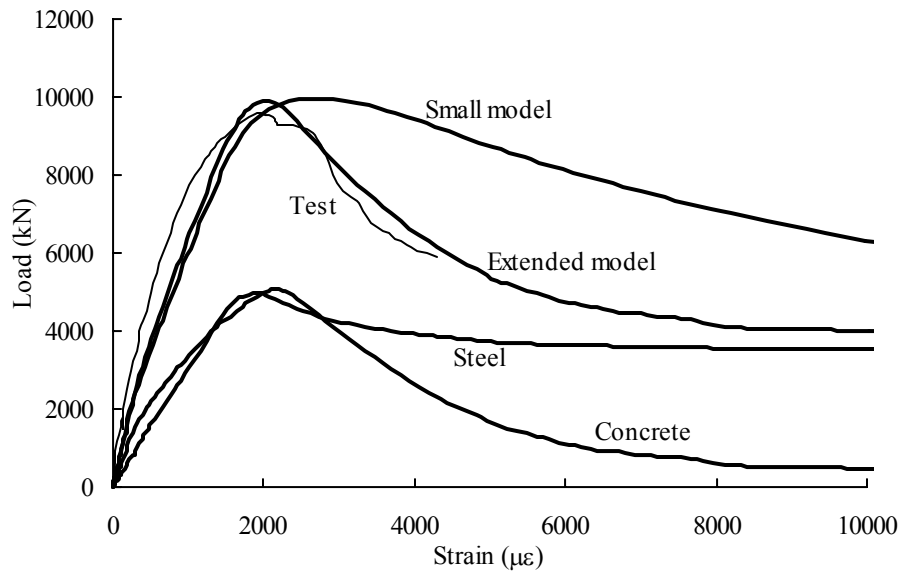
(b) Specimen C-3 (Tremblay et al. 1998)

**Figure 5.1 Experimental and Numerical Load versus Axial Strain Behaviour Using
Small and Extended Models**

114
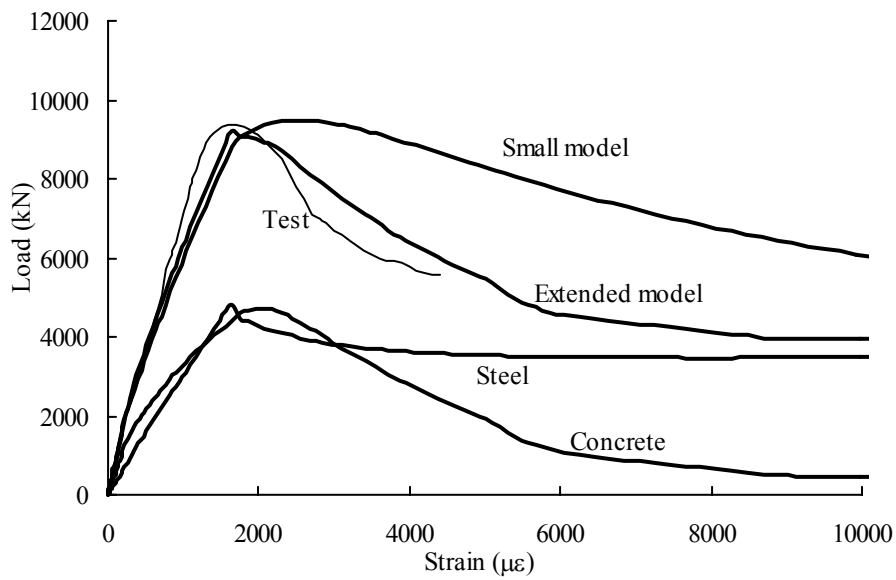
(c) Specimen C-4 (Tremblay et al. 1998)
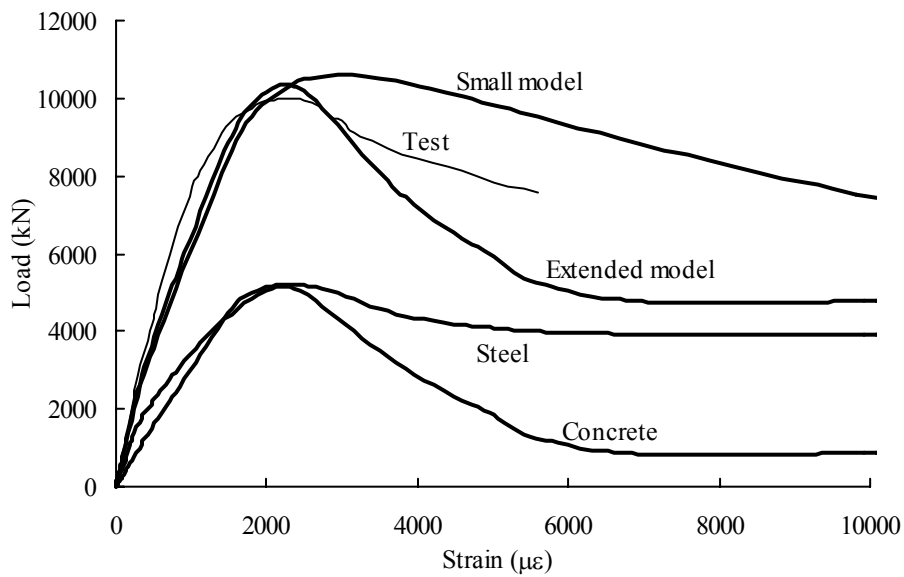
(d) Specimen C-5 (Tremblay et al. 1998)

Figure 5.1 (cont.) Experimental and Numerical Load versus Axial Strain Behaviour Using Small and Extended Models

115
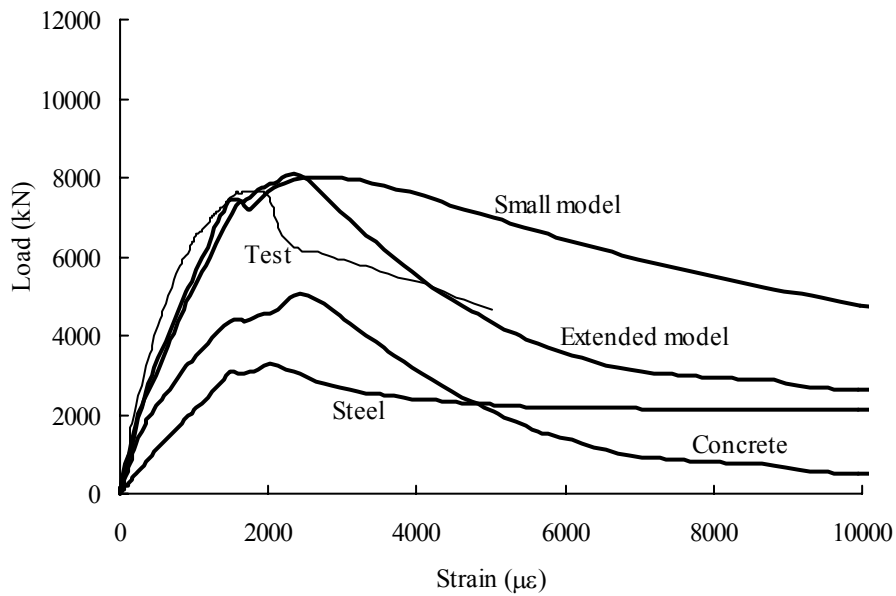
(e) Specimen C-6 (Tremblay et al. 1998)
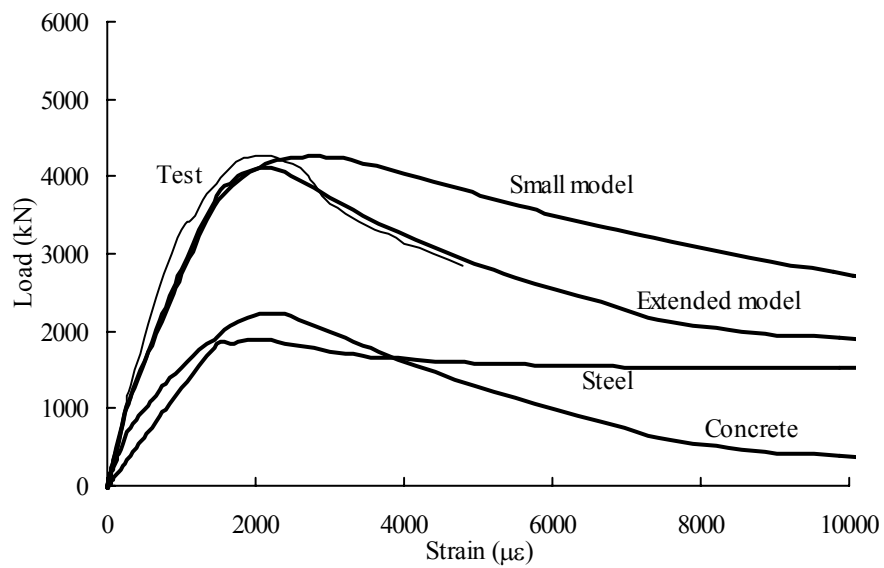
(f) Specimen C-7 (Tremblay et al. 1998)

Figure 5.1 (cont.) Experimental and Numerical Load versus Axial Strain Behaviour Using Small and Extended Models
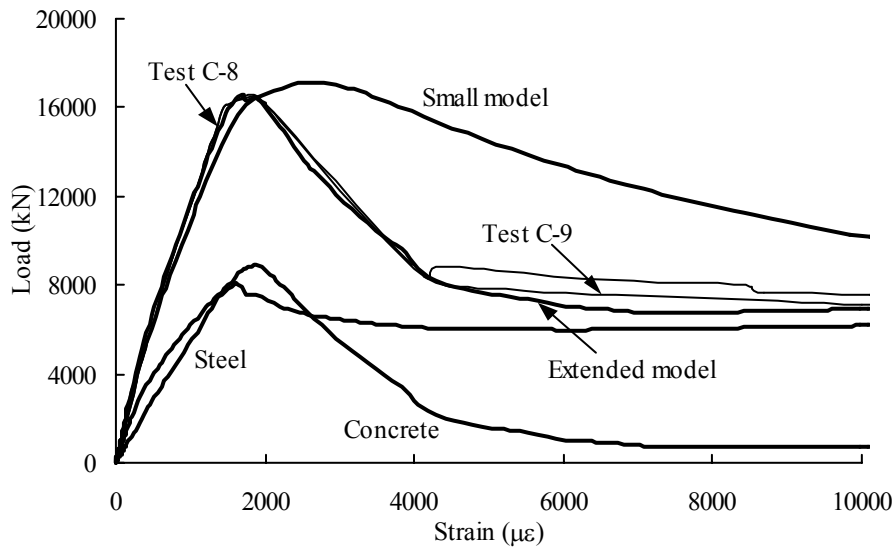
(g) Specimen C-8 and C-9 (Chicoine et al. 2002)
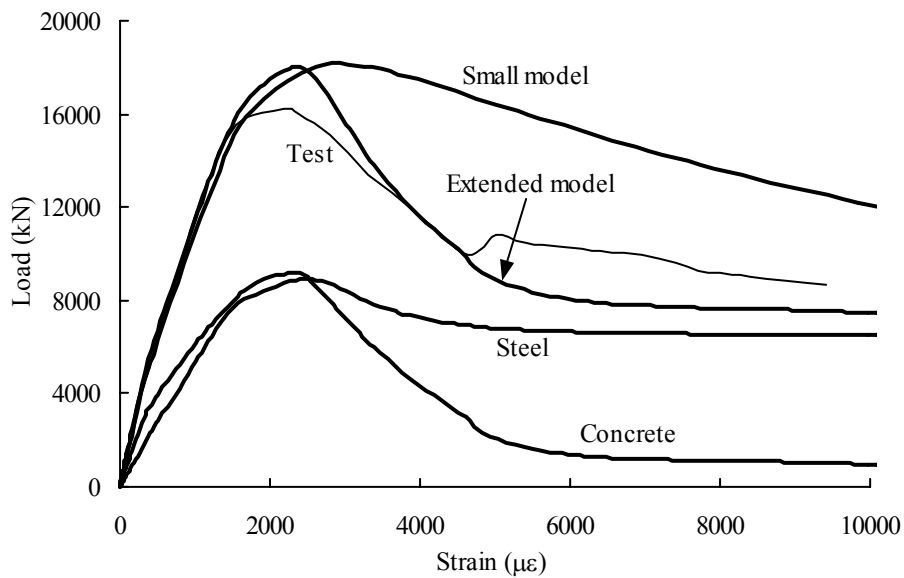
(h) Specimen C-10 (Chicoine et al. 2002)

Figure 5.1 (cont.) Experimental and Numerical Load versus Axial Strain Behaviour Using Small and Extended Models

117
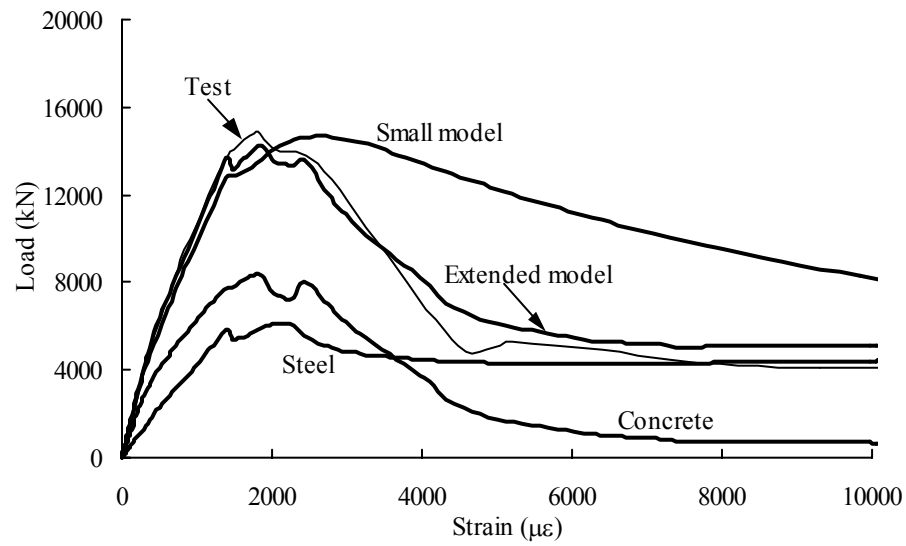
(i) Specimen C-11 (Chicoine et al. 2002)

Figure 5.1 (cont.) Experimental and Numerical Load versus Axial Strain Behaviour Using Small and Extended Models
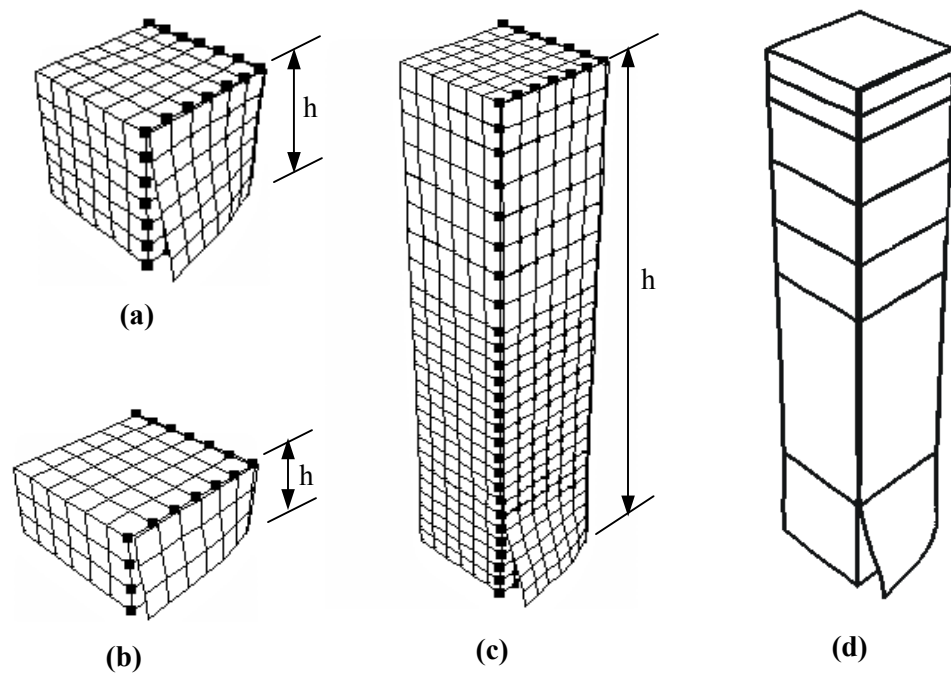
Figure 5.2 Failure Modes, (a) Small Model (h=s/2=d/2); (b) Small Model (h=s/2=d/4); (c) Extended Model (h=2.5s=2.5d) and (d) Extended Model (without displaying the mesh).
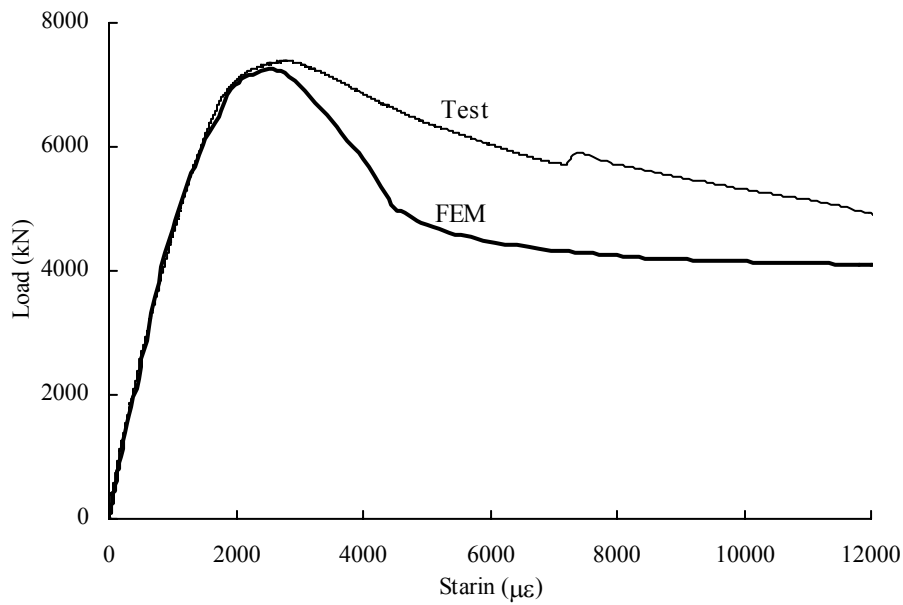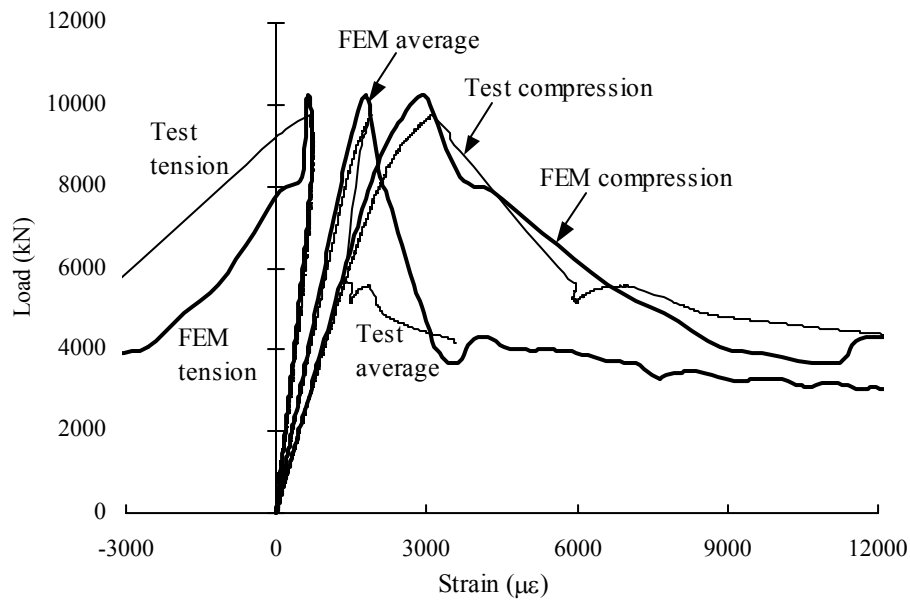
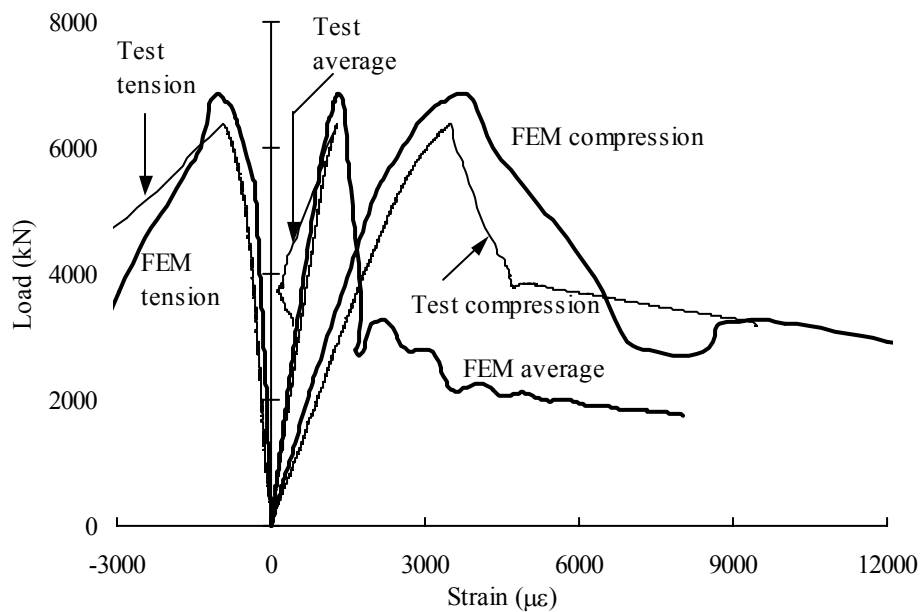**(a) Specimen H1 (Prickett and Driver 2006)**
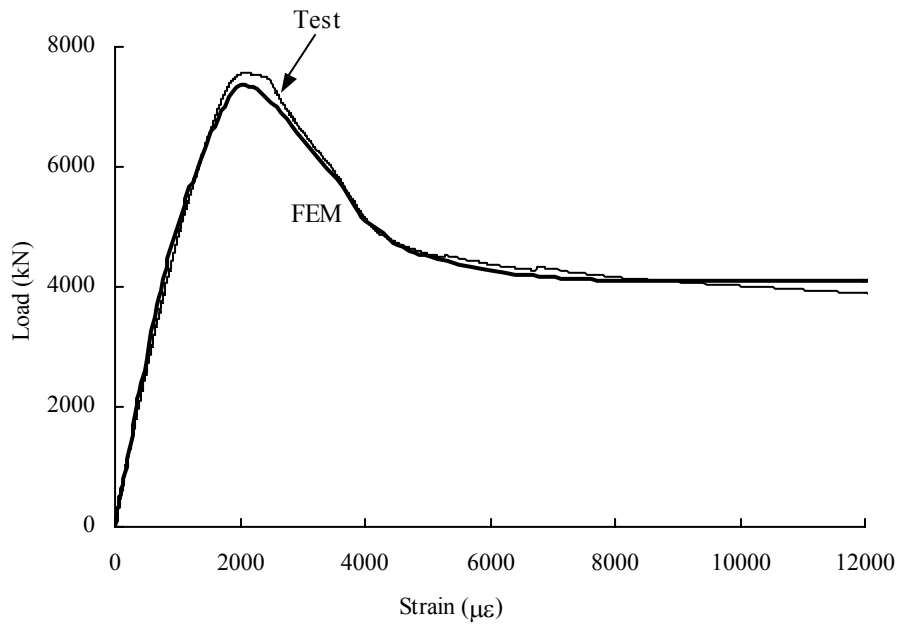
(b) Specimen H2 (Prickett and Driver 2006)

Figure 5.3 Experimental and Numerical Load versus Strain Behaviour (using Full Model) for Concentrically Loaded Short PEC Columns with NSC
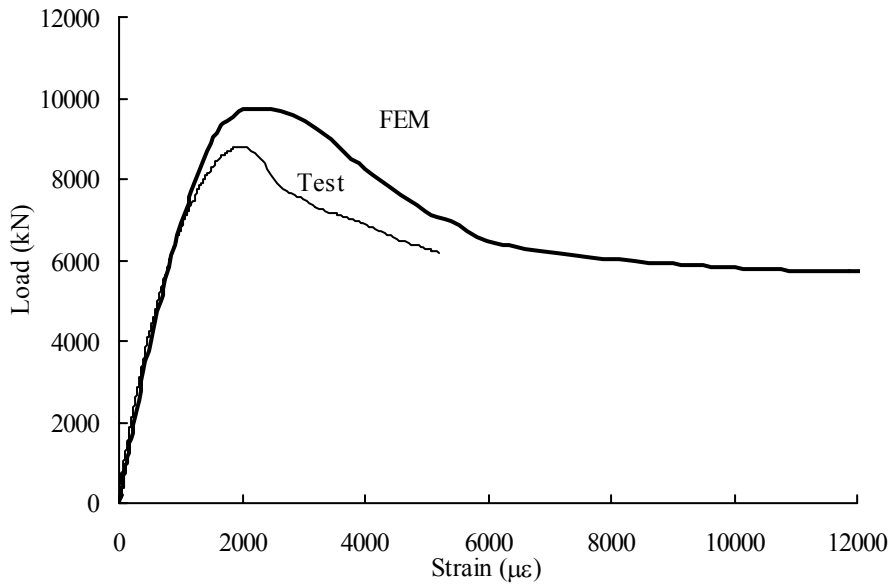
(c) Specimen B1-AX (Bouchereau and Toupin 2003)
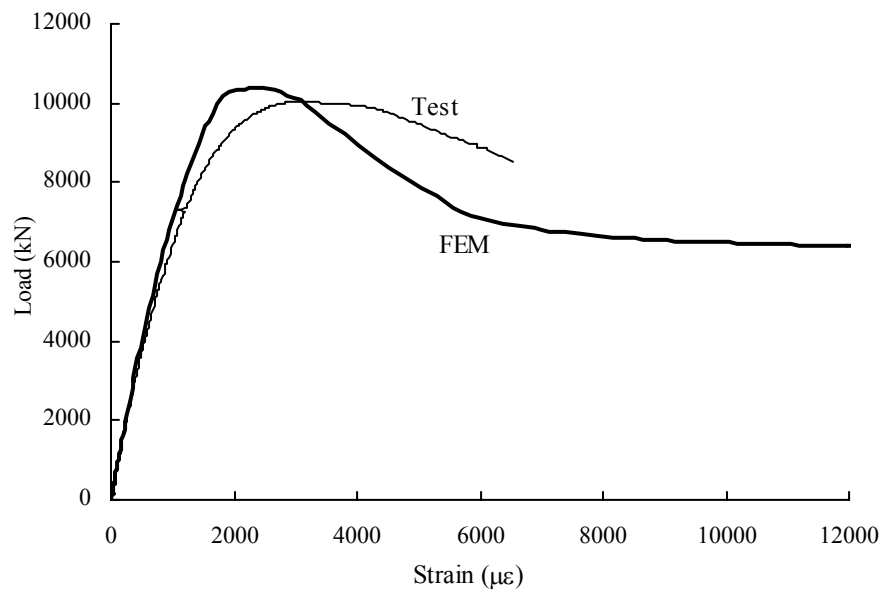
(d) Specimen B2-AX (Bouchereau and Toupin 2003)

Figure 5.3 (cont.) Experimental and Numerical Load versus Strain Behaviour (using Full Model) for Concentrically Loaded Short PEC Columns with NSC
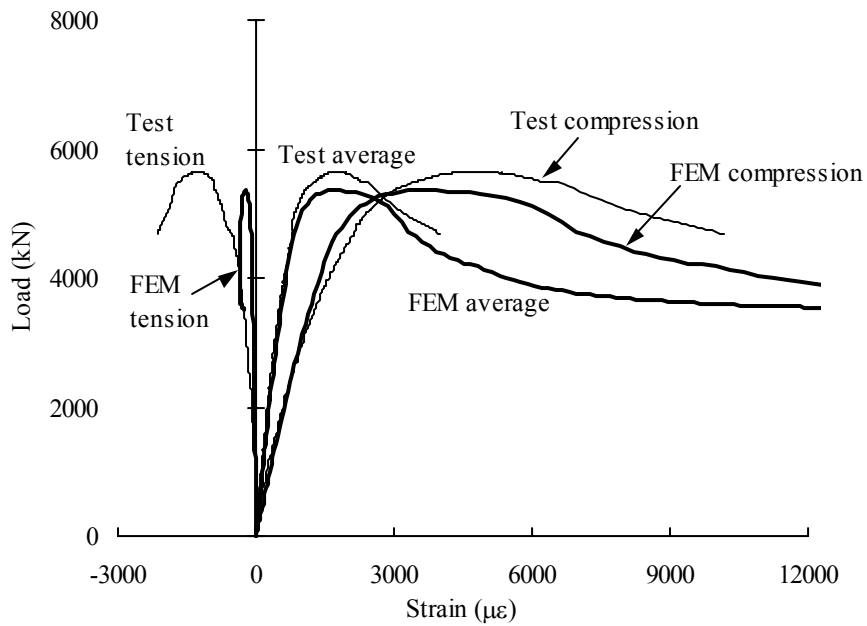
(a) Specimen B1-X1 (Bouchereau and Toupin 2003)
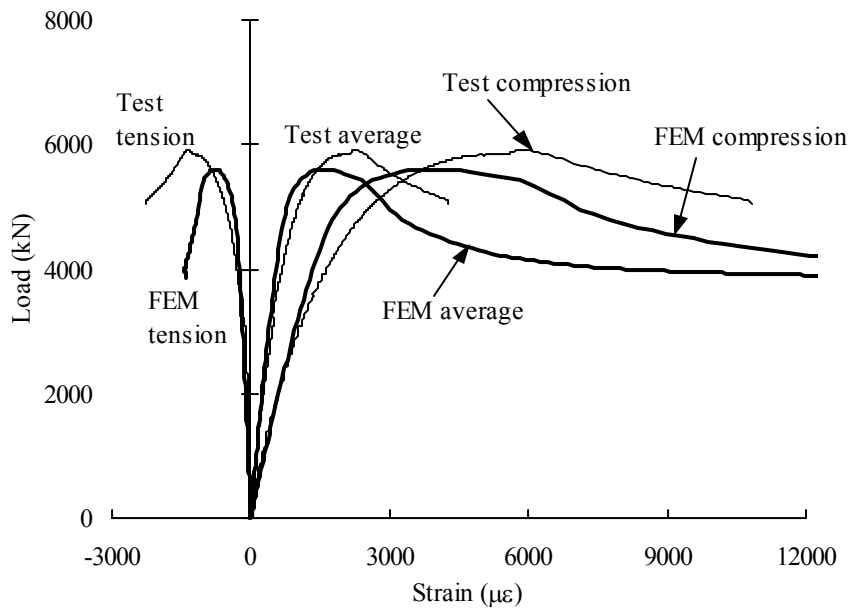
(b) Specimen B2-X1 (Bouchereau and Toupin 2003)

Figure 5.4 Experimental and Numerical Load versus Strain Behaviour (using Full Model) for Eccentrically Loaded Short PEC Columns with NSC
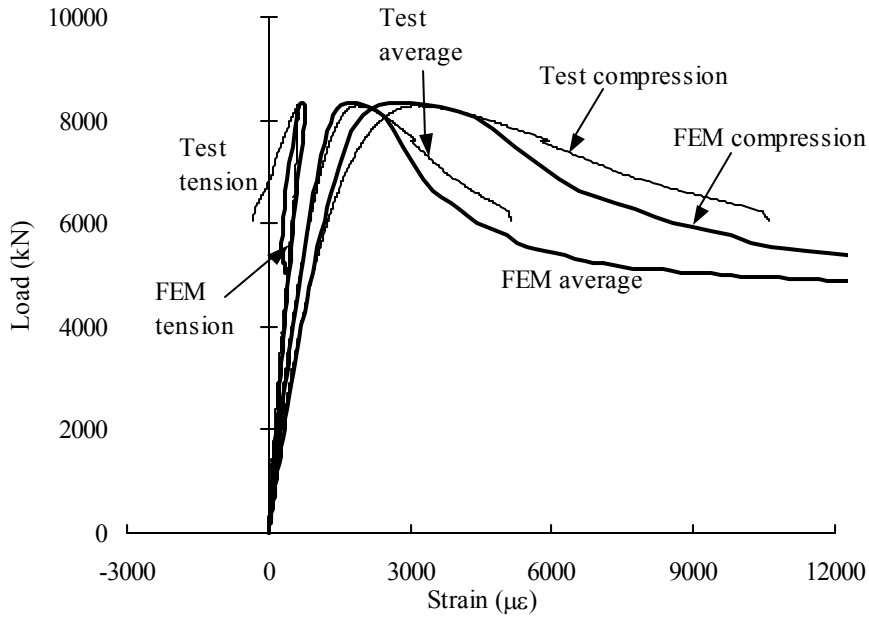
(c) Specimen B1-X3 (Bouchereau and Toupin 2003)
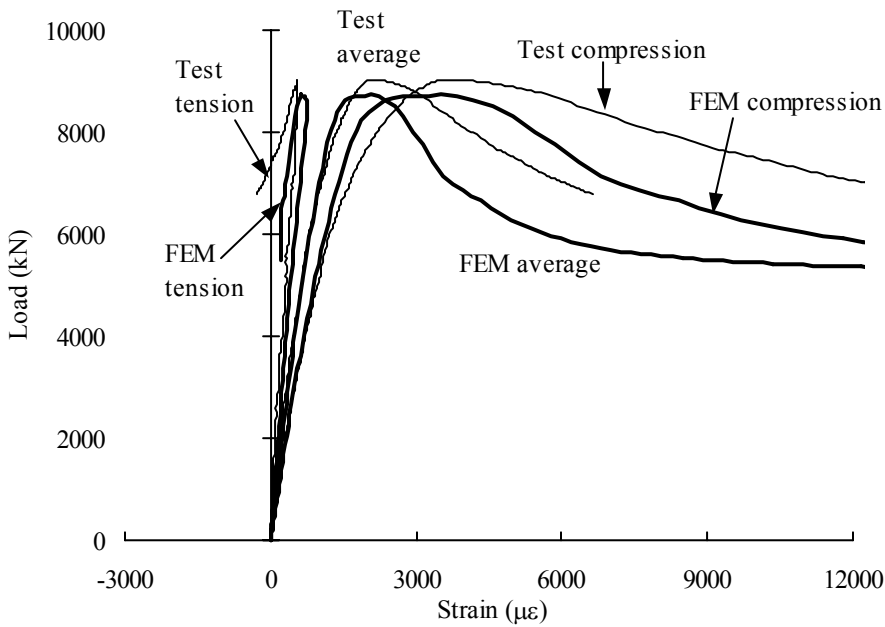
(d) Specimen B2-X3 (Bouchereau and Toupin 2003)

Figure 5.4 (cont.) Experimental and Numerical Load versus Strain Behaviour (using Full Model) for Eccentrically Loaded Short PEC Columns with NSC

123
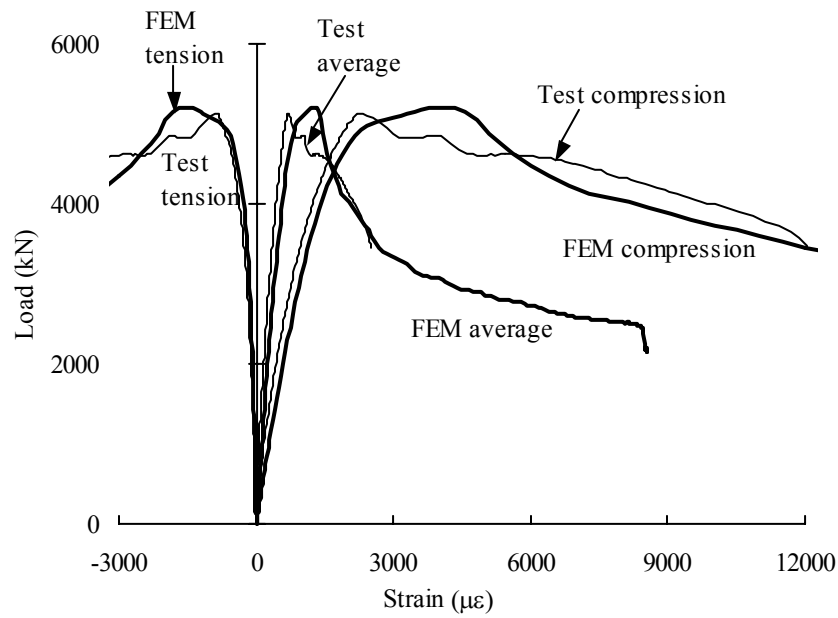
(e) Specimen B1-Y1 (Bouchereau and Toupin 2003)
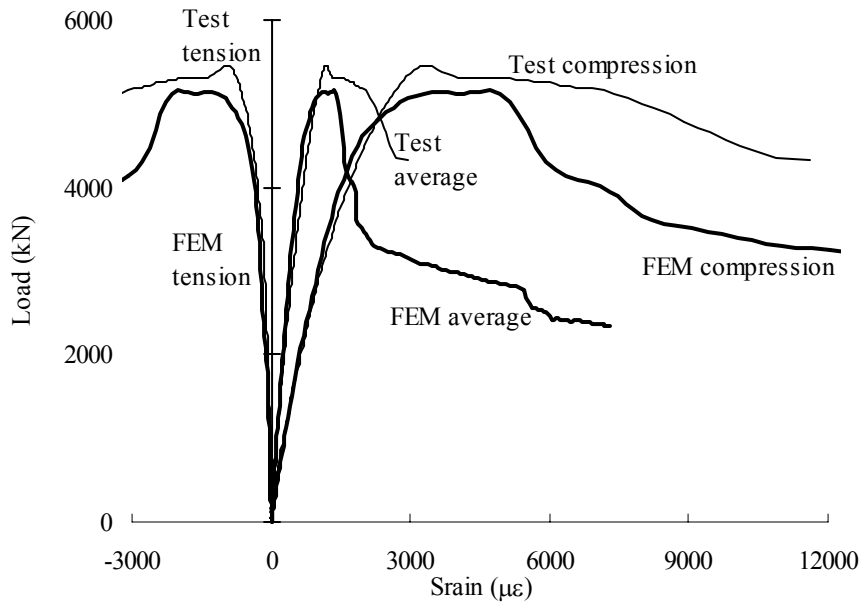
(f) Specimen B2-Y1 (Bouchereau and Toupin 2003)

Figure 5.4 (cont.) Experimental and Numerical Load versus Strain Behaviour (using Full Model) for Eccentrically Loaded Short PEC Columns with NSC

124
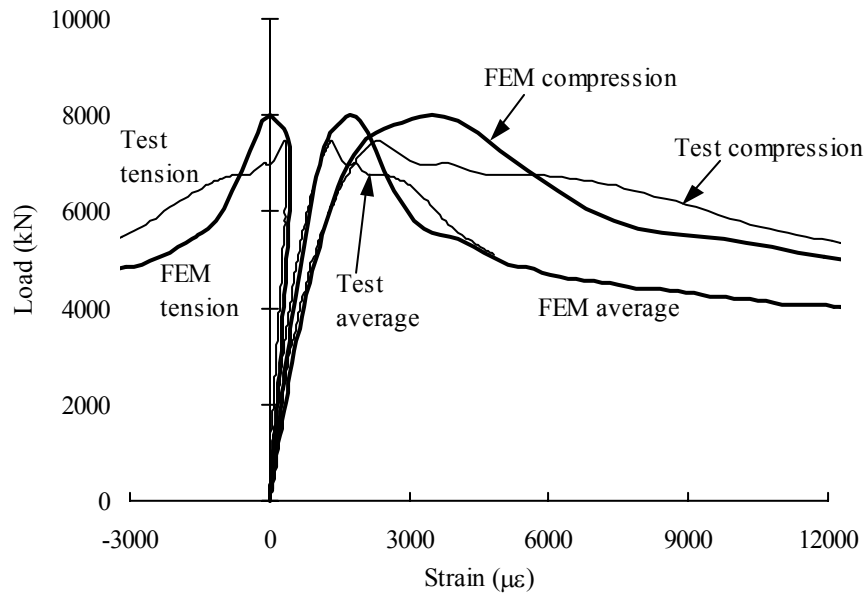
(g) Specimen B1-Y3 (Bouchereau and Toupin 2003)
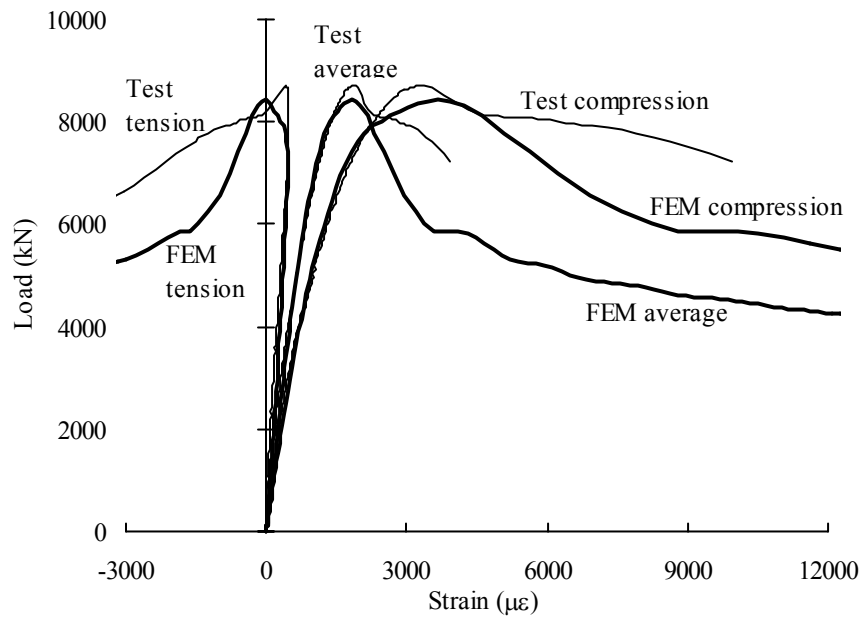
(h) Specimen B2-Y3 (Bouchereau and Toupin 2003)

Figure 5.4 (cont.) Experimental and Numerical Load versus Strain Behaviour (using Full Model) for Eccentrically Loaded Short PEC Columns with NSC

125
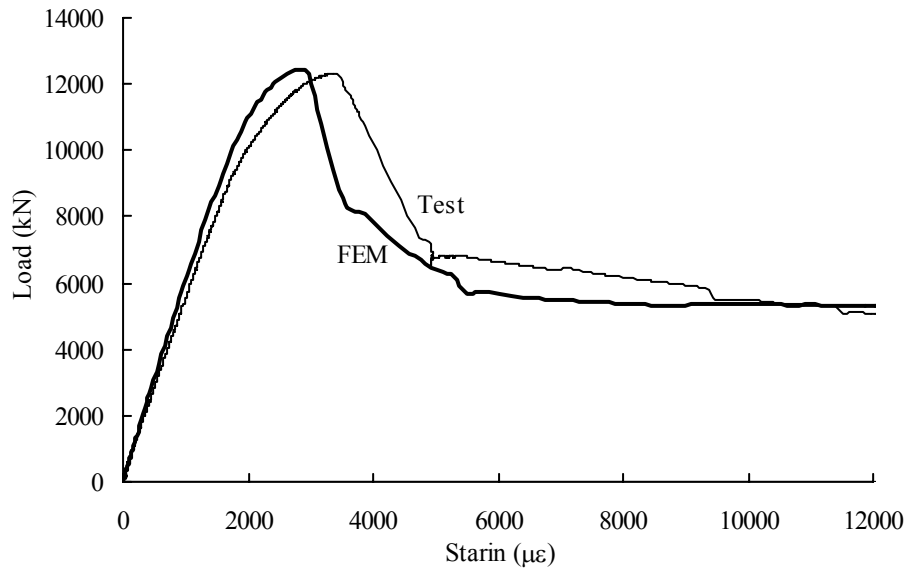
(a) Specimen H3 (Prickett and Driver 2006)
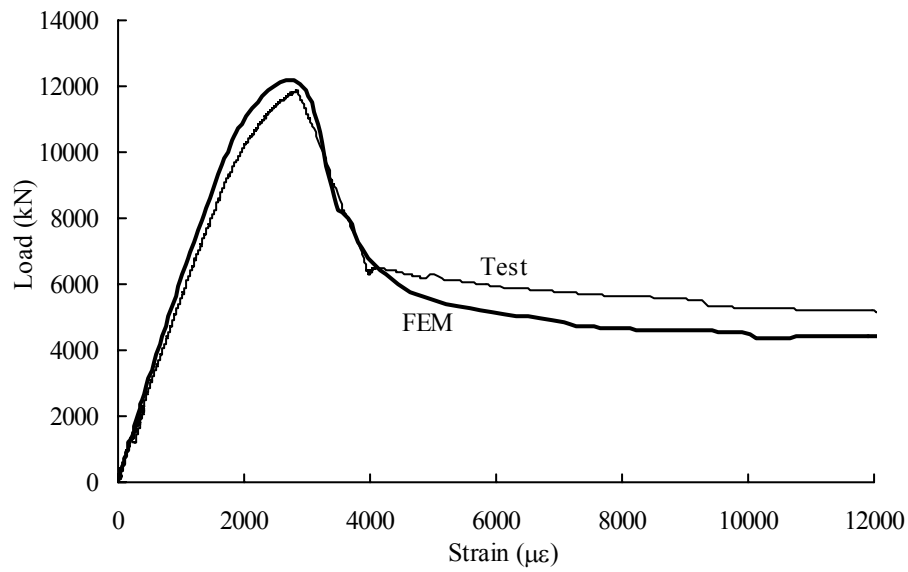
(b) Specimen H4 (Prickett and Driver 2006)

Figure 5.5 Experimental and Numerical Load versus Strain Behaviour (using Full Model) for Concentrically Loaded Short PEC Columns with HSC

126
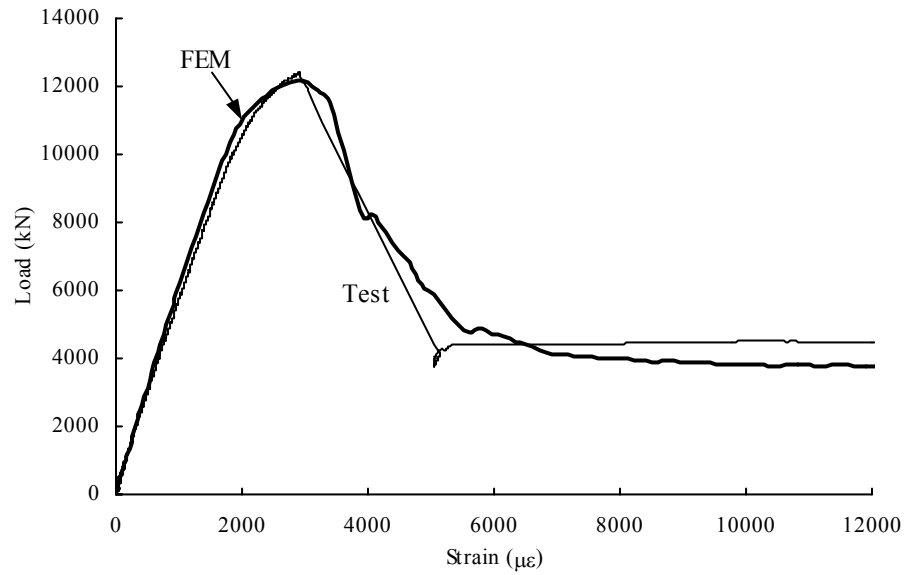
(c) Specimen H5 (Prickett and Driver 2006)

Figure 5.5 (cont.) Experimental and Numerical Load versus Strain Behaviour (using Full Model) for Concentrically Loaded Short PEC Columns with HSC
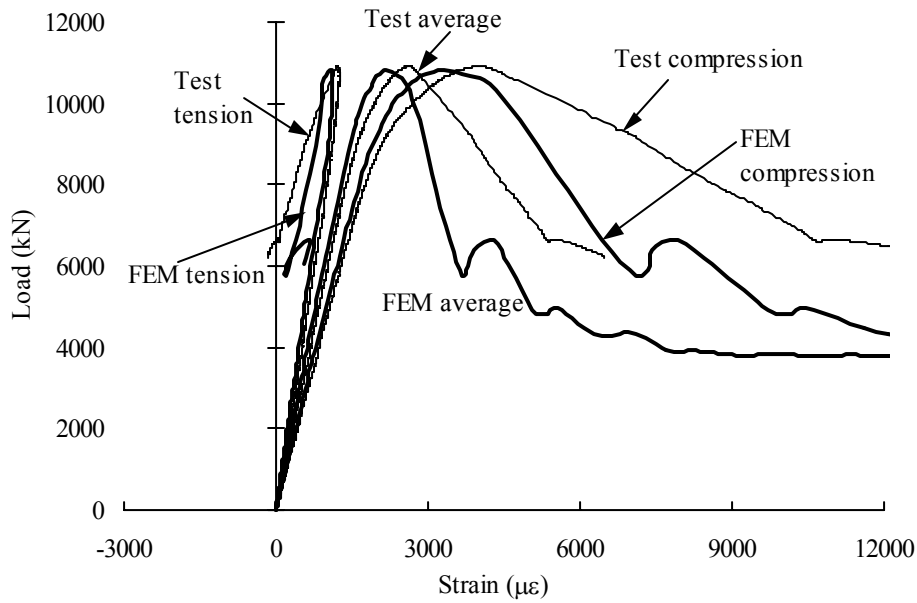
(a) Specimen H8 (Prickett and Driver 2006)
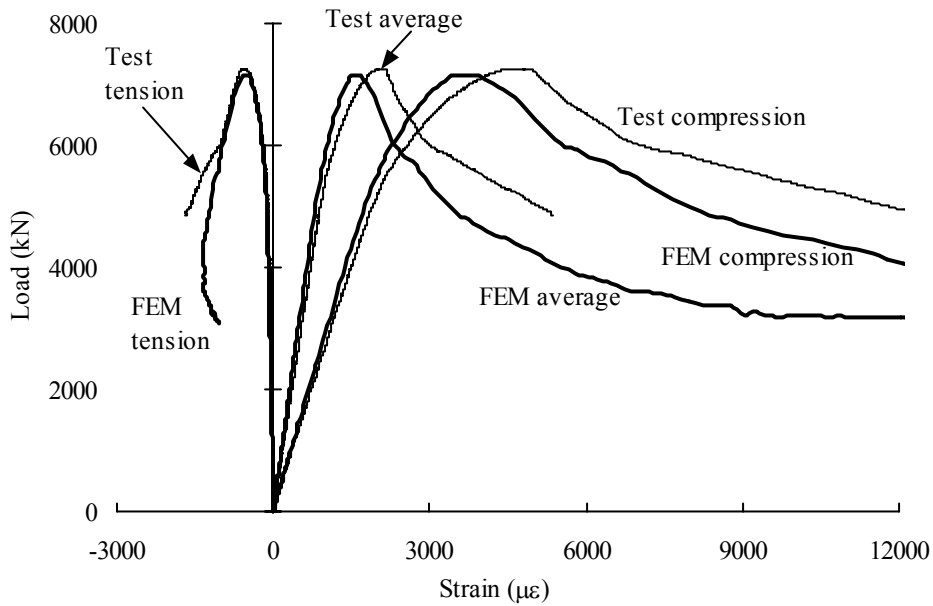
(b) Specimen H9 (Prickett and Driver 2006)

Figure 5.6 Experimental and Numerical Load versus Strain Behaviour (using Full Model) for Eccentrically Loaded Short PEC Columns with HSC

(c) Specimen H10 (Prickett and Driver 2006)

(d) Specimen H11 (Prickett and Driver 2006)

Figure 5.6 (cont.) Comparison of Experimental and Numerical Load versus Strain Behaviour (using Full Model) for Eccentrically Loaded Short PEC Columns with HSC
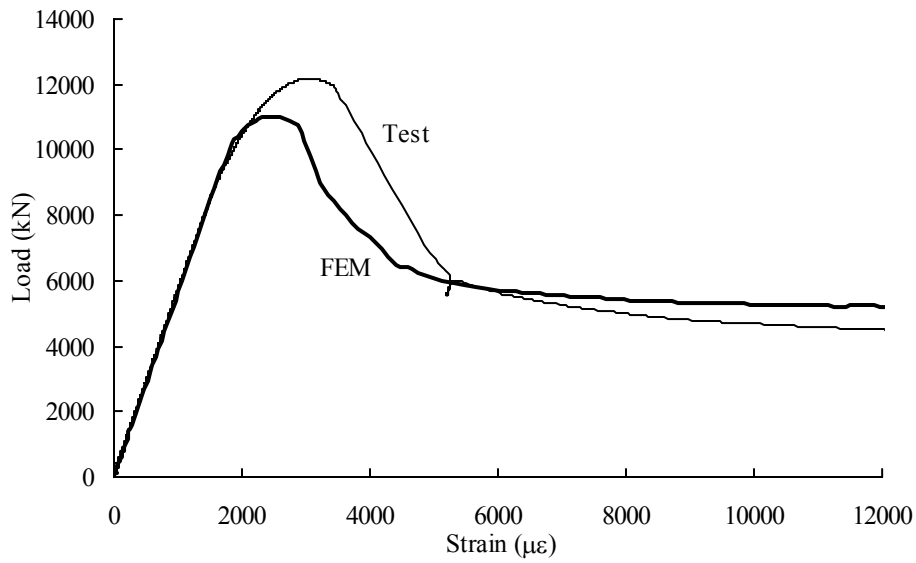
(a) Specimen H6 (Prickett and Driver 2006)
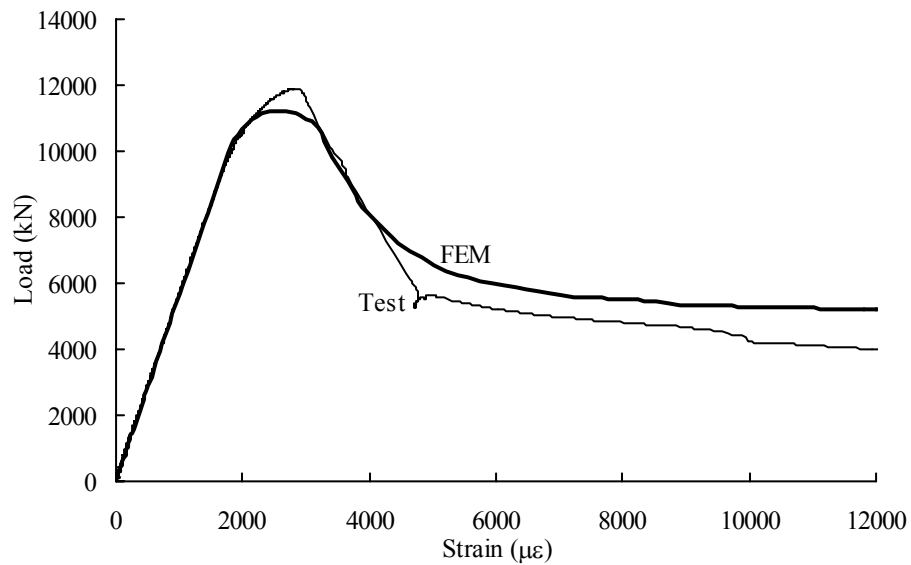
(b) Specimen H7 (Prickett and Driver 2006)

Figure 5.7 Experimental and Numerical Load versus Strain Behaviour (using Full Model) for Concentrically Loaded Short PEC Columns with HSFRC
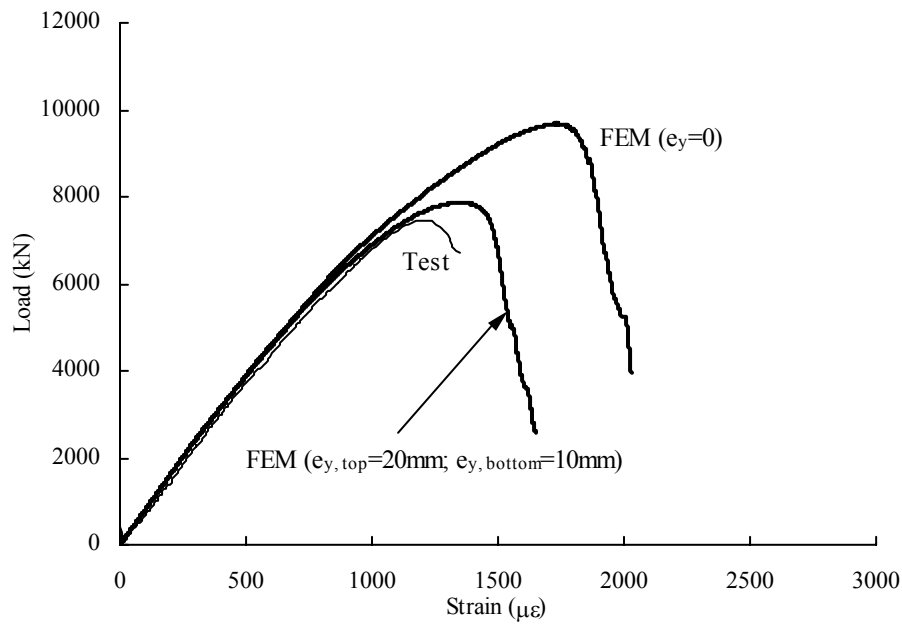
(a) Specimen CL-1 (Chicoine et al. 2000)
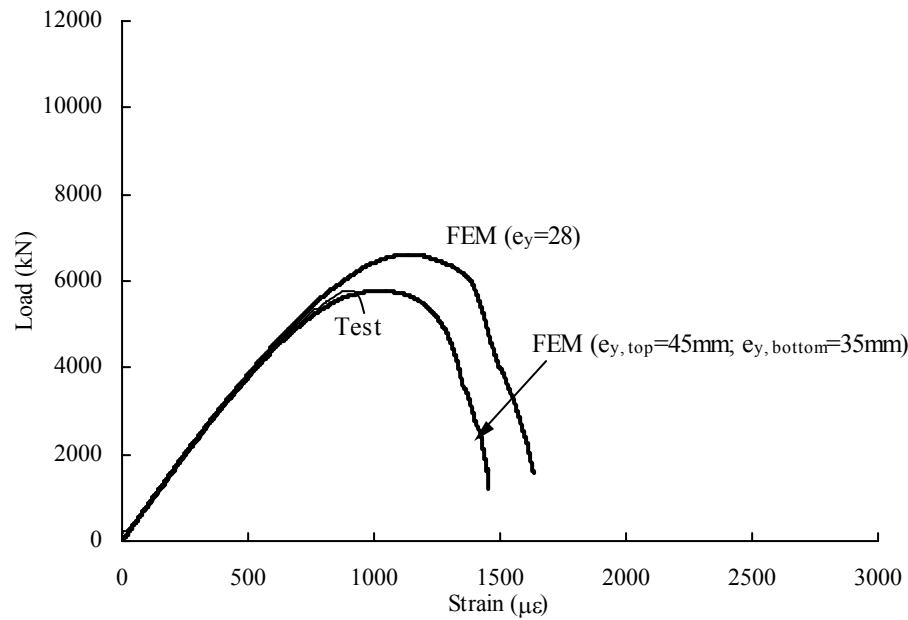
(b) Specimen CL-2 (Chicoine et al. 2000)

Figure 5.8 Experimental and Numerical Load versus Strain Behaviour for Long PEC Columns with NSC
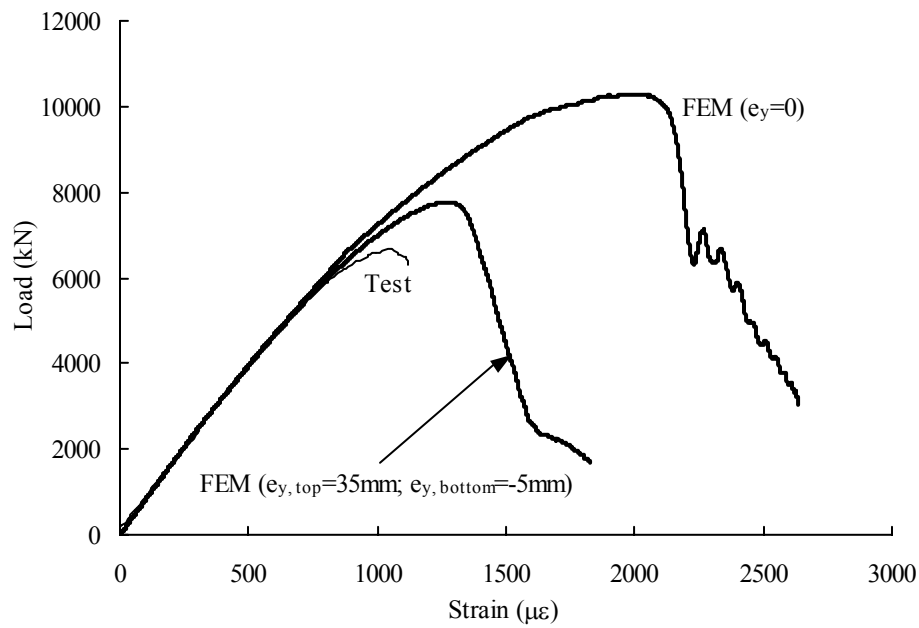
(c) Specimen CL-3 (Chicoine et al. 2000)

Figure 5.8 (cont.) Experimental and Numerical Load versus Strain Behaviour for Long PEC Columns with NSC
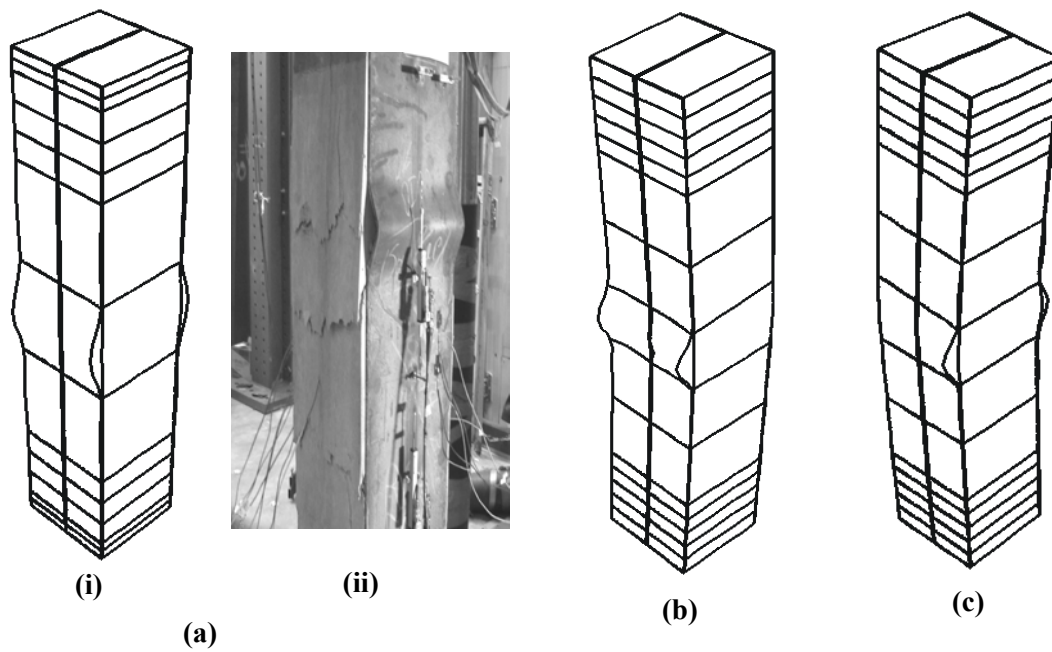
Figure 5.9 Failure Modes Obtained from the Full Column FE Model for Short PEC Columns, (a) Concentric Load, (i) Numerical and (ii) Experimental (Prickett and Driver 2006); (b) Eccentric Load (strong axis bending) and (c) Eccentric Load (weak axis bending)
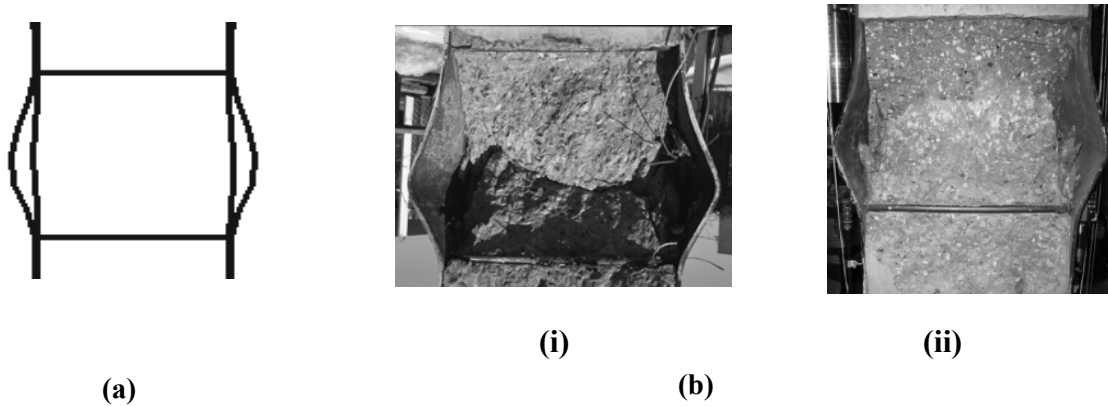
Figure 5.10 Comparison of Numerical and Experimental Local Buckling at Failure for Short PEC Columns, (a) Numerical; (b) Experimental (i) Chicoine et al. (2000) and (ii) Prickett and Driver (2006)

Local flange buckling and global flexural buckling
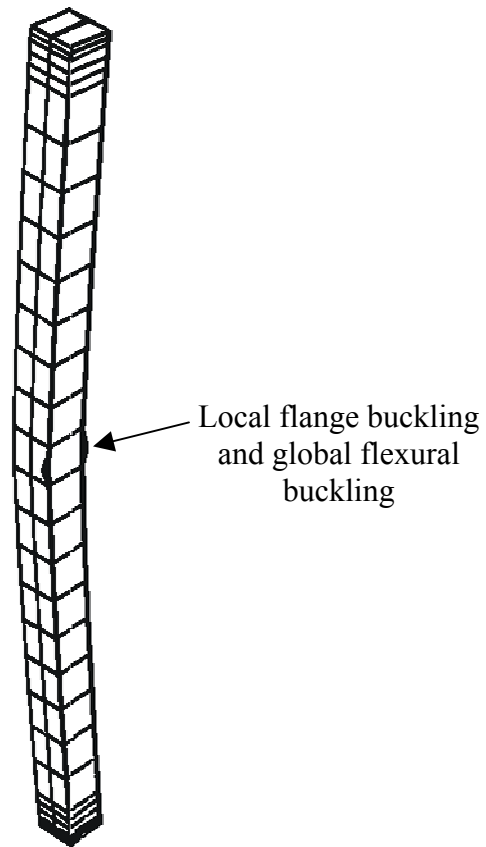
(a)
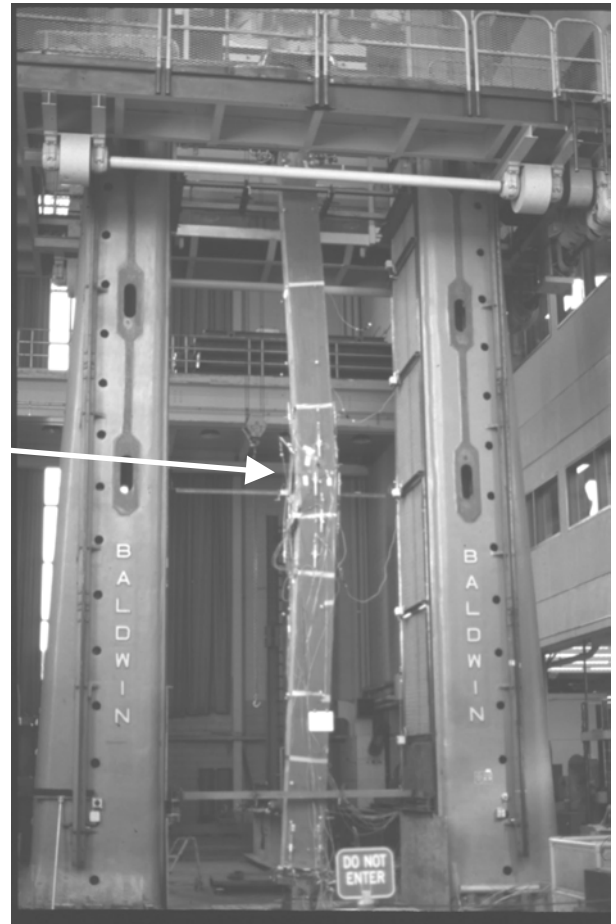
(b)

Figure 5.11 Comparison of Numerical and Experimental Failure Modes for Long PEC Columns, (a) Numerical and (b) Experimental (Chicoine et al. 2000)
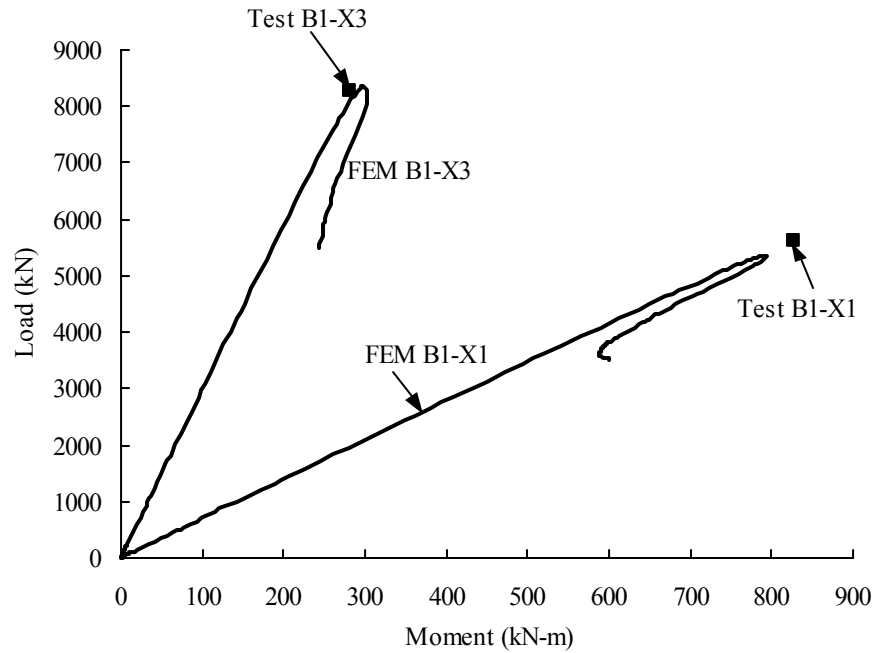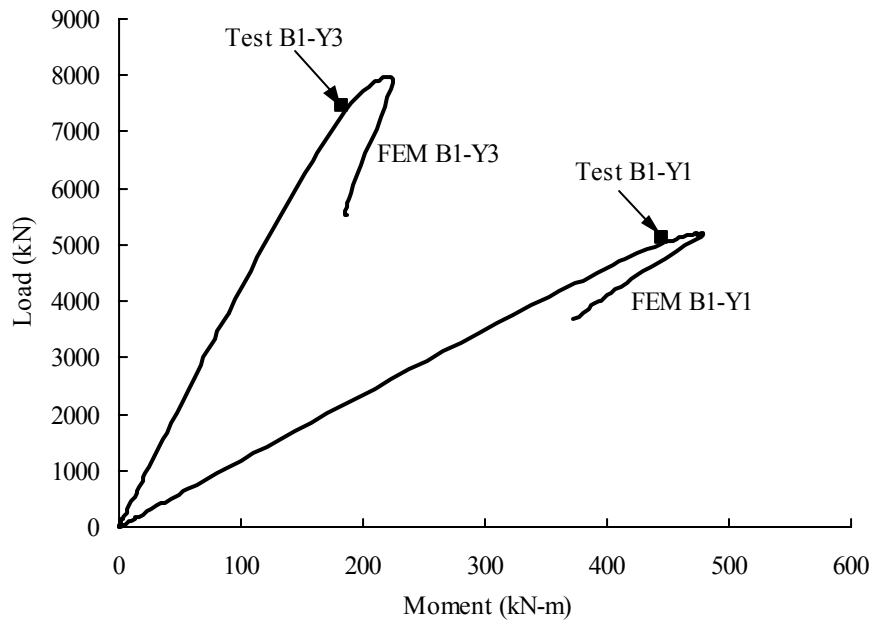
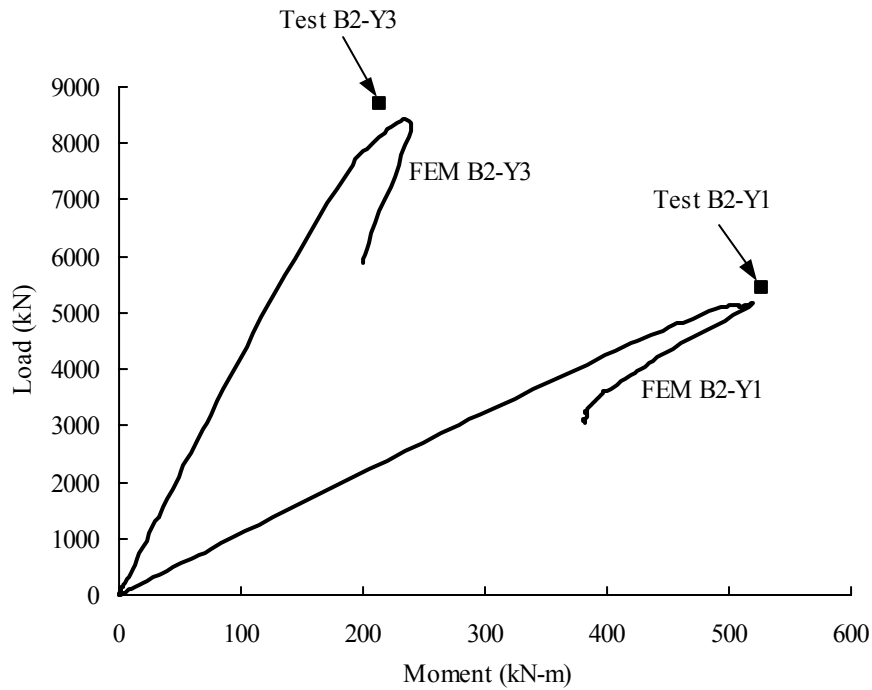**(a) Specimens B1-X1 and B1-X3 (Bouchereau and Toupin 2003)**
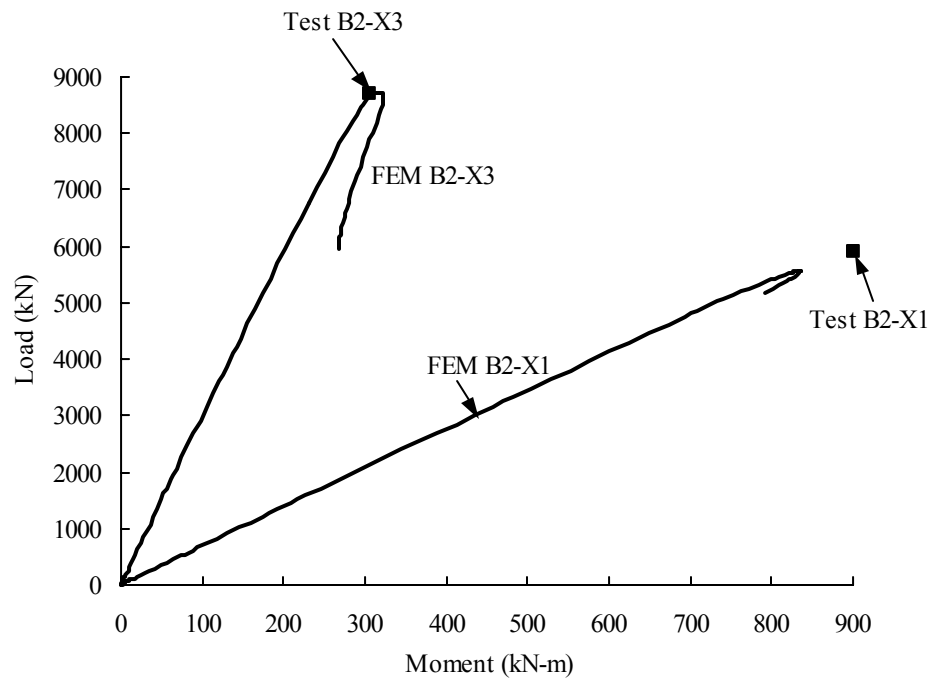
(b) Specimens B2-X1 and B2-X3 (Bouchereau and Toupin 2003)

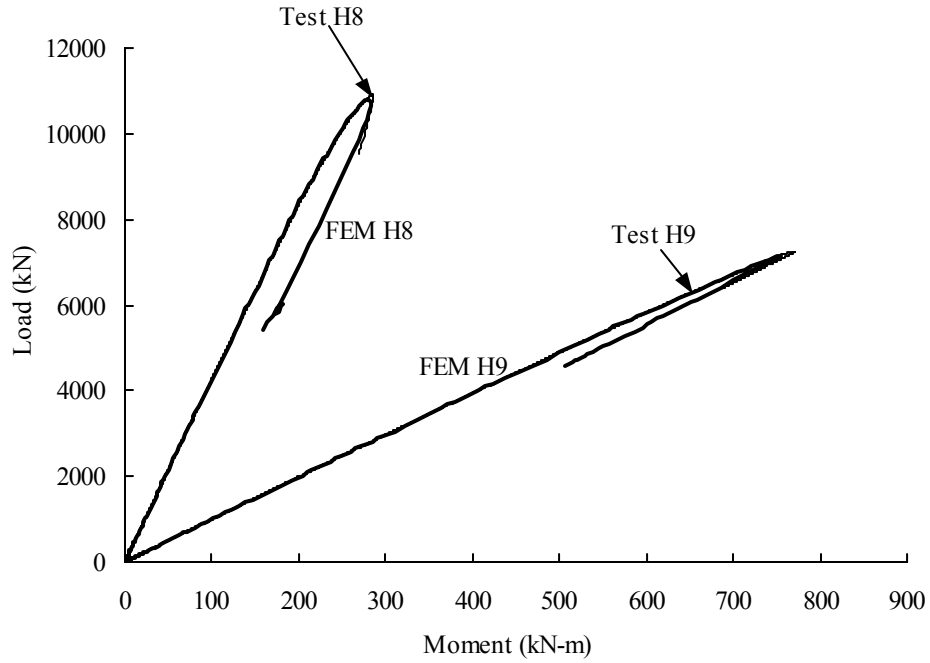**Figure 5.12 Numerical and Experimental Load versus Moment Curves for Short PEC Columns with Normal Strength Concrete**

(c) Specimens B1-Y1 and B1-Y3 (Bouchereau and Toupin 2003)
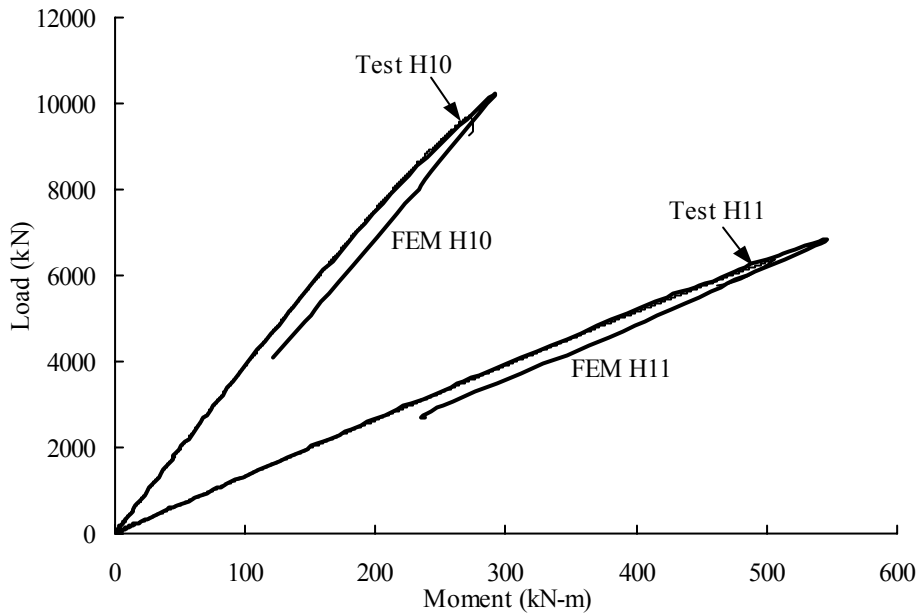

(d) Specimens B2-Y1 and B2-Y3 (Bouchereau and Toupin 2003)

Figure 5.12 (cont.) Numerical and Experimental Load versus Moment Curves for Short PEC Columns with Normal Strength Concrete
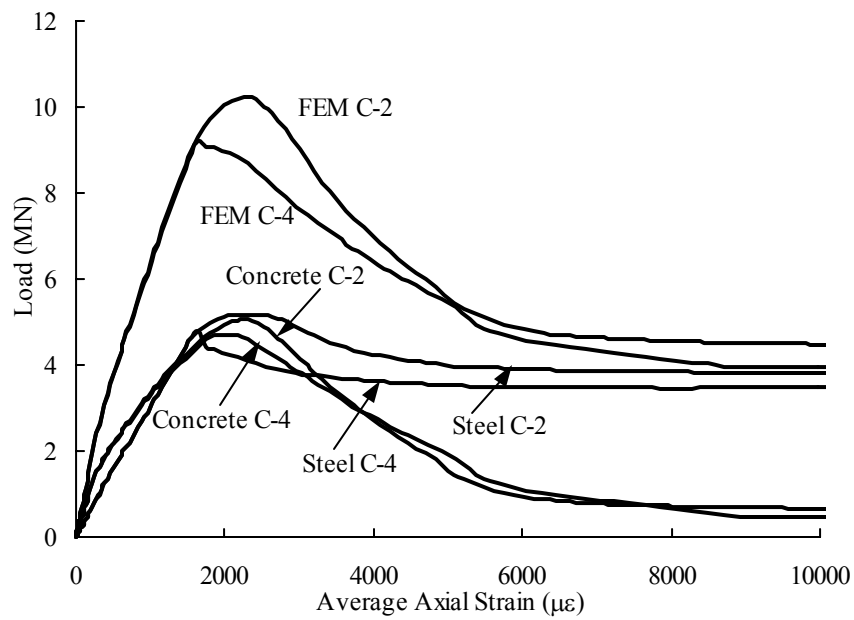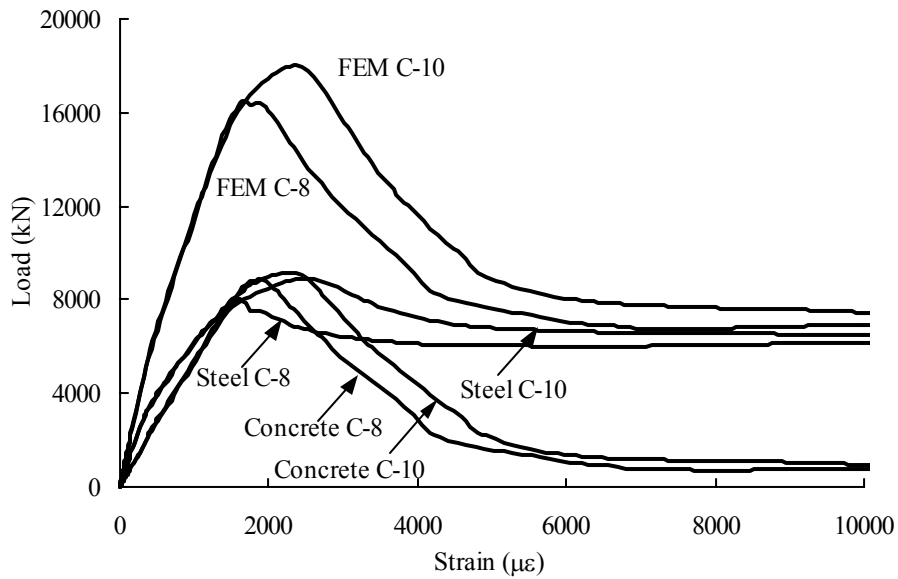
(a) Specimens H8 and H9 (Prickett and Driver 2006)

(b) Specimens H10 and H11 (Prickett and Driver 2006)

Figure 5.13 Numerical and Experimental Load versus Moment Curves
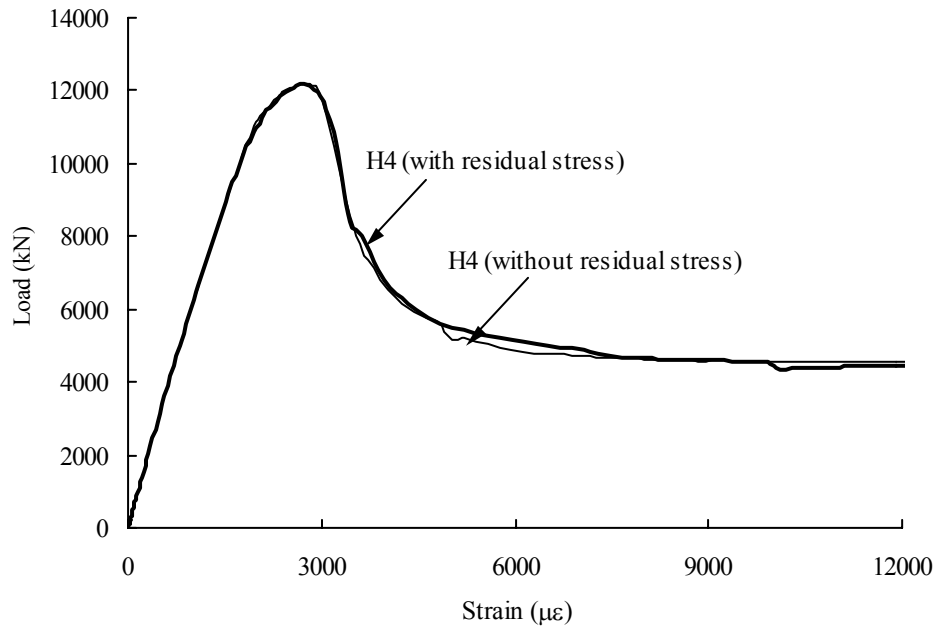**for Short PEC Columns with High Strength Concrete**

137
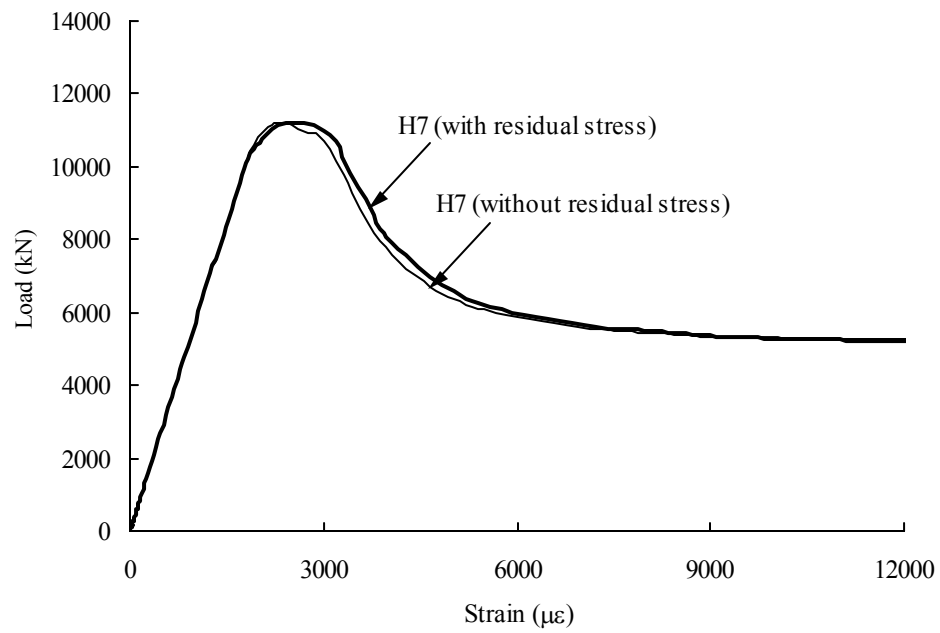
(a) Specimens C-2 and C-4 (Tremblay et al. 1998)

(b) Specimens C-8 and C-10 (Chicoine et al. 2002)

Figure 5.14 Effect of Link Spacing on Load versus Strain Behaviour

138

(a) Specimen H4 (Prickett and Driver 2006)

(b) Specimen H7 (Prickett and Driver 2006)

Figure 5.15 Effect of Residual Stress on Load versus Axial Strain Behaviour

6. PARAMETRIC STUDY

6.1 Introduction

Most of the early research on partially encased composite (PEC) columns investigated concentrically loaded applications, i.e., they were intended for use as "gravity" columns. The range of application of these columns can be expanded significantly by incorporating them as part of lateral load resisting systems such as braced steel frames or steel plate shear walls. In these cases, the columns are subjected to the combined action of bending moment and axial force and in some cases the moments can be substantial. Design rules for PEC columns constructed with normal strength concrete and subjected to concentric gravity loading have been incorporated into CSA S16-01 (CSA 2001). Based on large-scale experimental investigations, Prickett and Driver (2006) suggested that the design procedures in CSA S16-01 are also adequate for PEC columns made with high strength concrete, giving conservative predictions of strength. Prickett and Driver (2006) have also proposed design procedures for columns loaded under combined axial load and bending. They validated the design procedures against the test results of eccentrically loaded short PEC columns (L/d = 5), varying the initial load eccentricity and axis of bending. All of the PEC columns they tested had a flange b/t ratio of 25. Therefore, the researchers recommended that more tests should be performed on PEC columns having b/t ratios greater than 25, since this parameter is influential on local buckling of PEC columns. Moreover, the recommended design procedure for PEC columns under combined axial load and bending needs to be extended for columns with overall slenderness ratios, L/d, greater than 5. Experimental investigations are, however, time consuming and capital intensive, as well as being particularly cumbersome for long columns. Therefore, to extend the range of application of PEC columns constructed with both normal and high strength concrete subjected to axial compression and bending, a parametric analysis is required using a validated analytical model.

This study uses the full finite element model developed in Chapter 5 to assess the influence of important geometric and material parameters on the behaviour of PEC

columns. The efficiency and accuracy of the model were demonstrated through comparisons between the experimental and numerical results of a large number of PEC column tests with an array of parameters, as presented in Chapter 5. The model was found to be capable of tracing a stable and complete load–strain history with good accuracy for PEC columns with small and large cross-sections, constructed with normal and high strength concrete, and tested under concentric and eccentric loading conditions. Moreover, the model was able to simulate the observed failure mode well. In this chapter, the finite element model is used to expand substantively the pool of data from previous experimental research programs and, thereby, to explore the influences of several key parameters on the behaviour of PEC columns. Due to the broad range of parameters considered, to keep the project manageable the parametric study is confined to columns subjected to strong axis bending only, since this is the type of loading condition that most often occurs when the columns are a part of lateral load resisting systems. (Similar studies of PEC columns under weak axis or biaxial bending are recommended for future research.) The selection of the variable parameters and design of the parametric study, along with a discussion of the results, are presented in subsequent sections.

6.2   Design of Parametric Study

6.2.1   Selection of Parameters

For designing the parametric study, the geometric and material properties of PEC columns that can significantly affect their behaviour under axial compression and bending are identified as potential variables. Among these, the column cross-sectional dimensions, b_f (or b) and d, length of the column, L, longitudinal spacing of the transverse links, s, thickness of the steel flange and web plates, t and initial load eccentricity, e, are identified as the most important geometric variables. The compressive strength of concrete used in the column is included as the only material variable, since the grade of structural steel used is unlikely to be varied much by designers. The geometric properties listed here are non-dimensionalised for comparison in order to reflect anticipated combined influences and also to reduce the number of individual analyses

required. The definition of each parameter, along with its selected range for this study, is presented in turn below.

6.2.1.1   Overall Column Slenderness Ratio, L/d

The global stability of the column is controlled by the overall slenderness ratio, which is defined as the ratio of the length of the column, L, to the depth of the column cross-section, d. Three different slenderness ratios—5, 10 and 15—were employed in the parametric study to cover the range of short, intermediate and slender columns. Thereby, this study will help to fill the gap in the behaviour of PEC columns resulting from the paucity of experimental data for columns with L/d > 5. Although three tests on columns with L/d = 20 were used during the model verification exercises, it was decided to limit L/d in the parametric study to 15 until more experiments on slender columns are carried out. This upper limit slightly exceeds the limit prescribed by CSA S16-01 (CSA 2001) of 14.

6.2.1.2   Load Eccentricity Ratio, e/d

The behaviour of a PEC column under bending induced by an eccentrically applied axial load is greatly affected by the initial load eccentricity ratio, which is obtained by dividing the initial eccentricity, e, of the applied axial load by the depth of the column cross-section, d. Higher e/d ratios increase flexural compression in the cross-section, resulting in reduced load carrying capacity of the column as compared to a concentrically loaded column. The load eccentricity ratios used in this study are 0.05, 0.15 and 0.30. The load eccentricity ratio of 0.05 is intended to represent an "accidental" eccentricity that might occur in a column that is nominally designed as a gravity column. The upper limit of 0.30 explores cases with substantial bending moments.

6.2.1.3   Flange Plate Slenderness Ratio, b/t

The flange plate slenderness ratio is defined as the ratio of the half-width of the flange, b, to its thickness, t. This parameter was varied between 25 and 35, with an intermediate value of 30. The ultimate capacity and failure mode of a PEC column is significantly

affected by this parameter, since it controls the occurrence of local instability in the flange plate of the column. In other words, the ductility of this composite system is greatly affected by the flange plate slenderness ratio. The upper limit of 35 slightly exceeds the limit prescribed for PEC columns by CSA S16-01 (CSA 2001) of 32.

6.2.1.4 Link Spacing-to- Depth Ratio, s/d

Local flange buckling in a PEC column takes place in the unsupported length of the flange plate, i.e., in the flange panel between two successive links. Therefore, link spacing is clearly an important parameter affecting the behaviour of these columns. The effect of the link spacing is studied by varying the ratio of link spacing, s, to the depth of the column cross-section, d. Two values of the s/d ratio—0.5 and 0.7—were used in the parametric study. For comparison, the prescribed upper limit in CSA S16-01 for the link spacing is 0.67 of the least dimension of the column or 500 mm, whichever is less.

6.2.1.5 Concrete Compressive Strength

Compressive strength of concrete plays an important role in increasing the load carrying capacity of concrete, thereby reducing the required column size, and perhaps the amount of steel required, for a particular load. However, limited experimental investigations have been performed, to date, on PEC columns with high strength concrete and no such results were available prior to the publication date of the current edition of CSA S16-01 (CSA 2001). As a result, nominal concrete strengths greater than 40 MPa are currently not permitted in design. Thus, in the parametric study the concrete strength was varied from 30 MPa to 60 MPa to investigate the influence of high strength concrete in combination with other parameters.

6.2.2 Combinations of Parameters

As presented in the previous section, four non-dimensional geometric and one material parameter were varied in the parametric study. In designing the columns for the study, the overall column slenderness ratio, L/d, was considered the primary parameter. Other

parameters were combined in an optimum and systematic way for each value of the primary parameter to obtain their individual effects and interrelationships. To facilitate this approach, three reference columns, designated 'SN1', 'IN1' and 'LH1' (as shown in Table 6.1), are designed, where "S", "I" and "L" indicate short (L/d = 5), intermediate (L/d = 10) and long (L/d = 15) columns, respectively. The smallest value of each variable parameter is selected for SN1, the largest value of each for LH1, and intermediate values are used for IN1 in order to provide a broad perspective on the effects of the various parameters. To study the effect of each selected parameter, numerical analyses were performed by varying only that parameter for each of the reference columns.

Additional analyses were performed to study the combined effect of flange slenderness ratio, b/t, and link spacing-to-depth ratio, s/d, since these two parameters together control the local flange stability and, thereby, the ductility of the composite column. A high value of b/t ratio combined with large link spacing can significantly limit the capacity and influence the failure of these columns. In this study, for each value of flange b/t ratio (i.e., 25, 30 and 35) the s/d ratio was varied between 0.5 and 0.7 for each of the three reference columns.

In total, 31 columns were analysed for the parametric study, the details of which are given in Table 6.1. The first letter in the column designation refers to the overall column slenderness ratio. To differentiate between the normal strength and high strength concrete columns, letters "N" and "H" are included in the column designation. The number used in the column designation is simply the serial number as they appear in the table. The geometric and material properties of the parametric columns that were fixed for all columns are given in the following section.

6.3   Fixed Geometric and Material Properties of Parametric Columns

All of the columns have a square cross-section with outer dimensions of 450 mm × 450 mm. This is a moderate size for composite columns and might be suitable in the construction of mid-rise buildings. As a result of the fixed cross-sectional size,

each of the four non-dimensional geometric parameters were controlled by individually varying L, e, t and s. The transverse links used were of 12.7 mm diameter, which meets the requirements of CSA S16-01 (CSA 2001). For the two values of link spacing—0.5d and 0.7d—the transverse link arrangements along the height of the column are shown in Figures 6.1, 6.2 and 6.3 for short, intermediate and long columns, respectively. The links were distributed uniformly along the length of the columns for s = 0.5d for all three cases of the L/d ratio. However, for s = 0.7d, adjustments were required in the link spacing near the ends of the columns, as shown in the figures.

The parametric columns were assumed to be fabricated from CSA-G40.21 grade 350W steel plate. The nominal yield strength, F_y, of 350 MPa, the highest permitted by CSA S16-01 (CSA 2001) for PEC columns, was used in the analyses, and with an assumed modulus of elasticity of 200 GPa the yield strain, ε_y, was taken as 0.00175 mm/mm. The ultimate strength of the steel plate is taken as 450 MPa and the corresponding strain is assumed to be 100 times the yield strain, i.e., 0.175 mm/mm. The point delineating the onset of strain hardening is also required to define the trilinear stress–strain curve for steel used in the finite element model. This point is defined at a stress value of 350 MPa, with a strain of $10\varepsilon_y$. The Poisson's ratio used for the steel is 0.30.

Unlike the experimental columns, the parametric columns have uniform concrete strength along their entire length. Two types of concrete, with nominal strengths of 30 MPa and 60 MPa, were used in the parametric study. To define the concrete stress–strain curves for the finite element analyses of these columns, the strain corresponding to the uniaxial compressive strength, the elastic modulus and the Poisson's ratio are required. The strain at the ultimate compressive strength was calculated using the expression proposed by Almusallam and Alsayed (1995):

$$\varepsilon_{cu} = \left(0.2 f_{cu} + 13.06\right) \times 10^{-4} \tag{6.1}$$

which was developed based on experimental investigations of both normal and high strength concrete (up to 100 MPa).

The elastic moduli for the normal and high strength concrete were calculated using the following expression according to ACI 318-05 (ACI 2005):

$$E_c = 4730\sqrt{f_{cu}}$$ (6.2)

In Equations 6.1 and 6.2, f_{cu} is in MPa. The calculated values of elastic modulus and the strain at the ultimate compressive strength for concrete used in the parametric columns are listed in Table 6.1. The Poisson's ratio for concrete was taken as 0.20, as reported by Rashid et al (2002) for concrete with strengths ranging from 20 to 120 MPa. In generating the stress–strain curve for normal strength concrete, the strength reduction factor discussed in Chapters 2 and 4 was applied to the nominal strength (i.e., 30 MPa) of the concrete. However, no reduction factor was applied to reduce the strength of the high strength concrete, as was found to be appropriate in the validation exercises.

In the finite element model for the parametric columns, local imperfections in the flanges were not included since the axial capacity of PEC columns was found not to be affected significantly by the presence of local imperfections (see Section 5.5 of Chapter 5). However, global imperfections were included only in the slender columns (L/d = 15) with a maximum amplitude of L/2000 = 3.4 mm, considered to be a reasonable value that is somewhat lower than the codified limit. The imperfect shape was included in a similar way as implemented in the numerical model for long test specimens (as described in Chapter 4). The residual stresses in the steel plates of the parametric columns were also neglected based on the findings in Chapter 5 that the effect of residual stresses on the load–deformation response of PEC columns is negligible. The end conditions used for the parametric columns were similar to those used in the simulations for the eccentrically loaded columns with bending about the strong axis (as described in Chapter 4).

6.4 Results and Discussion

This section presents the influence of each parameter on the behaviour of short, intermediate and long PEC columns in comparison to the three associated reference columns (i.e., SN1, IN1 and LH1, respectively) selected for the parametric study. The output parameters that have been extracted from the analysis results are: axial load, P_u, moment, M_u, average axial strain, $\varepsilon_{a,u}$, and lateral displacement, $U_{3,u}$, at failure (i.e., at the peak axial load point). The term "moment" used in this section always refers to the total bending moment, i.e., including the second order effects. The axial load versus average axial strain, axial load versus lateral displacement, moment versus lateral displacement, axial load versus moment and moment versus curvature curves are also generated from the numerical analysis for each parametric column.

The average axial strain is calculated by dividing the average total displacement in the axial direction by the length of the column. In most cases, local buckling is observed in the segment (between two links) that includes the cross-section at the mid-height of the column. However, in four cases local buckling occurred two to three segments away from mid-height. The moment and curvature calculations for all columns are performed at the critical segment where local buckling took place. However, to minimize the effect of highly localized distortions, the critical section was taken right at the link level closest to the column mid-height that is adjacent to the buckled segment. The lateral displacement is extracted at the same link level and is used to determine the second order moment.

All the results obtained from the parametric analyses are organized and presented to highlight the individual effect of each parameter. To this end, the parametric columns that demonstrate the effect of a variable parameter for the three reference columns are divided into three sets: "Set 1", "Set 2" and "Set 3". "Set 1" includes the effect of the variable parameter on the short reference column, SN1, for which e/d=0.15, b/t=25 and s/d=0.5. "Set 2" demonstrates the effect on reference column IN1 (e/d=0.15; b/t=30; s/d=0.7). Finally, the effects of the variable parameter on the long reference column, LH1 (e/d=0.30; b/t=35; s/d=0.7), are included in "Set 3".

147

The failure mode in each of the 31 parametric columns is studied using the numerical model. In general the columns reached the peak load by concrete crushing either preceded, followed or accompanied by local buckling of the flanges. The load level where the first sign of local buckling was observed is reported. This was done by plotting the axial load versus axial strain curves at the outside, inside and middle surfaces of the shell element of the flange plate where local buckling had taken place. Load versus strain plots for the flange in the reference columns only are shown in Figure 6.4. However, the Appendix includes the load versus axial strain curve at the buckled flange for all 31 parametric columns. The ratio of the axial load at the initiation of local buckling to the peak load is given in Tables 6.2 to 6.5. Occurrence of local buckling before, at or after the attainment of the peak axial load is also reported in the tables.

In the following sections, only the significant observations from the parametric study are reported, along with the relevant figures. However, all figures regarding the influence of each parameter on the load versus average axial strain response, load versus lateral displacement response, moment versus lateral displacement response, load versus moment response and moment versus curvature response are included in the Appendix.

6.4.1 Effect of Overall Column Slenderness Ratio

6.4.1.1 Peak Load and Corresponding Moment

Table 6.2 shows the effect of the overall column slenderness (L/d) ratio on the selected output parameters at the peak load point. For Set 1 and Set 2, the effect of the L/d ratio has the same effect on the ultimate axial load and moment. For these columns, increasing the L/d ratio from 5 to 10 reduces the ultimate axial load capacity by 3%. On the other hand, increasing the L/d ratio to 15 results in an 8% reduction in the ultimate axial load. The moments at the peak load points for Sets 1 and 2 are increased by 9% and 31% for L/d ratios of 10 and 15, respectively, with respect to the moment for L/d = 5. The increase in the bending moment resulted from the increase in second order moments as the column gets increasingly slender.

The effect of the L/d ratio as observed in Set 3 is different than that observed in Sets 1 and 2. The ultimate load of column SH2 is observed to reduce by 7% and 18%, respectively, for L/d of 10 and 15. However, the moment at the peak load point is increased by 5% and 10%, respectively, for L/d ratios of 10 and 15 with respect to that obtained for L/d = 5. This increase in the moment at the peak load point is significantly less than that observed for Sets 1 and 2 because the high load eccentricity (e = 0.3d) for columns included in Set 3 reduces the effect of the increase in the second order displacements, as L/d ratio increases, on the bending moment of these columns.

6.4.1.2 Load versus Average Axial Strain Response

Figures 6.5(a), (b) and (c) show the effects of L/d ratios on the axial load versus average axial strain responses for Sets 1, 2 and 3, respectively. In Set 1, column SN1 shows a flatter peak and more gradual post-peak strength decline as compared to columns IN2 (L/d = 10) and LN2 (L/d = 15). These three columns had e/d = 0.15, b/t = 25, s/d = 0.5 and were constructed with 30 MPa concrete. As shown in Figure 6.5 (b), for the Set 2 analyses, no significant difference is observed in the load versus strain response of columns IN1 and LN3. However, column SN2 shows ductile behaviour as compared to the other two. These columns had e/d = 0.15, b/t = 30, s/d = 0.7 and were constructed with 30 MPa concrete. In Figure 6.5 (c), no significant difference is observed in the load versus average axial strain curves of columns SH2, IH2 and LH1, except in the peak zone. All three columns show steep decline from the ultimate axial capacity. The columns had e/d = 0.30, b/t = 35, s/d = 0.7 and were constructed with 60 MPa concrete.

Although the longer columns exhibit lower capacity and ductility in all sets, as expected, the effect on axial strength is far more pronounced for the columns with slender flange plates, the more severe eccentricity, and high strength concrete (i.e., Set 3). In some cases, significant differences in the failure mode are also revealed by changing the column slenderness. The clear benefit of the stockier flange plates (Set 1) on the failure mode of short columns diminishes as the columns become more slender. The difference in the brittleness of the failure mode as a function of column length is less distinct when

149

the flange plates themselves are slender (Set 3), although this may have also been influenced by the different character of the high strength concrete.

In the post-peak regions of the load versus strain responses undulations are observed, particularly for the intermediate and long columns. As presented in Chapter 4, a dynamic solution strategy was implemented in the numerical simulations of the quasi-static response of PEC columns. After the peak load, the steel plate experiences local instability in several locations along the column height as the applied displacement increases. Moreover, as the column gets slender global instability becomes significant at higher levels of applied displacement. The instability in the steel plates causes the inertial forces to be significant, resulting in spurious oscillations in the residual portion of the load versus deformation responses.

6.4.1.3 Load versus Lateral Displacement Response

The effect of the L/d ratio on the load versus lateral displacement response is shown in Figure 6.6. In all three sets, the pre-peak region of the load versus lateral displacement curves for the short columns (SN1, SN2 and SH2) show a steep slope and linear behaviour. As the slenderness ratio (L/d) increases, this region of the curve gets nonlinear with reduced initial slope. The nonlinear behaviour occurs due to the increased second order displacement in the slender columns. The short columns experience a sharp decline in the post-peak region of the load versus lateral displacement curve, whereas the long columns can withstand the peak axial load over a wide range of lateral displacement.

In this case, the effect of increasing the slenderness ratio does not seem to be affected greatly by the other parameters. All three sets show a much more rapid accumulation of lateral displacement as the global slenderness increases.

6.4.1.4 Load versus Moment Response

Figure 6.7 presents the load versus moment curves for short, intermediate and long columns in each analysis set. In all three cases, the load versus moment curve for the

short columns represent essentially linear behaviour. However, as the L/d ratio increases, the curve shows nonlinear behaviour resulting from the effect of second order displacements. The effect of global slenderness on the load versus moment curves is similar for the three sets, although the effect is somewhat less pronounced when the initial eccentricity is larger (Set 3) because the second order displacement are, relative to the initial eccentricity, smaller.

6.4.1.5 *Failure Mode*

The points of occurrence of local buckling in the reference columns (SN1, IN1 and LH1) for different L/d ratios are shown in Table 6.2. For column SN1 (e/d = 0.15, b/t =25, s/d = 0.5), local buckling occurred shortly after the peak load. Increasing the L/d ratio is observed to delay the initiation of local buckling slightly.

The local buckling in column IN1 (e/d = 0.15, b/t =30, s/d = 0.7) occurred after the crushing of concrete at 0.99 P_u . For this column, increasing the L/d ratio to 15 (column LN3) does not affect the failure mode. However, when the L/d ratio is reduced to 5 (i.e., column SN2), the local buckling was observed at the peak load accompanied by concrete crushing.

On the other hand, for the long reference column LH1 (e/d = 0.30, b/t =35, s/d = 0.7), local buckling occurred after the crushing of concrete at 0.92 P_u and reducing the L/d ratio is observed to delay the local buckling somewhat. Although the long reference column, LH1, had the largest b/t ratio (i.e., 35) combined with the larger link spacing (i.e., 0.7d), it experienced local buckling well after the peak load. This column was constructed with high strength concrete and had a higher e/d ratio as compared to columns SN1 and IN1.

6.4.2 Effect of Load Eccentricity Ratio

6.4.2.1 Peak Load and Corresponding Moment

The influence of the load eccentricity ratio on the axial load capacity of the PEC columns is observed to be significant (Table 6.3). For Sets 1 and 2, the peak loads corresponding to $e/d = 0.05$ are reduced by approximately 20% and 40% when e/d ratio is increased to 0.15 and 0.30, respectively. For Set 3, this reduction in capacity is even higher, with decreases of 25% and 49% for $e/d = 0.15$ and 0.30, respectively.

As observed in Table 6.3, for Set 1 and Set 2 the average value of the increase in the moment corresponding to the peak load was about 140% and 260% for e/d ratio of 0.15 and 0.30, respectively. For Set 3, however, the increase in moment was observed to be lower: 91% and 124%, respectively, for $e/d = 0.15$ and 0.30. The columns in Set 3 were constructed with high strength concrete and had an L/d ratio of 15.

6.4.2.2 Load versus Average Axial Strain Response

Figure 6.8 shows the effect of the load eccentricity ratio on the axial load versus average axial strain curve for the three sets of analyses. No difference is observed in the initial portion of the load strain behaviour within each set. However, the variation in the e/d ratio affects the peak and post-peak region of the load versus average axial strain response. In Sets 1 and 2, a flatter peak followed by a slightly more gradual post-peak strength decline is observed as the e/d ratio increases. On the other hand, all three columns in Set 3 experienced a sharp decline in the post-peak region. This indicates a negligible effect of the increased bending moment (resulting from the increase in the e/d ratio) in the level of brittleness in the behaviour of these columns. Conversely, the axial strain at the peak is significantly affected in Set 3; a 17% and 42% reduction in the axial strain at the peak load is observed for increasing the e/d ratio from 0.05 to 0.15 and 0.30, respectively.

The effect of increased bending moment on the axial capacity and corresponding axial strain is more pronounced as the column gets slender. The brittle failure mode of the long

152

reference column (which was constructed with high strength concrete and slender plates) is not affected at all by the e/d ratio. The capacities of the short and intermediate reference columns are reduced by 20% on an average, but with a better post-peak response, as the e/d ratio increases. These columns were constructed with normal strength concrete and had variations in plate slenderness and link spacing.

6.4.2.3   Load versus Lateral Displacement and Moment versus Lateral Displacement Responses

The effects of the load eccentricity ratio on the load versus lateral displacement response are presented in Figure 6.9. In all three sets, the lateral displacement at a particular load increases with an increase in the e/d ratio, as expected. The increase in lateral displacement is more pronounced in the cases of intermediate and long columns (Figures 6.9(b) and 6.9(c)) due to the lower flexural stiffness of the column. These figures also show that the peak region of the curve becomes relatively flat with a gradual drop in axial load capacity in the descending branch as the e/d ratio increases.

As shown in Figure 6.10, the moment at the column mid-height increases significantly with the increase in the e/d ratio in all three sets due to the significant differences in the end eccentricity. The lateral displacement at the peak moment also increases with increasing e/d ratios, but this effect is far more evident in the long columns (Set 3) due to the more influential second order effects. However, the moment versus lateral displacement curves for long columns (with high strength concrete) show a sharper decline in the descending branch as compared to the short (Set 1) and intermediate (Set 2) PEC columns.

6.4.2.4   Moment versus Curvature Response

The moment–curvature relationships for the three sets of analysis are shown in Figure 6.11. The initial stiffness of the column is not affected by the load eccentricity ratio due the behaviour being relatively linear. As the moment increases into the inelastic region, columns with higher e/d ratios bend more, which in turn enhances the geometric

nonlinearity in the PEC column. Consequently, the formation of the plastic hinge becomes less gradual as the eccentricity increases. In each set, columns loaded at high eccentricity show slightly less ductile behaviour at failure as compared to the columns with low eccentricity. Nevertheless, the cross-section is able to maintain the maximum moment, or near the maximum moment, under large curvatures in all cases.

6.4.2.5 Failure Mode

For Set 1 that includes the short columns, the occurrence of local buckling is not affected by the load eccentricity ratio as shown in Table 6.3. For all three values of load eccentricity ratio, the short columns experienced local buckling shortly after the peak at an axial load of $0.99P_u$. In the case of the intermediate reference column IN1 ($e/d = 0.15$, $b/t = 30$, $s/d = 0.7$), reducing the load eccentricity accelerates the occurrence of local buckling, which is observed in column IN3. On the other hand, when the load eccentricity ratio is increased to 0.30 (column IN4) no change is observed in the load corresponding to the first sign of local buckling. The flanges of columns IN1 and IN4 buckled at a load of $0.99P_u$ after reaching the peak, whereas column IN3 ($e/d = 0.05$) experienced buckling at $0.97P_u$ before reaching the peak load.

In Set 3, the long reference column LH1 also experiences local buckling earlier as the e/d ratio reduces to 0.15 and 0.05, in comparison with that observed with $e/d = 0.30$. Among all the long columns analysed for the parametric study, only column LH3 experienced local buckling well before reaching the peak load. This long column was also the only one loaded at $e/d = 0.05$, which indicates the presence of higher axial compression and lower bending moment as compared to the columns with higher e/d ratios.

For stockier flanges and closer link spacing, the occurrence of local buckling is not affected by the load eccentricity. For PEC columns with plate slenderness ratios of 30 and 35 accompanied with larger a link spacing, local buckling occurred earlier as the e/d ratio decreases. For the e/d ratio of 0.05, which is the accidental eccentricity case, the columns with slender plates experienced local buckling before the peak load. This was

observed for both normal strength and high strength concrete and for L/d ratios of 10 and 15.

6.4.3   Effect of Flange Plate Slenderness Ratio

6.4.3.1   Peak Load and Corresponding Moment

In Table 6.4, for Set 1 and Set 2, nearly identical changes are observed for the peak load and corresponding moment when the b/t ratio is changed from 25 to 30 and 35 for each s/d ratio. For long columns, which are included in Set 3, the reductions in the peak load and moment due to the increase in b/t ratio are slightly lower than those observed in Set 1 and Set 2.

Increasing the b/t ratio from 25 to 30 causes a 6 to 8% reduction in the axial load capacity of the PEC columns in all three sets for the two link spacings. The average reduction in axial capacity is 7.5%. The L/d ratio and concrete strength seemed to have little or no effect on the reduction in axial capacity due to the increase in plate slenderness. The average reduction in capacity for b/t = 35 is 13%, ranging from 11% (long columns) to 16% (short columns).

The average reduction in the moment corresponding to the axial load is 7% and 13% respectively, for b/t ratios of 30 and 35, with respect to the moment for b/t = 25. The minimum reduction was observed in long columns, i.e., 5% for b/t = 30 and 10% for b/t = 35. On the other hand, the maximum reduction was observed for short columns, i.e., 8% for b/t = 30 and 17% for b/t = 35. The variations in the link spacing seemed to have a negligible influence on these results.

6.4.3.2   Load versus Average Axial Strain Response

Figures 6.12, 6.13 and 6.14 present the effects of the plate slenderness, b/t, on the load versus average axial strain curves for short, intermediate and long columns, respectively, with two different link spacing. In the cases of short and intermediate columns, as the b/t

155

ratio increases the responses of the columns become less ductile as indicated by the flatness of the peak region of the curve. However, the b/t ratio has a more pronounced effect for s = 0.7d than s = 0.5d. As shown in Figures 6.12(b) and 6.13(b), columns SN8 and IN6 which had plates with b/t = 35 and s = 0.7d, demonstrated sudden failure as observed through the sharp decline from the peak load.

In the case of the slender columns, the plate slenderness ratio seemed to have no significant effect (see Figure 6.14) on the load versus average axial strain curve. This can be attributed to the fact that in these slender columns local buckling in the steel flanges occurred after the ultimate load point.

The plate slenderness ratio is more influential in short columns with larger link spacings. As the column becomes slender, the advantage of using a stockier flange plate diminishes for both values of s/d ratios (0.5 and 0.7).

6.4.3.3   *Failure Mode*

As shown in Table 6.4, for three different values of b/t ratio (i.e., 25, 30 and 35) the short reference column (SN1) which had an e/d = 0.15 and s/d = 0.5, local flange buckling occurred at the same load level ($0.99P_u$) after reaching the peak load. When the same column is fabricated with links spaced at 0.7d, increasing the plate b/t ratios from 25 to 35 accelerated the occurrence of local buckling in the flanges slightly. In column SN7, with b/t = 25 and s/d = 0.7, local buckling is observed at $0.99P_u$ after the crushing of concrete at the peak load. The same column when fabricated with plates having b/t ratios of 30 (column SN2) and 35 (column SN8), local buckling occurred with and before the crushing of concrete, respectively.

In case of intermediate columns (included in Set 2) with links spaced at 0.5d and plate b/t ratios of 25, 30 and 35, designated as IN2, IN7 and IN8, respectively, local buckling took place shortly after the peak axial load. The plate slenderness ratio is observed to have no significant effect on the failure modes of these columns. However, among the

intermediate columns with a 0.7d link spacing, column IN6, with b/t = 35, showed local buckling before the peak load, whereas columns IN5 (b/t = 25) and IN1 (b/t = 30) did not experience local buckling before reaching the peak load.

None of the long columns (Set 3) experienced local buckling before reaching the peak load, as shown in Table 6.4. Columns LH7 and LH1, which had the most slender plate (b/t = 35), experienced local buckling slightly earlier as compared to the columns with b/t = 25 and 30. All the longs columns in Table 6.4 were constructed with high strength concrete and were subjected to severe second order bending.

The effect of the b/t ratio on local buckling is more prominent for link the spacing s = 0.7d. The chance of the occurrence of local buckling before the peak load, as the plate gets slender, reduces with increased L/d ratios.

6.4.4   Effect of Link Spacing-to-Depth Ratio

6.4.4.1   Peak Load and Corresponding Moment

As shown in Table 6.5, changing the s/d ratio from 0.5 to 0.7 has no effect on the peak load and corresponding moment for short and intermediate PEC columns with b/t ratios of 25 and 30. When these columns are constructed with slender plates (b/t = 35), slight reductions in the peak load and moment (ranging from 1% to 4%) are observed for s/d = 0.7 with respect to s/d = 0.5. However, the axial capacities of the slender columns are not affected at all by the s/d ratios and the corresponding moments negligibly so.

6.4.4.2   Load versus Average Axial Strain Response

The load versus average axial strain curves for short columns (as shown in Figure 6.15) show increased ductility as the s/d ratio reduces from 0.7 to 0.5. However, this effect of link spacing is observed to become prominent for larger b/t ratios. For b/t ratios of 30 and 35, the peak load is sustained to a larger strain for s/d = 0.5 as compared to that for s/d = 0.7. As shown in Figure 6.16, the columns in Set 2, i.e., the intermediate columns,

also show similar responses when varying the s/d ratio between 0.5 and 0.7. The b/t ratio is found to have essentially no effect at all on the load versus axial strain responses for the columns in Set 3 (Figure 6.17), which are long columns, constructed with high strength concrete and had largest e/d ratio selected in this study.

Although the range of s/d ratio selected in this study does not affect the column axial capacity significantly for the b/t ratio ranging from 25 to 35, the load versus axial strain curves demonstrate more ductile response for lower s/d ratio. However, this effect is prominent in short columns with slender flanges and diminishes as the overall column slenderness increases.

6.4.4.3 *Failure Mode*

For b/t = 25, no change is observed in the failure mode of the short column by varying the link spacing from 0.5 to 0.7d. Both column SN1 (e/d = 0.15, b/t = 25, s/d = 0.5) and SN7 (e/d = 0.15, b/t = 25, s/d = 0.7) experienced local buckling at a load of $0.99P_u$, after the crushing of concrete. On the other hand, when the plate slenderness ratio of the short reference column is increased to 30 and 35, increasing the link spacing from 0.5d to 0.7d accelerated the occurrence of local buckling. Column SN2 (e/d = 0.15, b/t = 30, s/d = 0.7) and SN8 (e/d = 0.15, b/t = 35, s/d = 0.7) failed by local buckling followed by concrete crushing at the peak load. When the link spacing-to-depth ratio of these columns is changed to 0.5 from 0.7, the failure is observed to take place by crushing of concrete at the peak and local flange buckling occurred afterwards.

For the intermediate reference column (IN1), which had a b/t = 30, link spacings of 0.5d and 0.7d do not affect the failure mode significantly. For this column, local flange buckling occurred after reaching the peak axial load at load levels of $0.98P_u$ and $0.99P_u$, respectively, for s = 0.5d and 0.7d. The failure mode of the intermediate column having b/t = 25, is also not affected significantly by varying the link spacing from 0.5d (column IN2) to 0.7d (column IN5). However, for the limiting b/t ratio, i.e. 35, changing the link spacing affects the failure mode as shown in Table 6.5. The failure of

column IN6 (e/d = 0.15, b/t = 35, s/d = 0.7) was initiated by local buckling, whereas column IN8 (e/d = 0.15, b/t = 35, s/d = 0.5) attained the peak load by concrete crushing and local buckling of the flanges followed.

In the case of the long column LH1 constructed with b/t ratios of 25, 30 and 35, the two link spacings 0.5d and 0.7d did not affect the failure mode. In all six columns (Table 6.5), failure was initiated by concrete crushing. Local buckling occurred at loads ranging from $0.87P_u$ to $0.92P_u$, after reaching the peak capacity.

The initiation of local buckling is affected by the link spacing for short and intermediate PEC columns with slender plates. However, for long PEC columns (L/d = 15) the link spacing does not affect the failure behaviour even for b/t = 35, since the failure of the long columns are mainly due to global flexural buckling. The high e/d ratio used in the long columns also added to the increased bending moment in these columns.

6.4.5 Effect of Concrete Compressive Strength

6.4.5.1 Peak Load and Corresponding Moment

The effect of normal and high strength concrete with nominal strengths of 30 and 60 MPa, respectively, is studied in Table 6.6. The ultimate axial load of column SN1 (e/d = 0.15, b/t = 25, s/d = 0.5), IN1 (e/d = 0.15, b/t = 30, s/d = 0.7) and LN1 (e/d = 0.30, b/t = 35, s/d = 0.7), which were constructed with 30 MPa concrete, are increased by 57%, 60% and 48%, respectively, when high strength concrete of 60 MPa is used instead. The moment at the peak load is also increased by 55% for columns SN1 and LN1 and 69% for column IN1. The average increase in the peak load and corresponding moment for all three columns with different e/d, b/t and s/d ratios are 55% and 57%, respectively.

159

6.4.5.2 Load versus Average Axial Strain and Moment versus Curvature Responses

As expected, the behaviour of the PEC columns is greatly affected by the compressive strength of concrete for all three sets of analysis, as shown in Figure 6.18. The axial load versus average strain response for PEC columns with high strength concrete show steeper slopes in the initial portions of the curves due to the higher modulus of elasticity of high strength concrete. Columns SH1, IH1 and LH1 also demonstrate sharp post-peak strength declines as compared to columns SN1, IN1 and LN1, respectively. However, for the long columns (LN1 and LH1) the level of brittleness somewhat less affected by the concrete strength. This is because the brittle failures of the long columns are due to the effect of increased bending moment resulting from increased lateral displacements.

The moment versus curvature plot shown in Figure 6.19 presents the ductile nature of the plastic hinge in columns SN1, IN1, and LN1 as compared to the columns SH1, IH1 and LH1, respectively. This effect gets less pronounced as the overall column slenderness increases.

The axial load and moment capacities of PEC columns can be improved significantly by the use of high strength concrete. This is observed for a wide range of L/d, e/d and b/t ratios. However, the ductility of the column is observed to deteriorate significantly by the use of high strength concrete, which can be recovered to some extent by incorporating steel fibres in the concrete.

6.4.5.3 Failure Mode

The local flange buckling in column SN1 (e/d = 0.15, b/t = 25, s/d = 0.5) and IN1 (e/d = 0.15, b/t = 30, s/d = 0.7) occurred shortly after the crushing of concrete at a load of $0.99P_u$, as indicated in Table 6.6. When high strength concrete is used in these columns—columns SH1 and IH1—local buckling is observed to be delayed significantly. The load corresponding to the first sign of local buckling in the flanges were $0.89P_u$ and $0.94P_u$, respectively, for columns SH1 and IH1. However, the concrete compressive strength did not affect initiation of local buckling in the flanges of the long column

160

(LH1), since the long column behaviour is governed by global bending. Both of the long columns (LN1 and LH1), which had e/d = 0.30, b/t = 35 and s/d = 0.7, experienced local buckling at 0.92P_u after reaching the peak axial load.

6.5 Comparison between Numerical and Theoretical Load and Moment Capacities

The theoretical interaction diagrams, as shown in Figure 6.20, for the three reference columns—SN1, IN1 and LH1—are calculated using the method proposed by Prickett and Driver (2006) (as described in Chapter 2). Two theoretical interaction diagrams are drawn, one using the effective steel area (A_{se}) and the other using the total cross-sectional area (A_s) of the steel plates. Although their tests indicated that the total steel area could be used conservatively, Prickett and Driver (2006) recommended using the effective steel area (to account for potential local buckling before failure) for design since the b/t ratios in the tests did not exceed 25. In Figure 6.20 the numerical moment versus bending moment curves are also plotted for each of the reference columns for various e/d ratios. The numerical load and moment capacities for these columns are compared with the theoretical capacities in Table 6.7. In this table the theoretical capacities are extracted from the location where the numerical load versus moment curve intersects the interaction diagram based on the effective steel area. For Set 1 (which includes the short columns with normal strength concrete), the ratio of the numerical-to-theoretical load and moment capacities varied from 1.02 to 1.05. For intermediate columns with normal strength concrete (i.e., Set 2), the ratio of the numerical-to-theoretical peak load ranged from 1.06 (e/d = 0.30) to 1.10 (e/d = 0.05), with an average value of 1.08. However, the ratio of the numerical-to-theoretical moment capacities for the intermediate column is around 1.15. For the long columns the numerical moment capacity is also observed to exceed the theoretical capacity with numerical-to-theoretical ratio ranging from 1.18 to 1.36.

The effects of concrete strength on the numerical-to-theoretical capacities are also studied, as given in Table 6.8. For all three sets shown in Table 6.8 the ratios between the

numerical and theoretical (based on A_{se}) capacities for high strength concrete PEC columns are higher (ranging from 1.08 to 1.28 with an average ratio of 1.16) than those observed in columns with normal strength concrete. Figure 6.21 also shows the effect of concrete strength on the columns included in the three sets of analyses.

Using the total steel area in the calculation for the theoretical interaction diagrams is observed to reduce the differences between the theoretical and numerical capacities, especially for columns with high strength concrete (as shown in Figures 6.20 and 6.21). Although most of the parametric columns under axial compression and bending experienced local buckling after the peak load, the use of the effective steel area should be retained for design to account for the local buckling occurring before the peak load in PEC columns with the b/t ratio greater than 30 combined with the maximum allowable link spacing.

6.6 Summary

A comprehensive parametric analysis was performed to study the behaviour of PEC columns subjected to axial compression and bending about the strong axis. Four geometric and one material parameter were varied and their influences were demonstrated with respect to the peak axial load and corresponding moment, failure mode and overall column load–deformation responses. The important findings of the study presented in this chapter are summarized below.

The axial capacity of a PEC column reduces as the overall slenderness ratio increases, particularly for columns with slender plates. The ductility of the normal strength concrete column reduces as the column gets slender. However, the level of brittleness at failure for high strength concrete PEC columns is not affected significantly by the overall column slenderness parameter.

The presence of a higher bending moment (resulting from a high e/d ratio) reduces the column capacity significantly. The occurrence of local buckling is also affected by the e/d

162

ratio. The columns with lower e/d ratio experienced local flange buckling before or very shortly after the peak load.

As the plate slenderness ratio increases, the axial capacity of the column reduces, as expected, with increased brittleness in the failure behaviour. These effects are more prominent in short columns with a larger link spacing. On the other hand, the brittle behaviour of long PEC columns is not affected by the b/t ratio. Thus, the advantage of using stockier flange plates diminishes as the column becomes slender.

Varying the link spacing from 0.5d and 0.7d is found to have no significant effect on the capacity of the PEC column. Short and intermediate PEC columns with a flange b/t ratio of 35, when combined with the link spacing of 0.7d, experienced the most brittle and sudden failure among the parametric columns.

The axial capacity of the PEC column, with a variety of L/d, e/d, b/t and s/d ratios, is greatly (average increase is 55%) improved by the use of high strength (60 MPa) concrete instead of normal strength (30 MPa) concrete. However, the load–deformation response of high strength concrete PEC columns exhibited brittle failure as compared to the normal strength concrete columns.

The numerical capacities of 12 parametric columns were compared with the theoretical cross-sectional capacities and were observed to exceed the theoretical capacities in all of the 12 columns. For PEC columns with normal strength concrete, the numerical axial capacity exceeded the theoretical value by 2% (column SN1) to 10% (column IN3). For high strength concrete columns, the numerical capacity exceeded the theoretical capacity by 8% (column LH1) to 18% (column LH3). These numbers include the effect of the range of L/d, e/d, b/t and s/d ratios implemented in this study. Therefore, the theoretical interaction diagram based on the method used by Prickett and Driver (2006) for short PEC columns can be used for columns with $L > 5d$ and the wide range of b/t and s/d ratios applied in this study.

Table 6.1 Details of the PEC Columns for Parametric Study

Column designation	L/d	e/d	b/t	s/d	Global imperfection (mm)	f_{cu} (MPa)	ε_{cu} (μɛ)	E_c (MPa)
SN1[a]	5	0.15	25	0.5	0.0	30	1900	25000
SN2	5	0.15	30	0.7	0.0	30	1900	25000
SN3	5	0.05	25	0.5	0.0	30	1900	25000
SN4	5	0.3	25	0.5	0.0	30	1900	25000
SN5	5	0.15	30	0.5	0.0	30	1900	25000
SN6	5	0.15	35	0.5	0.0	30	1900	25000
SN7	5	0.15	25	0.7	0.0	30	1900	25000
SN8	5	0.15	35	0.7	0.0	30	1900	25000
SH1	5	0.15	25	0.5	0.0	60	2500	32600
SH2	5	0.3	35	0.7	0.0	60	2500	32600
IN1[a]	10	0.15	30	0.7	0.0	30	1900	25000
IN2	10	0.15	25	0.5	0.0	30	1900	25000
IN3	10	0.05	30	0.7	0.0	30	1900	25000
IN4	10	0.3	30	0.7	0.0	30	1900	25000
IN5	10	0.15	25	0.7	0.0	30	1900	25000
IN6	10	0.15	35	0.7	0.0	30	1900	25000
IN7	10	0.15	30	0.5	0.0	30	1900	25000
IN8	10	0.15	35	0.5	0.0	30	1900	25000
IH1	10	0.15	30	0.7	0.0	60	2500	32600
IH2	10	0.3	35	0.7	0.0	60	2500	32600
LN1	15	0.3	35	0.7	3.4	30	1900	25000
LN2	15	0.15	25	0.5	3.4	30	1900	25000
LN3	15	0.15	30	0.7	3.4	30	1900	25000
LH1[a]	15	0.3	35	0.7	3.4	60	2500	32600
LH2	15	0.3	25	0.5	3.4	60	2500	32600
LH3	15	0.05	35	0.7	3.4	60	2500	32600
LH4	15	0.15	35	0.7	3.4	60	2500	32600
LH5	15	0.3	25	0.7	3.4	60	2500	32600
LH6	15	0.3	30	0.7	3.4	60	2500	32600
LH7	15	0.3	35	0.5	3.4	60	2500	32600
LH8	15	0.3	30	0.5	3.4	60	2500	32600

[a]Reference column

Table 6.2 Effect of Overall Column Slenderness (L/d) Ratio

Set	Column designa-tion	Column properties					Magnitude of output parameters at peak load point				Percent difference		Occurrence of local buckling
		L/d	e/d	b/t	s/d	f_{cu} (MPa)	P_u (kN)	M_u (kN-m)	$\varepsilon_{a,u}$ (με)	$U_{3,u}$ (mm)	P_u (%)	M_u (%)	
	SN1[a]	5	0.15	25	0.5	30	6428	458	1382	3.7	0	0	after peak at 0.99P_u
Set 1	IN2	10	0.15	25	0.5	30	6240	498	1213	12.3	-3	9	after peak at 0.97P_u
	LN2	15	0.15	25	0.5	30	5922	601	1200	30.6	-8	31	after peak at 0.96P_u
	SN2	5	0.15	30	0.7	30	5892	421	1370	3.9	0	0	at peak
Set 2	IN1[a]	10	0.15	30	0.7	30	5724	460	1202	12.9	-3	9	after peak at 0.99P_u
	LN3	15	0.15	30	0.7	30	5410	551	1190	30.9	-8	31	after peak at 0.99P_u
	SH2	5	0.30	35	0.7	60	6701	945	1184	6.0	0	0	after peak at 0.88P_u
Set 3	IH2	10	0.30	35	0.7	60	6263	988	1008	22.8	-7	5	after peak at 0.91P_u
	LH1[a]	15	0.30	35	0.7	60	5521	1036	904	49.3	-18	10	after peak at 0.92P_u

[a]Reference column

Table 6.3 Effect of Load Eccentricity (e/d) Ratio

Set	Column designation	Column properties					Magnitude of output parameters at peak load point				Percent difference		Occurrence of local buckling
		L/d	e/d	b/t	s/d	f_{cu} (MPa)	P_u (kN)	M_u (kN-m)	$\varepsilon_{a,u}$ ($\mu\varepsilon$)	$U_{3,u}$ (mm)	P_u (%)	M_u (%)	
	SN3	5	**0.05**	25	0.5	30	7931	188	1547	1.2	0	0	after peak at $0.99P_u$
Set 1	SN1[a]	5	**0.15**	25	0.5	30	6428	458	1382	3.7	-19	144	after peak at $0.99P_u$
	SN4	5	**0.30**	25	0.5	30	4967	700	1334	5.8	-37	272	after peak at $0.99P_u$
	IN3	10	**0.05**	30	0.7	30	7268	195	1503	4.4	0	0	before peak at $0.97P_u$
Set 2	IN1[a]	10	**0.15**	30	0.7	30	5724	460	1202	12.9	-21	136	after peak at $0.99P_u$
	IN4	10	**0.30**	30	0.7	30	4287	678	1195	23.1	-41	247	after peak at $0.99P_u$
	LH3	15	**0.05**	35	0.7	60	10833	462	1546	16.8	0	0	before peak at $0.93P_u$
Set 3	LH4	15	**0.15**	35	0.7	60	8116	880	1288	37.6	-25	91	after peak at $0.97P_u$
	LH1[a]	15	**0.30**	35	0.7	60	5521	1036	904	49.3	-49	124	after peak at $0.92P_u$

[a]Reference column

Table 6.4 Effect of Plate Slenderness (b/t) Ratio with Different s/d Ratios

Set	Column designa-tion	Column properties					Magnitude of output parameters at peak load point				Percent difference		Occurrence of local buckling
		L/d	e/d	b/t	s/d	f_{cu} (MPa)	P_u (kN)	M_u (kN-m)	$\varepsilon_{a,u}$ (µε)	$U_{3,u}$ (mm)	P_u (%)	M_u (%)	
Set 1	SN1[a]	5	0.15	**25**	0.5	30	6428	458	1382	3.7	0	0	after peak at $0.99P_u$
	SN5	5	0.15	**30**	0.5	30	5917	422	1371	3.8	-8	-8	after peak at $0.99P_u$
	SN6	5	0.15	**35**	0.5	30	5548	395	1361	3.9	-14	-14	after peak at $0.99P_u$
	SN7	5	0.15	**25**	0.7	30	6406	456	1383	3.7	0	0	after peak at $0.99P_u$
	SN2	5	0.15	**30**	0.7	30	5892	421	1370	3.9	-8	-8	at peak
	SN8	5	0.15	**35**	0.7	30	5411	380	1119	2.7	-16	-17	before peak at $0.99P_u$
Set 2	IN2	10	0.15	**25**	0.5	30	6240	498	1213	12.3	0	0	after peak at $0.97P_u$
	IN7	10	0.15	**30**	0.5	30	5743	462	1203	12.9	-8	-7	after peak at $0.98P_u$
	IN8	10	0.15	**35**	0.5	30	5384	435	1193	13.3	-14	-13	after peak at $0.98P_u$
	IN5	10	0.15	**25**	0.7	30	6224	497	1214	12.4	0	0	after peak at $0.98P_u$
	IN1[a]	10	0.15	**30**	0.7	30	5724	460	1202	12.9	-8	-7	after peak at $0.99P_u$
	IN6	10	0.15	**35**	0.7	30	5327	420	1100	11.4	-14	-15	before peak at $0.99P_u$
Set 3	LH2	15	0.30	**25**	0.5	60	6200	1154	971	47.7	0	0	after peak at $0.88P_u$
	LH8	15	0.30	**30**	0.5	60	5814	1098	958	50.5	-6	-5	after peak at $0.88P_u$
	LH7	15	0.30	**35**	0.5	60	5548	1041	904	49.3	-11	-10	after peak at $0.92P_u$
	LH5	15	0.30	**25**	0.7	60	6200	1147	959	46.6	0	0	after peak at $0.87P_u$
	LH6	15	0.30	**30**	0.7	60	5797	1082	929	48.2	-7	-6	after peak at $0.87P_u$
	LH1[a]	15	0.30	**35**	0.7	60	5521	1036	904	49.3	-11	-10	after peak at $0.92P_u$

[a]Reference column

Table 6.5 Effect of Link Spacing-to-Depth (s/d) Ratio with Different b/t Ratios

Set	Column designation	Column properties					Magnitude of output parameters at peak load point				Percent difference		Occurrence of local buckling
		L/d	e/d	b/t	s/d	f_{cu} (MPa)	P_u (kN)	M_u (kN-m)	$\varepsilon_{a,u}$ ($\mu\varepsilon$)	$U_{3,u}$ (mm)	P_u (%)	M_u (%)	
Set 1	SN1[a]	5	0.15	25	**0.5**	30	6428	458	1382	3.7	0	0	after peak at $0.99P_u$
	SN7	5	0.15	25	**0.7**	30	6406	456	1383	3.7	0	0	after peak at $0.99P_u$
	SN5	5	0.15	30	**0.5**	30	5917	422	1371	3.8	0	0	after peak at $0.99P_u$
	SN2	5	0.15	30	**0.7**	30	5892	421	1370	3.9	0	0	at peak
	SN6	5	0.15	35	**0.5**	30	5548	395	1361	3.9	0	0	after peak at $0.99P_u$
	SN8	5	0.15	35	**0.7**	30	5411	380	1119	2.7	-2	-4	before peak at 0.99Pu
Set 2	IN2	10	0.15	25	**0.5**	30	6240	498	1213	12.3	0	0	after peak at $0.97P_u$
	IN5	10	0.15	25	**0.7**	30	6224	497	1214	12.4	0	0	after peak at $0.98P_u$
	IN7	10	0.15	30	**0.5**	30	5743	462	1203	12.9	0	0	after peak at $0.98P_u$
	IN1[a]	10	0.15	30	**0.7**	30	5724	460	1202	12.9	0	0	after peak at $0.99P_u$
	IN8	10	0.15	35	**0.5**	30	5384	435	1193	13.3	0	0	after peak at $0.98P_u$
	IN6	10	0.15	35	**0.7**	30	5327	420	1100	11.4	-1	-3	before peak at $0.99P_u$
Set 3	LH2	15	0.30	25	**0.5**	60	6200	1154	971	47.7	0	0	after peak at $0.87P_u$
	LH5	15	0.30	25	**0.7**	60	6200	1147	959	46.6	0	-1	after peak at $0.87P_u$
	LH8	15	0.30	30	**0.5**	60	5814	1098	958	50.5	0	0	after peak at $0.88P_u$
	LH6	15	0.30	30	**0.7**	60	5797	1082	929	48.2	0	-1	after peak at $0.87P_u$
	LH7	15	0.30	35	**0.5**	60	5548	1041	904	49.3	0	0	after peak at $0.92P_u$
	LH1[a]	15	0.30	35	**0.7**	60	5521	1036	904	49.3	0	0	after peak at $0.92P_u$

[a]Reference column

Table 6.6 Effect of Concrete Compressive Strength

Set	Column designa-tion	Column properties					Magnitude of output parameters at peak load point				Percent difference		Occurrence of local buckling
		L/d	e/d	b/t	s/d	f_{cu} (MPa)	P_u (kN)	M_u (kN-m)	$\varepsilon_{a,u}$ (µε)	$U_{3,u}$ (mm)	P_u (%)	M_u (%)	
Set 1	SN1[a]	5	0.15	25	0.5	**30**	6428	458	1382	3.7	0	0	after peak at $0.99P_u$
	SH1	5	0.15	25	0.5	**60**	10100	712	1538	2.9	57	55	after peak at $0.89P_u$
Set 2	IN1[a]	10	0.15	30	0.7	**30**	5724	460	1202	12.9	0	0	after peak at $0.99P_u$
	IH1	10	0.15	30	0.7	**60**	9160	776	1430	17.3	60	69	after peak at $0.94P_u$
Set 3	LN1	15	0.3	35	0.7	**30**	3736	667	926	40.2	0	0	after peak at $0.92P_u$
	LH1[a]	15	0.3	35	0.7	**60**	5521	1036	904	49.3	48	55	after peak at $0.92P_u$

[a]Reference column

Table 6.7 Comparison of Numerical and Theoretical Capacities for the Reference Parametric Columns with Various e/d Ratios

Set	Column designation	e/d	Numerical		Theoretical		Numerical/Theoretical	
			Load (kN)	Moment (kN-m)	Load (kN)	Moment (kN-m)	Load	Moment
	SN3	0.05	7931	188	7700	180	1.03	1.04
Set 1	SN1[a]	0.15	6428	458	6300	435	1.02	1.05
	SN4	0.30	4967	700	4850	675	1.02	1.04
	IN3	0.05	7268	195	6630	170	1.10	1.15
Set 2	IN1[a]	0.15	5724	460	5250	400	1.09	1.15
	IN4	0.30	4287	678	4050	595	1.06	1.14
	LH3	0.05	10833	462	9200	340	1.18	1.36
Set 3	LH4	0.15	8116	880	7000	660	1.16	1.33
	LH1[a]	0.30	5521	1036	5100	875	1.08	1.18

[a]Reference column

Table 6.8 Comparison of Numerical and Theoretical Capacities for the Reference Columns with Variable Concrete Strength

Set	Column designation	e/d	Numerical		Theoretical		Numerical/Theoretical	
			Load (kN)	Moment (kN-m)	Load (kN)	Moment (kN-m)	Load	Moment
Set 1	SN1[a]	0.15	6428	458	6300	435	1.02	1.05
	SH1	0.15	10100	712	9130	610	1.11	1.17
Set 2	IN1[a]	0.15	5724	460	5250	400	1.09	1.15
	IH1	0.15	9160	776	8200	605	1.12	1.28
Set 3	LN1	0.30	3736	667	3600	625	1.04	1.07
	LH1[a]	0.30	5521	1036	5100	875	1.08	1.18

[a]Reference column
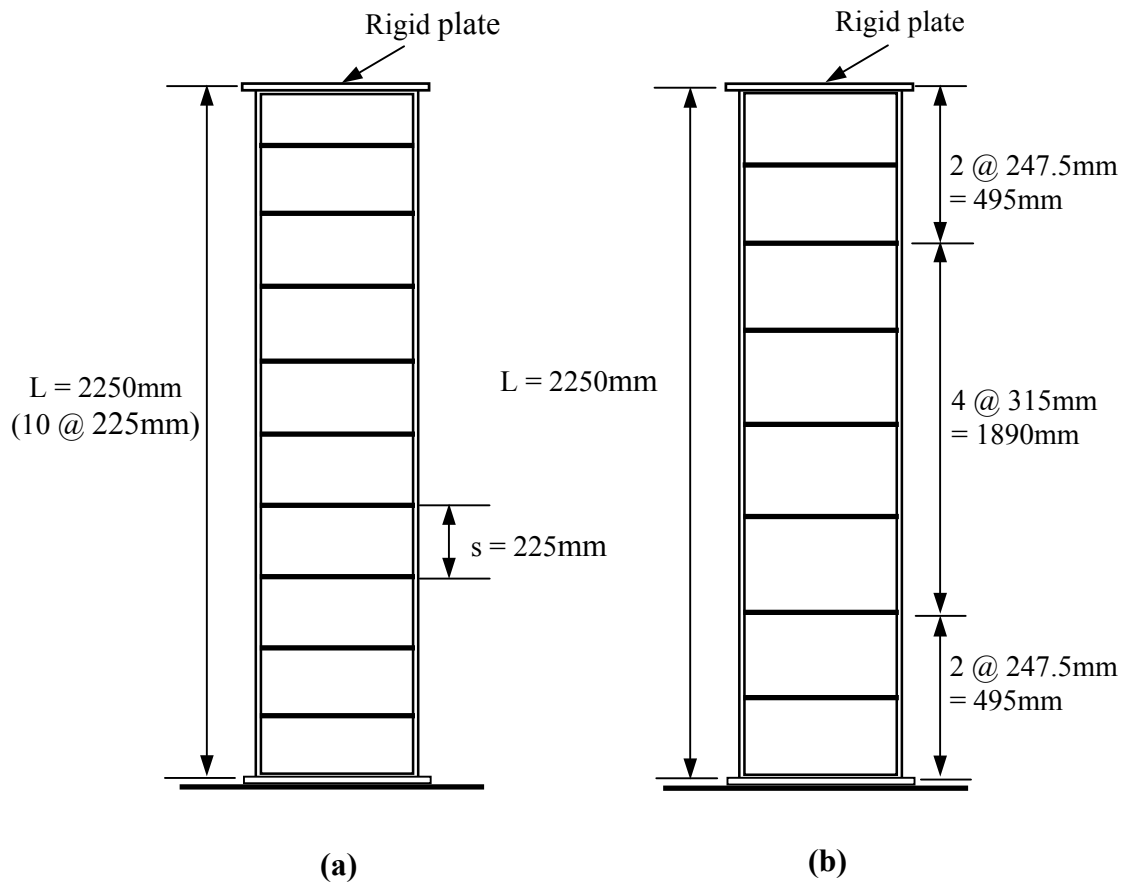
Figure 6.1 Link Arrangements in Short Parametric PEC Columns with:
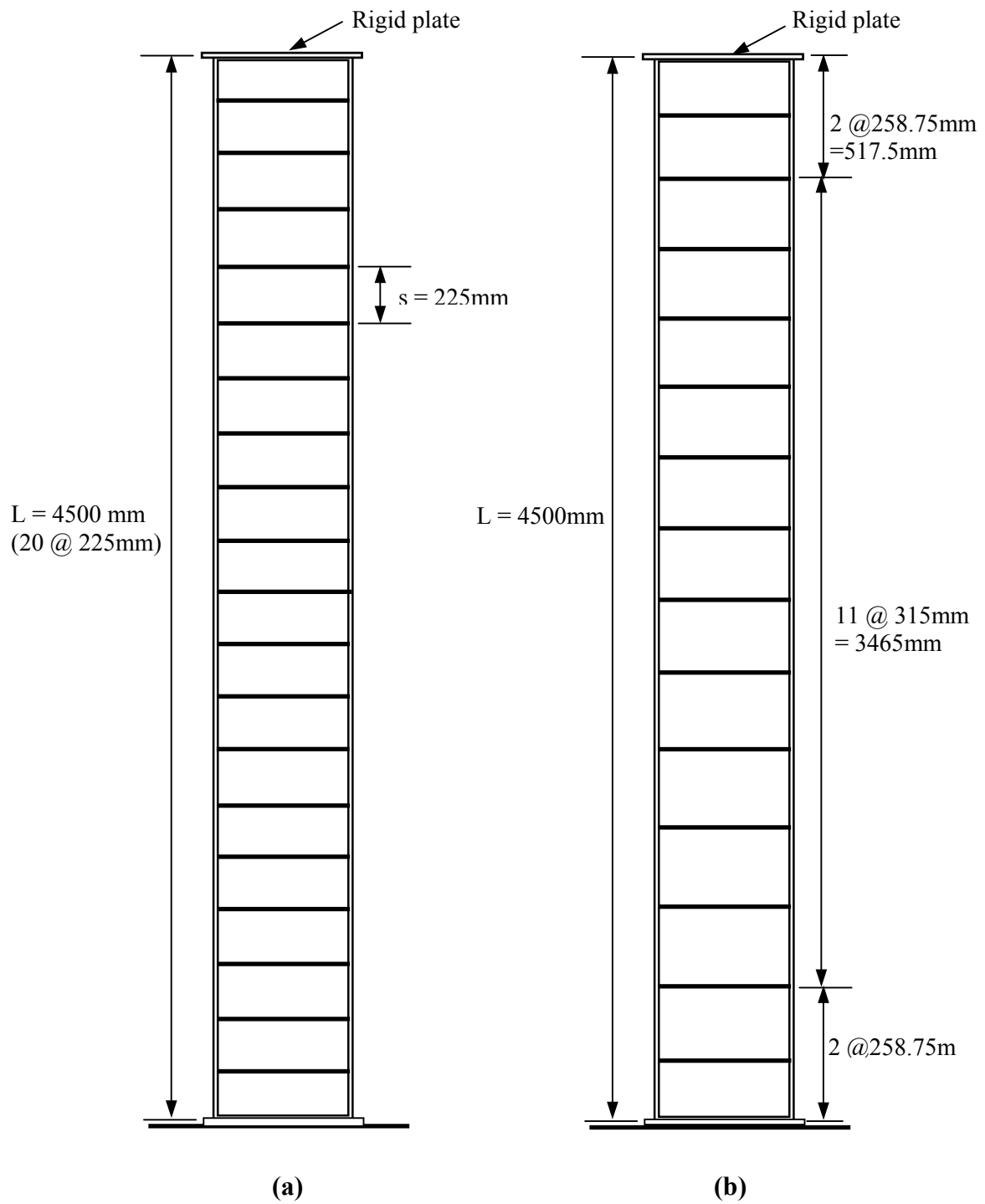
(a) s = 0.5d and (b) s = 0.7d

Figure 6.2 Link Arrangements in Intermediate Parametric PEC Columns with: (a) s = 0.5d and (b) s = 0.7d

172
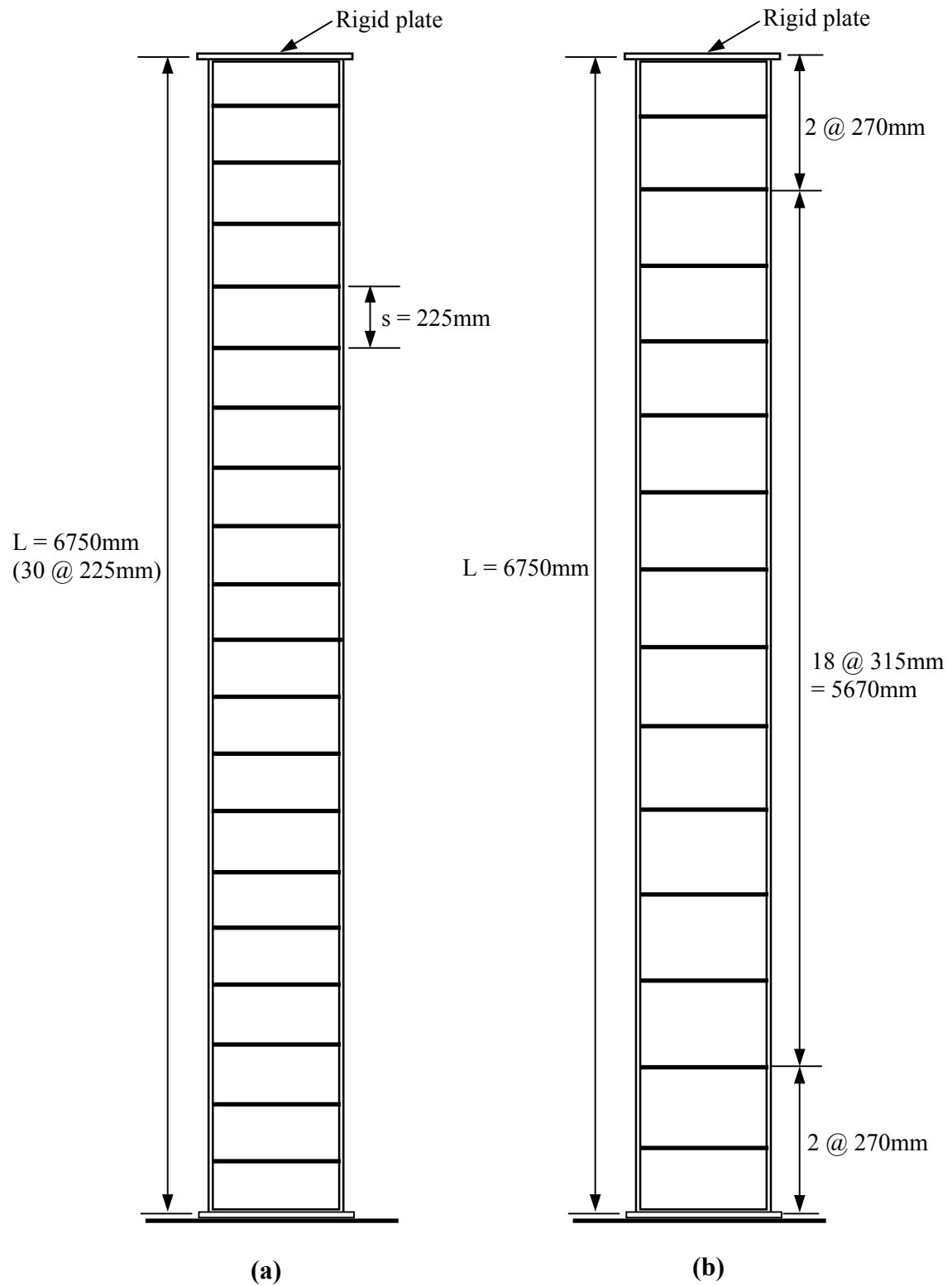
Figure 6.3 Link Arrangements in Long Parametric PEC Columns with:

(a) s = 0.5d and (b) s = 0.7d
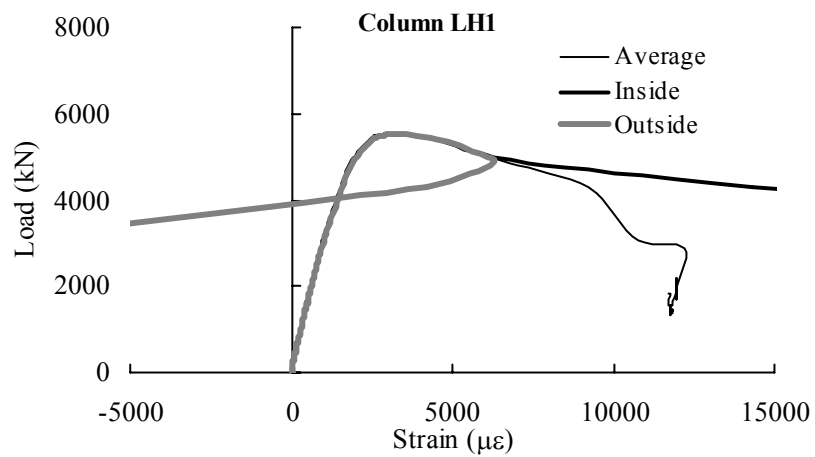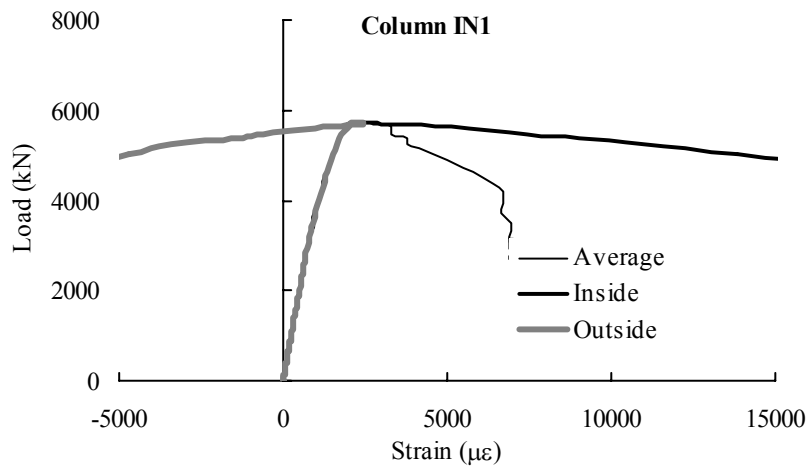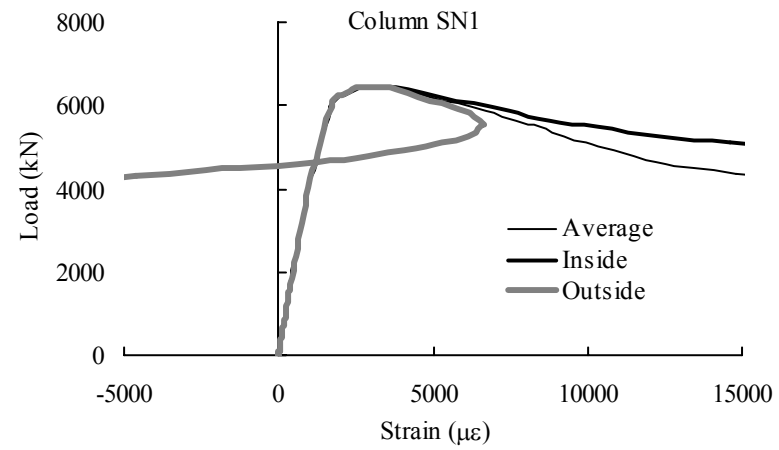
Figure 6.4 Load versus Axial Strain at the Locally Buckled Flange in the Reference Columns

174
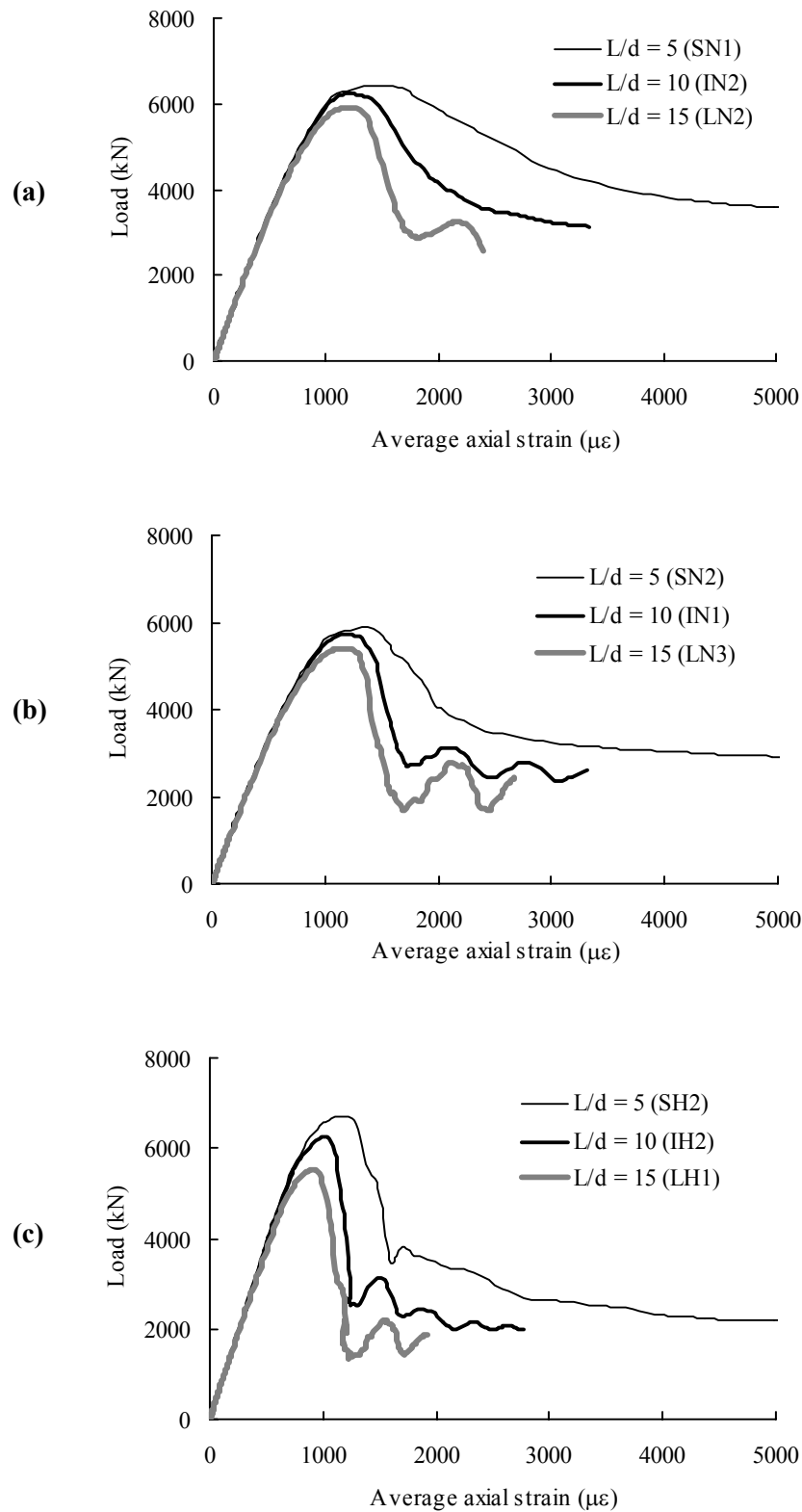
Figure 6.5 Effect of L/d Ratio on Load versus Average Axial Strain Curve, (a) Set 1, (b) Set 2 and (c) Set 3

175
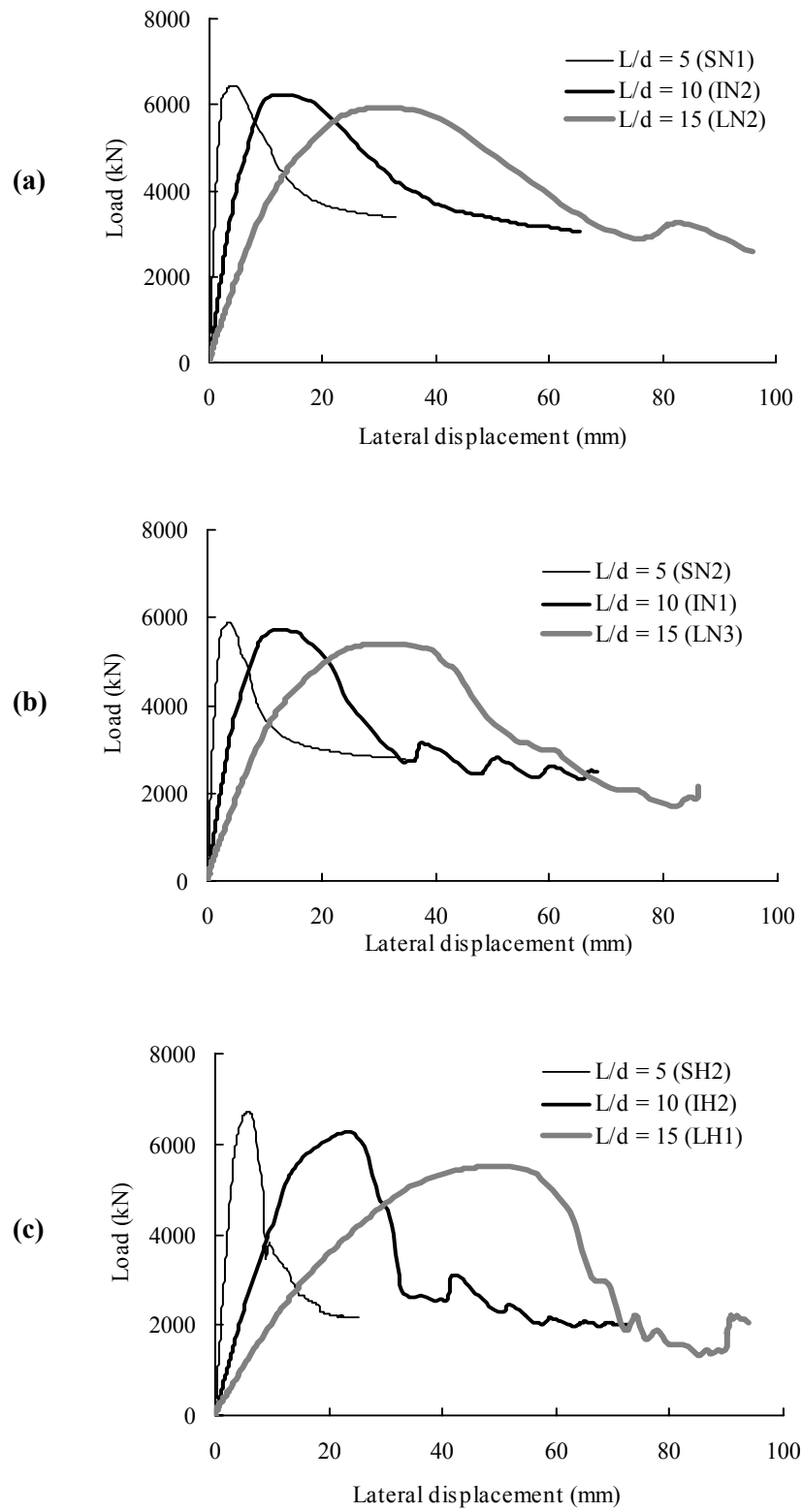
Figure 6.6 Effect of L/d Ratio on Load versus Lateral Displacement Curve, (a) Set 1, (b) Set 2 and (c) Set 3
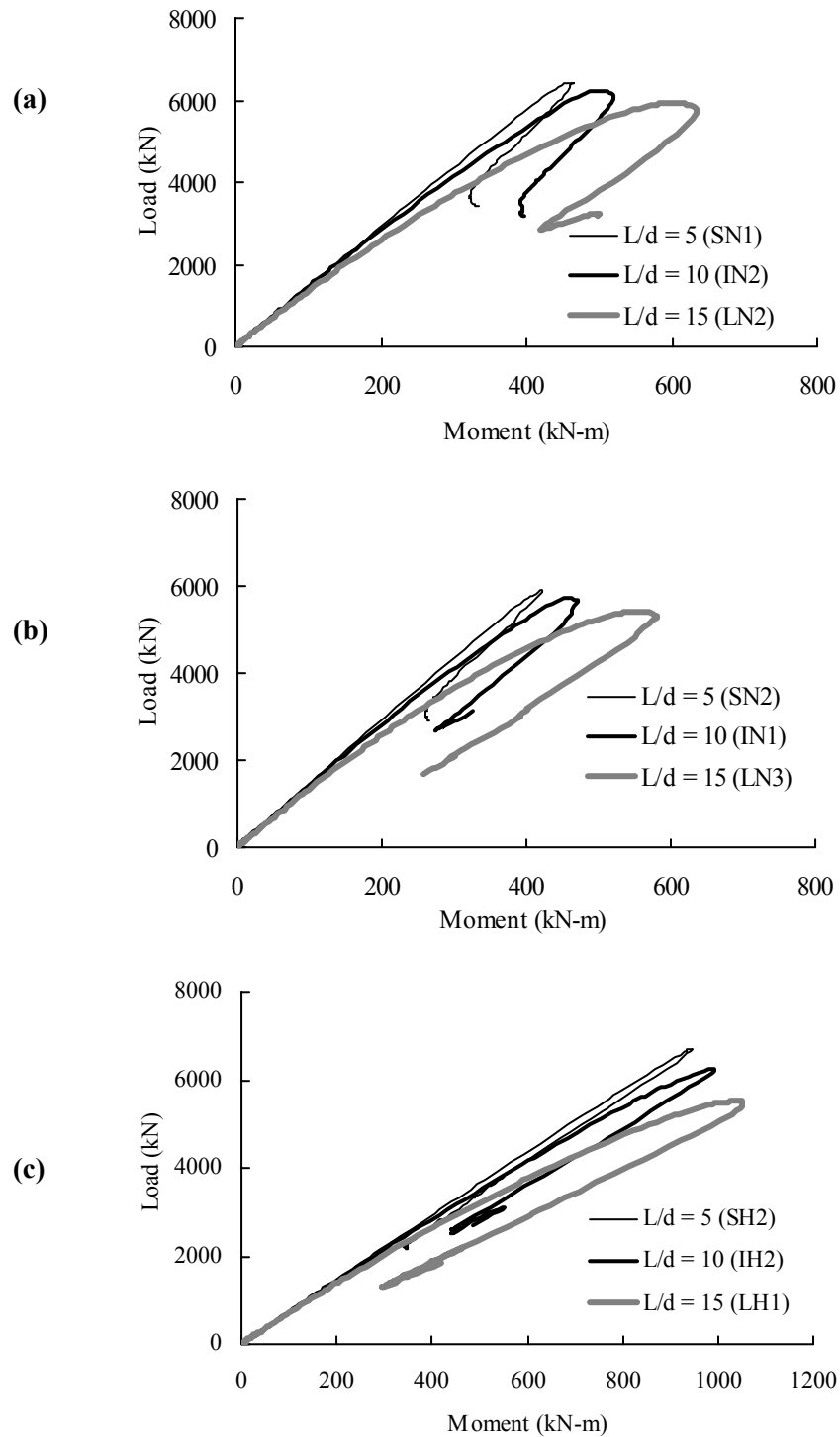
Figure 6.7 Effect of L/d Ratio on Load versus Moment Curve, (a) Set 1, (b) Set 2 and (c) Set 3

177
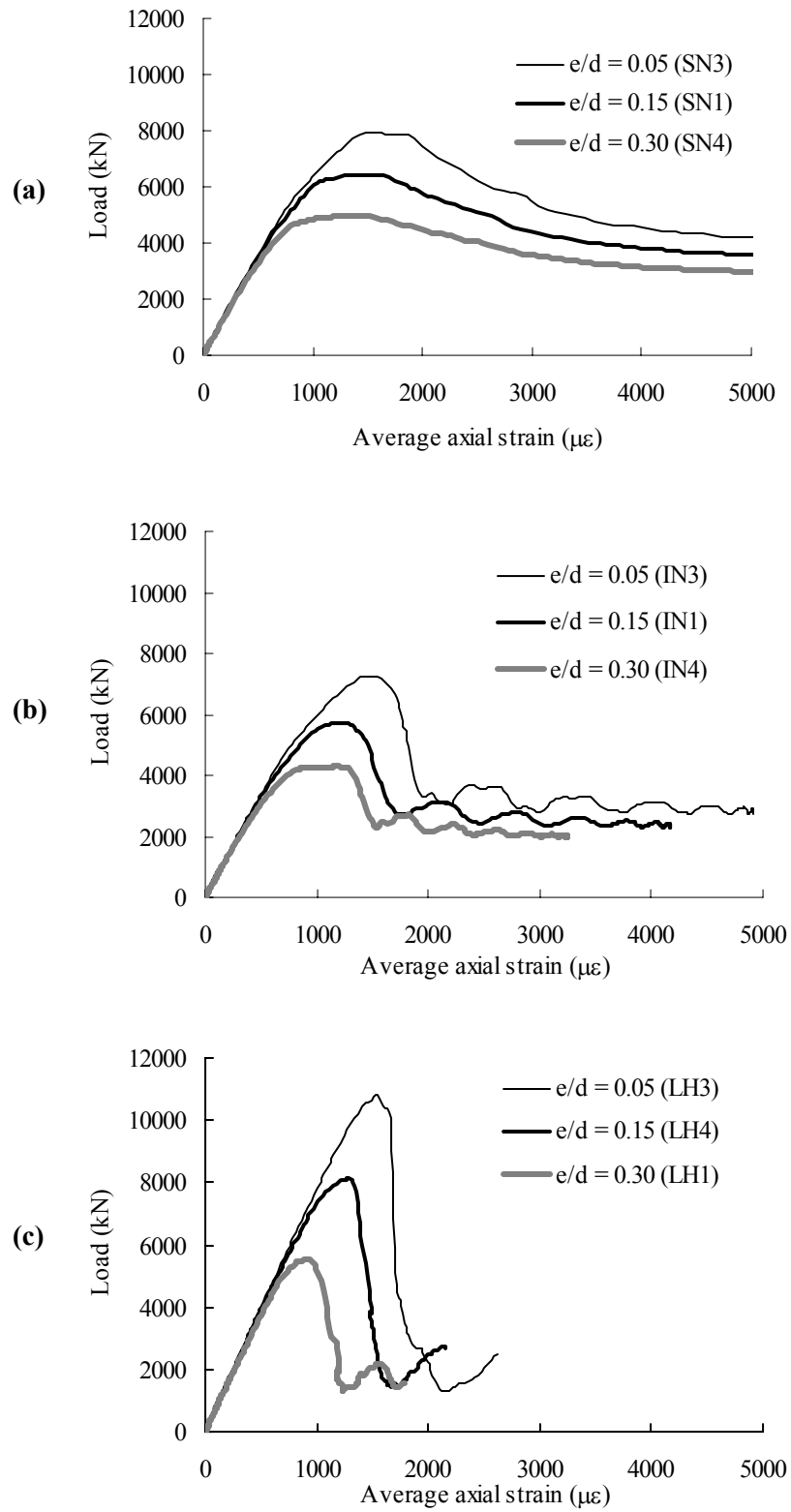
Figure 6.8 Effect of e/d Ratio on Load versus Average Axial Strain Curve, (a) Set 1, (b) Set 2 and (c) Set 3

178
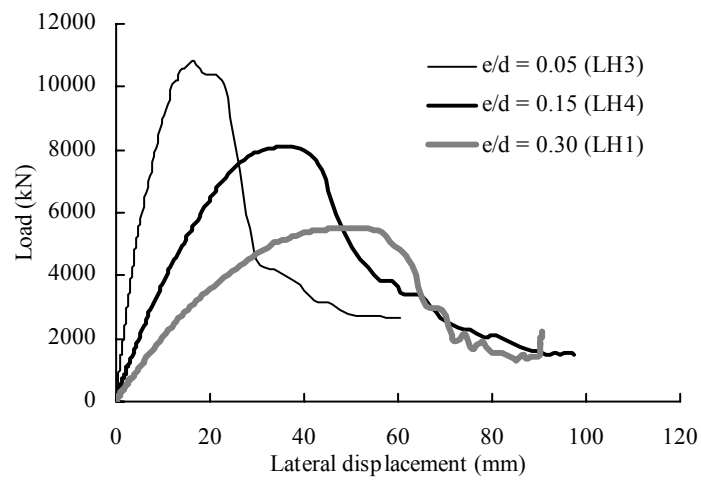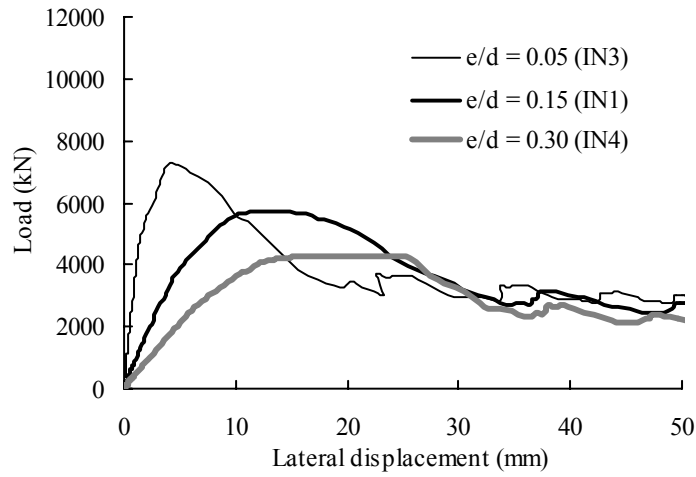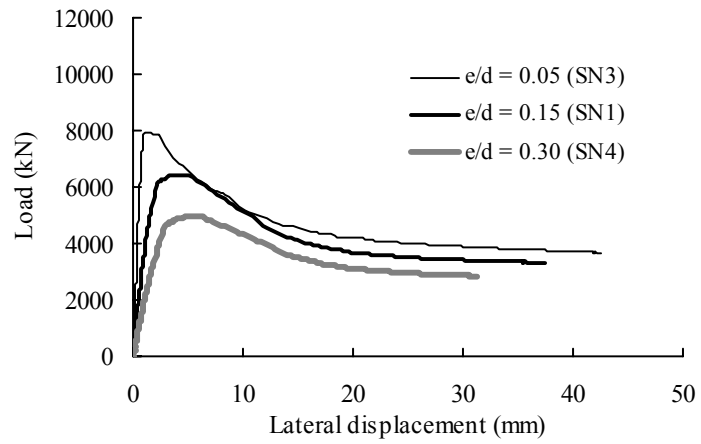
Figure 6.9 Effect of e/d Ratio on Load versus Lateral Displacement Curve, (a) Set 1, (b) Set 2 and (c) Set 3

179
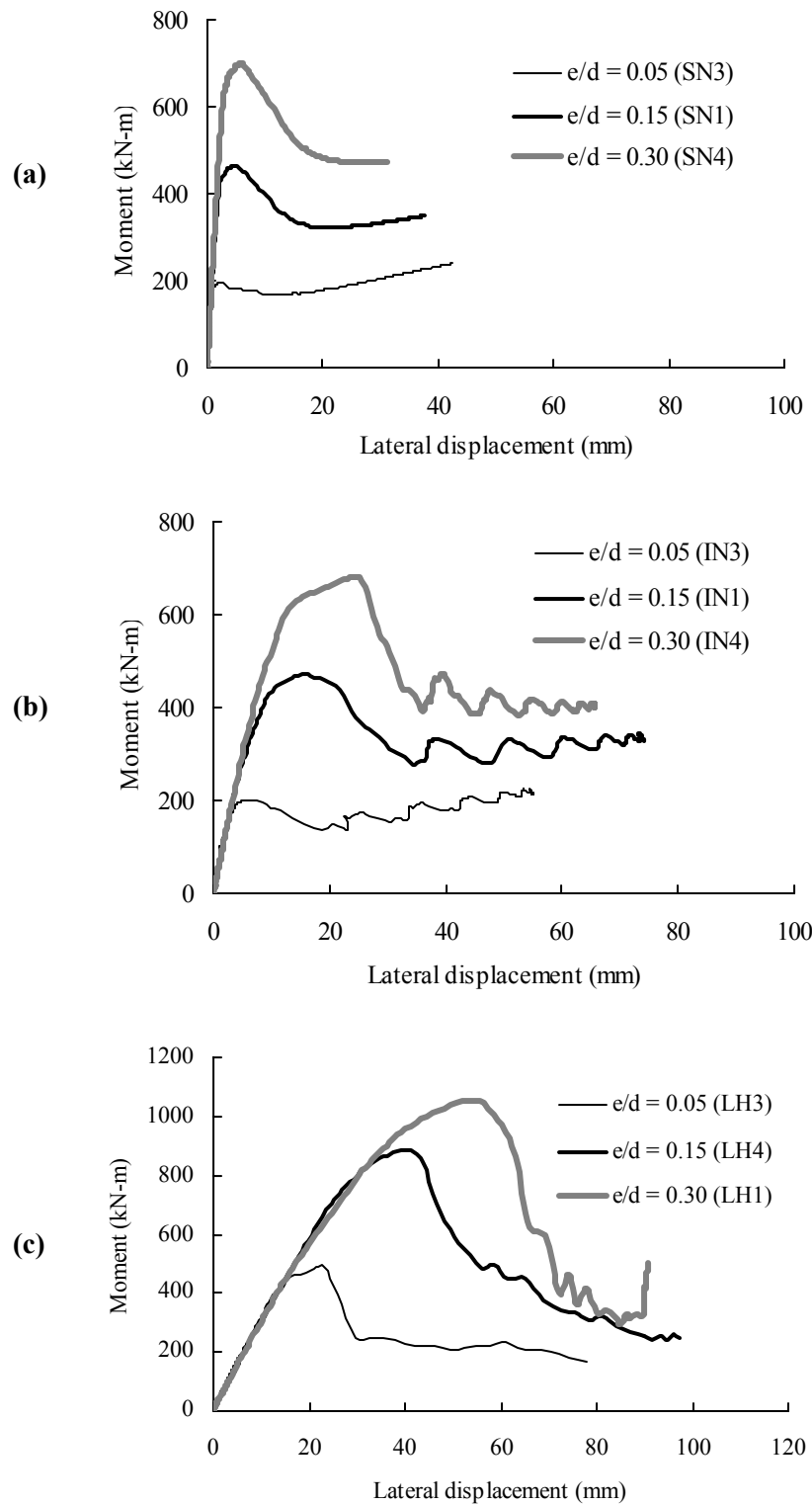
Figure 6.10 Effect of e/d Ratio on Moment versus Lateral Displacement Curve,

(a) Set 1, (b) Set 2 and (c) Set 3

180
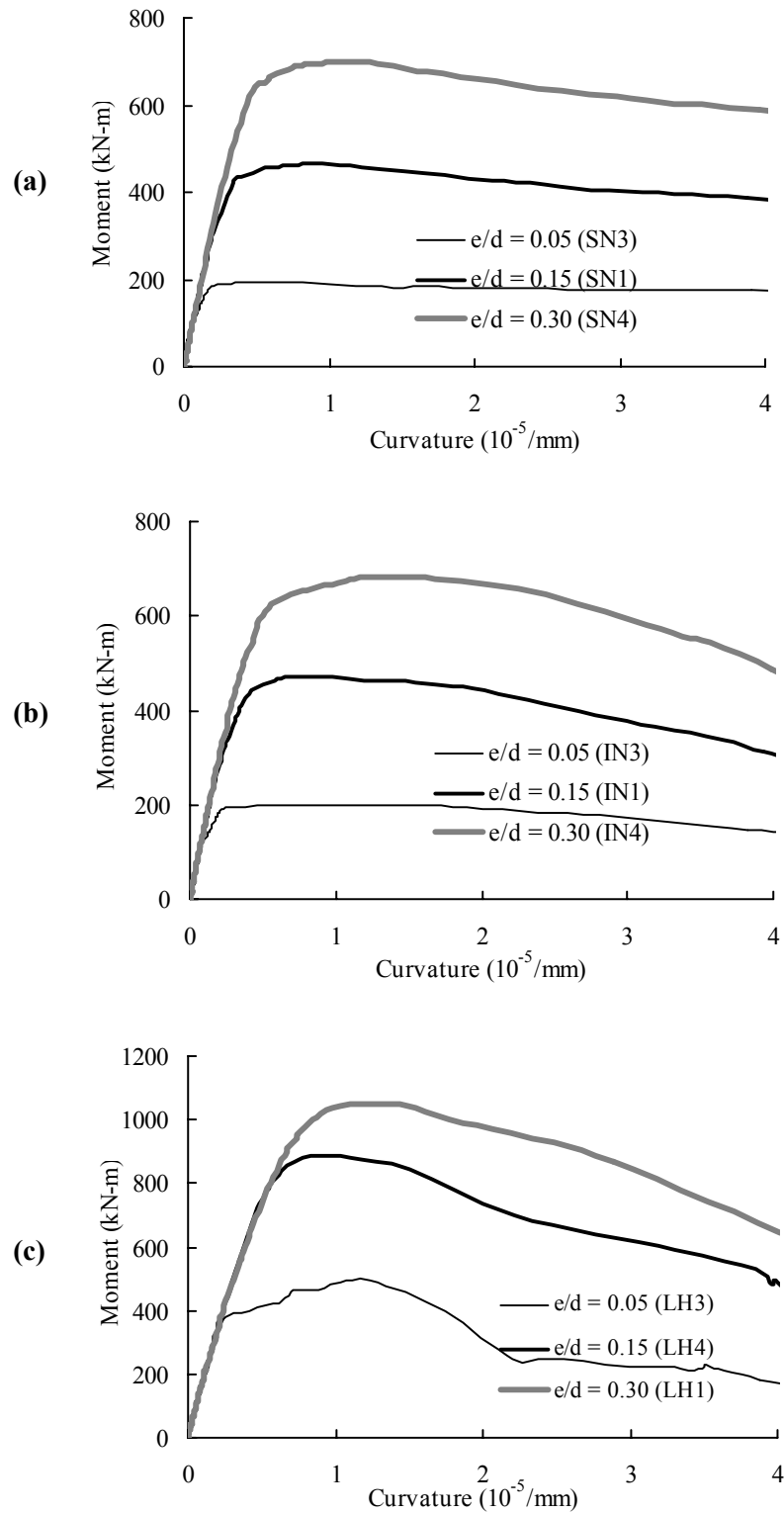
Figure 6.11 Effect of e/d Ratio on Moment versus Curvature Curve, (a) Set 1, (b) Set 2 and (c) Set 3
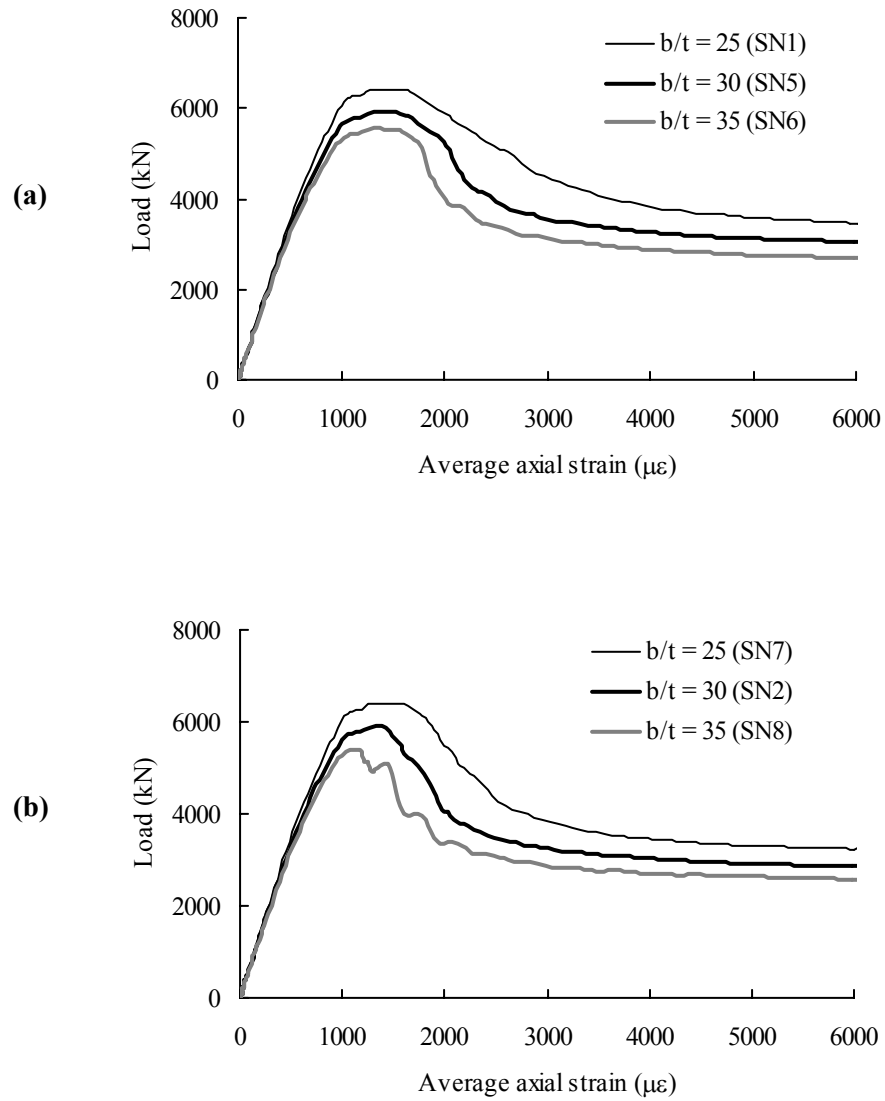
Figure 6.12 Effect of b/t ratio on Load versus Average Axial Strain Response for Short PEC Column (Analysis Set 1), (a) s = 0.5d and (b) s = 0.7d
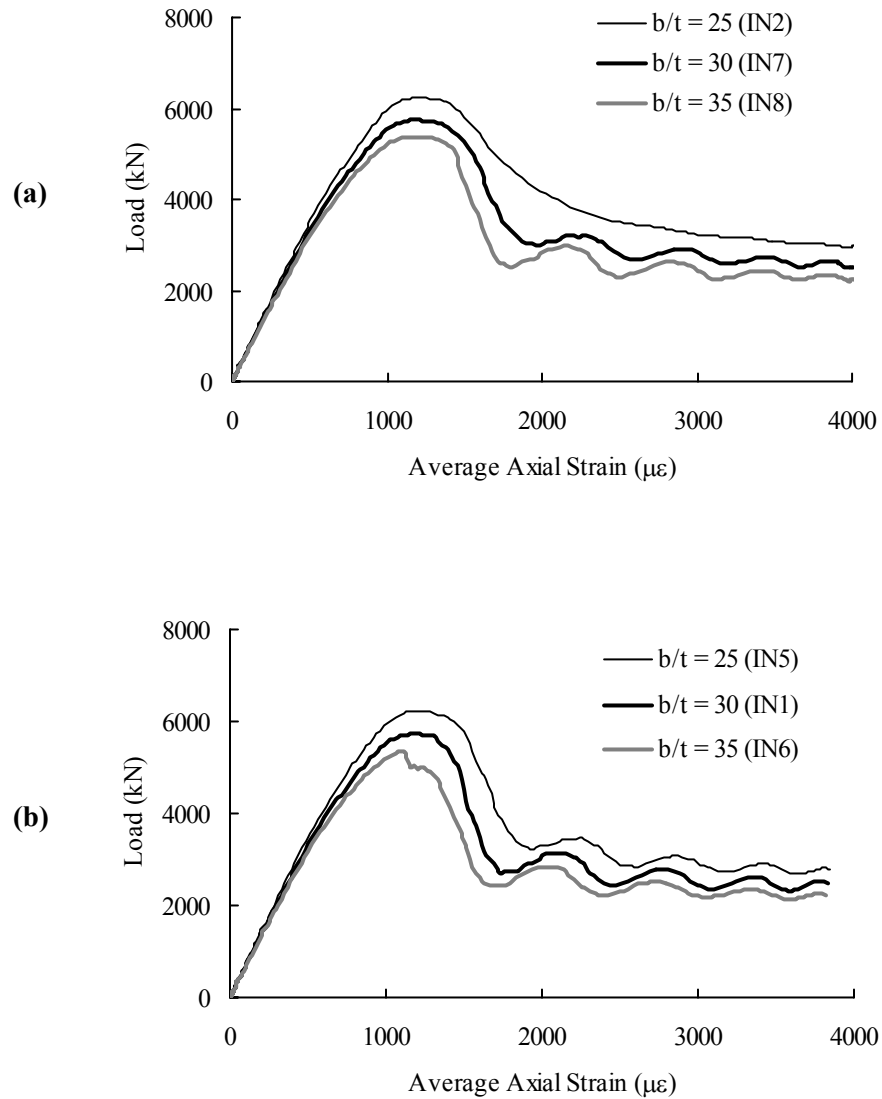
Figure 6.13 Effect of b/t ratio on Load versus Average Axial Strain Response for Intermediate PEC Column (Analysis Set 2), (a) s = 0.5d and (b) s = 0.7d
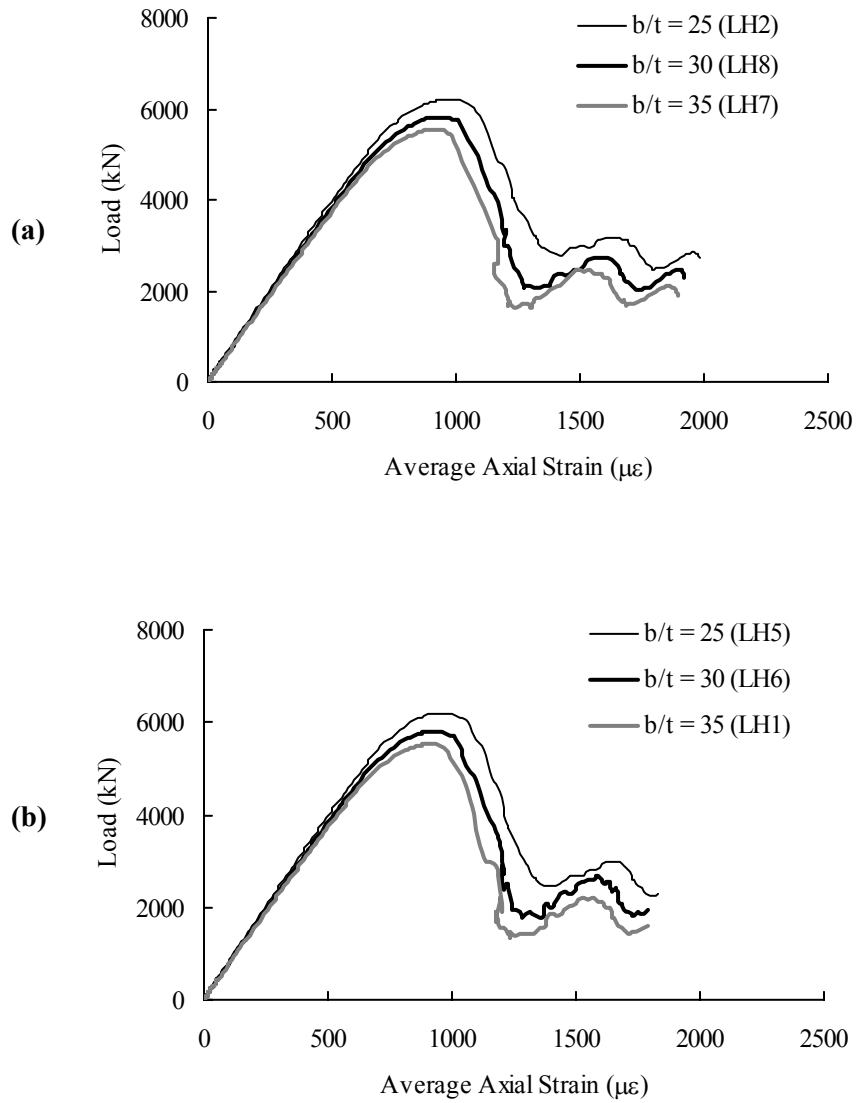
Figure 6.14 Effect of b/t ratio on Load versus Average Axial Strain Response for Long PEC Column (Analysis Set 3), (a) s = 0.5d and (b) s = 0.7d

184
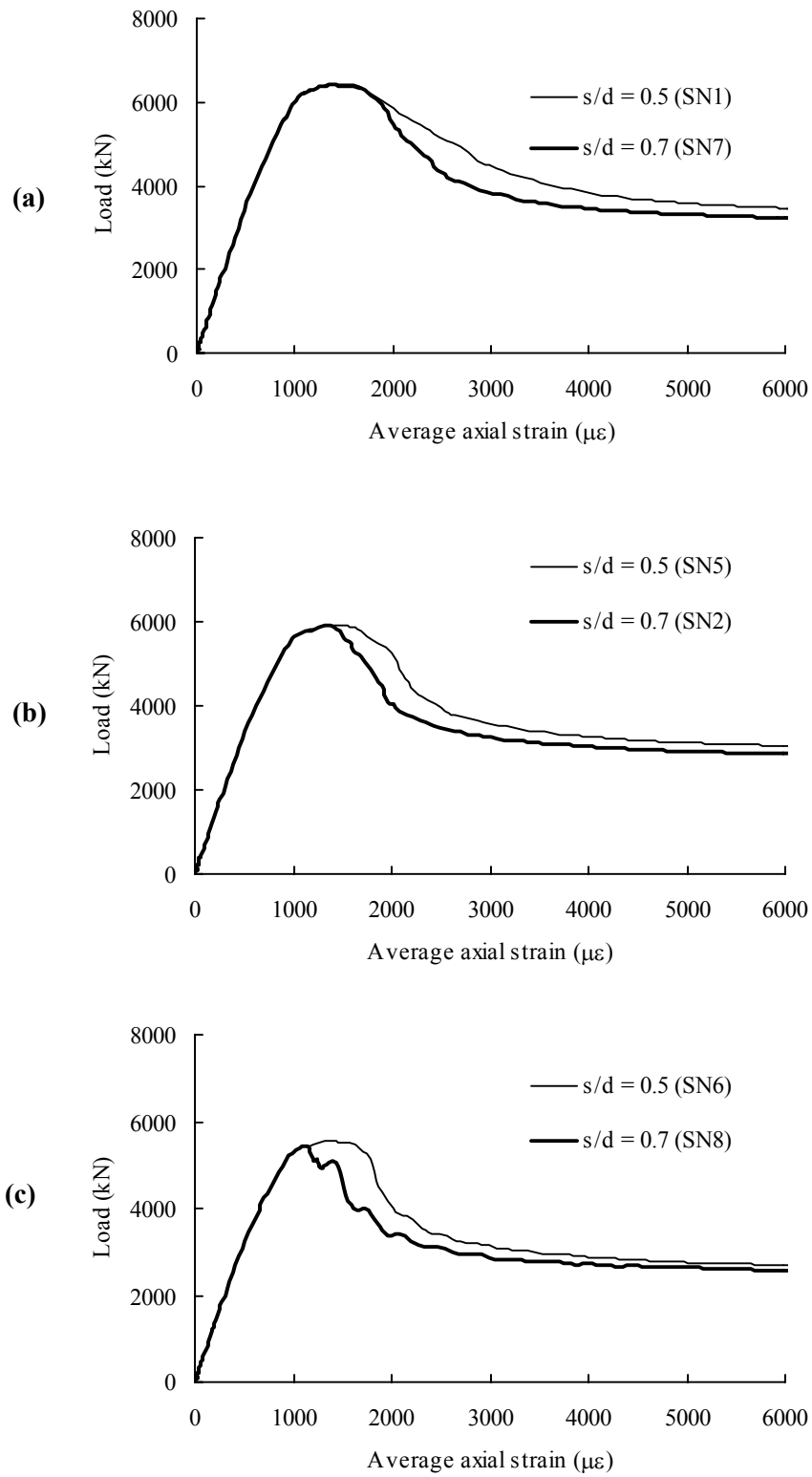
Figure 6.15 Effect of s/d Ratio on Load versus Average Axial Strain Response for Short PEC Column (Analysis Set 1), (a) b/t = 25, (b) b/t = 30 and (c) b/t = 35
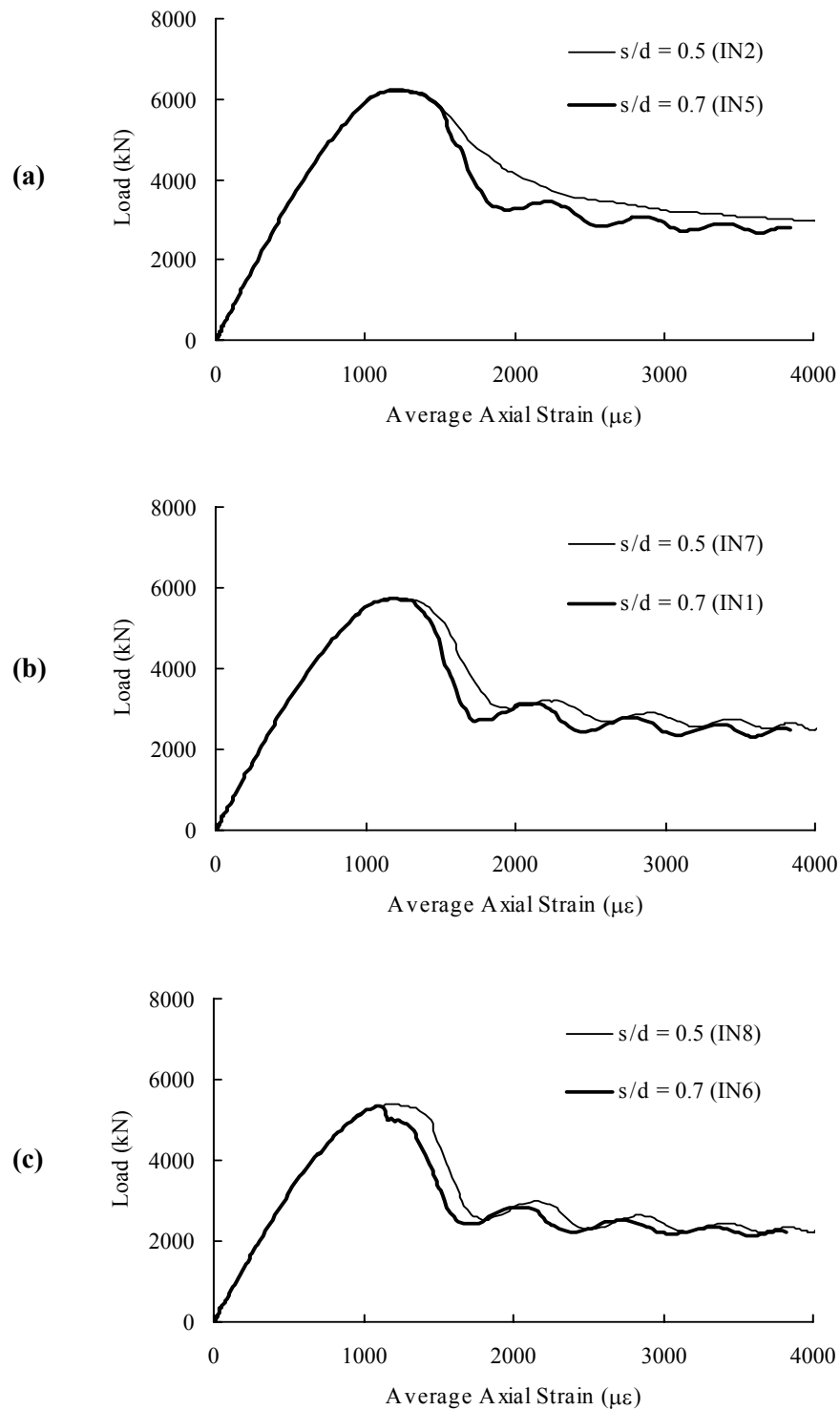
Figure 6.16 Effect of s/d Ratio on Load versus Average Axial Strain Response for Intermediate PEC Column (Analysis Set 2), (a) b/t = 25, (b) b/t = 30 and (c) b/t = 35
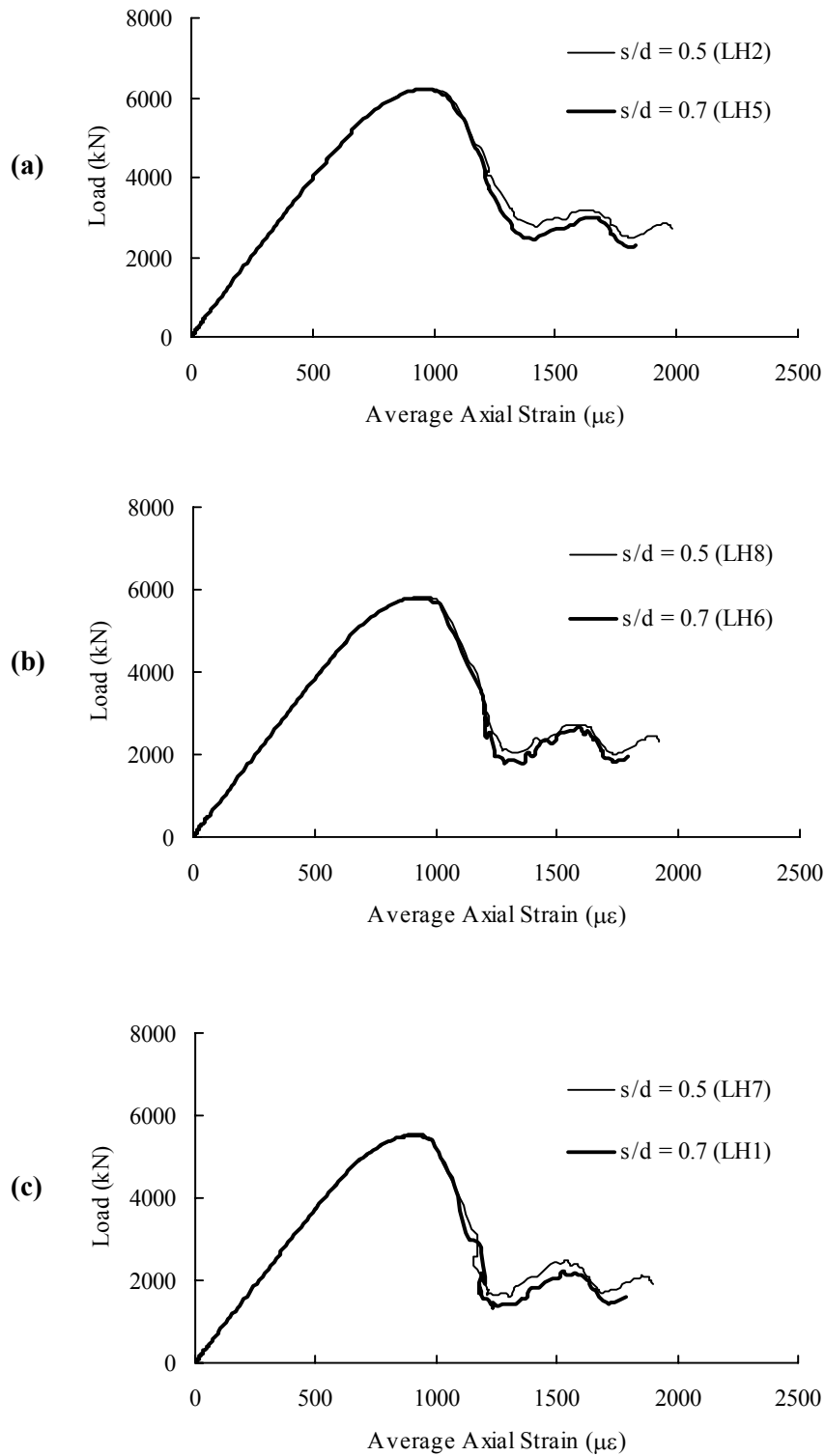
Figure 6.17 Effect of s/d Ratio on Load versus Average Axial Strain Response for Long PEC Column (Analysis Set 2), (a) b/t = 25, (b) b/t = 30 and (c) b/t = 35
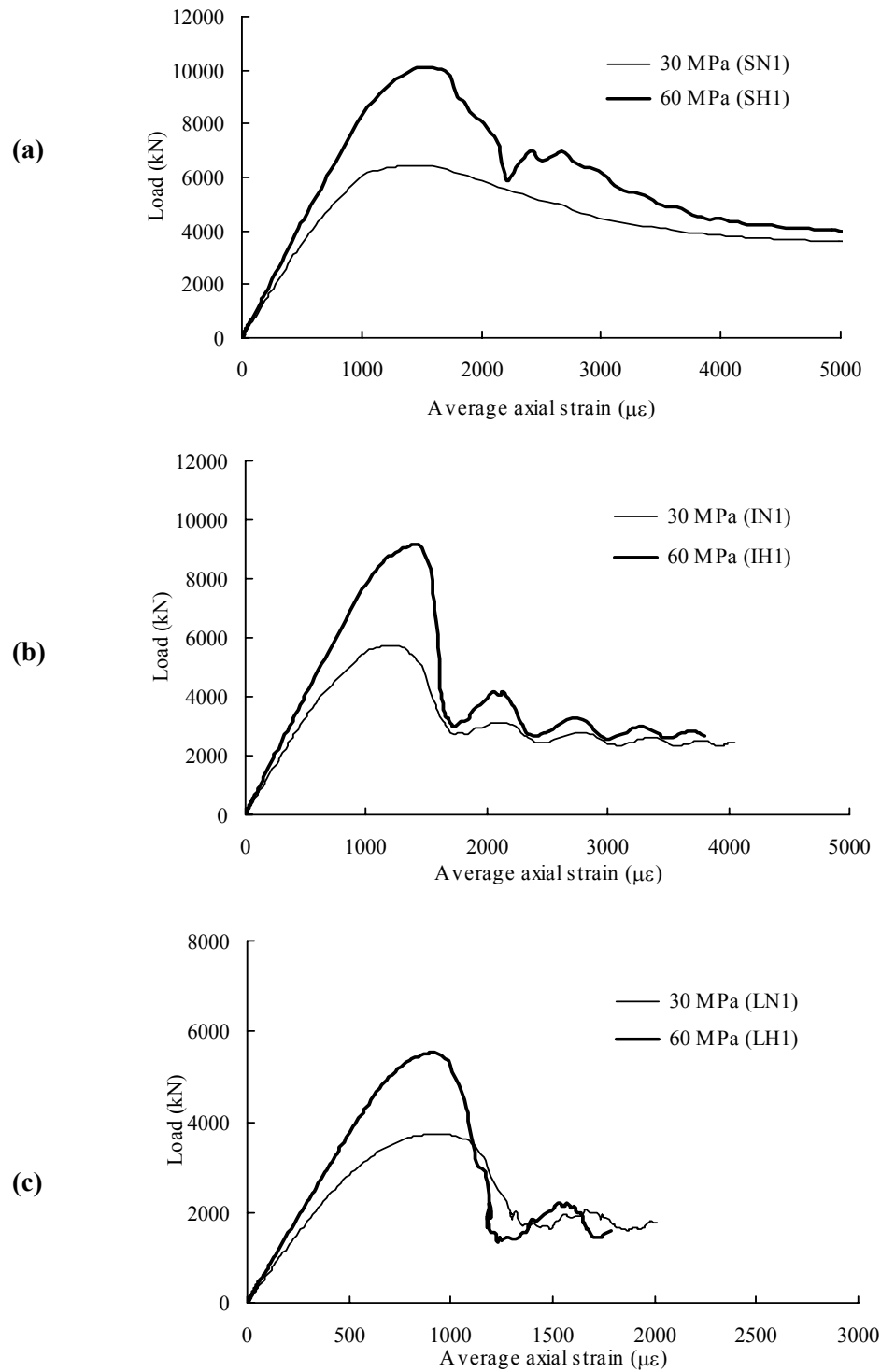
Figure 6.18 Effect of Concrete Compressive Strength on Load versus Average Axial Strain Curve, (a) Set 1, (b) Set 2 and (c) Set 3

188
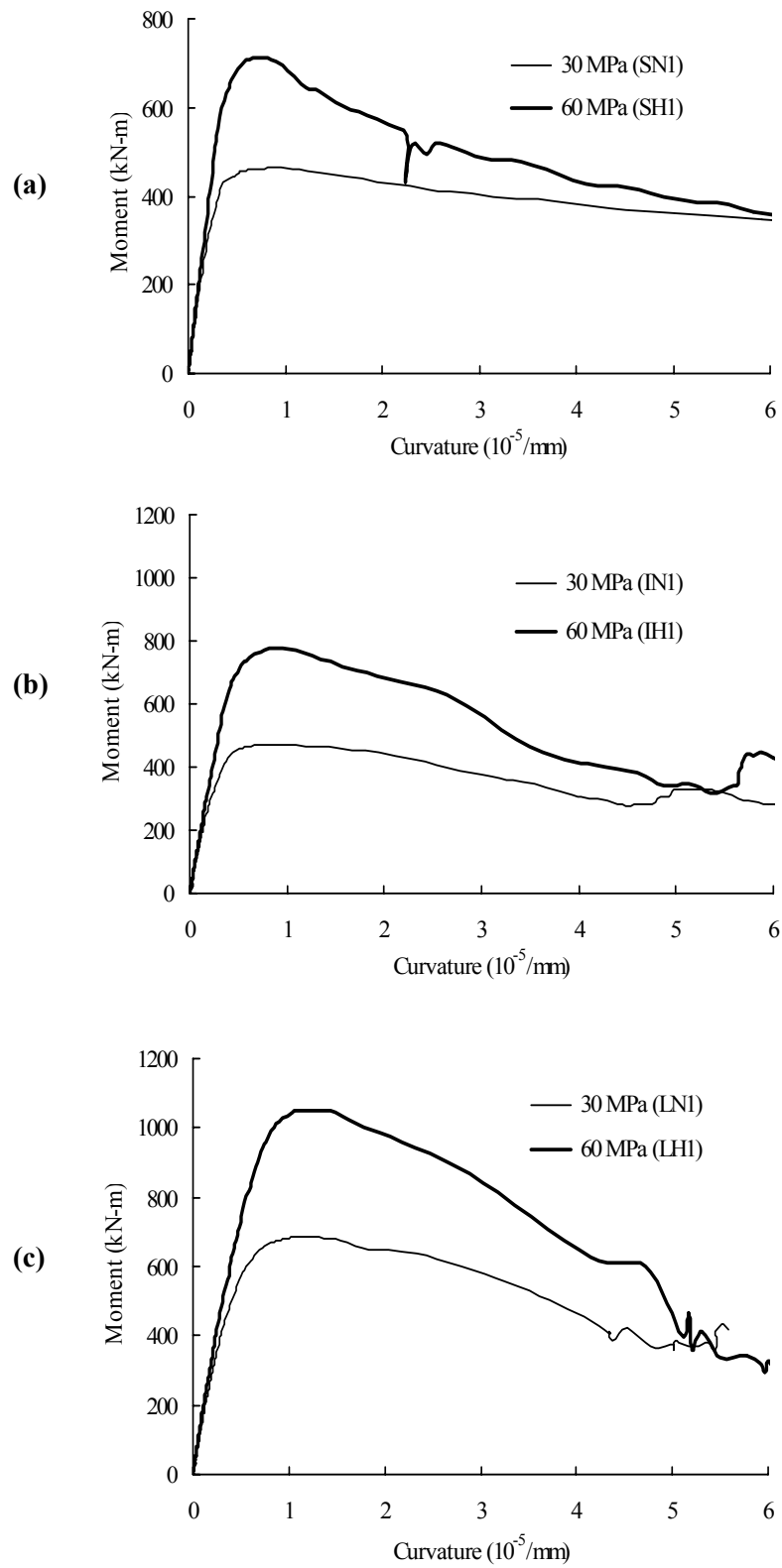
Figure 6.19 Effect of Concrete Compressive Strength on Moment versus Curvature Curve, (a) Set 1, (b) Set 2 and (c) Set 3
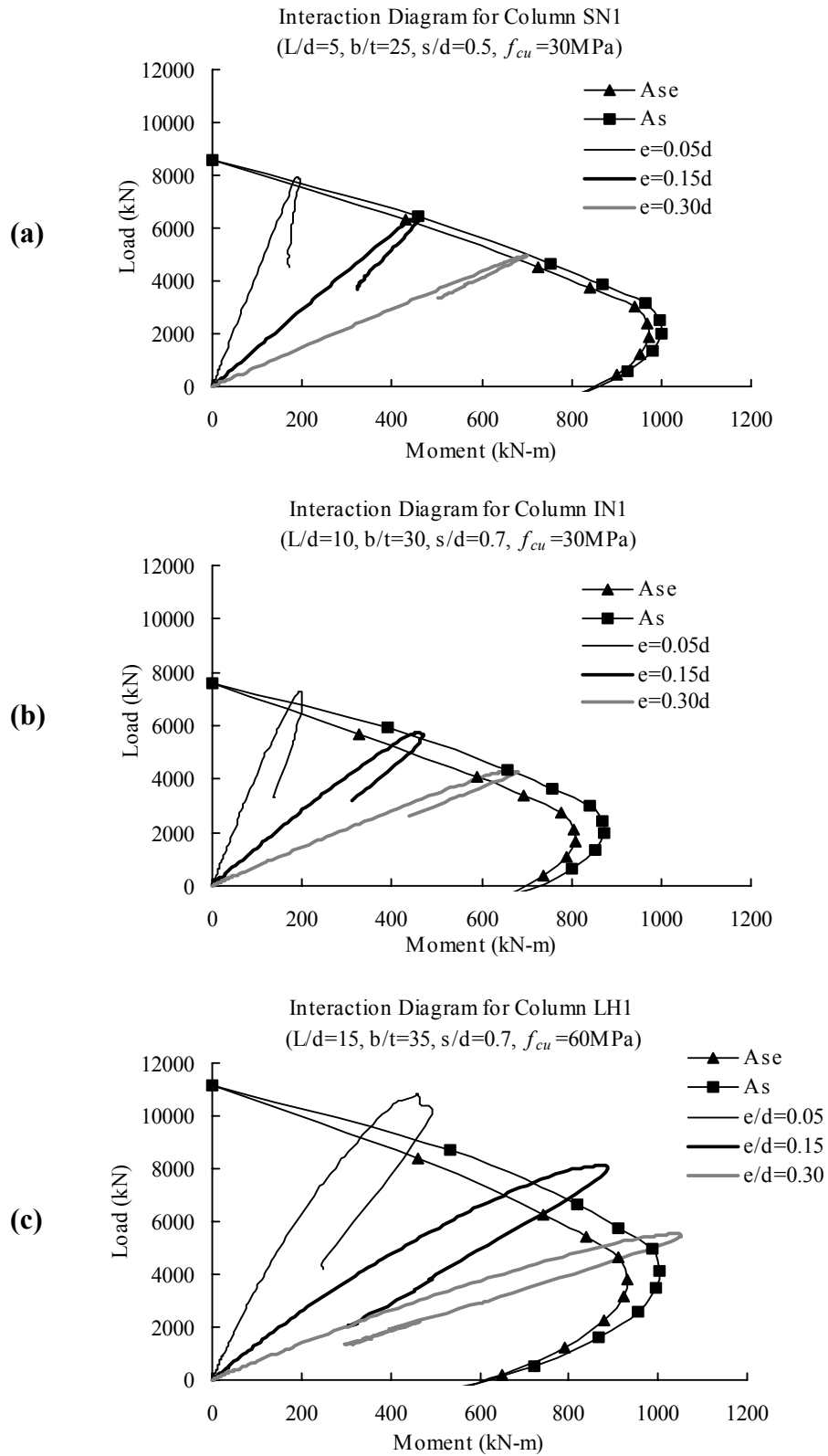
Figure 6.20 Load–Moment Interaction Diagrams,

(a) Column SN1, (b) Column IN1 and (c) Column LH1

190

(a)

(b)
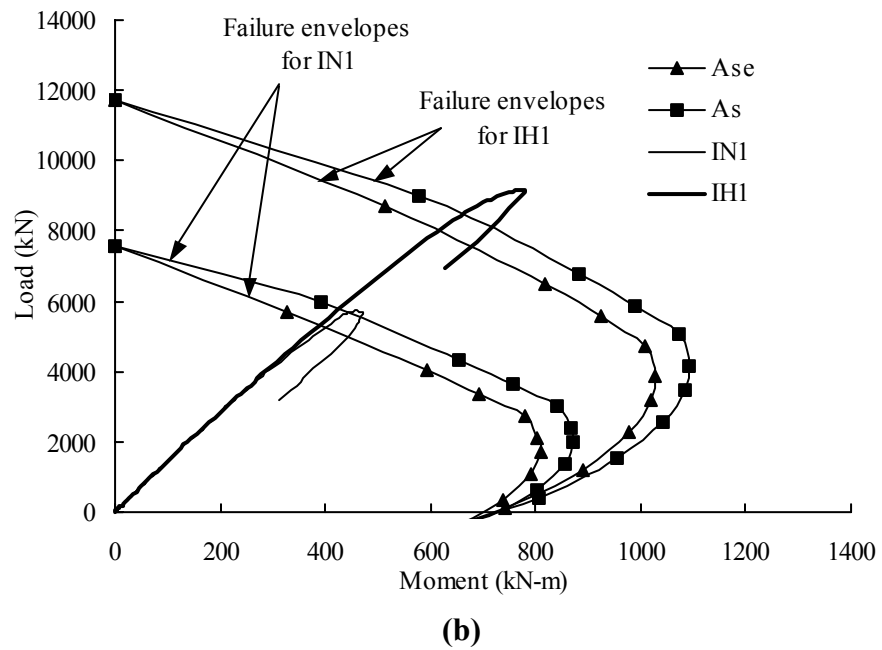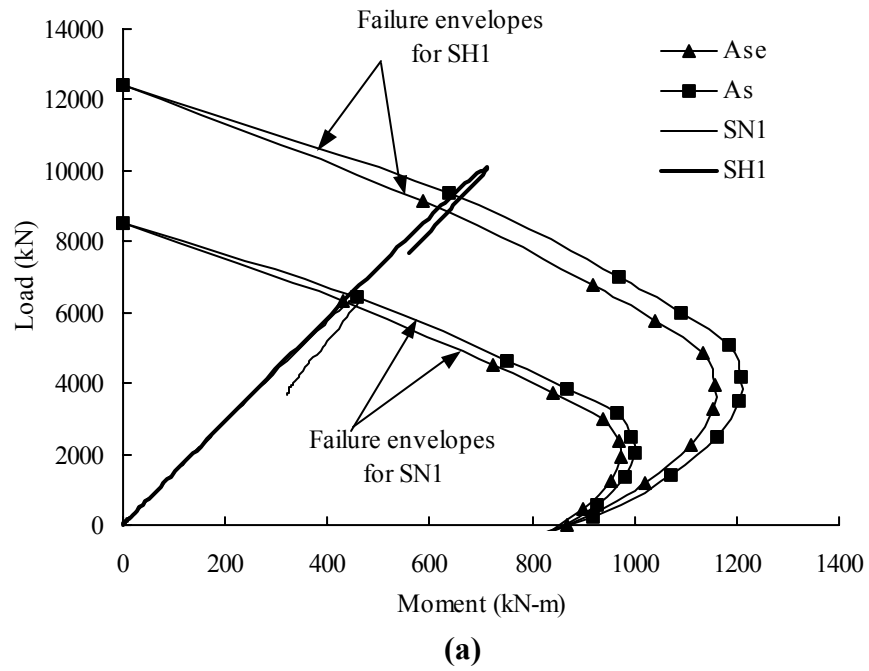
**Figure 6.21 Effect of Concrete Compressive Strength on the
Theoretical-to-Numerical Ratios of the Ultimate Capacities, (a) Short Column,
(b) Intermediate Column and (c) Long Column**

191
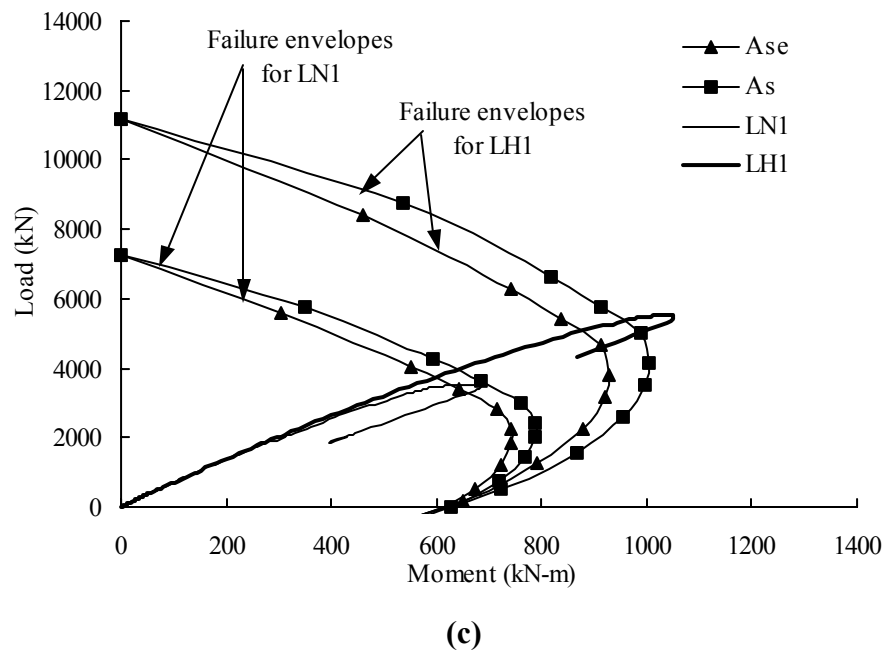
**Figure 6.21 (cont.) Effect of Concrete Compressive Strength on the
Theoretical-to-Numerical Ratios of the Ultimate Capacities, (a) Short Column,
(b) Intermediate Column and (c) Long Column**

7. SUMMARY, CONCLUSIONS AND RECOMMENDATIONS

7.1 Summary

Extensive numerical investigations were conducted to study the behaviour of partially encased composite (PEC) columns, which consist of a thin-walled welded steel shape with concrete placed between the flanges. Transverse links are welded between the flanges at regular intervals to improve the resistance to local instability of the thin steel flange. Previously, only limited research had been performed to develop a finite element model to study the behaviour of this new composite system and only axial loads were considered. In that work, significant challenges were identified in simulating the local instability of the thin flanges and the triaxial behaviour of the partially confined concrete in the column. This study was able to overcome these difficulties in the numerical simulation of the behaviour of PEC columns using the commercial finite element software ABAQUS.

The explicit module of ABAQUS finite element code was used to develop the numerical model for PEC columns. A dynamic explicit solution strategy was implemented in the numerical model to trace a stable post-peak response in the load–deformation curve. The steel–concrete interface in the composite column was simulated using a contact pair algorithm. To represent the concrete material behaviour under partial confinement, the damage plasticity model in ABAQUS was implemented. The performance of this model in representing the behaviour of concrete under various levels of lateral confinement was studied.

A small segment of the composite column consisting of one-fourth of the column cross-section was modelled initially to study the performance of the concrete material model and contact algorithm in modelling the steel–concrete interface. This model was then extended to establish a complete model for the PEC columns including the entire cross-

section, which was further used to simulate the column behaviour under the combined action of axial compression and flexure.

To validate the model, simulations were conducted for PEC column tests, reported in the literature, with normal strength concrete and high strength concrete with or without steel fibres. The short PEC columns constructed with normal strength concrete varied in cross-sectional size from 300 mm × 300 mm to 600 mm × 600 mm, including a variety of link spacings and diameters, and a range of flange plate slenderness ratios. Some of the normal strength concrete columns had additional longitudinal reinforcing bars and ties, which were also included in the numerical model. High strength concrete column specimens that were modeled are 400 mm × 400 mm in cross-section, with different link spacings and diameters. The loading conditions in both the normal strength and high strength concrete PEC columns ranged from concentric to eccentric loading with strong and weak axis bending and with variable load eccentricities. Furthermore, numerical analyses on three 9 m long PEC test columns with a 450 mm × 450 mm cross-section were performed to investigate the ability of the finite element model to reproduce the global buckling behaviour. The numerical model for long columns included the global imperfect shape of the test specimens resulting from the fabrication process. However, the local flange imperfections were excluded from the numerical model for all test specimens after a study had been conducted that demonstrated that the effect of local imperfections on the behaviour of these columns was very small. The effect of residual stress on the overall column behaviour was also studied for a series of test specimens and found to be negligible. The finite element model was also used to predict the effect of different link spacings on the behaviour of the PEC columns as well as determining the individual contributions of the steel and concrete to the total load carrying capacity.

A parametric study was conducted using the numerical model to investigate the effect of a full range of parameters on eccentrically loaded PEC columns subjected to strong axis bending. The parameters that were varied include the overall column slenderness ratio (L/d), load eccentricity ratio (e/d), link spacing-to-depth ratio (s/d), plate slenderness ratio (b/t) and concrete compressive strength (f_{cu}). The overall column slenderness (L/d) ratio

was chosen to be the primary variable with values of 5, 10 and 15. Other parameters were varied within each case of L/d ratio. The cross-section of the parametric columns was selected as 450 mm × 450 mm, which can be considered a typical size for a column used in medium to high–rise buildings. The effects of the selected parameters on the behaviour of PEC columns were studied with respect to the failure mode, the peak axial load, the axial load versus average axial strain curve, the axial load versus lateral displacement curve, the moment versus lateral displacement curve, the moment versus curvature curve and the load–moment interaction diagram. The load and moment capacities of the parametric columns obtained numerically were compared with theoretical capacities calculated based on the method used by Prickett and Driver (2006).

7.2 Conclusions

7.2.1 Performance of the Finite Element Model

In general the finite element models for PEC columns developed in this study were able to simulate the full behavioural histories of a variety of PEC columns tested under concentric and eccentric loading, with very good accuracy. The interaction between the steel and concrete and their separation at the common interface because of the local instability of the flange was successfully represented in the finite element analyses of the test specimens using the small, extended and full models developed herein. The numerical models also provided good representations of the peak load, axial deformation at the peak load and load versus axial strain curve, including the post-peak behaviour of the test columns. The small model overestimated the strain near and after the peak in the load versus axial strain curves of the test columns because the model only included a small region of the column where failure was forced to occur, whereas the test specimen strains were averaged over the length of the column. The extended and full models were able to represent the experimental strains near and after the peak with very good accuracy.

The full model, which is a complete model for PEC columns, was used to reproduce the test results of 12 normal strength, seven high strength and two steel fibre reinforced high

strength concrete PEC columns. The average experimental-to-numerical ratios of the peak load obtained were: 1.01, 0.99 and 1.08, respectively, for normal strength, high strength and steel fibre reinforced high strength concrete PEC columns with standard deviations all less than 0.05. Moreover, the numerical load versus axial strain responses for the test columns were in very good agreement with the experimental responses with only a few exceptions. Furthermore, the load versus moment curves obtained from the numerical analyses of the eccentrically loaded test columns represented the experimental curves with excellent accuracy, for strong axis bending as well as weak axis bending.

The full model also represented the axial capacity of the three long PEC test specimens (L/d = 20) with good accuracy with an average experimental-to-numerical ratio of 0.98 (excluding the specimen with premature failure). However, the numerical model overestimated the experimental strains around the peak region of the load versus axial strain curve.

Studies regarding the sensitivity of the column capacity to local flange imperfections and residual stresses revealed that neither had significant effects on the column behaviour, and therefore they were omitted from subsequent investigations.

7.2.2 Parametric Study

7.2.2.1 Effect of Overall Column Slenderness Ratio

For PEC columns constructed with normal strength concrete, higher L/d ratios resulted in brittle failure of the column. This behaviour was observed to be insignificantly affected by the plate slenderness ratio and link spacing. For PEC columns with high strength concrete, the L/d ratio seemed to have no significant effect on the level of brittleness of the failure mode of the column.

The axial load capacity of the normal strength concrete short PEC columns was reduced by 3% and 8%, when the L/d ratio was increased from 5 to 10 and 15, respectively. The change in the flange plate slenderness ratio from 25 to 30, along with the change in the

link spacing from 0.5d to 0.7d, did not affect the percent reduction in capacity. On the other hand, the use of high strength concrete (60 MPa) instead of normal strength concrete (30 MPa) along with b/t = 35 and higher eccentricity resulted in 7% and 18% reductions in the axial capacity of the short column, for L/d ratio of 10 and 15, respectively.

7.2.2.2 *Effect of Load Eccentricity-to-Depth Ratio*

The ratio of the initial load eccentricity to the overall depth of the column cross-section was observed to increase the lateral displacement of the columns significantly and was more pronounced for columns with L/d ratios greater than 5. The normal strength concrete PEC columns (with L/d ratios of 5 and 10) demonstrated a flatter peak and gradual post-peak strength decline in the load versus axial strain responses as the e/d ratio increases. On the other hand, the sharp decline in the post-peak region of the load versus axial strain response of the long reference column (which was constructed with high strength concrete and slender plates) was not affected by the e/d ratio.

The occurrence of local buckling in PEC columns was not affected much by increasing the e/d ratio from 0.15 to 0.30. However, an e/d ratio of 0.05, which is the accidental eccentricity case, causes local buckling before the peak load for PEC columns with slender plates (b/t = 30 and 35) and larger link spacing (s = 0.7d). The use of normal strength or high strength concrete does not affect this behaviour significantly.

The peak axial load was affected significantly by the e/d ratio. The average reduction in the axial capacity was 22% and 42% for e/d ratios of 0.15 and 0.30, respectively, with respect to the capacity with e/d = 0.05. These results include the effects of various L/d, b/t and s/d ratios selected for the parametric study and is also applicable for normal strength as well as high strength concrete PEC columns.

7.2.2.3 Effect of Flange Slenderness Ratio and Link Spacing

The parametric study was performed for flange slenderness ratios of 25, 30 and 35 in conjunction with the two values of link spacing: 0.5d and 0.7d. For all combinations of L/d, e/d and links spacing as well as concrete strength, the ductility of the PEC column reduces as the flange slenderness ratio increases. This effect is more prominent in short columns with a larger link spacing. However, the brittle failure behaviour of long PEC columns is not significantly affected by the b/t ratio.

The axial capacity of the PEC column with stockier flanges (b/t = 25) was found to be reduced by 6 to 8% (average of 7.5%) when the flange b/t ratio was changed to 30. Again, increasing the b/t ratio to 35 resulted in 11 to 16% reductions, with an average value of 13%, in the capacity corresponding to b/t = 25.

The axial capacity of the PEC column was observed to be nearly unaffected by the range of link spacings selected in the parametric study. However, the load versus axial strain curves for PEC columns demonstrate a more ductile response for lower values of link spacing. This effect is prominent in short columns with slender flanges and diminishes as the overall column slenderness increases.

7.2.2.4 Effect of Concrete Compressive Strength

The use of high strength (60 MPa) concrete in PEC column was observed to improve the capacity significantly, as expected, which was observed for a variety of PEC columns with the selected ranges of L/d, e/d, b/t and s/d ratios. The average increase in the axial capacity of the PEC column was found to be 55%, when the normal strength concrete with a nominal strength of 30 MPa is replaced by high strength concrete with a nominal strength of 60 MPa. However, the use of high strength concrete reduced the ductility of the failure mode of PEC columns, which can be improved somewhat by the use of steel fibres in the concrete.

7.2.2.5   *Performance of the Theoretical Interaction Diagram*

The theoretical interaction diagram based on the method used by Prickett and Driver (2006) for short PEC columns was found to provide accurate predictions of the numerical capacities of PEC columns with normal strength concrete and conservative predictions for PEC columns with high strength concrete.   The method used to construct the theoretical interaction diagrams is similar to that frequently used by designers for reinforced concrete columns. Therefore, the use of the theoretical interaction diagram for PEC columns should be suitable for the wide range of L/d, b/t and s/d ratios applied in this study and for columns with normal strength concrete as well as high strength concrete, although additional comparisons with physical tests would be desirable.

7.3   Recommendations for Future Research

The finite element model developed herein was verified for monotonic loading conditions only. However, in high-rise structures when these columns are constructed as a part of a lateral load resisting systems, cyclic bending moments will occur due to wind and earthquake loading. A limited number of tests have been performed to date on normal strength concrete PEC columns to address the effect of cyclic bending moment. Therefore, large-scale experimental investigations are required to address the effect of high performance concrete in PEC columns subjected to cyclic loading and to validate the finite element model for PEC columns developed in this study against these test results.

The accuracy of the design equation in CSA S16-01 for PEC columns with an L/d ratio greater than 5 has not been completely verified because of the lack of sufficient experimental investigations. The current study provided some information to this end. However, only three long columns tests were available to validate the model for L/d ratios greater than 5. Moreover, no experimental investigations have been performed to address the effect of using high performance concrete in PEC columns with L/d ratios greater than 5. Experimental investigations are therefore needed on PEC columns with

L/d ratios greater than 5 with normal strength and high strength concrete, the results of which will help to support the findings of the parametric study performed herein.

The level of concrete confinement in these columns should be more systematically quantified and a study should be performed to observe the effect of link spacing and loading conditions on the confining pressure of the concrete. Thereby, the concrete material model can be modified to capture the axial strains more accurately for the maximum level of confining pressure that can occur in a PEC column. Moreover, in the numerical simulation of PEC columns the additional reinforcement bars should be modelled using beam elements instead of the truss elements used in the current study. This may improve the ability of the numerical model to capture the enhanced concrete confinement because of the representation of the flexural stiffness of the bars.

A similar parametric study to the one conducted herein should be performed on PEC columns subjected to weak axis bending and biaxial bending to further extend the range of application of these columns in medium to high-rise buildings. In addition, the effects of cyclic bending moment with variable geometric and material properties need to be addressed. Finally, design guidelines should be proposed to include the effect of cyclic loading and high performance concrete in PEC columns.

REFERENCES

ACI (2005). "Building Code Requirements for Structural Concrete." *ACI 318R-05*, *American Concrete Institute,* Detroit.

ACI (1997). "State–of–the–Art Report on High Strength Concrete." (Reapproved 1997*), ACI 363R–92*, *American Concrete Institute,* Detroit.

Almusallam, T. H. and Alsayed, S. H. (1995). "Stress–Strain Relationship of Normal, High Strength and Lightweight concrete." *Magazine of Concrete Research*, 47 (170), 39-44.

Barr, B., and Lee, M. K. (2003). "Modelling the Strain-Softening Behaviour of Plain Concrete using a Double-Exponential Model." *Magazine of Concrete Research,* 55 (4), 343-353.

Begum, M., Elwi, A. E., and Driver, R. G. (2004). "Numerical Simulation of the Behaviour of Partially Encased Composite Columns." *Proc., 5th Structural Specialty Conference of the Canadian Society for Civil Engineering*, Saskatoon, Saskatchewan, Canada, ST-127-1 to 127-10.

Begum, M., Driver, R. G. and Elwi, A. E. (2005). "Strength and Stability Simulations of Partially Encased Composite Columns under Axial Load". *Proc.* SSRC/NASCC *Joint Annual Stability Conference*, Montreal, Quebec, Canada, 241-255.

Begum, M., Driver, R. G. and Elwi, A. E. (2007). "Finite Element Modeling of Partially Encased Composite Columns using the Dynamic Explicit Solution Method." *Journal of Structural Engineering*, *ASCE*, 133 (3), in press for printing.

Bouchereau, R., and Toupin, J.-D. (2003). "Étude du Comportement en Compression-Flexion des Poteaux Mixtes Partiellement Enrobés." *Report EPM/GCS-2003-03*, Dept. of Civil, Geological and Mining Engineering, Ecole Polytechnique, Montreal, Canada.

Broderick, B. M. and Elnashai, A. S. (1994). "Seismic Resistance of Composite Beam–Columns in Multi–Storey Structures. Part 2: Analytical Model and Discussion of Results." *Journal of Construction Steel Research*, 30, 231–258.

Carreira, D. J. and Chu, K. M. (1985). "Stress–Strain Relationship for Plain Concrete in Compression." *ACI Journal*, 82 (6), 797–804.

CEB (1990). "CEB-FIP Model Code 1990". Bulletin d'information, No. 203, Paris, France.

Chicoine, T., Tremblay, R., Massicotte, B., Yalcin, M., Ricles, J., and Lu, L.-W. (2000). "Test Programme on Partially-Encased Built Up Three-Plate Composite Columns." *Joint Report EPM/GCS No. 00-06*, February, Dept. of Civil, Geological and Mining Engineering, Ecole Polytechnique, Montreal, Canada – ATLSS Engineering Research Centre, No. 00-04, Lehigh University, Bethlehem, Pennsylvania, USA.

Chicoine, T., Tremblay, R. and Massicotte, B. (2001). "Finite Element Modelling of the Experimental Response of Partially Encased Composite Columns." *EPM/GCS No. 2001-06*, Dept. of Civil, Geological and Mining Engineering, Ecole Polytechnique, Montreal, Canada.

Chicoine, T., Tremblay, R., Massicotte, B., Ricles, J., and Lu, L.-W. (2002a). "Behavior and Strength of Partially-Encased Composite Columns with Built Up Shapes." *Journal of Structural Engineering*, *ASCE*, 128 (3), 279-288.

Chicoine, T., Tremblay, R. and Massicotte, B. (2002b). "Finite Element Modelling and Design of Partially Encased Composite Columns." *Steel and Composite Structures*, 2 (3), 171–194.

Chicoine, T., Massicotte, B. and Tremblay, R. (2003). "Long–term Behavior and Strength of Partially-Encased Composite Columns with Built Up Shapes." *Journal of Structural Engineering*, *ASCE*, 129 (2), 141–150.

CSA. (2001). "CSA S16-01, Limit States Design of Steel Structures." Canadian Standards Association, Toronto, ON.

CSA. (2004a). "CSA A23.3-04, Design of Concrete Structures." Canadian Standards Association, Rexdale, ON.

CSA. (2004b). "CSA G40.21-04, Structural Quality Steel." Canadian Standards Association, Rexdale, ON.

Desayi, P. and Krishnan, S. (1964). "Equation for Stress–Strain Curve of Concrete." *ACI Journal*, 61 (3), 345–350.

Du, J., Yon, J. H., Hawkins, N. M., Arakawa, K. and Kobayashi, A. S. (1992). "Fracture Process Zone for Concrete for Dynamic Loading." *ACI Material Journal*, 89 (3), 252-258.

Elghazouli, A.Y. and Elnashai, A.S. (1993). "Performance of Composite Steel/Concrete Members under Earthquake Loading. Part II: Parametric Studies and Design Considerations." *Earthquake Engineering and Structural Dynamics*, 22 (4), 347–368.

Elnashai, A.S. and Broderick, B.M. (1994). "Seismic Resistance of Composite Beam-Columns in Multi-Storey Structures. Part 1: Experimental Studies." *Journal of Constructional Steel Research*, 30 (3), 201–229.

203

Elnashai, A.S. and Elghazouli, A.Y. (1993). "Performance of Composite Steel/Concrete Members under Earthquake Loading. Part I: Analytical Model." *Earthquake Engineering and Structural Dynamics*, 22 (4), 315–345.

Elnashai, A.S., Takanashi, K., Elghazouli, A.Y. and Dowling, P.J. (1991). "Experimental Behaviour of Partially Encased Composite Beam-Columns under Cyclic and Dynamic Loads." *Proceedings – Institution of Civil Engineers*, Part 2: Research and Theory, v 91, June, 259–272.

Fanella, D. and Naaman, A. (1985). "Stress–Strain Properties of Fibre Reinforced Mortar in Compression." *ACI Journal*, 82 (4), 475–483.

Filion, I. (1998) "Étude Expérimentale des Poteaux Mixtes Avec Section d'acier de classe 4", *Report n^o. EPM/GCS-1998-06,* Dept. of Civil, Geological and Mining Engineering, Ecole Polytechnique, Montreal, Canada.

Foote, R. M. L., Mai, Y. W. and Cotterell, B. (1986). "Crack Growth Resistance Curves in Strain–Softening Material." *Journal of Mechanics and Physics of Solids*, 34 (6), 593–607.

Gopalaratnam, V. S. and Shah, S.P. (1985). "Softening Response of Plain Concrete in Direct Tension." *ACI Journal*, 82 (3), 310-323.

Gorst, N. J. S., Williamson, S. J., Pallet, P. F. and Clark, L. A. (2003). "Friction in Temporary Works." *Research Report 071*, Health and Safety Executive, University of Birmingham, Birmingham, UK.

Gysel, V. A. and Taerwe, L. (1996). "Analytical Formulation of the Complete Stress–Strain Curve for High Strength Concrete." *Materials and Structures*, vol.29, November, 529–533.

Hibbitt, Karlsson and Sorensen, Inc. (HKS) (2003). *ABAQUS/ Explicit User's Manual*, Version 6.3.

Hillerborg, A., Modeer, A. and Peterson, P. E. (1976). "Analysis of Crack Formation and Crack Growth in Concrete by Means of Fracture Mechanics and Finite Elements." *Cement and Concrete Research*, 6, 773-782.

Hognestad, E. (1951). " A Study of Combined Bending and Axial Load in Reinforced Concrete Members." *Bulletin No. 399*, University of Illinois Engineering Experimental Station, Urbana, Champaign.

Hsu, L. S. and Hsu, T. C.–T. (1994a). "Complete Stress–Strain Behaviour of High Strength Concrete Under Compression." *Magazine of Concrete Research*, 46 (169), 301–312.

Hsu, L. S. and Hsu, T. C.–T. (1994b). "Stress–Strain Behaviour of Steel Fibre High Strength Concrete under Compression." *ACI Materials Journal*, 91 (4), 448–457.

Hunaiti, Y. M., and Fattah, B. Abdel (1994). "Design Considerations of Partially Encased Composite Columns." *Proc. Inst. Civ. Eng., Struct. Build.,* 106 (2), 75-82.

Kupfer, H., Hilsdorf, K. H. and Rusch, H. (1969). "Behaviour of Concrete Under Biaxial Stresses." *ACI Journal*, August, 656–666.

Kützing, L. and König, G. (1999). "Design Principals for Steel Fibre Reinforced Concrete—A Fracture Mechanics Approach." *Leipzig Annual Civil Engineering Report Lacer*, No. 4, 175–183.

Lee, K. M. and Barr, B. I. G. (2004). "A Four–Exponential Model to Describe the Behaviour of Fibre Reinforced Concrete." *Materials and Structures,* 37, 464–471.

Lee, J., and Fenves, G. L. (1998). "Plastic-Damage Model for Cyclic Loading of Concrete Structures." *Journal of Engineering Mechanics*, 124 (8), 892–900.

Loov, R. (1996). "A Simple Equation for Axially Loaded Steel Column Design Curve." *Canadian Journal of Civil Engineering*, 23, 272–276.

Lubliner, J., Oliver, J., Oller, S. and Onate, E. (1989). "A Plastic-Damage Model for Concrete." *International Journal of Solids and Structures,* 25 (3), 229-326.

Maranda, R. (1998) "Analyses par Éléments Finis de Poteaux Mixtes Avec Sections d'acier En I de Classe 4" *Report n^o. EPM/GCS-1998-11*, Dept. of Civil, Geological and Mining Engineering, Ecole Polytechnique, Montreal, Canada.

Marzouk, H. and Chen, Z. (1995). "Fracture Energy and Tension Properties of High-Strength Concrete." *Journal of Materials in Civil Engineering,* 7 (2), 108-116.

Muise, J. (2000). "Behaviour of Simple Framing Connections to Partially Concrete Encased H Section Columns." Master's Thesis, Dept. of Civil Engineering, University of Toronto, Toronto, Canada.

Popovics, S. (1970). "A Review of Stress–Strain Relationships for Concrete." *ACI Journal Proceedings*, 67 (3), 243–248.

Popovics, S. (1973). "A Numerical Approach to the Complete Stress–Strain Curve of Concrete." *Cement and Concrete Research*, 3(4), 583–599.

Prickett, B. S. and Driver, R. G. (2006). "Behaviour of Partially Encased Composite Columns Made with High Performance Concrete." *Structural Engineering Report No 262*, Dept. of Civil and Environmental Engineering, University of Alberta, AB, Canada.

Rashid, M. A., Mansur, M. A. and Paramasivum, P. (2002). "Correlation between Mechanical Properties of High Strength Concrete." *Journals of Materials in Civil Engineering, ASCE*, 14 (3), pp.230–238.

Sfer, D., Carol, I., Gettu, R. and Etse, G. (2002). "Study of the Behavior of Concrete under Triaxial Compression." *Journal of the Engineering Mechanics,* ASCE, 128 (2), 156–162.

Tremblay, R. (2003). "Flexural Demand on Partially Encased Composite Columns in Multi–Storey Concentrically Braced Steel Frames." STESSA 2003: Proceedings of the Conference on Behaviour of Steel Structures in Seismic Areas, 9–12 June, Naples, Italy, 479–485.

Tremblay, R., Chicoine, T., and Massicotte, B. (2000b). "Design Equation for the Axial Load Capacity of Partially Encased Non-Compact Columns." *Proc., Composite Construction in Steel and Concrete IV, ASCE*, ed. by J.F. Hajjar, M. Hosain, W.S. Easterling, and B.M. Sharooz, ASCE, Reston, VA, pp. 506-517.

Tremblay, R., Chicoine, T., Massicotte, B., Ricles, J., and Lu, L.-W. (2000a). "Compressive Strength of Large Scale Partially-Encased Composite Stub Columns." *Proc., 2000 SSRC Annual Technical Session & Meeting,* Memphis, 262-272.

Tremblay, R., Massicotte, B., Filion, I., and Maranda, R. (1998). "Experimental Study on the Behaviour of Partially Encased Composite Columns Made with Light Welded H Steel Shapes under Compressive Axial Loads." *Proc., SSRC Annual Technical Session & Meeting*, Atlanta, 195-204.

Tsai, W.T. (1988). "Uniaxial Compression Stress–Strain Relation of Concrete." *Journal of Structural Engineering*, ASCE, 114 (9), 2133–2136.

Vincent, R. and Tremblay, R. (2001). "An Innovative Partially Encased Composite Column System for High-Rise Buildings." *Proc., North American Steel Construction Conf.*, Fort Lauderdale, FL., 30-3 to 30-17.

Wang, P. T., Shah, S. P., and Naaman, A. E. (1978). "Stress–Strain Curves of Normal and Lightweight Concrete in Compression." *ACI Journal*, 75 (11), 603–611.

Wee, T. H., Chin, M. S., and Mansur, M. A. (1996). "Stress–Strain Relationship of High–Strength Concrete in Compression." *Journal of Materials in Civil Engineering*, ASCE, 8 (2), 70–76.

APPENDIX

The appendix presents the load versus longitudinal strain curves at the buckled flange for all 31 columns used for the parametric study as well as the influences of each variable parameter on the load versus average axial strain, load versus lateral displacement, moment versus lateral displacement, load versus moment and moment versus curvature responses. Some figures from Chapter 6 have been repeated here in order to provide a complete set of graphs in one location for convenience.

The appendix is structured as follows:

Figures A.x: Load versus Axial Strain at the Locally Buckled Flange of the Parametric Columns

Figures B.x: Effect of L/d Ratio

Figures C.x: Effect of e/d Ratio

Figures D.x: Effect of b/t ratio

Figures E.x: Effect of s/d Ratio

Figures F.x: Effect of Concrete Compressive Strength
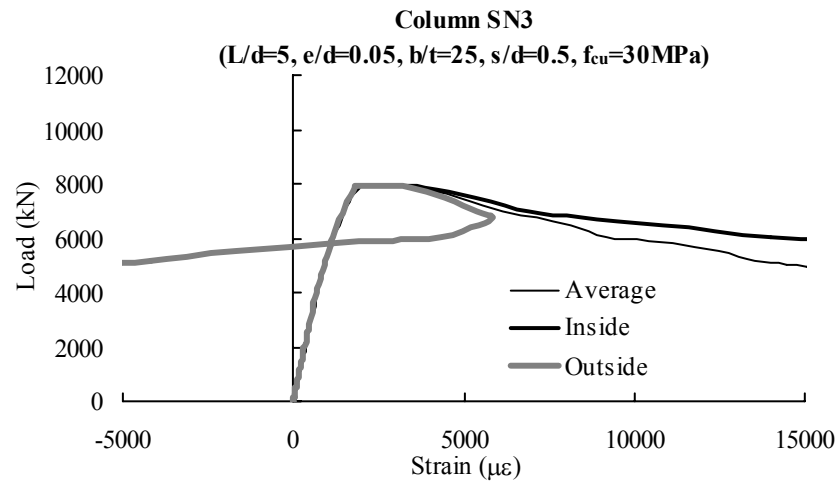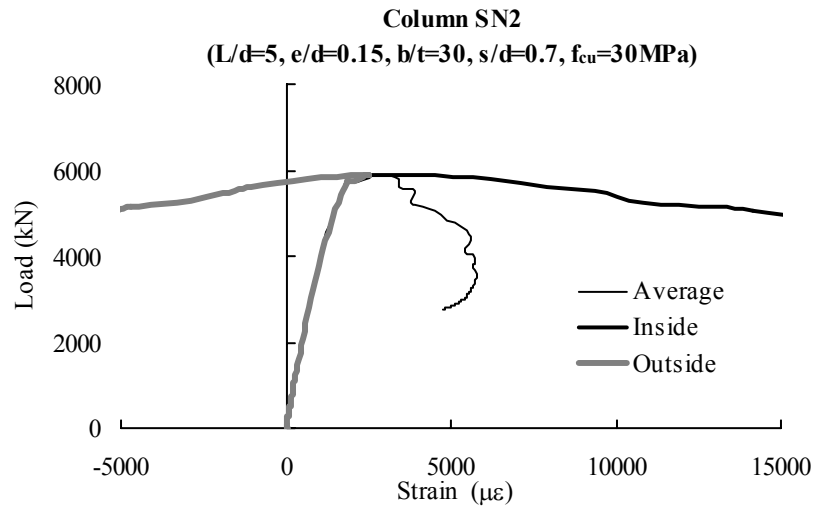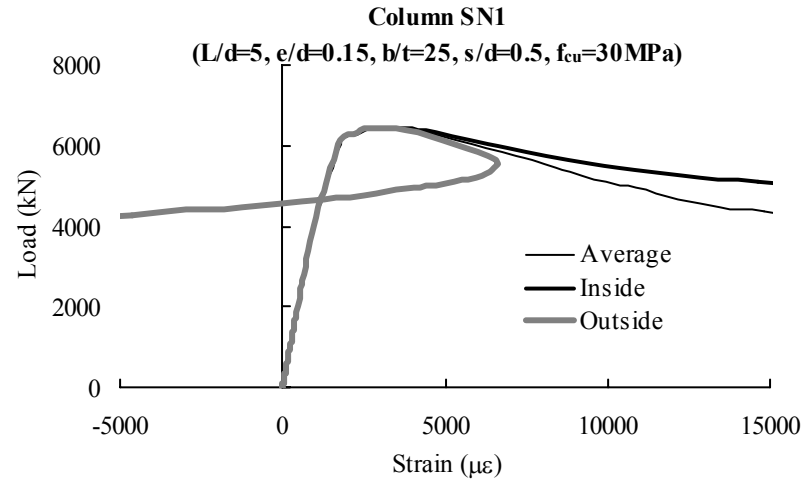
Figure A.1 Load versus Axial Strain at the Locally Buckled Flange of the

Parametric Columns

Column SN4

(L/d=5, e/d=0.30, b/t=25, s/d=0.5, f$_{cu}$=30MPa)

Column SN5

(L/d=5, e/d=0.15, b/t=30, s/d=0.5, f$_{cu}$=30MPa)

Column SN6

(L/d=5, e/d=0.15, b/t=35, s/d=0.5, f$_{cu}$=30MPa)

Figure A.1 (cont.) Load versus Axial Strain at the Locally Buckled Flange of the Parametric Columns

211

Figure A.1 (cont.) Load versus Axial Strain at the Locally Buckled Flange of the Parametric Columns

Column SH2

(L/d=5, e/d=0.30, b/t=35, s/d=0.7, f_cu=60MPa)

Column IN1

(L/d=10, e/d=0.15, b/t=30, s/d=0.7, f_cu=30MPa)

Column IN2

(L/d=10, e/d=0.15, b/t=25, s/d=0.5, f_cu=30MPa)

Figure A.1 (cont.) Load versus Axial Strain at the Locally Buckled Flange of the Parametric Columns

213

Figure A.1 (cont.) Load versus Axial Strain at the Locally Buckled Flange of the Parametric Columns

Column IN6
(L/d=10, e/d=0.15, b/t=35, s/d=0.7, f$_{cu}$=30MPa)

Column IN7
(L/d=10, e/d=0.15, b/t=30, s/d=0.5, f$_{cu}$=30MPa)

Column IN8
(L/d=10, e/d=0.15, b/t=35, s/d=0.5, f$_{cu}$=30MPa)

Figure A.1 (cont.) Load versus Axial Strain at the Locally Buckled Flange of the

Parametric Columns

215

Column IH1
(L/d=10, e/d=0.15, b/t=30, s/d=0.7, f$_{cu}$=60MPa)

Column IH2
(L/d=10, e/d=0.30, b/t=35, s/d=0.7, f$_{cu}$=60MPa)

Column LN1
(L/d=15, e/d=0.30, b/t=35, s/d=0.7, f$_{cu}$=30MPa)

Figure A.1 (cont.) Load versus Axial Strain at the Locally Buckled Flange of the Parametric Columns

216

Column LN2
(L/d=15, e/d=0.15, b/t=25, s/d=0.5, f_{cu}=30MPa)

Column LN3
(L/d=15, e/d=0.15, b/t=30, s/d=0.7, f_{cu}=30MPa)

Column LH1
(L/d=15, e/d=0.30, b/t=35, s/d=0.7, f_{cu}=60MPa)

Figure A.1 (cont.) Load versus Axial Strain at the Locally Buckled Flange of the

Parametric Columns

Column LH2
(L/d=15, e/d=0.30, b/t=25, s/d=0.5, f_cu=60MPa)

Column LH3
(L/d=15, e/d=0.05, b/t=35, s/d=0.7, f_cu=60MPa)

Column LH4
(L/d=15, e/d=0.15, b/t=35, s/d=0.7, f_cu=60MPa)

Figure A.1 (cont.) Load versus Axial Strain at the Locally Buckled Flange of the

Parametric Columns

Column LH5
(L/d=15, e/d=0.30, b/t=25, s/d=0.7, f_cu=60MPa)

Column LH6
(L/d=15, e/d=0.30, b/t=30, s/d=0.7, f_cu=60MPa)

Column LH7
(L/d=15, e/d=0.15, b/t=35, s/d=0.7, f_cu=60MPa)

Figure A.1 (cont.) Load versus Axial Strain at the Locally Buckled Flange of the

Parametric Columns

219

Column LH8
(L/d=15, e/d=0.30, b/t=30, s/d=0.5, f_cu=60MPa)

Figure A.1 (cont.) Load versus Axial Strain at the Locally Buckled Flange of the

Parametric Columns

Figure B.1 Effect of L/d Ratio on Load versus Average Axial Strain Curve, (a) Set 1, (b) Set 2 and (c) Set 3
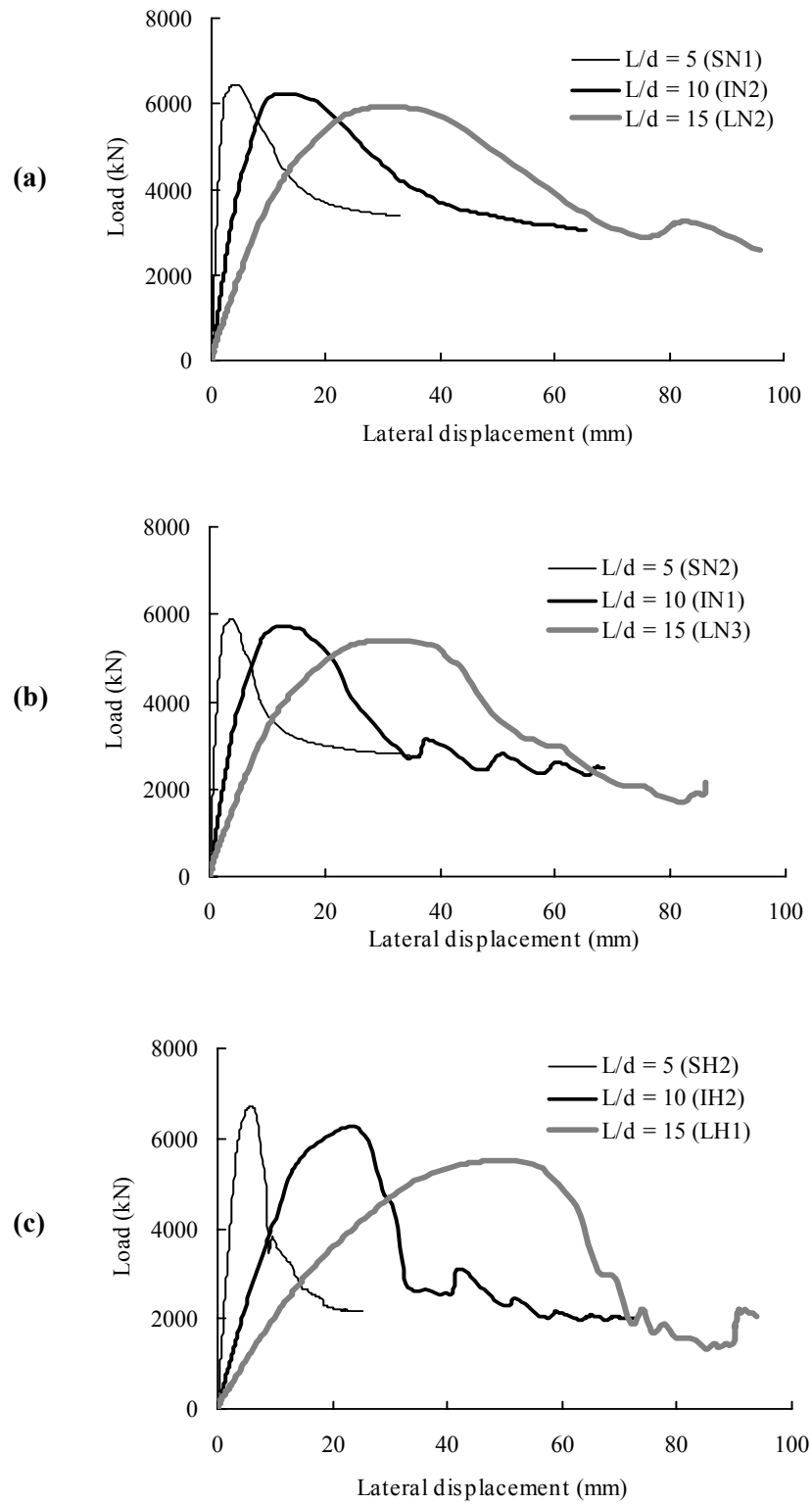
Figure B.2 Effect of L/d Ratio on Load versus Lateral Displacement Curve,

(a) Set 1, (b) Set 2 and (c) Set 3
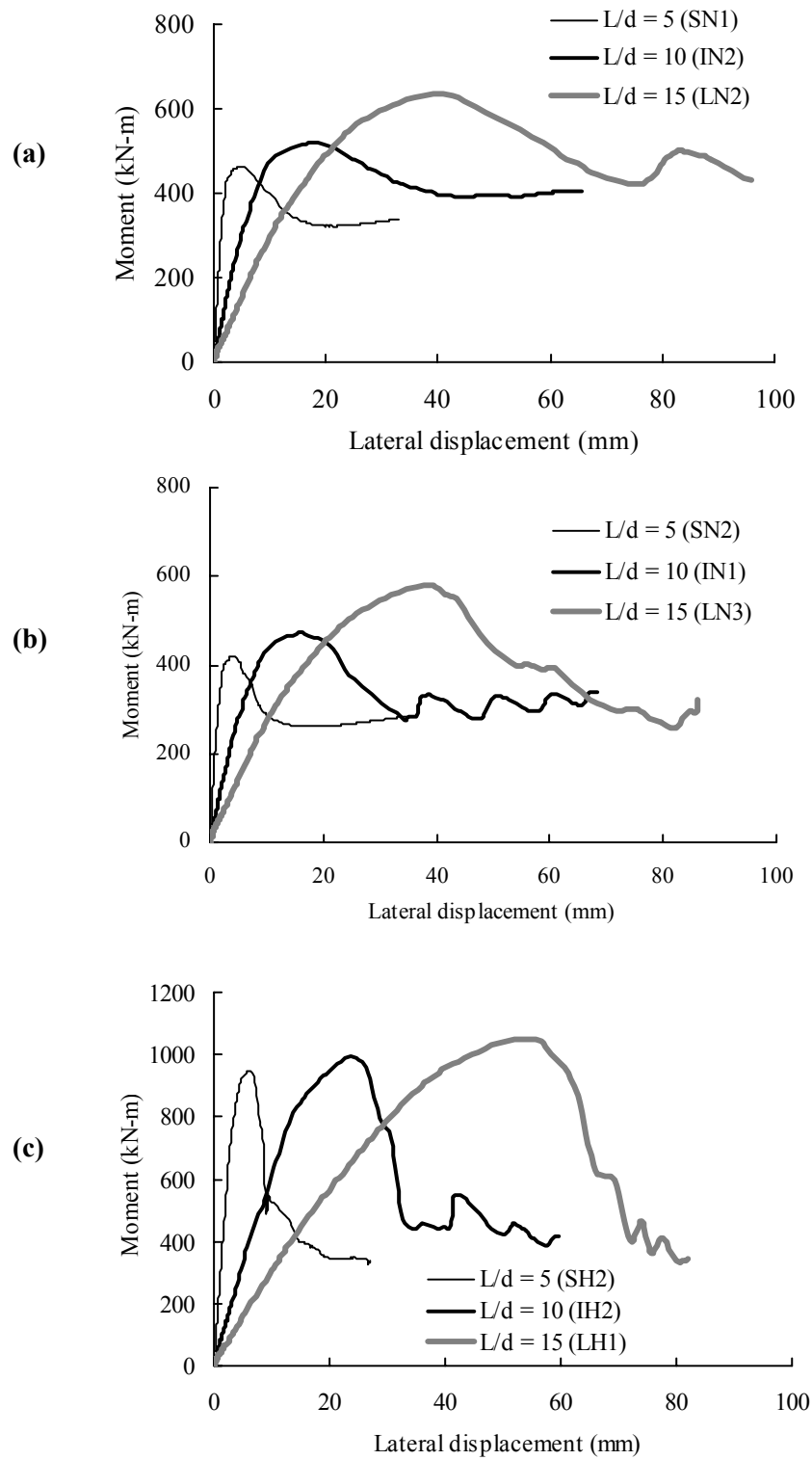
Figure B.3 Effect of L/d Ratio on Moment versus Lateral Displacement Curve,

(a) Set 1, (b) Set 2 and (c) Set 3

223
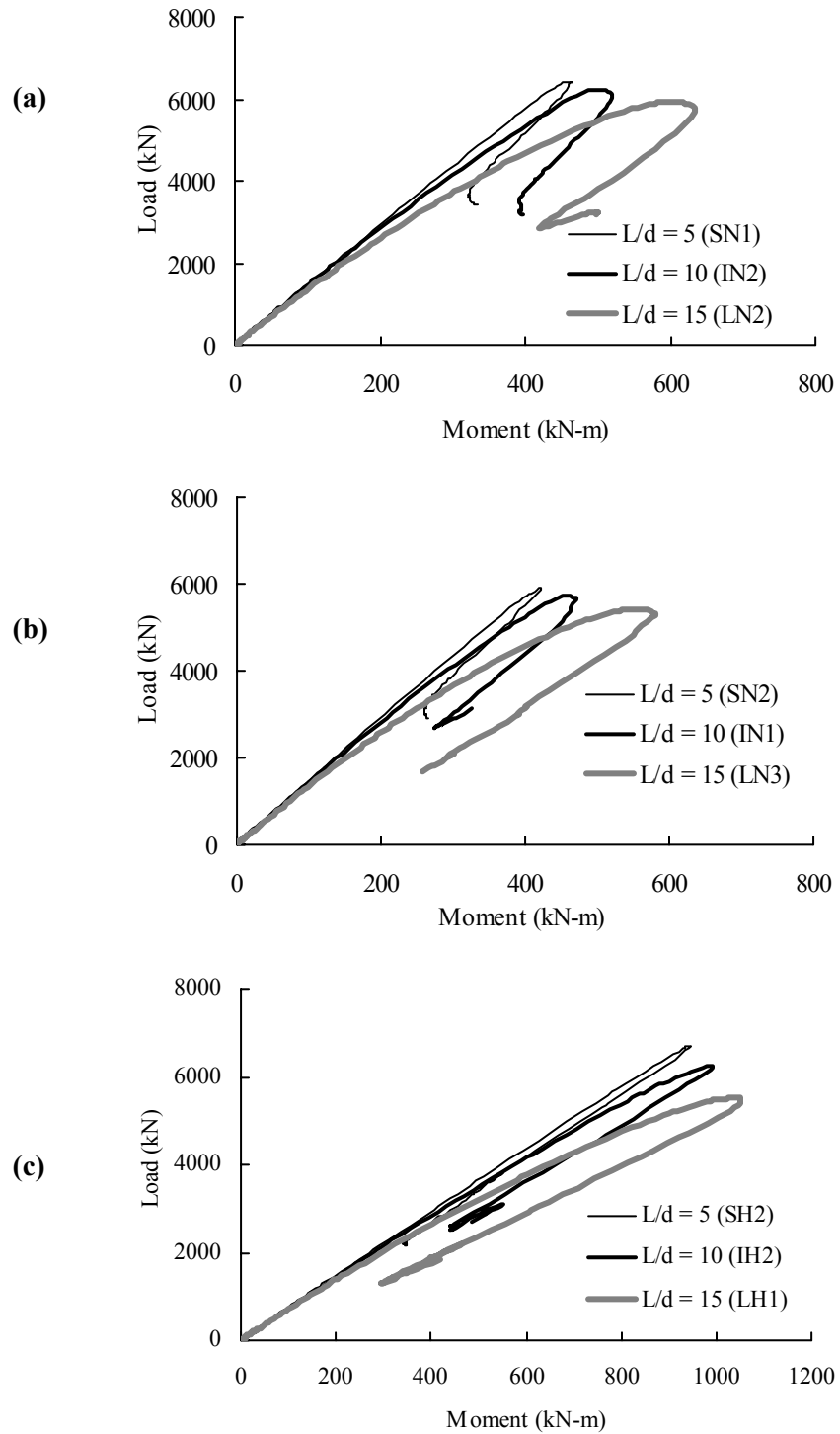
Figure B.4 Effect of L/d Ratio on Load versus Moment Curve, (a) Set 1, (b) Set 2 and (c) Set 3

224
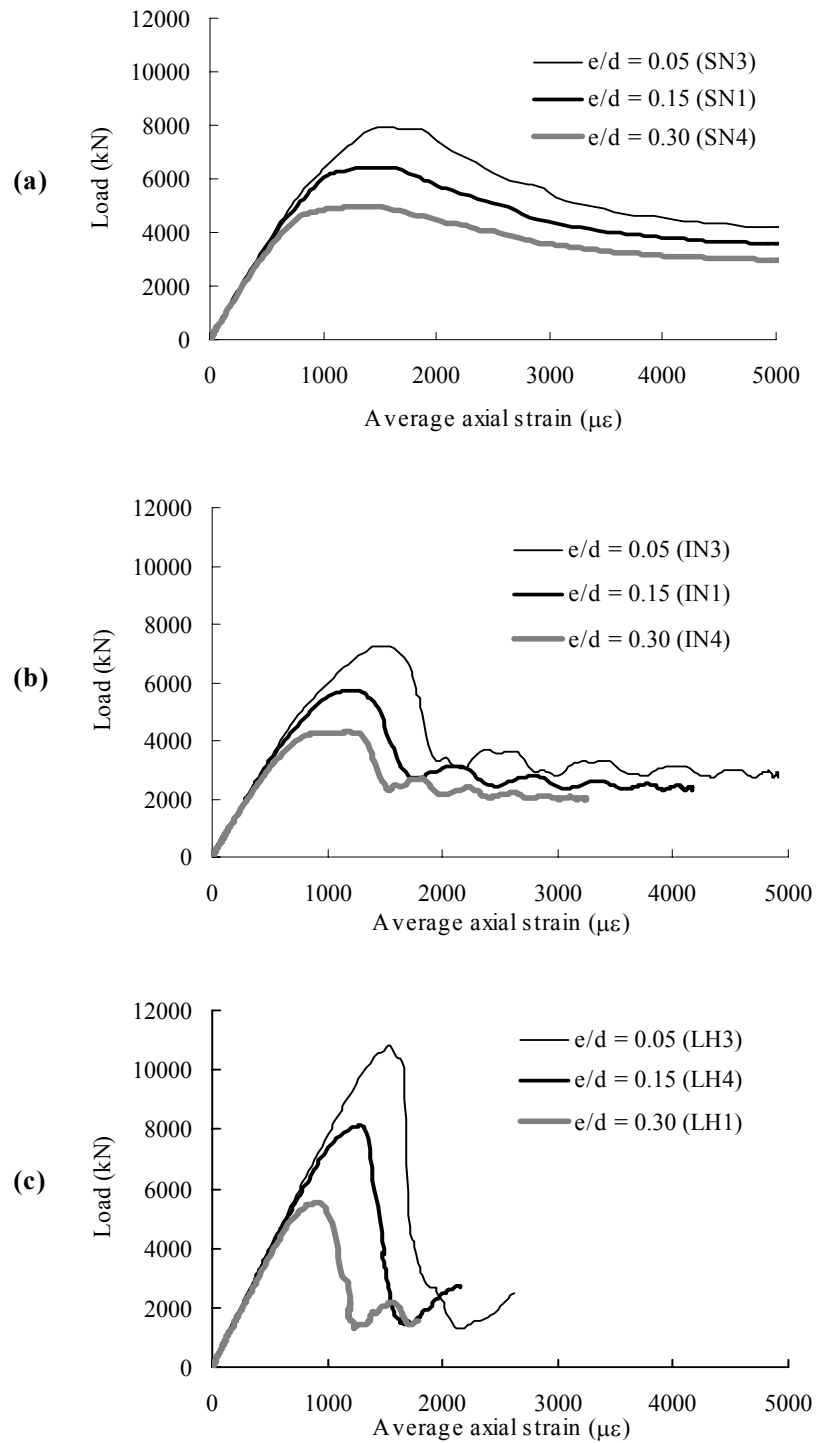
Figure C.1 Effect of e/d Ratio on Load versus Average Axial Strain Curve, (a) Set 1,
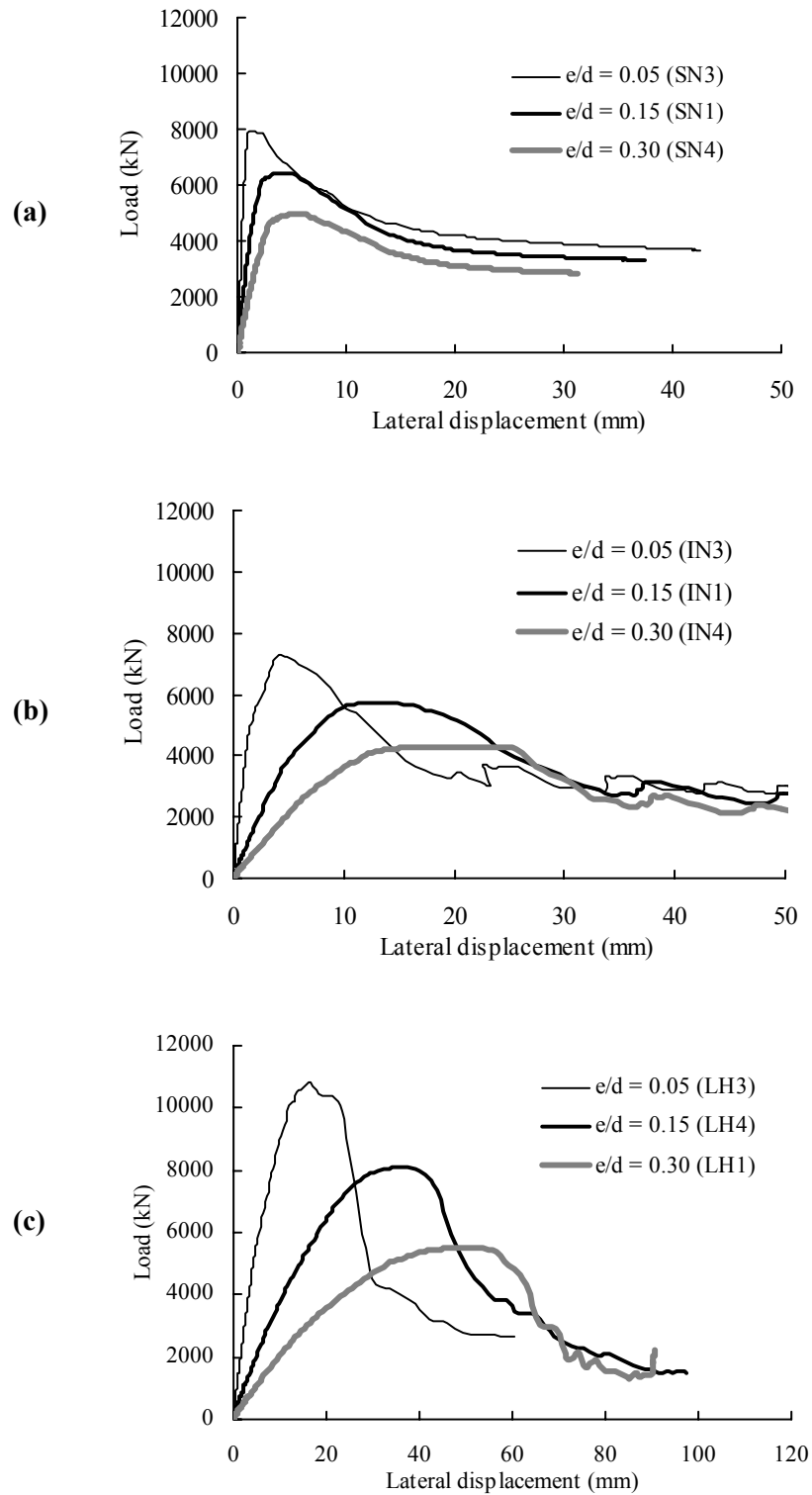
(b) Set 2 and (c) Set 3

Figure C.2 Effect of e/d Ratio on Load versus Lateral Displacement Curve, (a) Set 1, (b) Set 2 and (c) Set 3
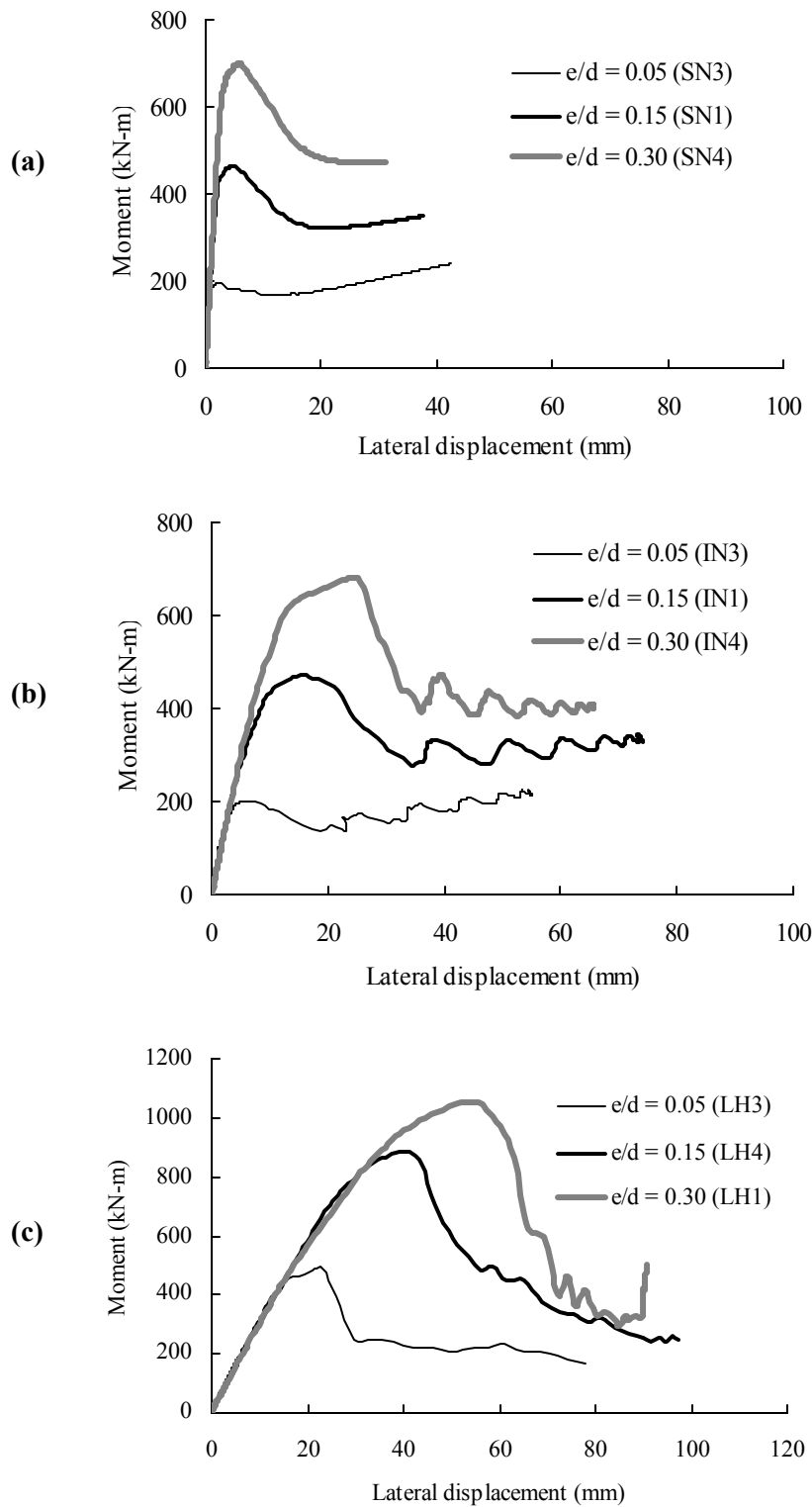
Figure C.3 Effect of e/d Ratio on Moment versus Lateral Displacement Curve, (a) Set 1, (b) Set 2 and (c) Set 3
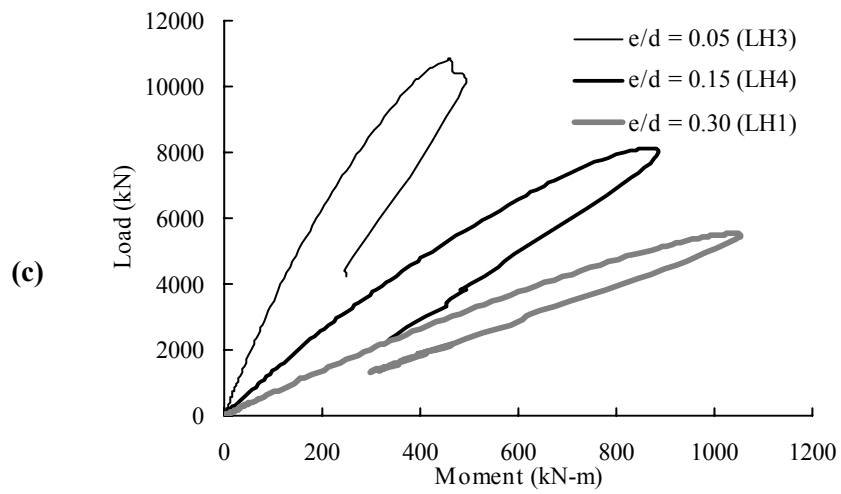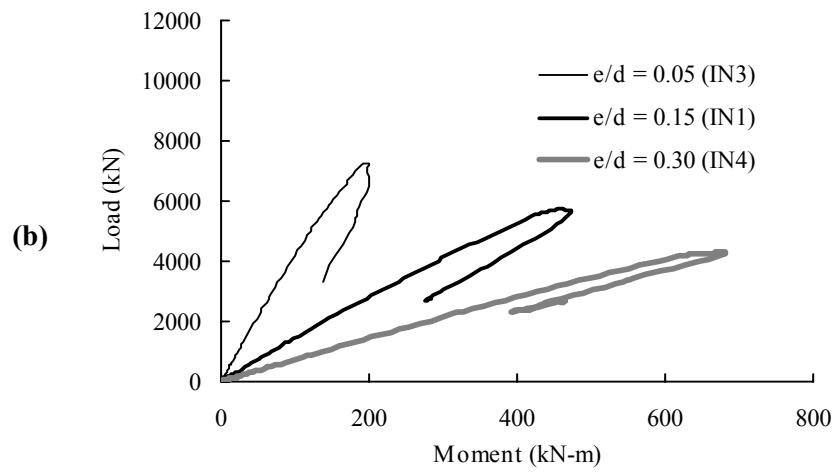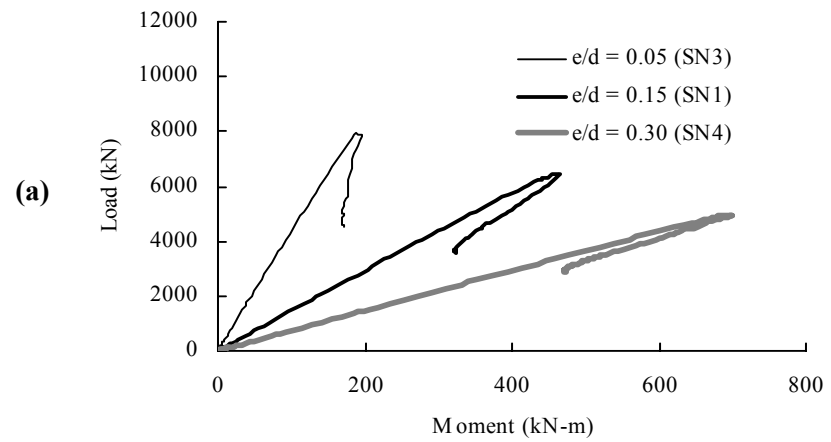
Figure C.4 Effect of e/d Ratio on Load versus Moment Curve, (a) Set 1, (b) Set 2 and (c) Set 3

228
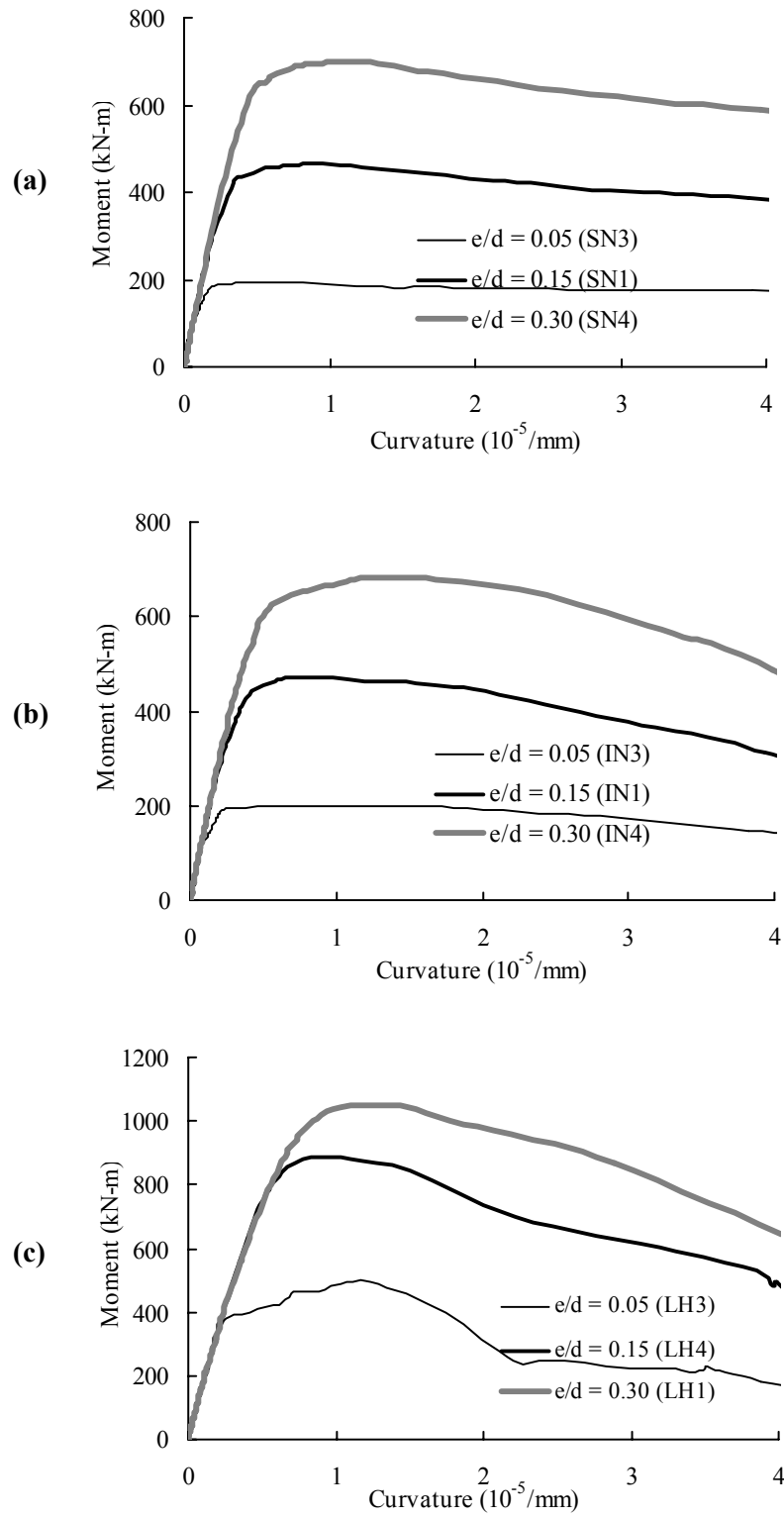
Figure C.5 Effect of e/d Ratio on Moment versus Curvature Curve, (a) Set 1,

(b) Set 2 and (c) Set 3

(a)

(b)
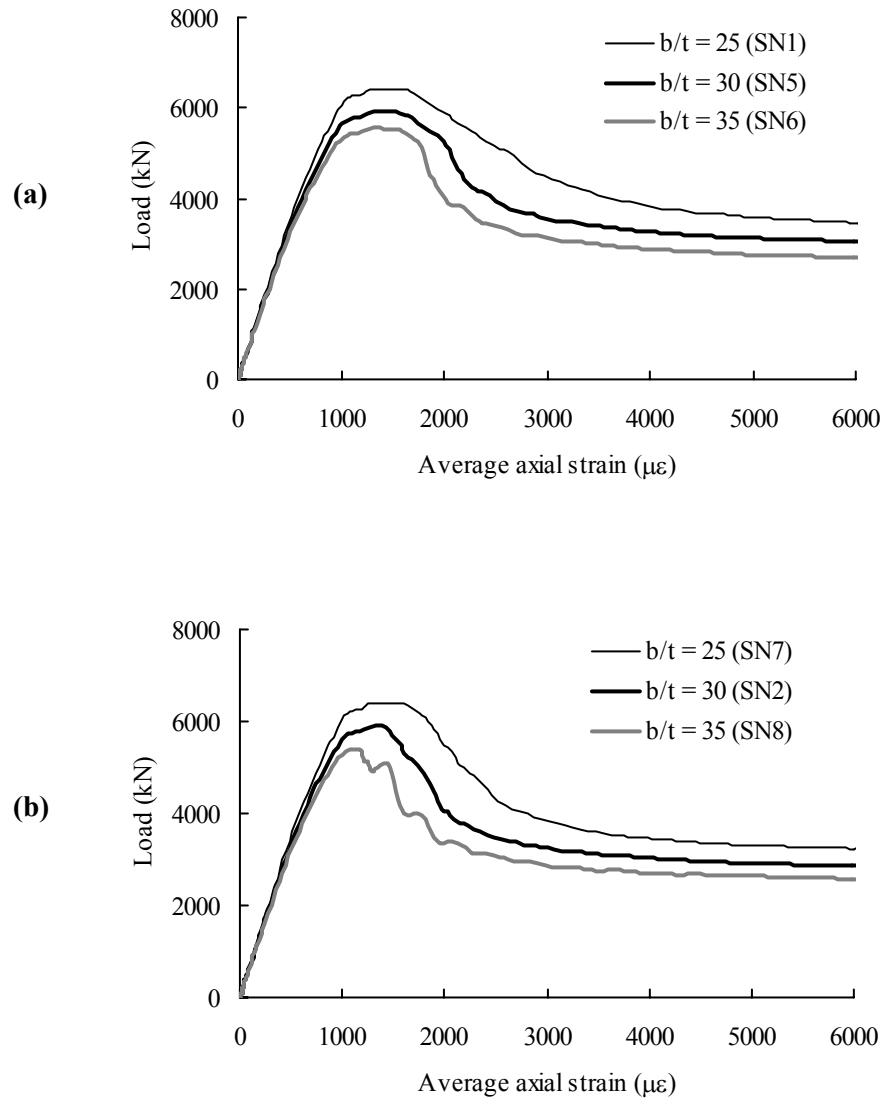
Figure D.1 Effect of b/t ratio on Load versus Average Axial Strain Curve for Short PEC Column (Analysis Set 1), (a) s = 0.5d and (b) s = 0.7d
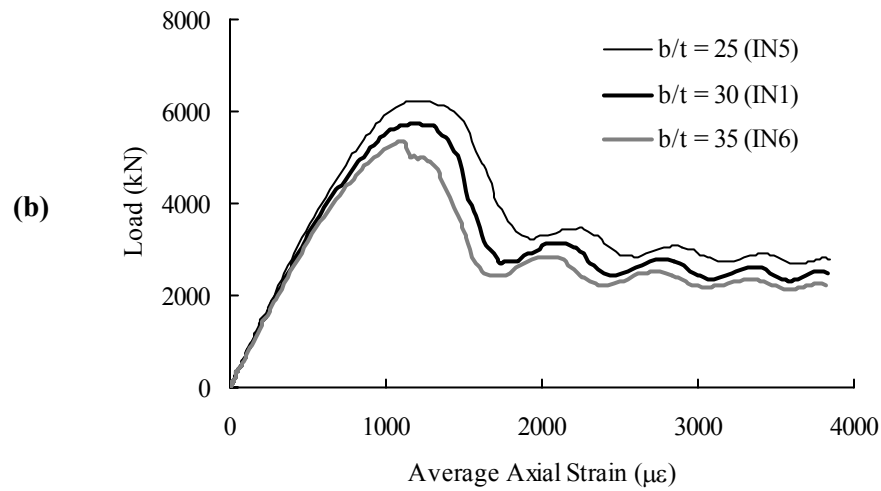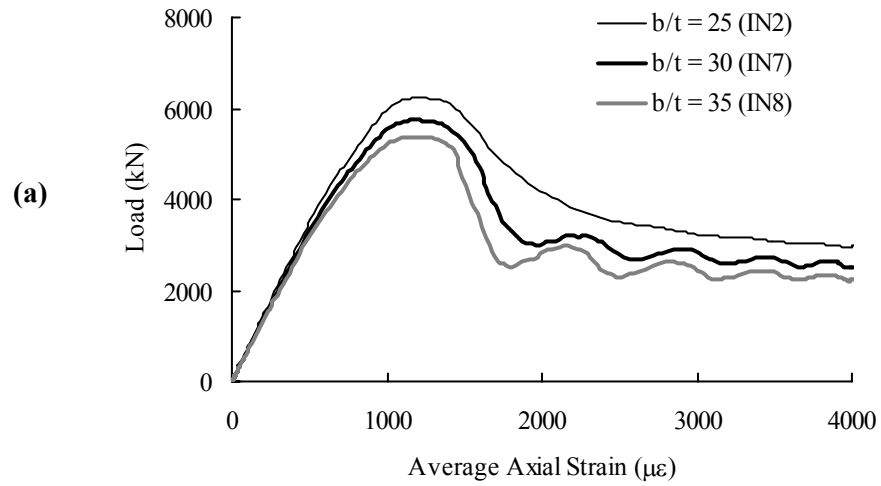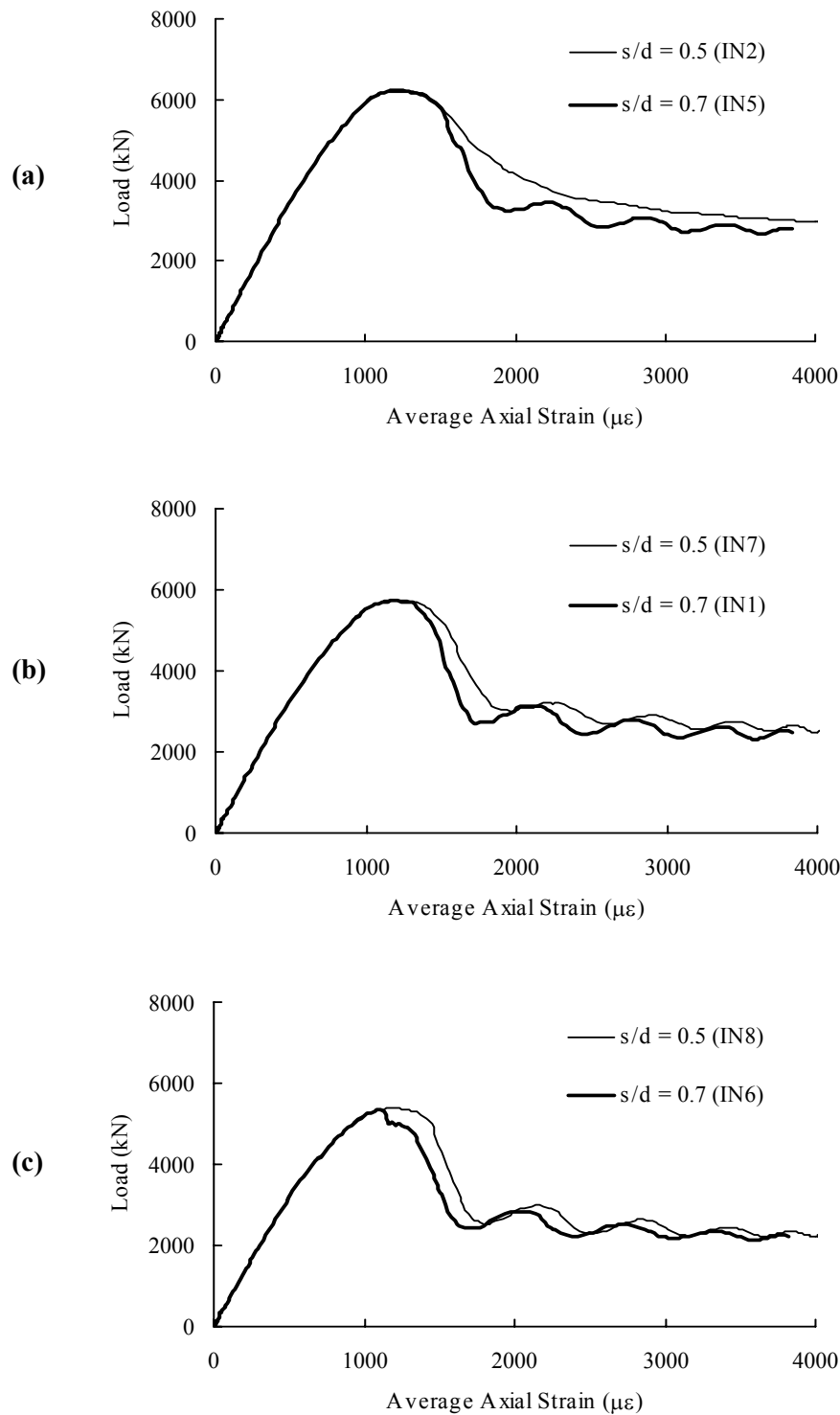
Figure D.2 Effect of b/t ratio on Load versus Average Axial Strain Curve for Intermediate PEC Column (Analysis Set 2), (a) s = 0.5d and (b) s = 0.7d

(a)

(b)
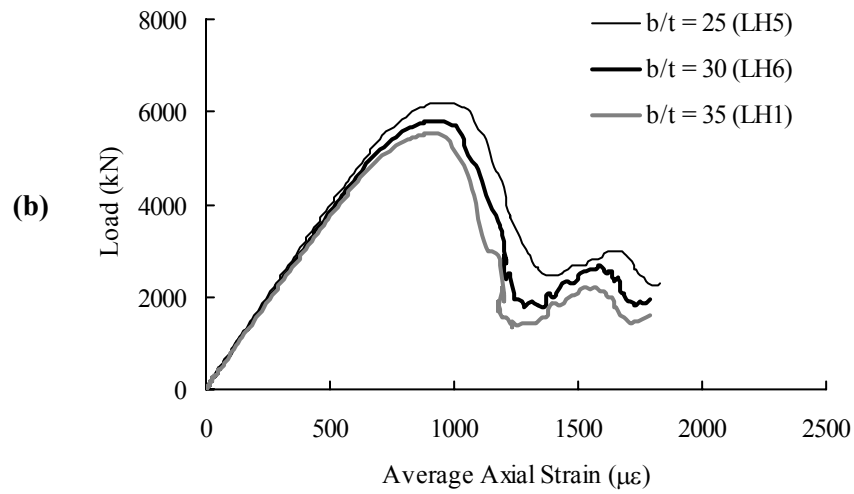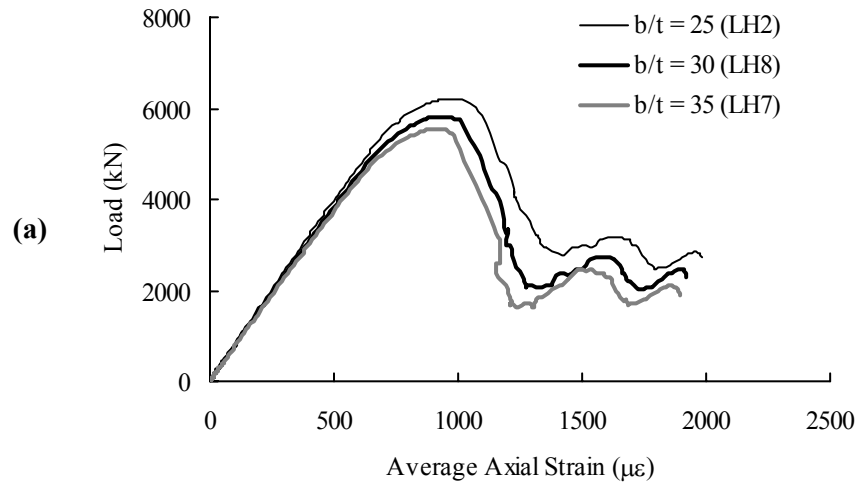
Figure D.3 Effect of b/t ratio on Load versus Average Axial Strain Curve for Long PEC Column (Analysis Set 3), (a) s = 0.5d and (b) s = 0.7d

(a)

(b)
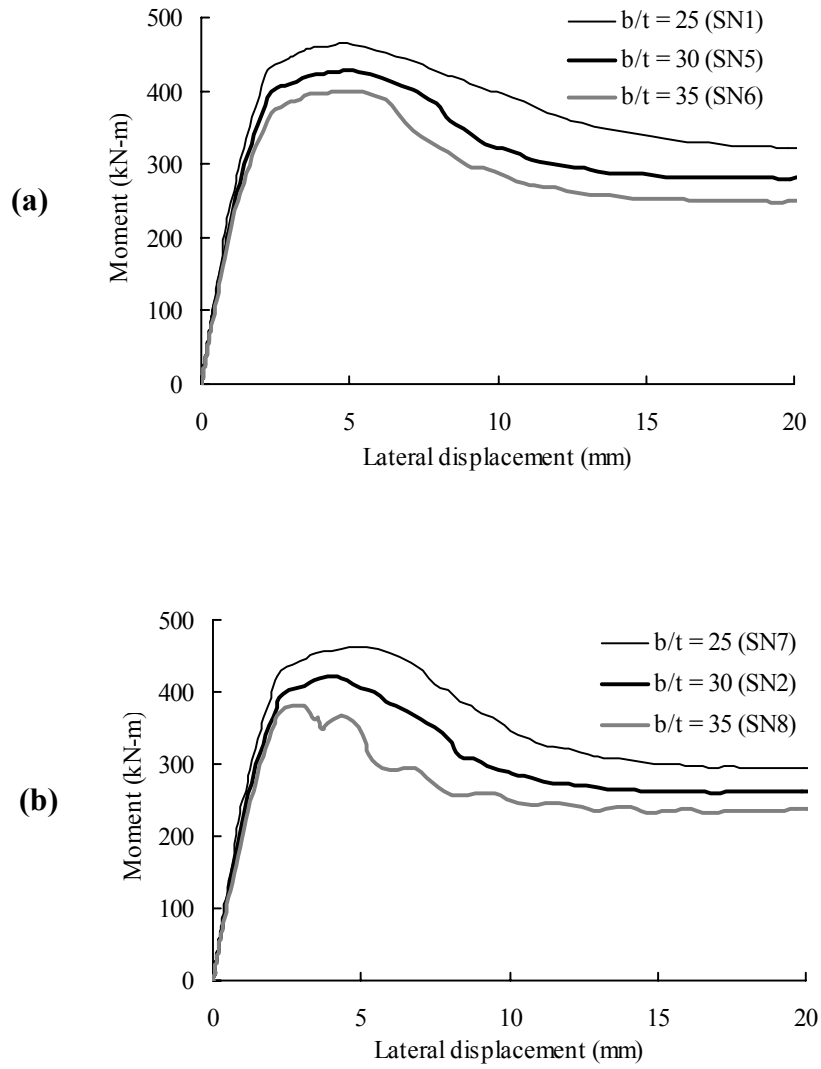
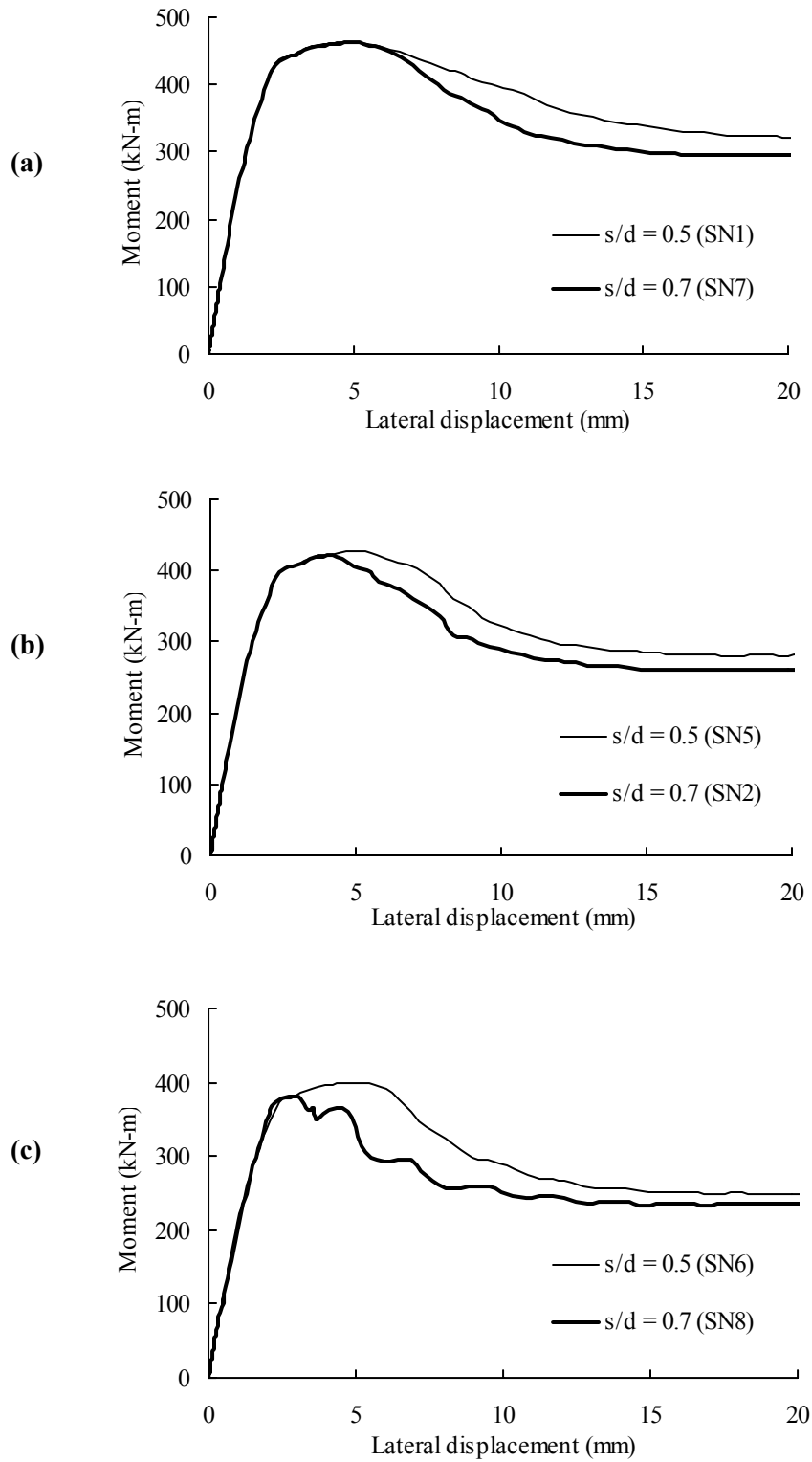**Figure D.4 Effect of b/t ratio on Moment versus Lateral Displacement Curve for Short PEC Column (Analysis Set 1), (a) s = 0.5d and (b) s = 0.7d**
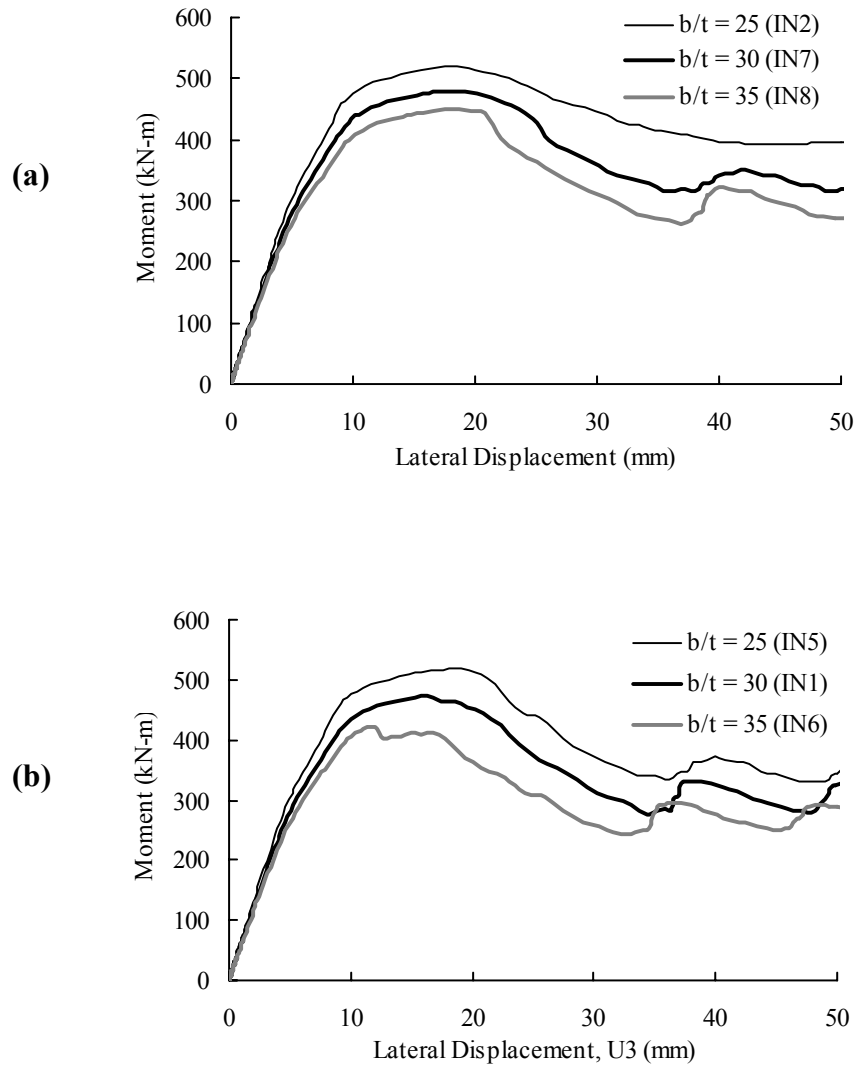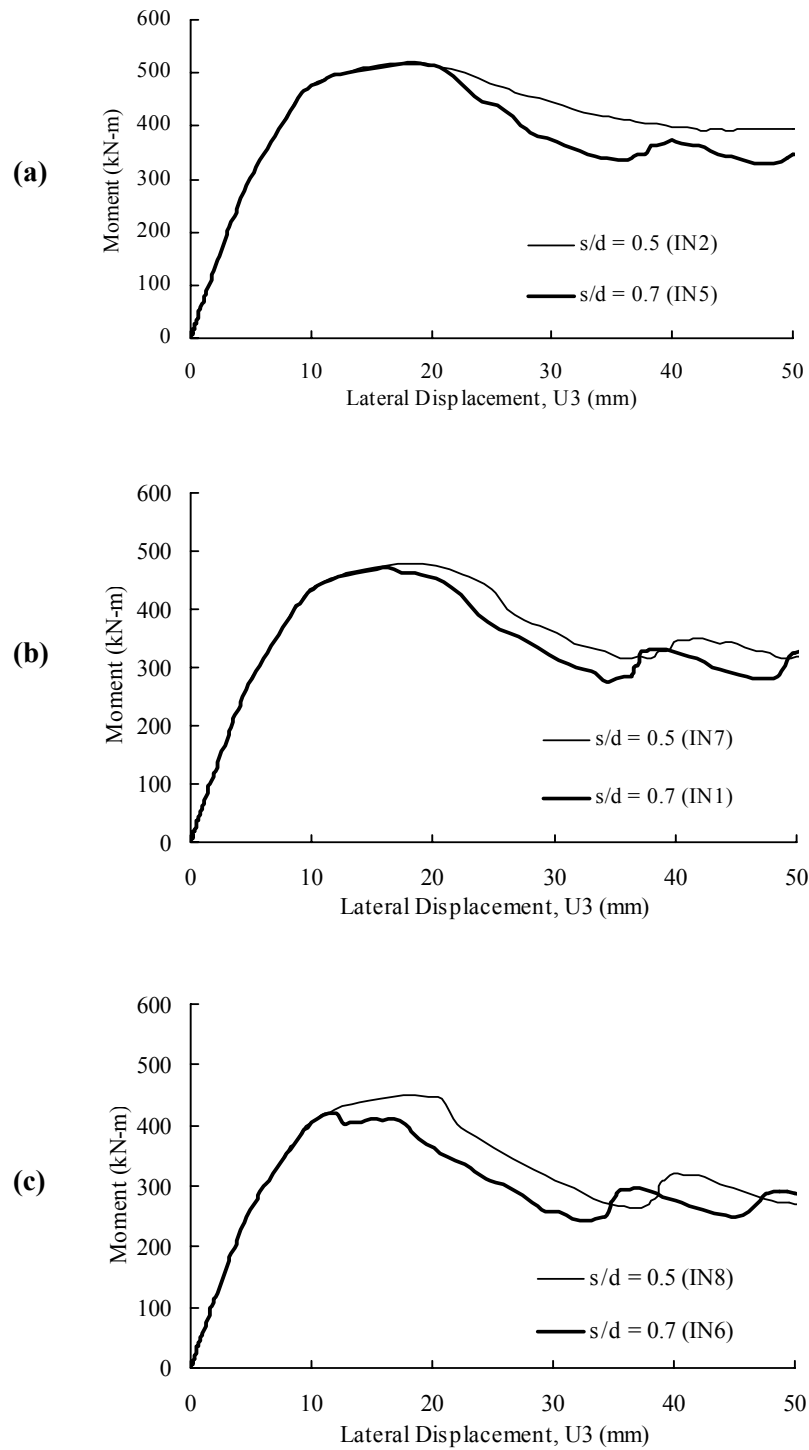
Figure D.5 Effect of b/t ratio on Moment versus Lateral Displacement Curve for Intermediate PEC Column (Analysis Set 2), (a) s = 0.5d and (b) s = 0.7d
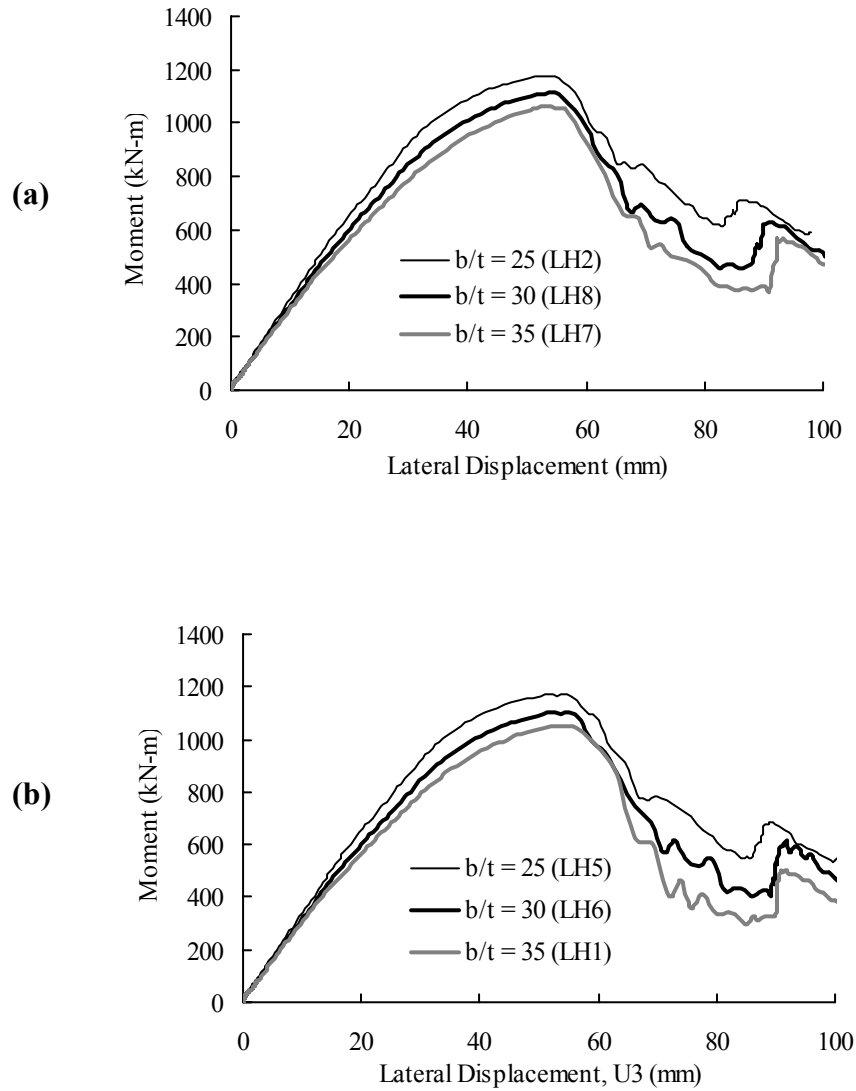
Figure D.6 Effect of b/t ratio on Moment versus Lateral Displacement Curve for Intermediate PEC Column (Analysis Set 2), (a) s = 0.5d and (b) s = 0.7d
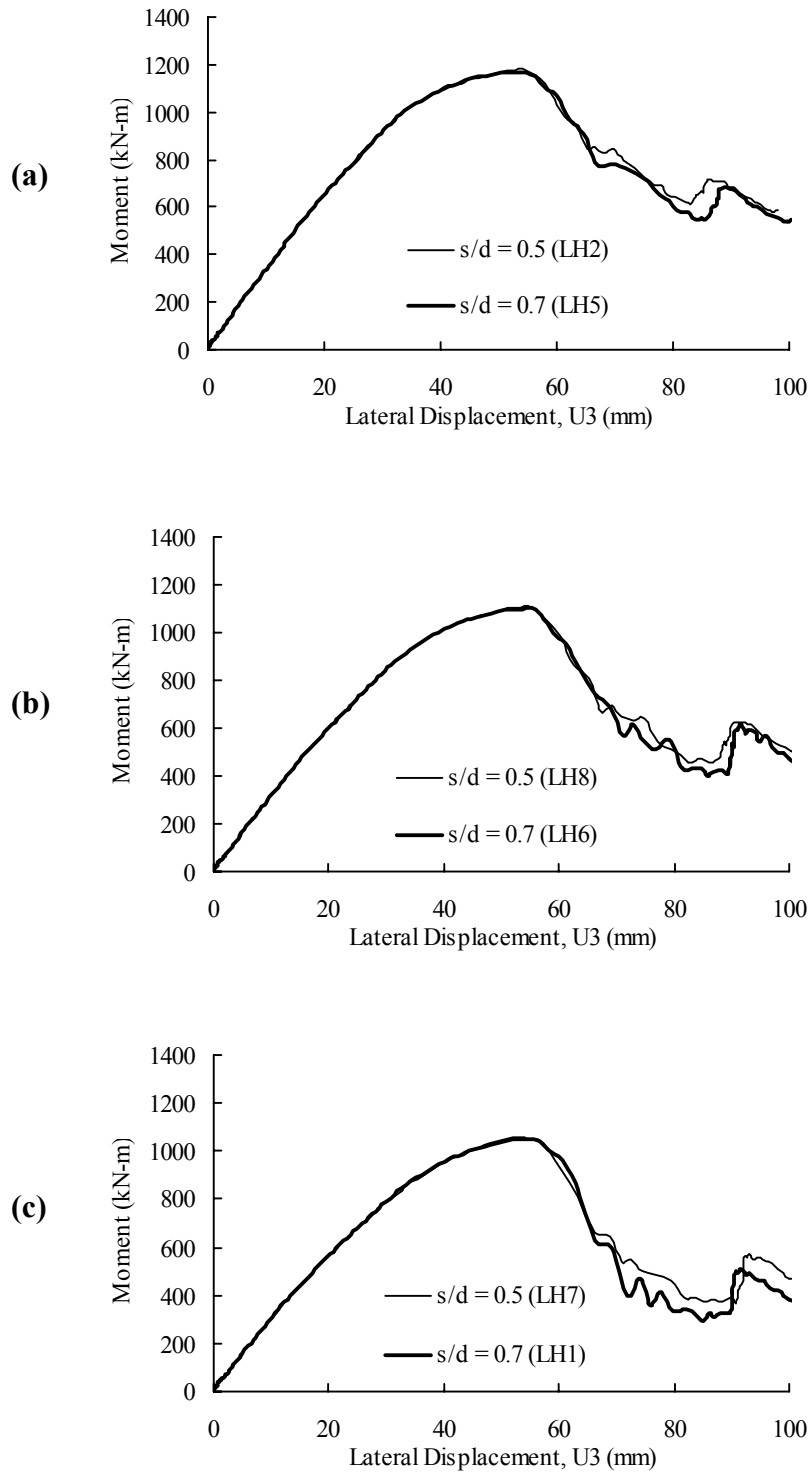
(a)

(b)
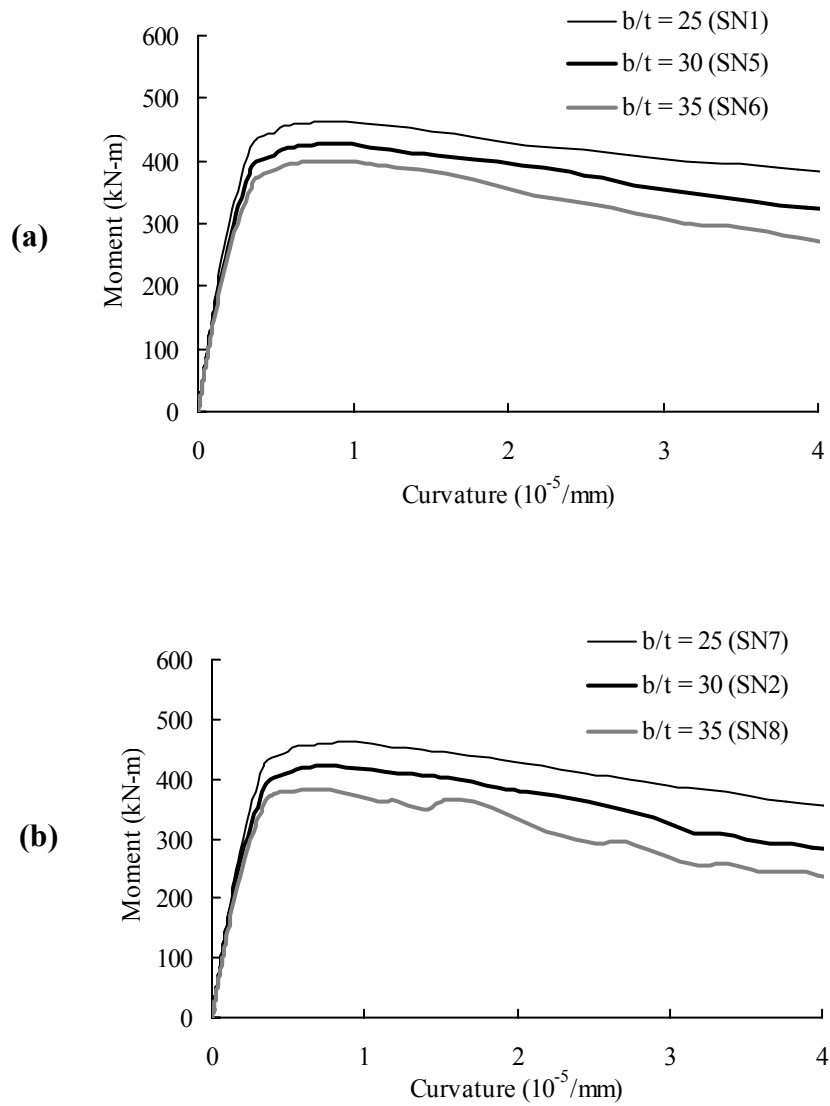
Figure D.7 Effect of b/t ratio on Moment versus Curvature Curve for Short PEC Column (Analysis Set 1), (a) s = 0.5d and (b) s = 0.7d

(a)

(b)
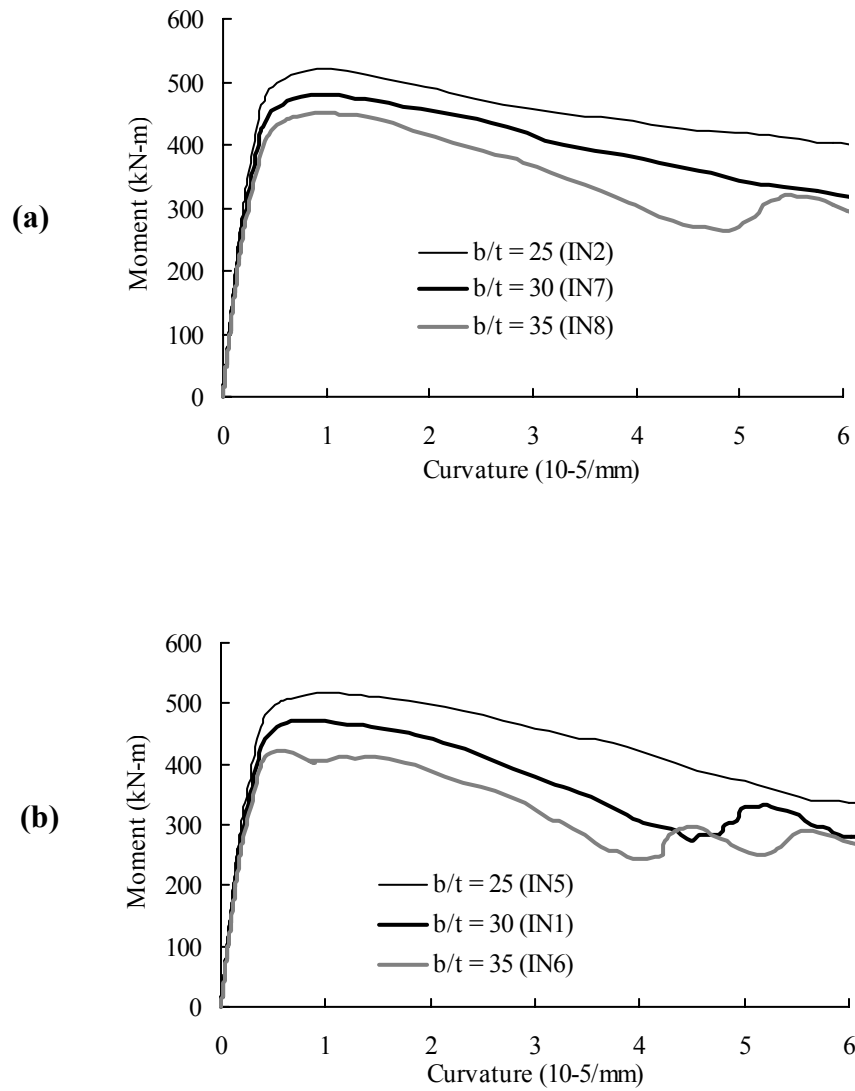
Figure D.8 Effect of b/t ratio on Moment versus Curvature Curve for Intermediate PEC Column (Analysis Set 2), (a) s = 0.5d and (b) s = 0.7d

(a)

(b)
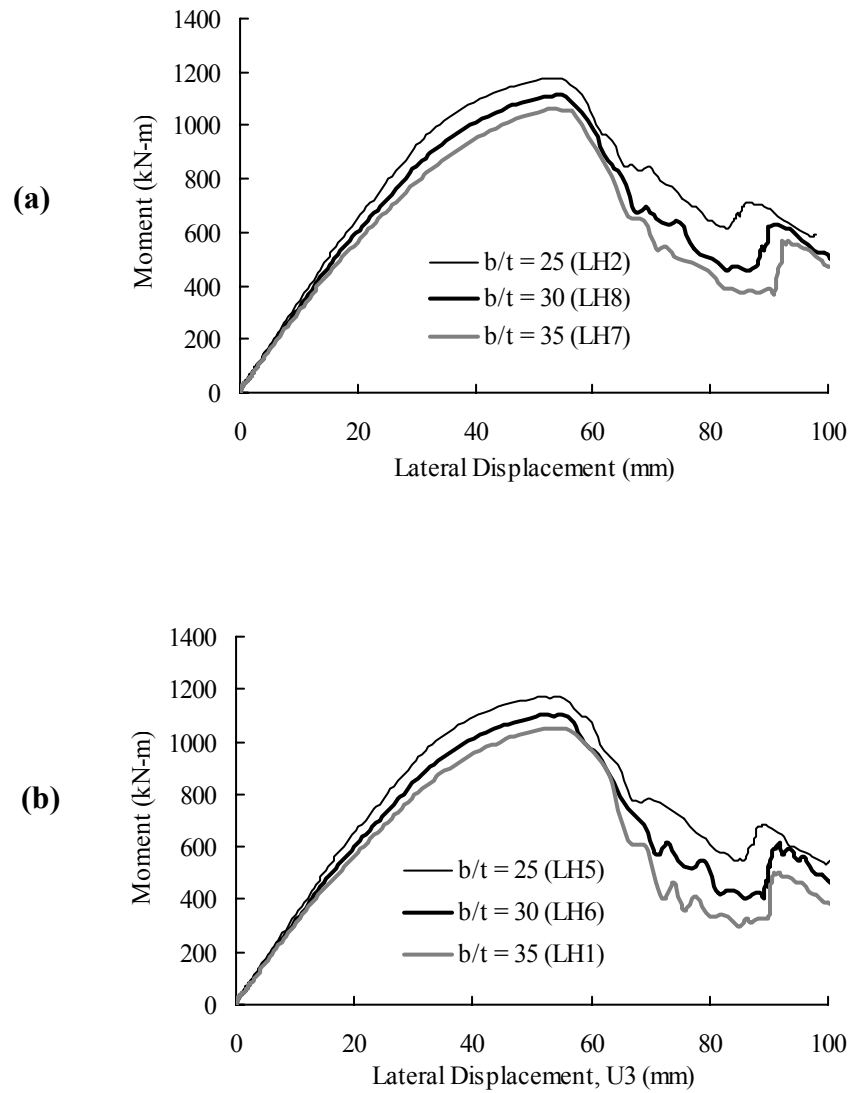
Figure D.9 Effect of b/t ratio on Moment versus Curvature Curve for Long PEC Column (Analysis Set 3), (a) s = 0.5d and (b) s = 0.7d
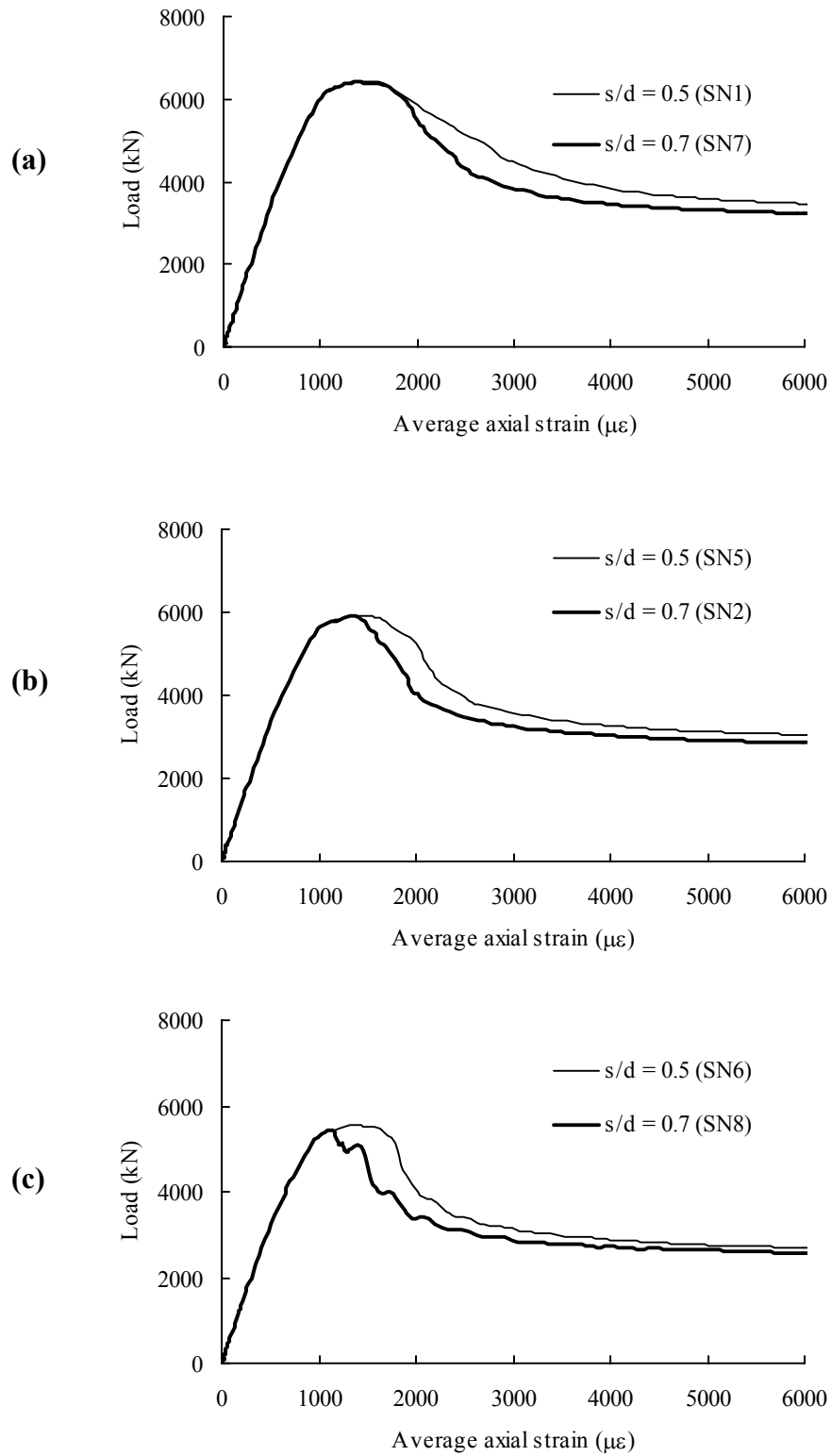
Figure E.1 Effect of s/d Ratio on Load versus Average Axial Strain Response for Short PEC Column (Analysis Set 1), (a) b/t = 25, (b) b/t = 30 and (c) b/t = 35

Figure E.2 Effect of s/d Ratio on Load versus Average Axial Strain Response for Intermediate PEC Column (Analysis Set 2), (a) b/t = 25, (b) b/t = 30 and (c) b/t = 35

(a)

(b)

(c)
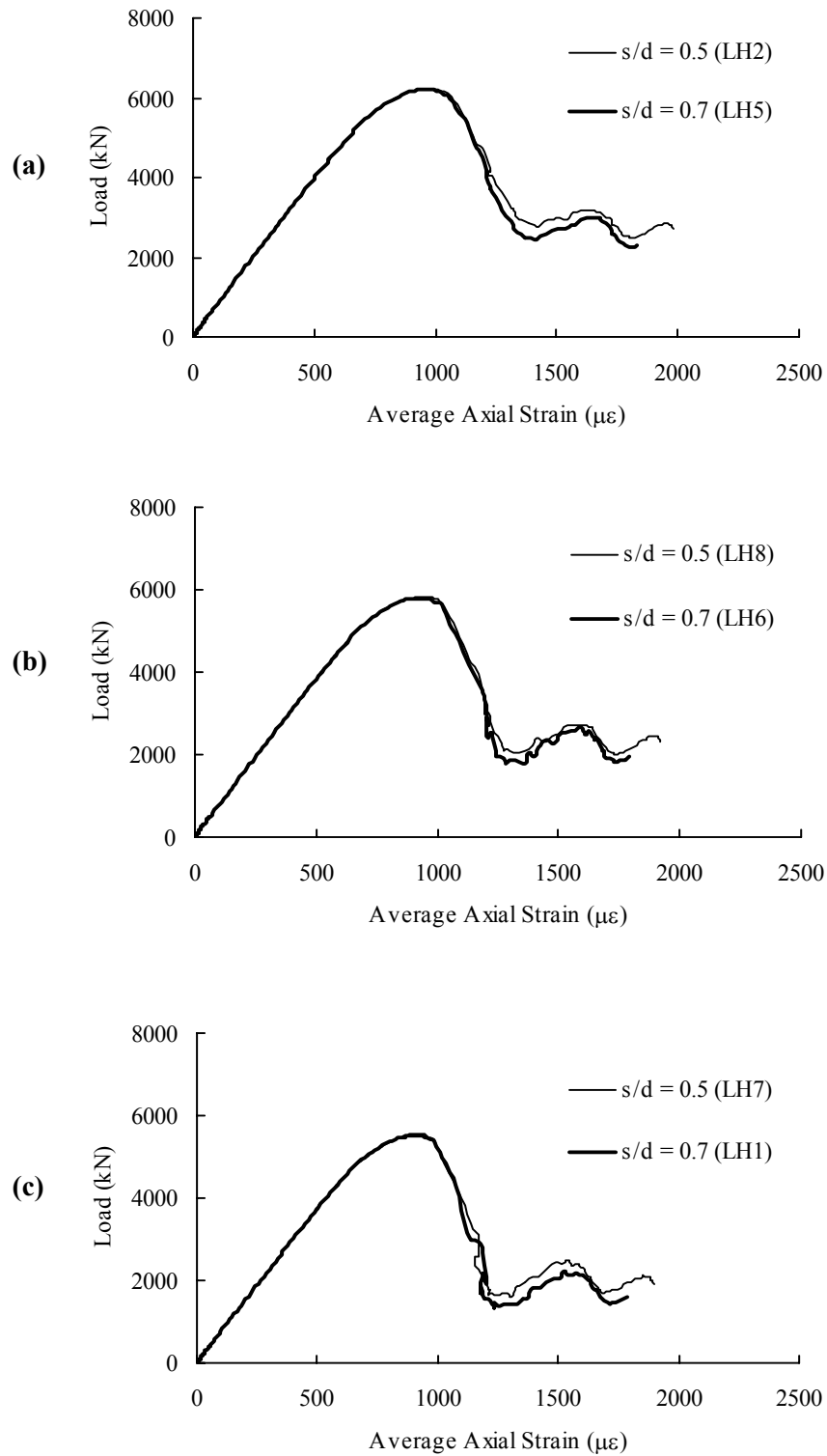
Figure E.3 Effect of s/d Ratio on Load versus Average Axial Strain Response for Long PEC Column (Analysis Set 2), (a) b/t = 25, (b) b/t = 30 and (c) b/t = 35

Figure E.4 Effect of s/d Ratio on Moment versus Lateral Displacement Curve for Short PEC Column (Analysis Set 1), (a) b/t = 25, (b) b/t = 30 and (c) b/t = 35
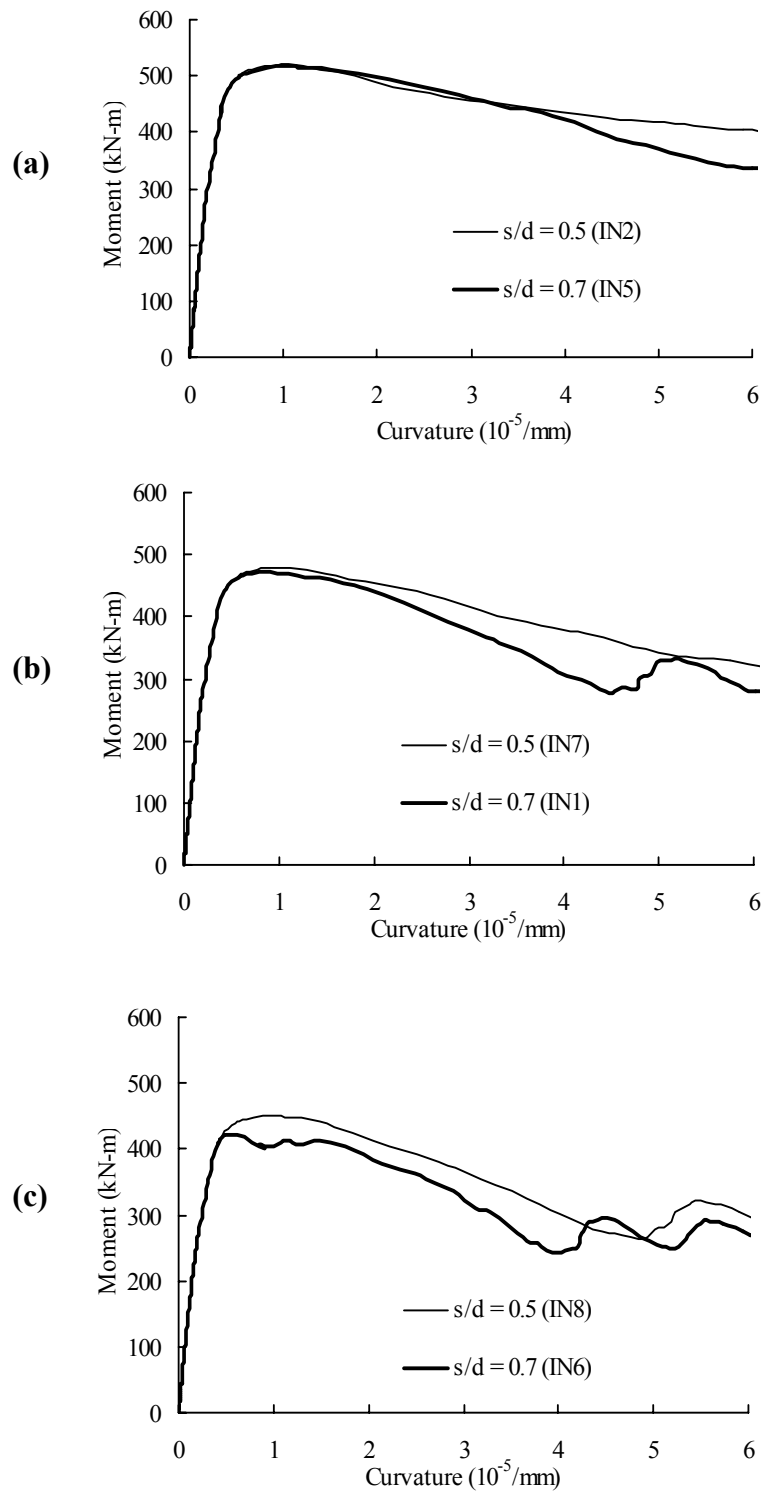
Figure E.5 Effect of s/d Ratio on Moment versus Lateral Displacement Curve for Intermediate PEC Column (Analysis Set 2), (a) b/t = 25, (b) b/t = 30 and (c) b/t = 35
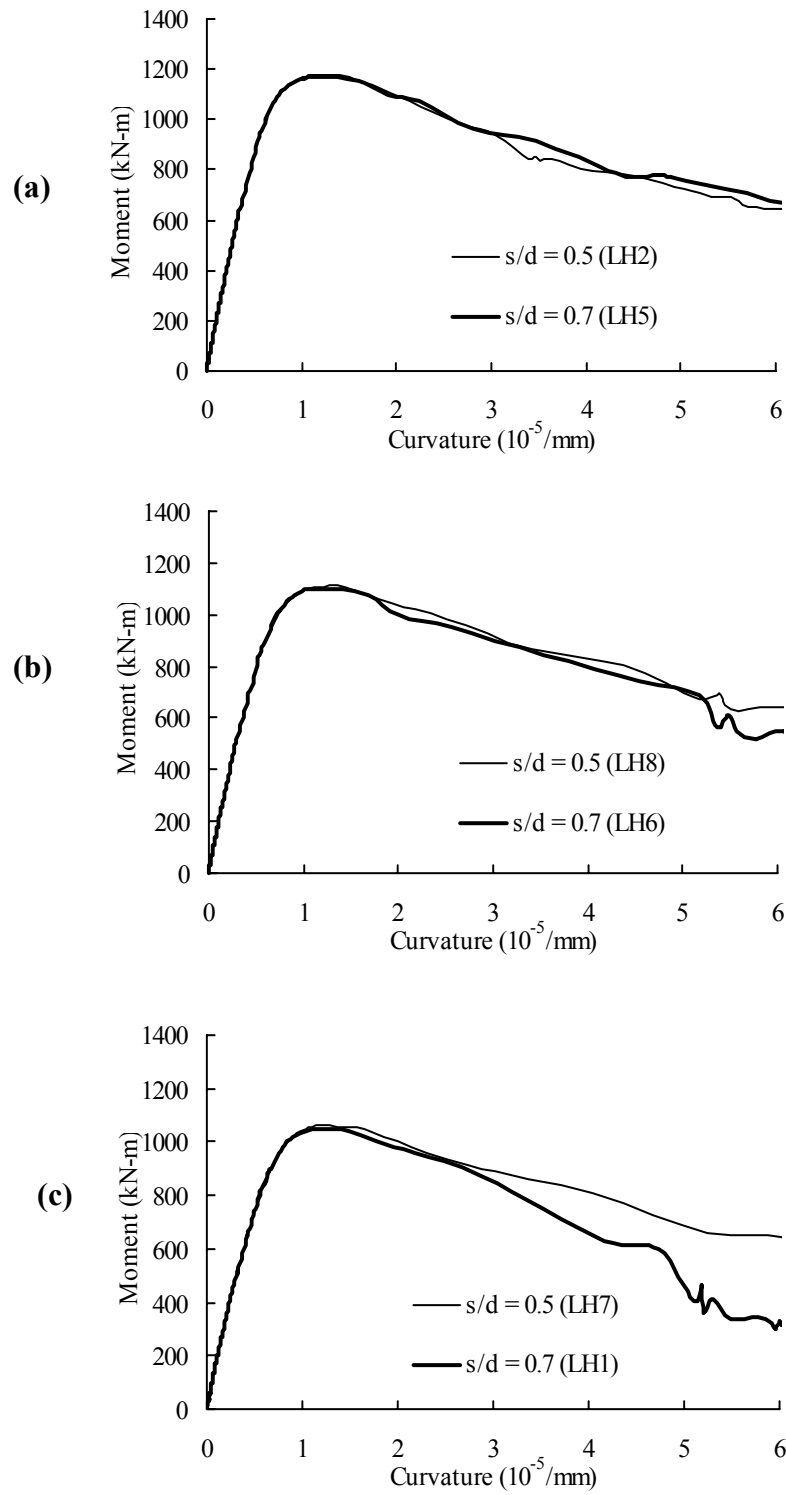
243

**Figure E.6 Effect of s/d Ratio on Moment versus Lateral Displacement Curve for
Long PEC Column (Analysis Set 3), (a) b/t = 25, (b) b/t = 30 and (c) b/t = 35**

244
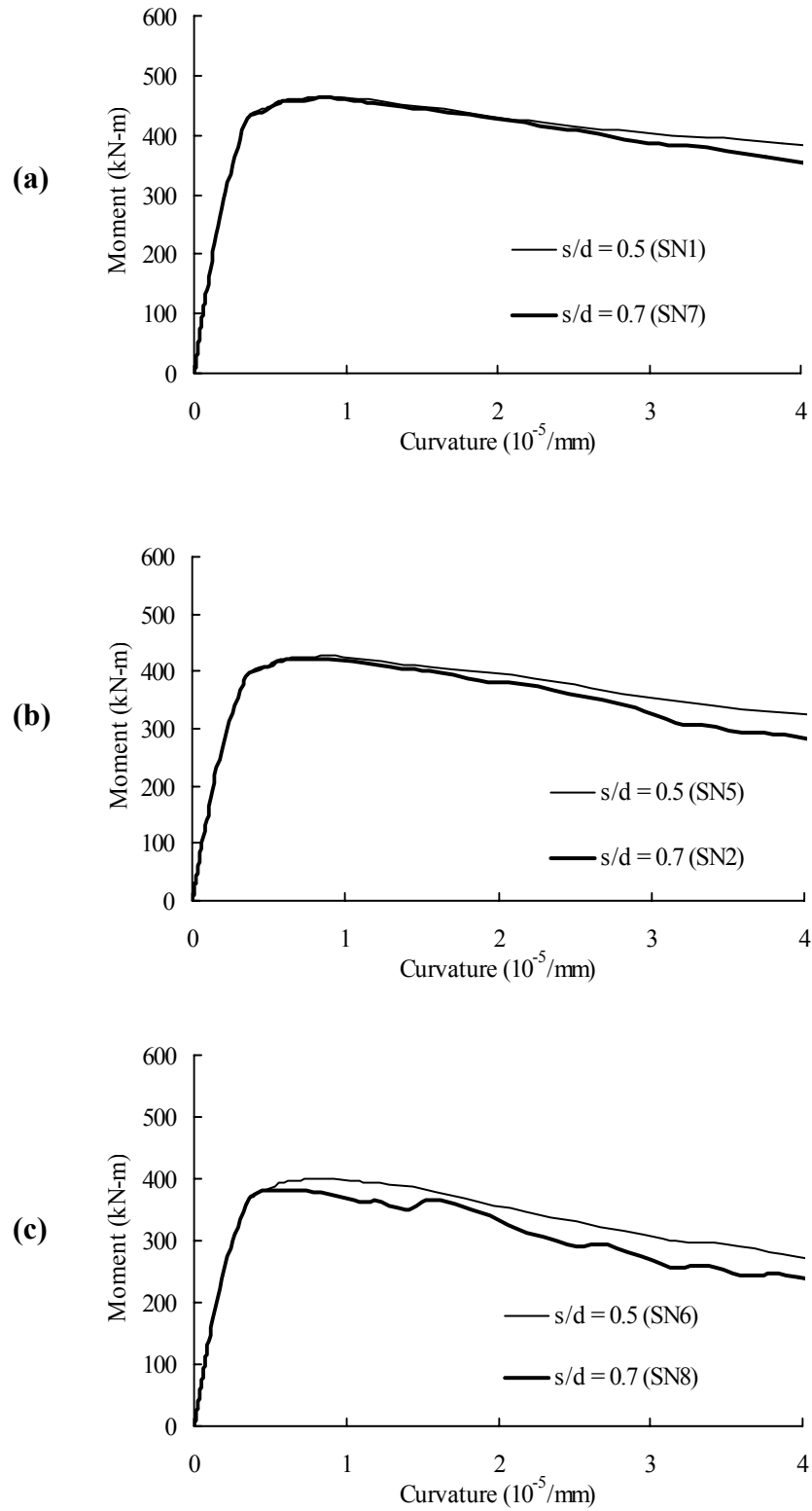
Figure E.7 Effect of s/d Ratio on Moment versus Curvature Curve for Short PEC Column (Analysis Set 1), (a) b/t = 25, (b) b/t = 30 and (c) b/t = 35

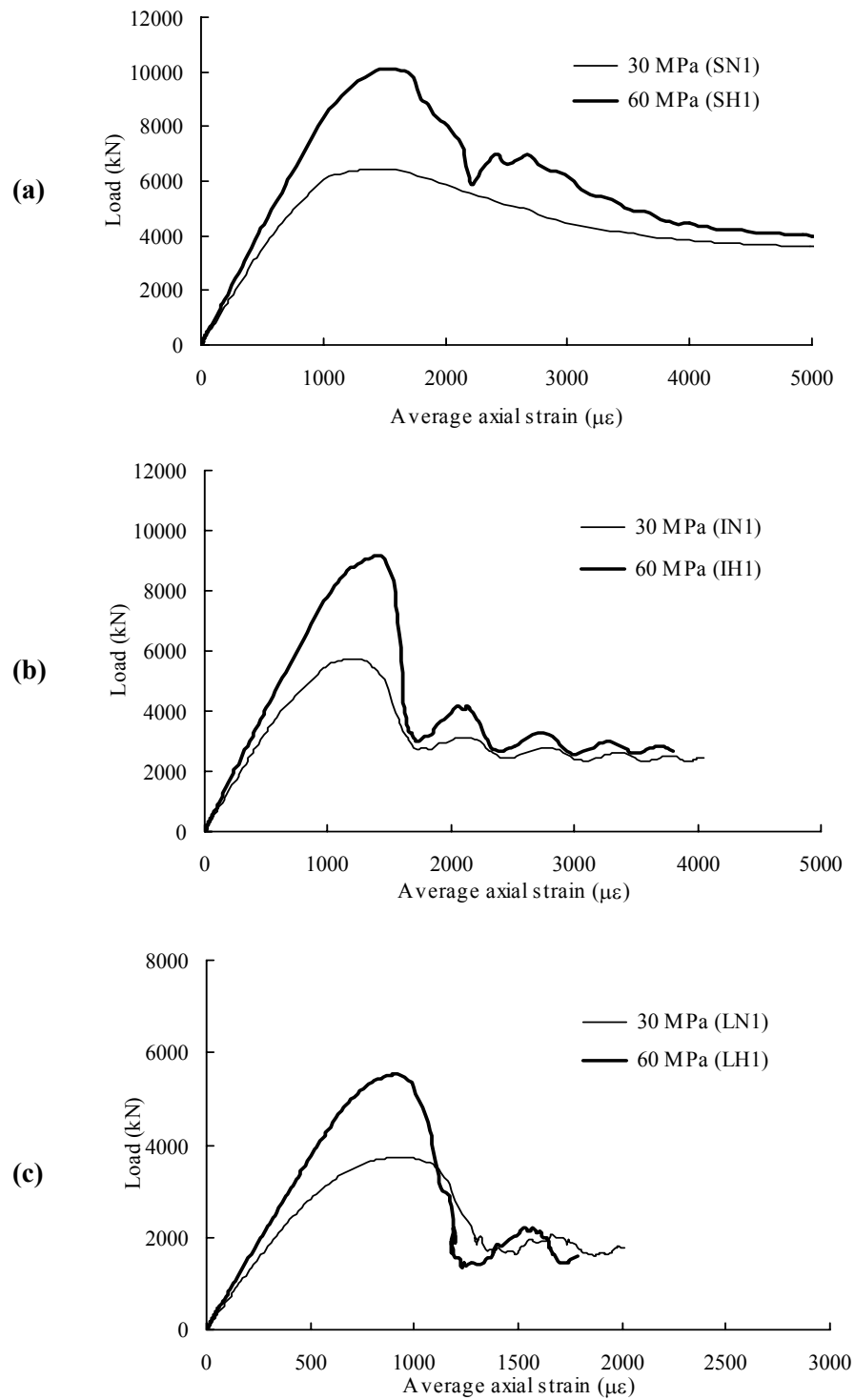**Figure E.8 Effect of s/d Ratio on Moment versus Curvature Curve for Intermediate PEC Column (Analysis Set 2), (a) b/t = 25, (b) b/t = 30 and (c) b/t = 35**

Figure E.9 Effect of s/d Ratio on Moment versus Curvature Curve for Long PEC Column (Analysis Set 3), (a) b/t = 25, (b) b/t = 30 and (c) b/t = 35

Figure F.1 Effect of Concrete Compressive Strength on Load versus Average Axial Strain Curve, (a) Set 1, (b) Set 2 and (c) Set 3
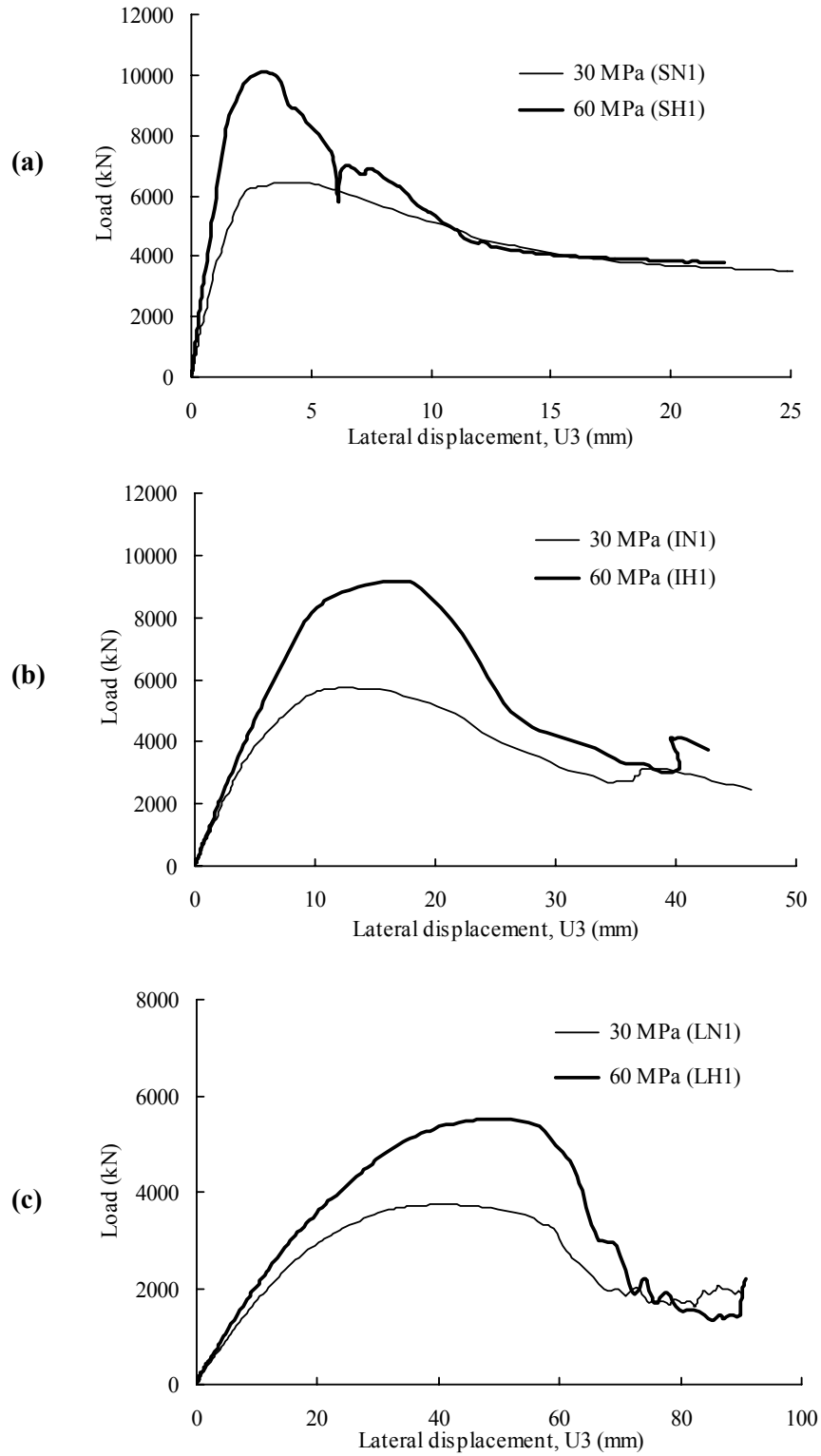
Figure F.2 Effect of Concrete Compressive Strength on Load versus Lateral Displacement Curve, (a) Set 1, (b) Set 2 and (c) Set 3
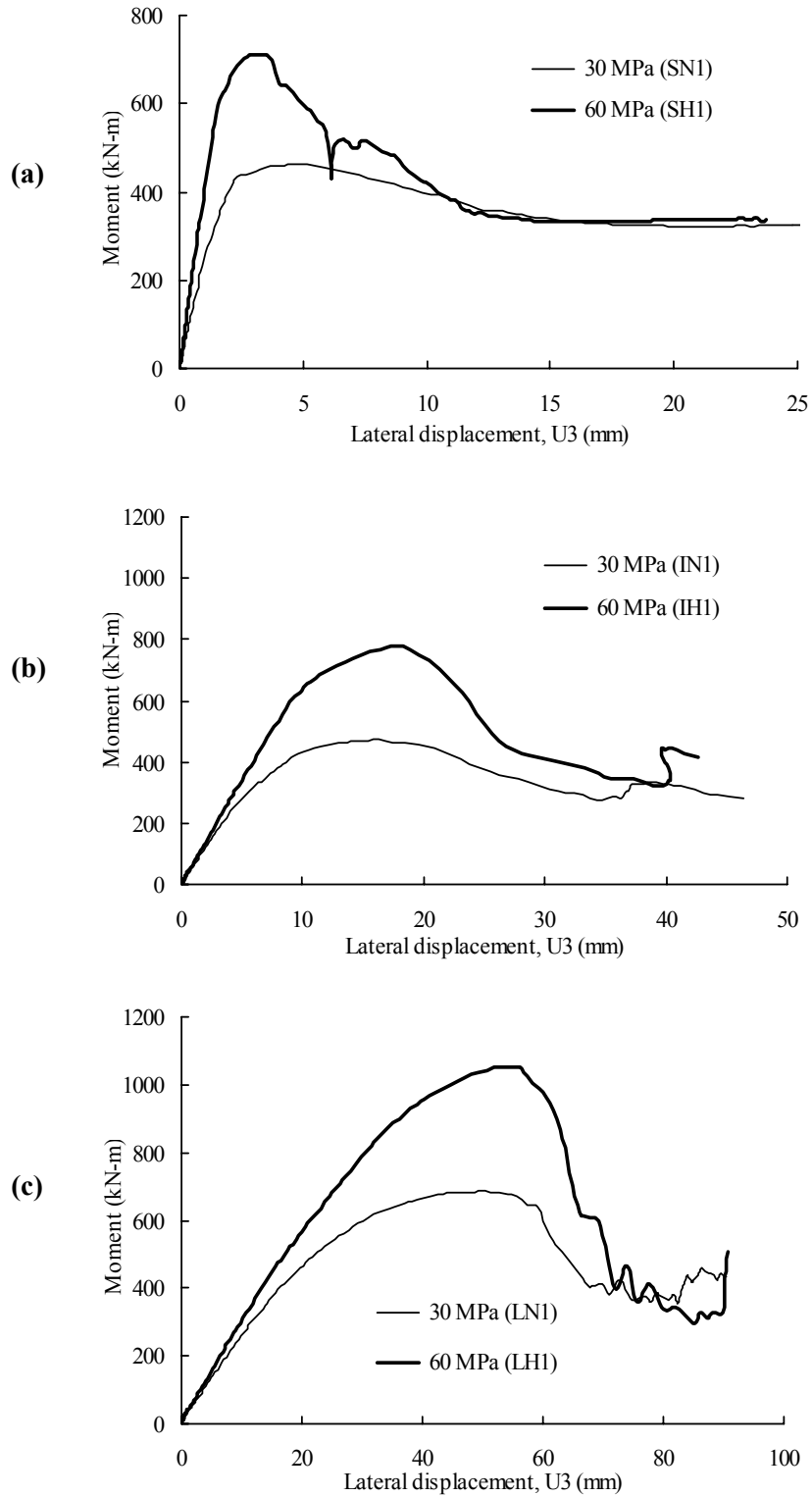
Figure F.3 Effect of Concrete Compressive Strength on Moment versus Lateral Displacement Curve, (a) Set 1, (b) Set 2 and (c) Set 3
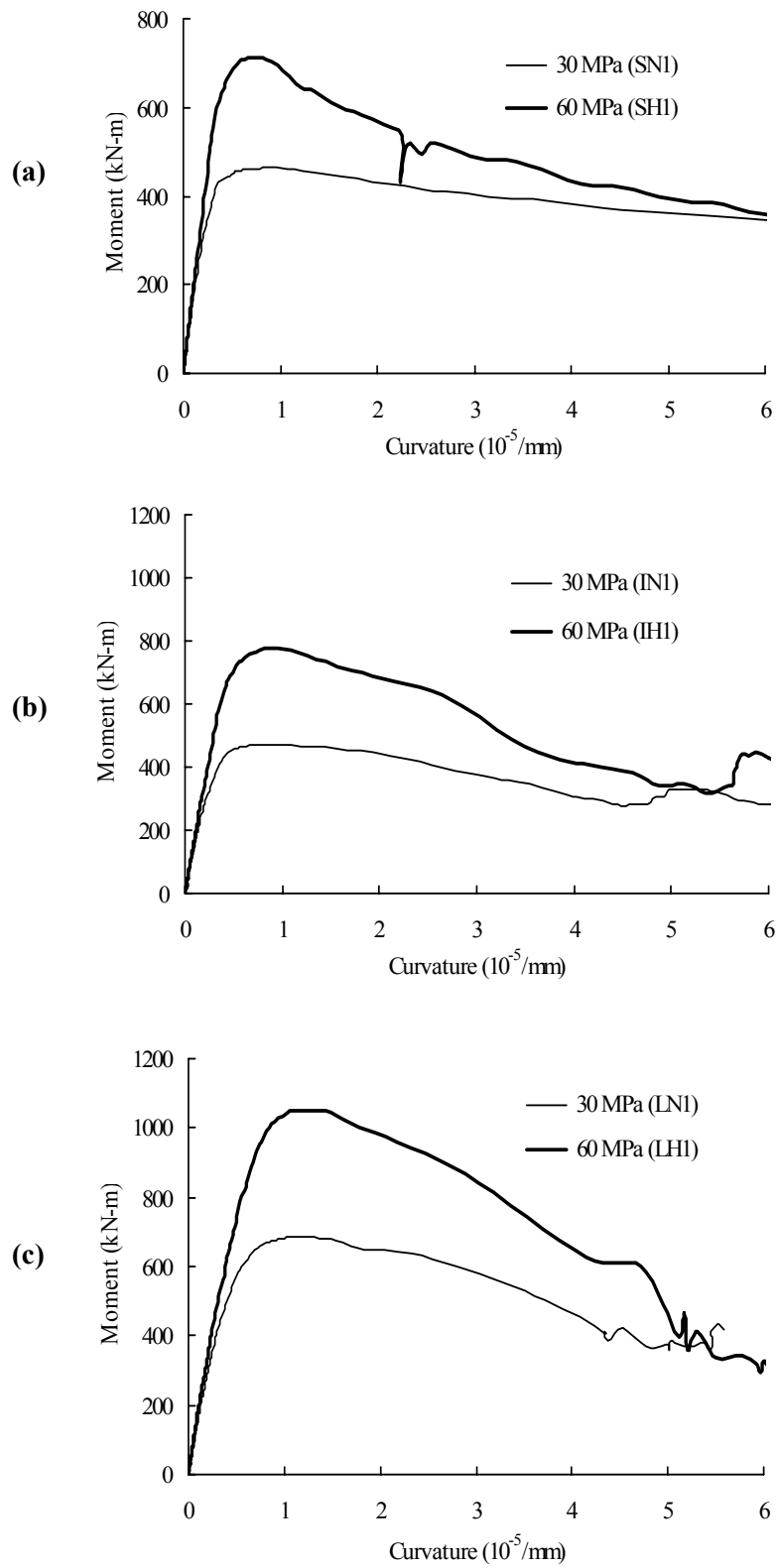
Figure F.4 Effect of Concrete Compressive Strength on Moment versus Curvature Curve, (a) Set 1, (b) Set 2 and (c) Set 3

251